CHEMICAL REVIEWS

pubs.acs.org/CR

Review

Bacterial Metallostasis: Metal Sensing, Metalloproteome Remodeling, and Metal Trafficking

Daiana A. Capdevila,* Johnma J. Rondón, Katherine A. Edmonds, Joseph S. Rocchio, Matias Villarruel Dujovne, and David P. Giedroc*

Cite This: *Chem. Rev.* 2024, 124, 13574−13659

Read Online

ACCESS | Metrics & More | Article Recommendations

ABSTRACT: Transition metals function as structural and catalytic cofactors for a large diversity of proteins and enzymes that collectively comprise the metalloproteome. Metallostasis considers all cellular processes, notably metal sensing, metalloproteome remodeling, and trafficking (or allocation) of metals that collectively ensure the functional integrity and adaptability of the metalloproteome. Bacteria employ both protein and RNA-based mechanisms that sense intracellular transition metal bioavailability and orchestrate systems-level outputs that maintain metallostasis. In this review, we contextualize metallostasis by briefly discussing the metalloproteome and specialized roles that metals play in biology. We then offer a comprehensive perspective on the diversity of metalloregulatory proteins and metal-sensing riboswitches, defining general principles within each sensor superfamily that capture how specificity is encoded in the sequence, and how selectivity can be leveraged in downstream synthetic biology and biotechnology applications. This is followed by a discussion of recent work that highlights selected metalloregulatory outputs, including metalloproteome remodeling and metal allocation by metallochaperones to both client proteins and compartments. We close by briefly discussing places where more work is needed to fill in gaps in our understanding of metallostasis.

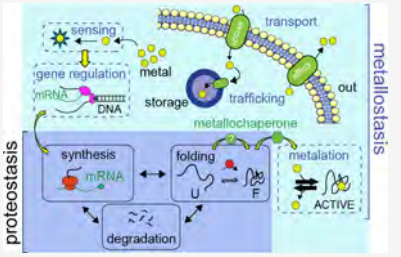

CONTENTS

Received: April 9, 2024
Revised: November 1, 2024
Accepted: November 6, 2024
Published: December 10, 2024

https://doi.org/10.1021/acs.chemrev.4c00264
Chem. Rev. 2024, 124, 13574−13659

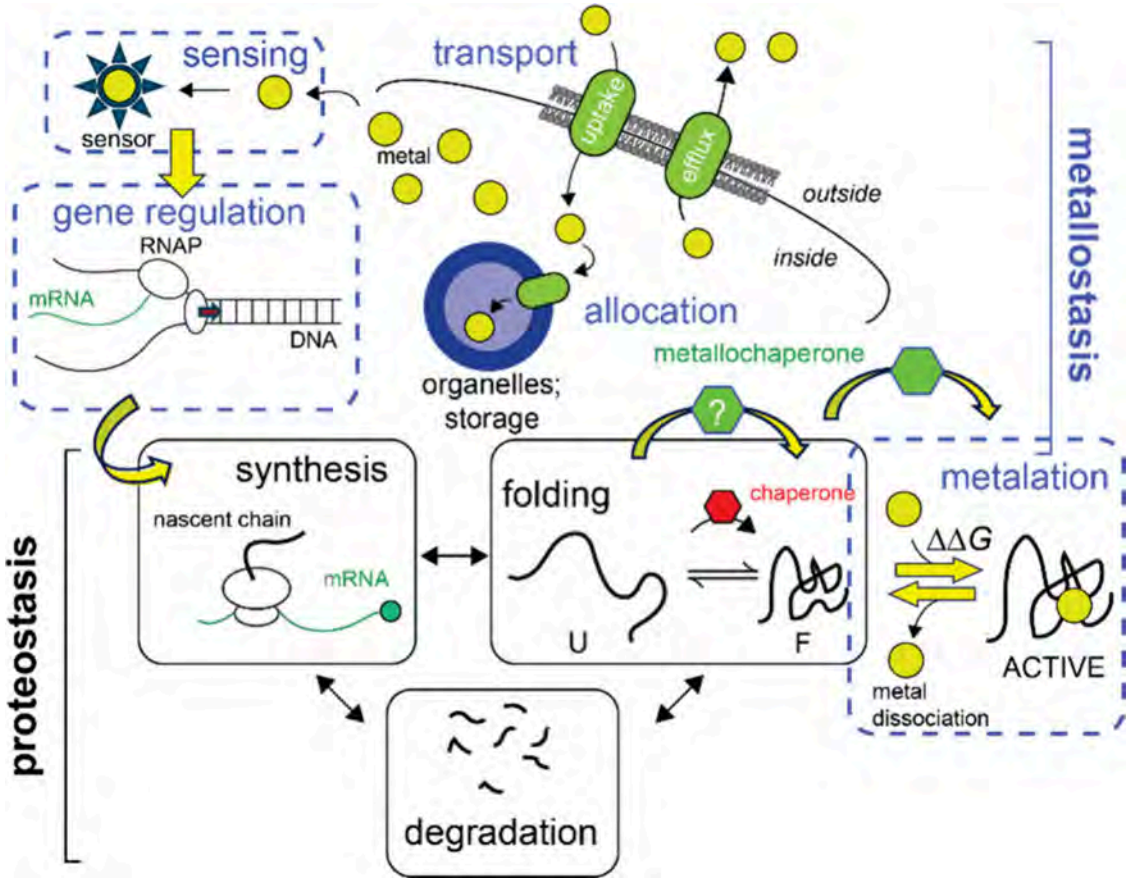

Figure 1. Metallostasis (blue) is a subdomain of the proteostasis network (black) that is integrated into the synthesis-folding-degradation paradigm. Metallosensors function at the apex of the metallostasis network and sense cellular bioavailable metal. This results in the regulation of the genes that encode components of the network, and includes proteins involved in metal transport, storage and allocation, and as enzyme paralogs (not shown here). The adaptive response to metal overload or starvation collectively mediated by the metallostasis network enforces an appropriate free energy of metalation ($\Delta\Delta G$) of the metalloproteome, thereby maintaining its functional integrity.

https://doi.org/10.1021/acs.chemrev.4c00264
Chem. Rev. 2024, 124, 13574−13659

1. INTRODUCTION

1.1. Metallostasis

All cells, whether free-living in a particular microenvironment, or part of community of cells in a tissue or a microbial biofilm, must acquire metal ions from the extracellular milieu, bring them across a lipid bilayer and put them to use. Metals generally function as metallocofactors in enzymes that are required to catalyze an enormous diversity of chemical transformations at rates and efficiencies compatible with cellular needs, while also responsive to prevailing metabolic conditions. These metalloproteins, ranging from proteins that use a metal as an enzymatic cofactor to structural metals that stabilize the protein fold, play many roles in biological systems.[1] Approximately one-third to 40% of a typical proteome is a metalloprotein,[2] and cells must ensure that the metalloproteome is metalated with integrity, defined by binding of the cognate or native metal under all growth conditions, yet is sufficiently plastic or adaptable, so as to effectively respond to metal limitation while avoiding metal toxicity.[3]

Metallostasis is the cellular homeostasis of metal ions and encompasses all processes that ultimately impact the status or integrity of the metalloproteome. Metallostasis integrates all mechanisms that ensure proper metalation, including those that function at the transcriptional level, mediated by protein- and RNA-based metallosensors, cotranslationally during protein synthesis, or post-translationally, where metal is inserted into a folded apoprotein (Figure 1). Metallostasis is analogous to, and a subdomain of, proteostasis or protein homeostasis, defined as the dynamic regulation of a balanced and functional proteome (Figure 1). While proteostasis is governed by a "network" that collectively controls the biogenesis, folding, trafficking, and degradation of proteins present within and outside the cell, metallostasis is likewise controlled by a network of metal sensing, transport, speciation and ultimately trafficking of these finite inorganic resources to a specific task (Figure 1). Metallostasis becomes particularly important under environmental conditions that induce metal limitation or starvation. In bacteria, the evolution of protein "paralogs" that perform identical functions in cells, but with distinct inorganic cofactor requirements or none at all, is a particularly dramatic and sometimes overlooked example of metabolic and evolutionary adaptation to bioavailable metals.[4] Examples of these proteins can be found particularly in central carbon metabolism that becomes essential in an infection under these conditions[5,6] and in DNA synthesis[7,8] and, more generally, nucleic acid metabolism.[4,9] In humans, nutritional immunity, where host mechanisms have evolved to limit bacterial pathogen access to nutrient metals, alongside host-mediated metal intoxication, are central aspects of the "tug-of-war" between host and pathogen in infectious disease.[10−12] In addition, dietary metal nutrient deficiency, metal toxicity or impaired metal transport, trafficking and allocation caused by a wide range of human genetic disorders figure prominently in human biology and pathology.[13−17]

1.2. Scope of this Review

Metallostasis is dedicated to ensuring the structural and functional integrity of the metalloproteome (Figure 1). We focus on specific mechanisms discovered from work published within the last 10 or so years, nearly exclusively in bacteria, as representative of the diversity of the adaptive responses in these simple organisms, with reference to eukaryotic mechanisms when parallels may inform bacterial metallostasis systems. In each section, we provide historical context for a discussion of the more recent work that follows, referring the reader to this earlier work as needed. We begin by briefly discussing the metalloproteome and specialized roles that metals play in biology, with a focus on general principles and specific illustrations of what constitutes structural, regulatory and catalytic metal sites in proteins. Metallostasis is tightly orchestrated by upstream "sentinels", metallosensors, specialized proteins or RNAs specific for a cognate metal that detects the bioavailability of that metal in the cell, and by doing so, control the expression of genes that encode other players in the metallostasis network (Figure 1). We discuss these proteins in detail, emphasizing general concepts that have emerged from comprehensive studies of these model "allosteric" switches[18] and more recent efforts to employ metallosensors in synthetic biology and biotechnology applications.[19] This is followed by a discussion of enzyme paralogs as a remarkable example of metalloproteome remodeling, albeit one generally limited to bacteria.[4] We then discuss the trafficking of metals to downstream metalloenzyme targets, contextualizing this discussion around the concept of a metallochaperone, focusing first on the biogenesis or maturation of metallocofactors in specific enzymes, followed by moving metals across a membrane. We close by briefly discussing places where more work is needed to fill in gaps in our understanding of metallostasis, and how this new knowledge might be leveraged to develop new therapeutic strategies to combat infectious disease.

2. THE METALLOPROTEOME

2.1. Metals in Biology

2.1.1. Overview. The metalloproteome comprises all of those proteins that bind a specific or cognate metal ion, or in rare cases a number of closely related metal ions, to execute a well-defined biological function. These metal ions can function as structural, regulatory or catalytic cofactors when bound to a protein through coordinate covalent bonds. In the context of this Review, we explicitly consider the first-row, late 3*d*-block metal ions from manganese (Mn; d^5 in the 2^+ oxidation state or Mn^{II}) to zinc (Zn; d^{10}) and including all the elements between these two: iron (Fe; d^6), cobalt (Co; d^7), nickel (Ni; d^8) and copper (Cu; d^9) (Figure 2). We limit our discussion to these metals, since, with the exception of nickel,[20] each plays important roles in all kingdoms of life and cells are known to sense and actively regulate their intracellular availability through the mechanisms we discuss here.[21,22] The reader is referred to other recent articles, reviews or collections of articles that discuss biological metals and processes beyond these metals, notably nitrogenase and the maturation of the molybdenum cofactor (Moco)[23] and other molybdenum-containing enzymes[24] in bacteria,[25,26] plants and photosynthetic organisms,[27,28] and humans,[29] as well as tungsten and vanadium-cofactored enzymes.[20,30] In addition, we do not discuss recent exciting findings on the chemistry and biology of trivalent lanthanides[31,32] and associated emerging work on employing the basic science of rare earth element molecular recognition to develop robust separations technologies designed for field-deployment.[33] Finally, we do not consider the major metalloid selenium (Se), which functions in proteins in a twenty-first

https://doi.org/10.1021/acs.chemrev.4c00264
Chem. Rev. 2024, 124, 13574−13659

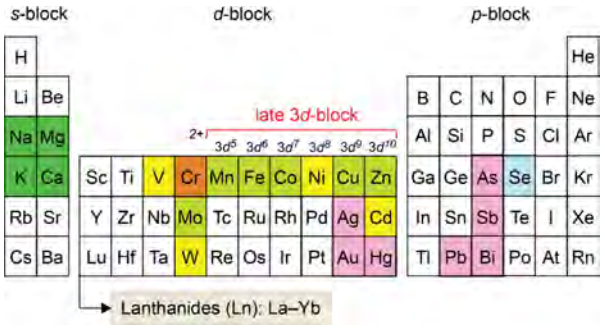

Figure 2. Abbreviated version of the periodic table of the elements highlighting the biologically important metals. *s*-block mono- and divalent metals (dark green); essential *d*-block metals (light green); *d*-block metals that play roles in some forms of life (yellow); chromium (orange) and the metalloid selenium (light cyan) are also indicated. The early lanthanides (tan; La) are used by some archaea,[32] notably the methylotrophs, which incorporate Ln into methanol dehydrogenases. Other elements from both *d*- and *p*-blocks are considered xenobiotics and sensed by metallosensors (light pink) (Section 3). The biologically relevant metals discussed are from the late 3*d*-block, from Mn to Zn.[21]

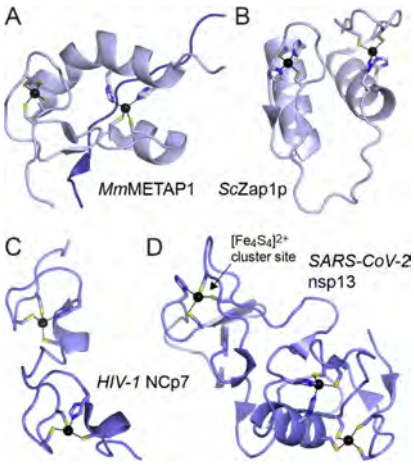

Figure 3. Zinc finger protein gallery illustrating the structural diversity of coordinatively saturated, approximately tetrahedral Zn^{II} complexes involved in protein−protein and protein-nucleic acid interactions. A) Cross-brace-like (ring-finger-like) double zinc-finger domain of murine METAP1 (7SEK);[56] B) Zinc-sensing site of the yeast Zap1p, illustrating a tandem array of canonical Cys_2-His_2 sites (1ZW8);[40] C) Tandem array of the two canonical CCHC retroviral-type zinc-fingers (1AAF);[57] D) SARS-CoV-2 nsp13 ring finger domain superficially related to the METAP1 domain, harboring a third CCHC Zn^{II} binding domain that is known to coordinate a [4Fe-4S] cluster in solution (6ZSL).[58]

amino acid, selenocysteine, with the selenoproteome playing important roles in both bacteria and eukaryotes.[34,35]

2.1.2. Structural Metal Sites. A structural metal ion stabilizes the protein fold and might be considered the inorganic analog of a long-lived disulfide bond that is found in proteins that reside in, or transit the endoplasmic reticulum in eukaryotic cells, and fulfills its function in the more oxidizing environment of the extracellular space. Since the reducing potential of the cytoplasm of a bacterial cell and the cytosolic compartment of a plant cell or a eukaryotic cell often precludes the widespread formation of thermodynamically stable disulfide bonds (see below), a metal ion like Zn^{II}, which is stable in the 2^+ oxidation state and refractory to oxidation−reduction chemistry, can perform such a function. Structural Zn^{II} coordination sites typically adopt tetrahedral coordination geometries as classically observed in zinc finger (ZF) proteins or domains (Figure 3A). ZF domains typically incorporate cysteine (Cys) thiolate coordination but can also harbor histidine (His) imidazole and mono- or bidentate carboxylate donors from aspartate (Asp) and glutamate (Glu) in these sites. These structural ZF sites are coordinatively saturated, i.e., they lack a solvent-accessible or "open" coordination site and are thought to be kinetically and/or thermodynamically stable, exhibiting very slow off rates.[36,37] A structural Zn^{II} atom nucleates folding around four metal−liganding residues that are often closely spaced in the primary structure, which then induces the folding of a subdomain of a protein, organizing a surface that promotes protein−protein or protein-nucleic acid (DNA or RNA) interactions. In the case of a ZF, these are "mini-folds" that lack a conventional hydrophobic core, and thus do not stably fold in the absence of metal−ligand bonds. Indeed, ZF proteins adopt to a wide diversity of folds that differ in the type and arrangement of metal ligands in the primary structure, e.g., CCHH, CCCH and CCHC, respectively, suggesting strongly divergent evolutionary solutions to a common protein folding problem (Figure 3A-D).

Canonical Cys_2His_2 (CCHH) ZF domains that adopt a $\beta\beta\alpha$ structure are nearly always tandemly repeated, "beads on a string" proteins (Figure 3B) are often nuclear and typically function by binding to a specific DNA sequence in the promoter regions of regulated genes, and thus are transcription factors in eukaryotes and all multicellular organisms. The presence of hundreds of Cys_2-His_2 ZF proteins in eukaryotes is the major reason why 9−10% of a typical eukaryotic proteome consists of zinc metalloproteins, while this fraction tends to be only 5−6% in bacteria.[36] It should be emphasized that the extent to which the structural integrity of these ZF sites, as major contributors to the zinc metalloproteome, is dictated by the cellular zinc bioavailability is unknown and remains an exciting and largely unresolved area of study.[38] It is known, however, that the major zinc-sensing transcription factors in eukaryotic cells, exemplified by vertebrate MTF-1 and Zap1p in *Saccharomyces cerevisiae* (Figure 3B) employ one or more ZF motifs as "sensors" of cellular zinc status, which results in the regulation of transcription of genes that encode enzymes that re-establish zinc homeostasis.[37,39,40]

The thermodynamic stability of structural ZF sites should also not be taken to suggest that they are unreactive. In fact, recent work reveals that the Cys residues in a canonical RNA-binding CCCH ZF protein, tristetraprolin (TTP) involved in regulating inflammation, are subject to persulfidation by hydrogen sulfide (H_2S) and molecular oxygen, which may involve the intermediacy of hydrogen disulfide radical anion and superoxide anion, followed by disulfide bond formation and zinc release.[41] A cysteine within a CCHH zinc-finger structure is also known to react with the signaling molecule, nitric oxide (NO•), in a global regulatory response to a nitric oxide burst as part of the plant immune response to infection.[42] These findings follow on many years of work to develop electrophilic molecules, notably aromatic thioesters, that target the Cys residues in one of the two retroviral nucleocapsid protein ZF domains of the Gag polyprotein (Figure 3C), mediating zinc release or "zinc ejection", as a promising antiretroviral strategy.[43−46] The extent to which this oxidative chemistry is regulatory in cells during the course of normal cellular metabolism remains to be explored but

https://doi.org/10.1021/acs.chemrev.4c00264
Chem. Rev. 2024, 124, 13574−13659

may be a means to connect the redox stress response to fluxes in cellular zinc that result from this oxidative chemistry.

Indeed, there is emerging evidence in support of the idea that what were once assumed to be "structural" zinc sites may be far richer in bioinorganic redox chemistry than previously imagined. The presence of four closely clustered metal−liganding Cys and/or His residues as in canonical ZF proteins, are often simply assumed to bind Zn^{II} often with little empirical evidence.[47] There is now significant support to suggest that a subset of these ZF sites do not bind Zn^{II} at all, but instead coordinate either an [2Fe-2S] or a [4Fe-4S] cluster, some of which are redox-active.[48−50] An important early example of this was found in Cleavage and Polyadenylation Specificity Factor 30 (CPSF30), which plays a role in mRNA pre-mRNA processing.[47,51] This is consistent with the general finding that some DNA and RNA metabolizing modifying enzymes incorporate an Fe−S cluster, which modulates enzyme activity, and may well mediate long-range electron transport through the nucleic acid to regulate and coordinate enzyme activity during DNA replication and repair processes.[48,52,53] Indeed, in recent work, at least two viral proteins encoded by severe acute respiratory syndrome coronavirus 2 (SARS-CoV-2), including the RNA-dependent RNA polymerase (nonstructural protein 12, nsp12) as well as the nsp13 helicase (Figure 3D), each harbor a redox-active and labile [4Fe-4S] cluster, that are potential targets for antiviral therapies.[54,55]

2.1.3. Regulatory Metal Sites. Structural metal sites, like some of the Fe−S cluster sites described above, can also play regulatory roles in the absence of metal oxidation or reduction. These sites are either allosteric, which function "at a distance" from the active site, or "competitive" with the binding of substrate or the catalytic chemistry in the active site. Identification of these regulatory sites relies on some functional discovery followed by biochemistry, and thus are typically much more difficult to identify in a complex proteome. A paradigm example of reversible modulation of enzyme activity by transition metals is the inhibition of protein tyrosine phosphatase 1B (PTP1B) by Zn^{II},[59,60] which contrasts sharply with that of Mg^{II}, which is an activator.[61] PTP1B is important target for the development of a potential therapy for obesity and insulin resistance. Both Zn^{II} and Mg^{II} compete for the same site in the active site region of the enzyme, which becomes available only following formation of the phosphorylated Cys intermediate (Figure 4A). Zn^{II} negatively impacts activation of a metal-coordinated water molecule that is required for hydrolysis of the phosphothioester linkage.[61] Zn^{II} binds to PTP1B with a dissociation equilibrium constant (K_d) in the low pM range, consistent with its physiological impact on this enzyme in cells (see Section 2.2).

In other cases, the regulatory Zn^{II} coordination site may be at or very near the protein surface where it functions at a distance as an allosteric modulator of protein function. These sites are formally analogous to the metalloregulatory metal sites in metallosensors (Section 3), except that they reversibly control enzyme activity. Regulatory sites like these are often difficult to identify *a priori*, and are often discovered using crystallographic methods and working backward using reverse genetic approaches, toward establishing functional significance, or through the use of coevolution- or structure-based metal site prediction algorithms, e.g., MetalNet,[62] Metal3D[63] and related approaches,[64−67] the predictions of which can be tested experimentally using biochemical methods. These approaches often rely on the conservation of the metal−ligand residues in the primary structure in a group of closely related enzymes using pattern-matching, and recent computational methods have been used to distinguish adventitious from physiologically relevant sites worthy of detailed study[65] as well as distinguish catalytic from noncatalytic structural sites[66] have recently been reported. The use of neural networks and machine learning approaches promises to impact the precision and accuracy of these predictions, which will require experimental validation using metalloproteomics approaches.[68]

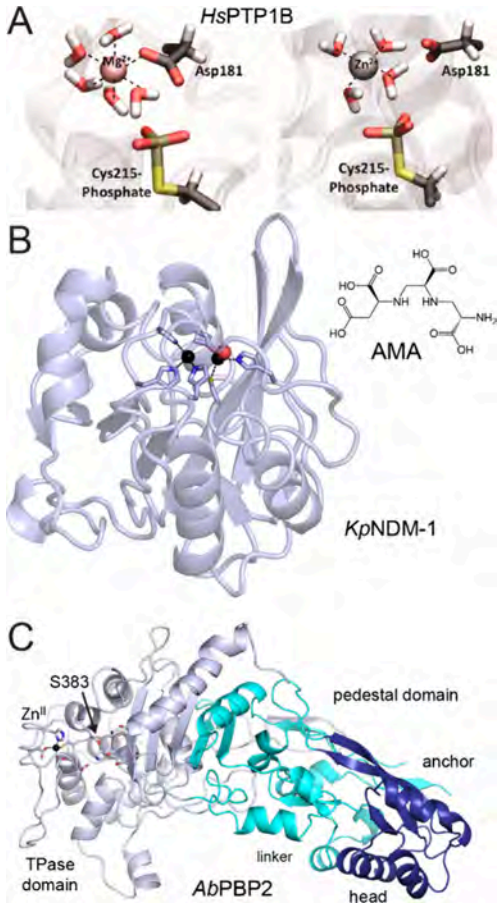

Figure 4. A) Active site of human PTP1B in a representative snapshot at the end of QM/MM MD simulations, bound to Mg^{II} (*left*) and Zn^{II} (right). Residues C215-phosphate, D181, and water molecules coordinating the metal are shown as sticks. B) Ribbon diagram of *Klebsiella pneumoniae* NDM-1, with Zn^{II} ions shown as black spheres, bound water shown as a red sphere, and metal-binding side chains shown as sticks (*left*). Chemical structure of aspergillomarasmine A (AMA, *right*), and inhibitor metallo-β-lactamases. C) Ribbon diagram of *Ab*PBP2, with the TPase domain colored light blue, linker region cyan, and head region dark blue. Conserved active site residues and metal binding residues are shown as sticks including C384, with the active site serine, S383, labeled. Panel A was reprinted with permission from *J. Am. Chem. Soc.* **2018**, 140, 4446−4454. Copyright 2018, American Chemical Society.

2.1.3.1. Regulatory Metal Sites and Nutritional Immunity. One recent example of the discovery of a new regulatory metal site using crystallographic approaches is in a periplasmic, high molecular weight (HMW) penicillin-binding protein, PBP2, from bacterial nosocomial pathogen, *Acinetobacter baumannii*.[69] PBP2 is a transpeptidase that is an important component of the "elongasome" that maintains the rod-shaped morphology of the bacterium and a major target for the β-lactam antibiotics from the carbapenem family of antibiotics. These are the same

https://doi.org/10.1021/acs.chemrev.4c00264
Chem. Rev. 2024, 124, 13574−13659

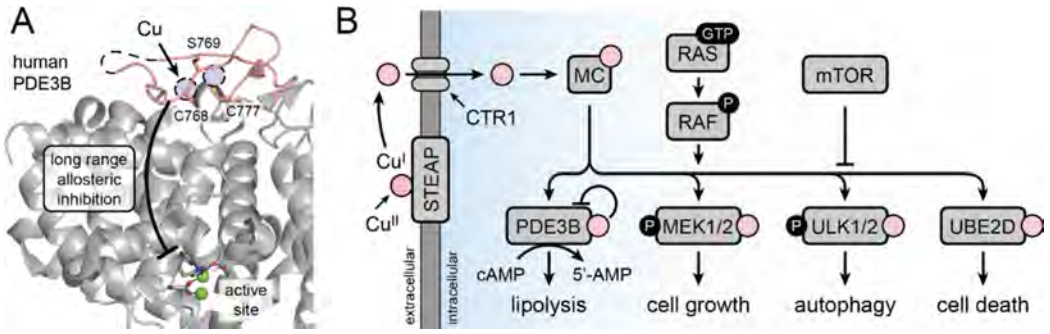

Figure 5. Copper metalloallostery in vertebrate systems. A) Ribbon diagram of the structure of human PDE3B with the active site a strong candidate Cu binding site that negatively modulates the activity of the enzyme. B) Excess cellular Cu (pink sphere) impacts the specific activities of a number of signal transduction pathways in the various cells. STEAP is a metalloreductase that reduces Cu^{II} to Cu^{I},[97] which is transported down a concentration gradient, picked up by a metallochaperone (MC) and trafficked to various signaling proteins, with distinct biological outcomes.[81,94]

antibiotics that are inactivated by bacterially encoded β-lactamases, including the metallo-β-lactamases (MBLs) that require Zn^{II} for their hydrolytic activity (Figure 4B). Nutrient zinc starvation is a key feature of "nutritional immunity", a potent antimicrobial strategy employed by the infected host to keep pathogens from causing infections beyond the initial site of colonization.[10,70−72] The crystallographic structure of *Ab*PBP2 revealed an unexpected and conserved tetrahedral SNO_2 Zn^{II} coordination complex that is just 10 Å from the catalytic serine (Figure 4C). Mutagenesis of any of the metal ligands, notably the single thiolate ligand, C384 (Figure 4C) disrupts metal binding, and induces a thermal destabilization on par with metal removal by EDTA. More importantly, mutant *A. baumannii* strains harboring one of these mutations which are expressed at wild-type-like levels are far more susceptible to growth inhibition by two β-lactam antibiotics that do not specifically target PBP2. In addition, all four missense mutations lead to a cell-widened, spherical morphology, identical to that of the Δ*pbp2* strain. These compelling biological data, coupled with the conservation of this zinc-binding motif in PBP2s from many β- and γ-classes of Proteobacteria, suggest that host-derived metal restriction predisposes *A. baumannii* strains to antibiotic susceptibility. Zn^{II} limitation also induces the expression of a low-zinc "paralog" of a housekeeping *D,D*-carboxypeptidase, ZrlA, that enhances resistance to cell wall envelope stress under the same conditions.[73] Left for future work is the mechanism by which Zn^{II} binding to this site in *Ab*PBP2 is truly reversible and sensitive to changes in bioavailable metal in the bacterial periplasm, and how Zn^{II} binding protects PBP2 from antibiotic acylation.

Nonetheless, studies like these illustrate the considerable complexity of "nutritional immunity" as an important weapon in the arsenal of host defenses used to combat bacterial invaders. Further, they highlight cell wall homeostasis as an important target of zinc-limitation in these and likely other ways. Indeed, recent work reveals that MBLs, in particular those derived from subclass B1 from carbapenem-resistant organisms, including the New Delhi MBL (NDM), Verona integrin-encoded MBL (VIM), and imipenemase (IMP)-type enzymes, are a potential target of host-mediated metal restriction in the periplasm, given a binuclear Zn^{II} active site, where the more weakly bound Zn_2 metal appears more susceptible to chelation by metal chelators including a secondary metabolite of fungal origin, aspergillomarasmine A (AMA), an aminopoly(carboxylic acid) with K_d^{Zn} of ≈0.2 nM (Figure 4B).[74,75] While NDM-1 β-lactamase is susceptible to inhibition by AMA, a more recently appearing allelic variant, NDM-6, is not, which is at least partly explained by ≈20-fold higher zinc affinity relative to NDM-1. Indeed, the evolution of increased zinc-affinity appears rather well-established in NDM-type MBLs, of which more than 20 new allelic variants have arisen within the past decade, all with increased zinc affinity.[76,77] Although Zn^{II}-removal increases the rate of protein degradation in bacterial cells in an MBL-specific way,[77] recent data for NDMs suggest that this picture is far more complex, with recently arising mutations linked to an enhanced kinetic and conformational stability and therefore increased lifetime of the β-lactamase in the periplasm, i.e., the proteostasis network (Figure 1), with Zn^{II} affinity just one, albeit important aspect of this evolution.[78]

2.1.3.2. Allosteric Copper Sites: Lipid metabolism, Cancer and Beyond. Copper homeostasis is now known to have a profound impact on many aspects of mammalian physiology and human disease, beyond serving as a catalytic cofactor in cuproenzymes.[79−81] For example, intracellular copper status, altered either pharmacologically or genetically in cultured vertebrate cells, was shown to be an important regulator of lipolysis, the catabolism of fats. The evidence suggests that Cu^{I} binding allosterically inhibits the activity of a cyclic-AMP-degrading phosphodiesterase, PDE3B, by coordinating a pair of Cys residues found only in the PDE3 subtype of phosphodiesterases (Figure 5A, *left*; Figure 5B).[81] This observation, building on previous work in cancer biology, has led to the general concept of "copper signaling"[80] and "metalloallostery"[82] where variations in intracellular or organellar Cu bioavailability, mediated by Cu-specific transporters that transport copper across membranes,[83] regulates enzyme activity and signal transduction via as yet largely unknown mechanisms.

This PDE3B-specific model of Cu-dependent regulation of enzyme activity in lipolysis may well be general, as Cu is known to regulate the activity of a number of protein kinases involved in various cell signaling pathways (Figure 5A).[84] These include pathways that are upregulated as part of the host immune response against bacterial infection,[85] and most prominently in cancer cells, consistent with the higher cellular demand of cancer cells for this micronutrient.[86] Enzymes that appear to be regulated by direct binding of Cu including mitogen-activated protein kinase kinase 1/2 (MEK1/2), which is required for downstream phosphorylation and activation of ERK1/2 and thus potentiation of the mitogen-activated protein (MAP) kinase pathway indeed, the MAP kinase pathway is a significant repository of oncogenic mutations and a long-standing target of cancer therapies (Figure 5B).[87,88] Subsequent studies suggested

https://doi.org/10.1021/acs.chemrev.4c00264
Chem. Rev. 2024, 124, 13574−13659

that the copper chaperone for superoxide dismutase (CCS) is responsible for chaperoning Cu to MEK1/2,[89] which would be required given the extremely limited bioavailability of Cu^{I} in cells (Section 2.2).[90] The other major Cu chaperone in mammalian cells, ATOX1, may also impact MAP kinase signaling pathway,[91,92] although the mechanistic details are not in. Finally, Cu is known to function as a positive allosteric modulator of autophagy in cancer biology, again via direct binding to a specific kinase in the P13K phosphoinositide 3-kinases)/AKT signaling pathway.[93−95] The extent to which cuprous vs cupric copper is the signaling moiety in these processes is an important mechanistic question not yet fully resolved. The recent development of a robust Cu^{II}-specific small molecule sensor strongly suggests that Cu^{II}, rather than Cu^{I}, mediates at least some of these Cu-dependent signaling processes described to date.[96] These processes are collectively coined *cuproplasia*, defined as regulated copper-dependent cell growth and proliferation.[94]

2.1.4. Catalytic Metal Sites. Catalytic metal sites are defined as those metal coordination sites that bind and activate substrates directly via coordinate covalent bonds. Catalytic metal sites are structurally diverse and encompass a remarkable breadth of catalytic power, as members of all seven major classes of enzymes as categorized by the Enzyme Commission (EC): oxidoreductases (EC 1), transferases (EC 2), hydrolases (EC 3), lyases (EC 4), isomerases (EC 5), ligases (EC 6), and translocases (EC 7).[66,98] Catalytic metal ions derive their catalytic power by the precise arrangement of donor atoms that define structure and geometry of the first and more distal coordination shells around the metal. Metals can be bound to proteins via a specialized and unique arrangement of coordination bonds, integrated into a metallocofactor, either one that is purely inorganic, e.g., in Fe−S clusters, as part of an organic chelate, e.g., heme or more generally Fe-porphyrin complexes and molybdopterin (Mo),[23] or as a more exotic organometallic cofactor, featuring metal−carbon bonds, and including cobalamin (Co)[99] and nickel pyridinium-3,5-dithiocarboxylic acid mononucleotide (Ni) and others.[100]

Comprehensive metalloprotein databases, more recently advanced by machine learning approaches,[20] and recent monographs on this topic reveal a number of general functional features.[22] Fe enzymes are more abundant in prokaryotes than eukaryotes, and generally come in three flavors: nonheme Fe enzymes, Fe−S cluster-containing enzymes and heme enzymes.[101] Fe enzymes play roles in electron transport and oxygen activation chemistry and many other types of oxidation−reduction (redox) chemistries. Zn^{II} enzymes are nature's preferred hydrolytic catalyst and are incorporated into more than 100 distinct structural superfamilies. This unique feature of Zn^{II} metalloenzymes has motivated the deployment of *de novo* protein design to create highly efficient novel Zn^{II} catalysts in a diversity of biomolecular scaffolds[102,103] in a way that extends far beyond zinc metalloenzymes themselves.[104,105] Fe and Zn are the most cell-abundant transition metals in most cells, rising to tenths of millimolar or higher, when simple estimates for total bacterial cell volumes are used,[106] and are required for virtually all life, with some exceptions.[107] Mg^{II}, a main group element and hard Lewis acid, is present at even higher concentrations than Zn^{II} and Fe, generally in the single-digit millimolar range, and is an important cofactor of cellular energy metabolism. Mg^{II} is present in chlorophyll and also in enzymes, where it is deployed by nucleotide (ATP, GTP) binding proteins to facilitate nucleotide hydrolysis, e.g., in ATPases and phosphatases or transesterification reactions.[108]

Cu and Mn are typically approximately 10-fold lower than Zn and Fe, with cell-associated Ni and Co about 10-fold lower still.[109,110] There are bacteria, however, exemplified by the radiation-resistant bacterium *Deinococcus radiodurans*, that possess Mn quotas on par with those of Fe, in contrast with the general trend indicated above. These have been termed Mn-centric bacteria.[110] Cu is a redox-active metal that cycles between oxidized cupric Cu^{II} and cuprous Cu^{I} oxidation states, with Cu^{I} forming low coordination complexes that generally function in oxygen activation chemistry.[111,112] Mn^{II} plays many diverse roles in biology,[113] including that of Lewis acid in transformations that do not require a change in oxidation state, e.g., in phosphatases, arginase and a number of metabolic enzymes, but also in other contexts where Mn^{III} and higher oxidation states are reached, including Mn-superoxide dismutase, some ribonucleotide reductases, and the oxygen evolving complex in plants. Ni and Co play far more specialized roles in biology. Although fewer than ten Ni-metalloenzymes are known, they punch far above their weight by producing gases in bacteria, algae and plants that drive the global carbon, nitrogen and oxygen cycles.[114] Ni^{II}, like Zn^{II} and Mn^{II}, can perform Lewis acid chemistry, exemplified by two hydrolytic enzymes, the dinuclear Ni^{II} enzyme urease (Section 5.1.2) and the mononuclear glyoxylase-I, but also functions as a cofactor in [NiFe]-hydrogenase and Ni-superoxide dismutase, among others, where both the Ni^{I} and Ni^{III} oxidation states must be accessible.[114,115] Co, on the other hand, functions prominently in the context of two enzymes dependent on the organometallic cofactor vitamin B_{12}, or cobalamin, found in all kingdoms of life.[99] These are methionine synthase and methylmalonyl-CoA mutase (MCM) and closely related CoA mutases which catalyze a methyl transfer and an isomerization reaction, respectively, where the Co center cycles through Co^{I} and Co^{III} oxidation states (Section 5.1.3).

2.2. The Metallostasis Set-Point Model

2.2.1. Overview. It is well established that the total concentration of metal that can be measured by inductively coupled plasma-mass spectrometry (ICP-MS) in a cell lysate or in a tissue, and often expressed in units of concentration (mol L^{-1}) greatly exceeds, by many orders of magnitude, the metal concentration that is "bioavailable" (see below).[106,109,116,117] The implication of this is that cells and tissues possess an extraordinary overcapacity to chelate metal ions; however, this says nothing about the extent to which these bound metals contribute to a buffered "pool", which for Zn^{II} and Cu^{II}/Cu^{I} that form high affinity coordination complexes with proteins. may well be small. Only those metal sites that rapidly equilibrate with this pool will be sensitive to small perturbations in bioavailable metal concentration that result from cellular metal toxicity or metal restriction.[118] A collection of metallosensors (Section 3) are widely accepted to surveil this pool and are thus "tuned" to effect a regulatory response, over some 12 orders of magnitude of metal concentration;[119] these metal sensing sites are generally near the protein surface, characterized by fast metal association rates and dissociation rates that can be modulated by one or more components of the cytoplasmic "buffer".[120,121] The chemical composition of this buffered pool is not known, although a handful of spectroscopic and analytical methods[122,123] have been developed to explore the coordination chemistry of this pool, or alternatively, identify those major

https://doi.org/10.1021/acs.chemrev.4c00264
Chem. Rev. 2024, 124, 13574−13659

buffering species in cells. Histidine is clearly implicated as an important component of this buffering pool.[119,124,125] We view this pool as coordinatively unsaturated, readily exchangeable,[85] "mobile" or "labile", which we collectively term "*bioavailable*". We note that metals in these pools are not technically "free", which is rigorously and correctly defined only as a fully solvated ion; the term "bioavailable" as proxy for *free* avoids the obvious confusion of "less than one *free* metal atom per cell"[90,109,126] which obfuscates, rather than clarifies.

2.2.2. The Set-Point Model. A metallosensor is a single-component signal transduction system, in that inducer "sensing" and "regulation" of gene expression occurs within the same polypeptide chain. This contrasts with bacterial two-component systems (TCS) where sensing and regulation require two proteins and a post-translational modification as the signaling moiety. In a single-component system, cognate metal binding or some other modification "signals" to the DNA binding domain of metallosensor via some intramolecular connection, classically defined as an *allosteric* connection.[18,127,128] Allostery couples metal binding to DNA binding of transcriptional activation in metallosensors in distinct ways depending mainly upon the structural family to which they belong (Section 3). Metallosensors elicit a transcriptional outcome in response to a range of intracellular metal concentrations over which their cognate metals fluctuate in cells.[119,129] These metalloregulatory proteins function as metal-dependent derepressors,[130,131] metal-dependent corepressors,[132−134] and metal-dependent activators,[135] of transcription (Figure 6A). Coordination of the cognate metal thus drives transcriptional derepression (an ON switch mediated by allosteric inhibition of DNA operator binding by metal) (Figure 6A, *top*), transcriptional corepression (an OFF switch mediated by allosteric activation of DNA binding) of downstream genes (Figure 6A, *middle*), or transcriptional activation (an ON switch mediated by metal-dependent conformational changes in the bound DNA, converting a weak promotor to a strong promoter) (Figure 6A, *bottom*).

Quantitative biochemical investigations of the metallosensor-DNA and metallosensor-metal binding equilibria allow one to determine the affinity and selectivity that a particular regulator has for its cognate inducer and the DNA operator. For a regulatory protein with two distinct ligands (metal, DNA), these equilibria can be cast as a coupled or "linked" equilibrium with four states from the perspective of the unliganded metallosensor (Figure 6B). This thermodynamic framework allows the quantitative determination of this allosteric connection, embodied in the allosteric coupling free energy, ΔG_c.[18,138] The magnitude and sign of ΔG_c quantifies the extent to which metal binding impacts DNA binding, either negatively ($+\Delta G_c$; Figure 6A, *top*) or positively ($-\Delta G_c$, Figure 6A, *middle*). This framework is particularly useful, for example, in the search for repressor mutants that *uncouple* metal and DNA binding to variable degrees ($\Delta\Delta G_c$), thus providing fundamental insights into the *mechanism* of allosteric connectivity.[139−141] Although this thermodynamic framework applies directly to transcriptional repressors,[18] it can also be applied to allosteric activation of transcription where inducer recognition does not necessarily affect DNA binding affinity but instead impacts RNA polymerase recruitment and/or DNA promoter architecture.[142,143] Here, K_c^t is simply substituted by k_c^t, the ratio of sensor-dependent transcription initiation rates in the presence and absence of cognate metal (Figure 6B).

The currently accepted set-point model that incorporates this thermodynamic framework is that cells effectively buffer

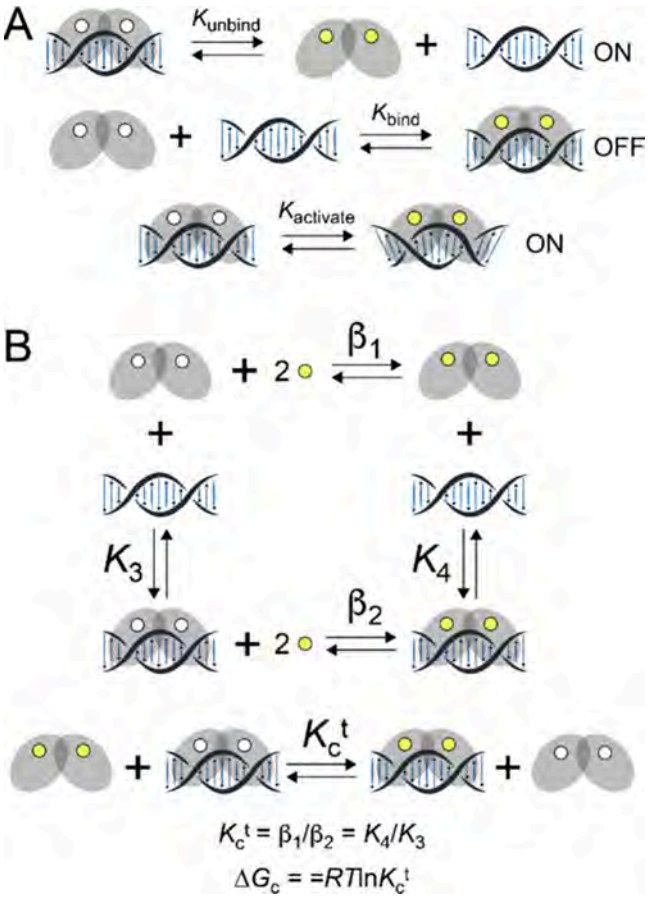

Figure 6. Metallostasis set-point model.[121,136,137] A) Schematic renderings of the three allosteric mechanisms used by metallosensors (gray) described here (Section 3) and their biological output (expression of the metallosensor regulon; ON or OFF). K_i (K_{unbind}, K_{bind}, and $K_{activate}$) are indicated. The set-point for each sensor, K_d^S is the metal concentration at which these $K_i = 1$ ($\Delta G = 0$). B) Generic thermodynamic cycle where β_1 and β_2 are overall Zn^{II} binding affinities for the apoprotein dimer and protein−DNA complex. The allosteric coupling free energy, ΔG_c, describes the overall ligand exchange reaction shown.[138]

transition metal concentration in a bioavailable pool so as to ensure that a particular metalloprotein can capture its cognate metal under virtually any cellular condition.[146] This buffering capacity goes as the inverse order of the stability complexes formed a series of divalent metals, known as the Irving-Williams series (Figure 7),[144] and is collectively maintained by the cellular repertoire of metallosensors, each of which is "tuned" to a set-point, K_d^S, allowing each to modulate transcription of their regulons over a relatively narrow range of metal concentration (Figure 8A).[119,121] K_d^S is the cognate metal concentration in cells at which the equilibrium constants for each of the three equilibria shown (Figure 6A, K_i) are equal to 1.0, and defines the point at which fractional expression of gene expression is 0.5 (Figure 8A). Once all parameters derived from the thermodynamic cycle shown (Figure 6B) as well as the impact of the cellular buffer and any change in the number of sensor molecules per cell (in high and in low metal) for each metallosensor are considered, response curves centered on K_d^S that relate fractional transcription output to the intracellular availability of the cognate metal are obtained (Figure 8A).[121]

Early work showed that the equilibrium affinity of a zinc efflux regulator for Zn^{II}, $K_{d,Zn}$, was $\approx 10^{-11}$ M.[147] This implies a

https://doi.org/10.1021/acs.chemrev.4c00264
Chem. Rev. 2024, 124, 13574−13659

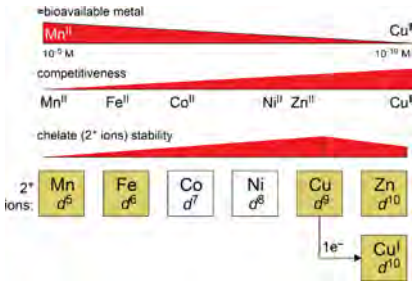

Figure 7. Schematic rendering of the Irving-Williams series of stability constants for 2^+ metal ions of the first-row late 3*d*-block metals,[144,145] with the extent to which each is competitive with other metals (*middle*), which is inversely proportional to their general bioavailability is cells (*top*).

transcriptional response that is tuned to change in bioavailable or weakly chelated [Zn] of 10^{-12} M to 10^{-10} M (corresponding to one log on either side of K_d^S which covers 10−90% of a canonical transcriptional response) (Figure 8A).[116,129] In contrast, Fe^{II} is buffered to $\geq 10^{-6}$ M; as a result, an Fe-containing metalloprotein that binds Fe^{II} with $K_{d,Fe}$ of 10^{-7} M and Zn^{II} with $K_{d,Zn}$ of 10^{-10} M^{-1}, for example, will not be mismetalated with Zn^{II} in the cell unless free Zn^{II} is allowed to rise far above its buffered range ($>10^{-11}$ M) in this example (Figure 8B).[148] This is the central feature of the set-point model of cellular metallostasis since the relationship between the metal dissociation constant and the bioavailable metal concentration defines the sign on the conditional free energy of metal loading; a + $\Delta\Delta G$ will be unfavorable and a − $\Delta\Delta G$ will be favorable (Figure 8B). This, in turn, is thought to dictate the metalation status of the metalloproteome.[121] This is so because metal sensor proteins minimally (in nearly all cases) regulate the expression of metal transporters that uptake or efflux a specific metal into or from the cytoplasm, respectively. These transporters are thought to function to quickly restore metallostasis in the case of an acute response, or maintain metallostasis in the event of chronic metal limitation or toxicity.[149]

2.2.2.1. Limitations of the Set-Point Model. A major strength of the metallostasis set-point model is its conceptual simplicity, which allows robust, quantitative predictions of the extent to which a single metalloprotein will be metalated with a *spectrum* of metals in a cell.[148] This has led to the development of the web-based metalation calculator tool, which allows a user to input known metal binding equilibrium constants for their protein of interest and calculates the degree to which that protein will metalated with a particular metal in an "idealized cytoplasm."[146,152] The lack of an unbiased validation of the predictions of this model, however, remains both a significant limitation and a considerable analytical challenge, for two reasons. The first is that experimental measurements of the concentrations of the bioavailable pool for these transition metals (Figure 8B) remain incomplete, in particular for the "idealized" cytoplasm of a bacterial cell on which the calculator was created. The only measurement of the concentration of exchangeable Zn^{II} in *E. coli* grown on a minimal growth medium using a carbonic anhydrase-based sensor is ≈20 pM, which is, gratifyingly, just inside the range predicted by the model (Figure 8A). Significant progress continues to be made here, with the development of dynamically highly responsive ratiometric fluorescent protein-based FRET biosensors optimized for eukaryotic cells and organelles,[153] alongside more recent

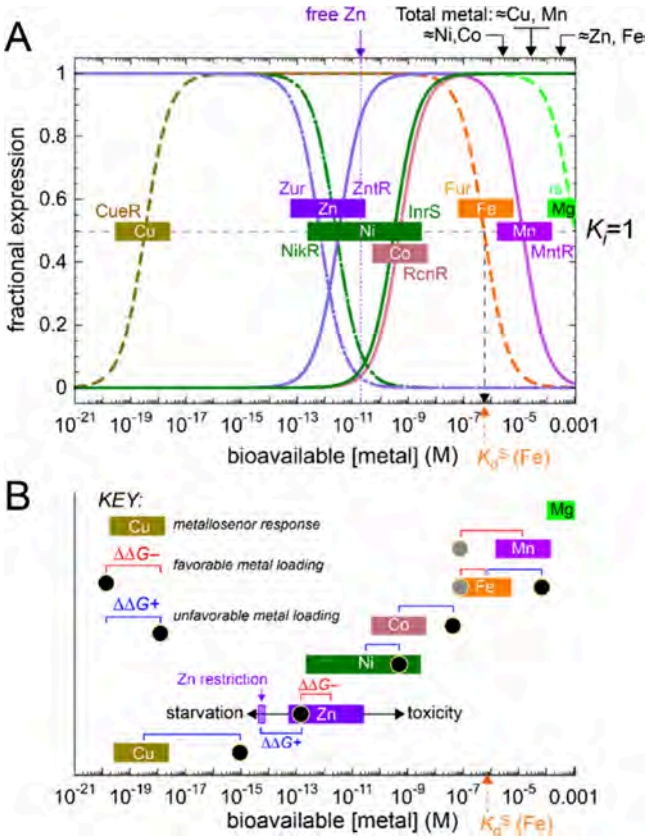

Figure 8. Metallostasis set-point model.[121,136,137] A) A plot of the fractional responsiveness (0−1; 0.5 is where K_i = 1, from Figure 6A) of each of the metallosensor proteins shown in an idealized bacterial (*Salmonella*) cytoplasm based on their experimentally determined set-points.[121,137] These set-points, K_d^S, quantitatively integrate negative or positive allosteric linkage of metal binding to DNA binding (Figure 6B)[18] as well as changes in sensor concentration with metal added to cells. Efflux regulation changes the expression of the regulated genes from 0−1 (ON), via transcriptional derepression (InrS, RcnR) or activation of transcription (CueR, ZntR) while uptake regulators induce a change in gene expression from 1−0 (OFF) (Zur, NikR, Fur, MntR and the Mg^{II}-sensing riboswitch).[150] The predicted range of bioavailable metal under unstressed conditions is indicated by the filled bar and is color-coded for each metal, and spans a fractional change in gene expression from 0.1−0.9 for a single sensor, or from the combined action of a 0.1 response for the uptake repressor and a 0.9 response for the efflux sensor. The total cell-associated metal and one experimental measurement of the exchangeable Zn (free Zn) are indicated above the plot.[151] B) The midpoint of a metallosensor response range (from Figure 6A) is proposed to define the free energy of metal binding to the buffering species, ΔG^{buf}, which is $\Delta G^{buf} = RT\ln K_d^S$ to which each sensor is tuned (or represents the average K_d^S for an uptake and efflux sensor pair). The metalation status of two hypothetical proteins (P1, black circle; P2, gray circle) are overlaid onto this thermodynamic construct. The various K_d for metal binding to P1, K_d^{P1} are indicated, where $\Delta G^{P1} = RT\ln K_d^{P1}$. The relative magnitude of the change in free energy upon metalation, $\Delta\Delta G = \Delta G^{P1} - \Delta G^{buf}$ thus defines the extent to which P1 will be bound (at equilibrium) to each metal in this idealized cytoplasm. In the hypothetical case of a zinc-specific metalloprotein, P1, only the $\Delta\Delta G$ of metalation by Zn^{II} is favorable (−$\Delta\Delta G$), despite the fact that Cu^I binds ≈10^4-fold more tightly. In the case of P2, metalation by Mn^{II} will be preferred over Fe^{II} despite the fact that each binds with a similar dissociation constants, K_d^{P2}. Note that under conditions of Zn^{II} restriction (*lower left*); purple arrow), the buffered pool may fall precipitously, which makes the free energy of metalation, $\Delta\Delta G$, positive for P1, leading to undermetalation of P1 and perhaps other components of the metalloproteome. Metal toxicity, on the other hand, moves the

https://doi.org/10.1021/acs.chemrev.4c00264
Chem. Rev. 2024, 124, 13574−13659

Figure 8. continued

bioavailable pool dramatically to the right (to higher bioavailable [metal]), which makes metalation of noncognate sites by more strongly binding metals, notably Zn^{II} and Cu^{I}, favorable ($-\Delta\Delta G$), particularly when these concentrations exceed the capacity of the buffering molecules, thus approaching total metal (*upper right*).

biosensor designs that originate with other fluorescent modalities that do not require molecular oxygen for maturation.[154]

A second analytical challenge is that validation of the set-point model requires an independent determination of holistic metal occupancy of a protein(s) to compare with prediction. Two-dimensional liquid chromatography inductively coupled plasma mass spectrometry (2D-LC-ICP-MS) and polyacrylamide gel electrophoresis laser ablation (GE-LS).[155,156] ICP-MS approaches on cell lysates prepared under nondenaturing conditions remain the most popular ways to do this.[107,157−159] Both approaches, however, require that metal complexes, even those bound to weakly bound metals, not dissociate during workup.[160] 2D LC-ICP-MS holds considerable promise for biologically required metals discussed here, potentially capable of detecting a change in metalation status as a function of growth conditions, for example, but appears to be readily applied to a quantitative analysis of only the most abundant protein-metal complexes of high thermodynamic (Cu^{I}, Zn^{II}) or kinetic stability.[157] On the one hand, a considerable strength of the 2D LC-ICP-MS workflow is to identify the (mis)metalation targets of metallodrugs containing abiological metals, which benefits from a very low signal background, as long as care is taken to stabilize what might be labile metallodrug−protein adducts.[160,161]

2.2.3. Mismetalation of Proteome Metal Sites. For the reasons discussed above, the cellular factors that control the metalation status of the proteome remain incompletely defined. Recent efforts based on thermodynamic principles alone have led to the concept that the relative free energies of metalation by cell-abundant metals ($\Delta\Delta G$, Figure 6B) is the primary determinant as to whether a metalloprotein is metalated with the cognate metal or one of a number of other noncognate metal ions (Section 2.2.2). Thus, cells incorporate extraordinary measures to ensure that the relative concentrations of metals are buffered in a range that allows these relative free energies to manifest themselves (Figures 6-8). Simply put, if the metal affinity of a recipient metalloprotein is in the nM range, the bioavailable metal concentrations must be in the nM range or higher in order to significantly populate that metal site, as dictated by the law of mass action (Figure 6B).

Mismetalation of a metalloprotein occurs at a point in time when capacity of the cell to buffer a noncognate metal is exceeded. This is indeed a major antimicrobial weapon the infected vertebrate host will deploy against bacteria, particularly those with intracellular lifestyles, e.g., in the phagolysosome.[162−164] Cu^{I} and Zn^{II} are often used this way given the fact that they are tight-binding metals, on the "competitive" side of the Irving-Williams series (Figure 7), and readily displace more weakly bound metals, including Fe. An important target of Cu^{I} toxicity is the Fe−S cluster biogenesis machinery,[165−167] as well as Fe−S clusters of mature enzymes, including dehydratases, where Cu^{I} displaces one or more Fe atoms on what are essentially solvent exposed clusters,[168] potentiating oxidative stress through Fenton chemistry. In addition, other work has stablished that Cu toxicity directly inhibits heme biosynthesis in the obligate human pathogen *Neisseria gonorrheae*.[169] In *Staphylococcus aureus*, Cu negatively modulates flux through the pentose phosphate pathway by direct binding to phosphoribosylpyrophosphate synthetase (Prs), which synthesizes phosphoribosyl diphosphate (PRPP), a key metabolite that is used to synthesize the purine and pyrimidine nucleobases and nicotinamide dinucleotides. Prs is generally thought to be a Mg^{II}-dependent enzyme, and the speculation is that Cu^{I} prevents Mg^{II} from binding.[170] While it is true that more weakly bound metals could in theory displace more tightly bound ones if their bioavailability becomes sufficiently high. as predicted by the relative free energies of metalation (Figure 8), examples of this kind of metal toxicity may well be rare.

Ionophores are membrane crossing channels that allow transition metals to pass, and are being developed as antimicrobial agents to induce Cu^{I} or Zn^{II} poisoning; indeed, recent work with the zinc ionophore and 8-hydroxyquinoline PBT2 reveals that a strategy of Zn^{II} intoxication may be particularly efficacious in "breaking" the resistance of *A. baumannii* to tetracycline class antibiotics, an important finding.[171] In other work long the same lines, it has recently been shown that the host actively leverages the metal promiscuity of the bacterially produced nicotianamine-like metallophore, staphylopine,[172,173] which is produced by *Staphylococcus aureus* during the response to "nutritional immunity" in an effort to capture metal from the extracellular milieu.[174] The host makes extracellular Cu^{II} bioavailable here, which is then brought into the bacterial cell as a Cu^{II}-metallophore complex, thus driving bacterial copper poisoning.[174] At least one of the targets of Cu^{I} toxicity is the glycolytic enzyme, glyceraldehyde-3-phosphate dehydrogenase,[174] which while not a metalloenzyme, has a pair conserved Cys residues in the active site that are proposed to coordinate Cu^{I}.[175] Indeed, there is abundant evidence to suggest in a wide range of the bacteria that Cu toxicity broadly impacts Zn homeostasis although the mechanisms may well vary, and perhaps to a lesser degree Mn homeostasis in a subset of organisms.[176]

There are a number of examples where bacterial Zn stress results in the mismetalation of the Mn^{II}-dependent enzymes. In *S. pneumoniae*, a Mn-centric bacterium,[110] Zn^{II} is an inhibitor of Mn^{II} uptake by the ATP-binding cassette (ABC) transporter, PsaBCA,[106] where it forms a coordination complex that is very nearly isostructural with that of Mn^{II}, but fails to transport Zn^{II} across the pneumococcal membrane, thus inducing cellular Mn^{II} starvation.[177,178] This may be a consequence of the very slow off-rate of bound Zn^{II} in this inhibited complex, relative to the more weakly bound Mn^{II} which upon engagement of the transmembrane domain readily releases Mn^{II} into the transport channel. An intracellular feature of the same Mn−Zn cross-talk is the Zn^{II}-dependent inhibition of the Mn^{II}-cofactored protein phosphatase PhpP, which functions in the regulation of cell division. Under conditions of Mn^{II} stress, this enzyme is hyperactive, leading to significantly elongated cells; under conditions of Zn^{II}-supplemented Mn^{II} limitation, PhpP is inhibited, thus leading to shorted cells, analogous to the Mg−Zn crosstalk that characterizes PTP1B (Figure 4A).[179] This work in *S. pneumoniae* suggests a regulatory model where the bioavailable Mn:Zn ratio impacts Mn^{II}-dependent metabolic activity. Indeed, this hypothesis is consistent with subsequent studies that showed that the Mn:Zn ratio impacts the activity of the Mn^{II}-dependent phosphoglucomutase, which interconverts glucose-1-phosphoate and glucose-6-phosphate, and thus modulates the biosynthesis of the polysaccharide capsule.[180]

https://doi.org/10.1021/acs.chemrev.4c00264
Chem. Rev. 2024, 124, 13574−13659

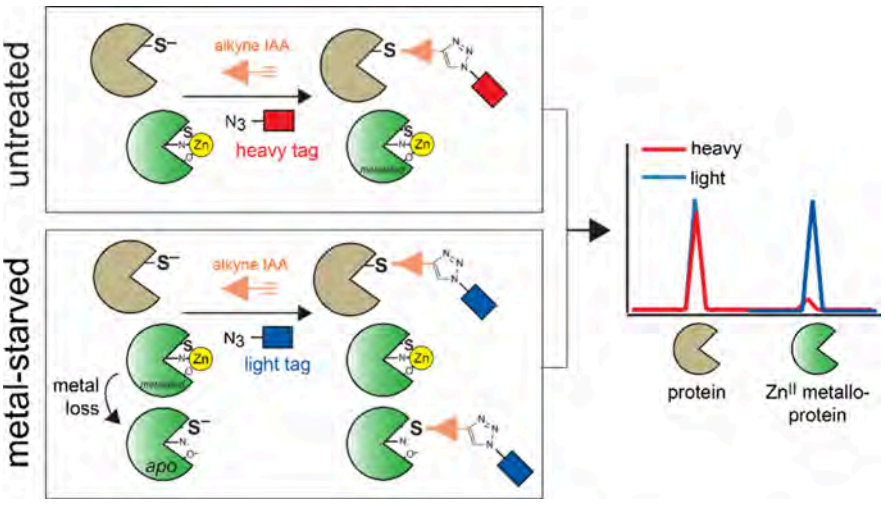

Figure 9. Global chemoproteomics strategy to probe the status of the metalloproteome under conditions of transition metal restriction.[183,184] Both proteome samples are capped with thiol-specific iodoacetamide derivative that harbors an alkyne and then subjected to Cu-catalyzed azide−alkyne cycloaddition (CuAAC) with the a "heavy" or "light" enrichment moiety as indicated. The two lysates are mixed 50:50 and subjected to a bottom-up proteomics workflow and the "heavy"/"light" ratio quantified for all Cys-containing peptides by mass spectrometry. Nonmetalloproteins with surface-accessible cysteines will be labeled to the same extent with the "heavy" and "light" probes (tan protein, right); those metalloproteins that lose the metal under conditions of metal starvation will feature more light vs heavy counts in the MS1 spectrum (green protein, right).

Recent work in *Staphylococcus aureus*, although not mismetalation *per se*, reveals that cells upregulate the expression of metal-independent paralogs (Section 4) of two obligate Mn^{II}-requiring glycolytic enzymes, phosphoglycerate mutase and fructose-1,6-biphosphate aldolase, under conditions of cellular Mn^{II}-starvation mediated by calprotectin.[5,6] In a striking illustration of mismetalation for "good", the strategic deployment of a truly cambialistic enzyme that is equally active with Mn^{II} or Fe^{II} results in metalation of a cambialistic superoxide dismutase with Fe under conditions of host-mediated Mn^{II} restriction (Section 4.3.5).[181]

2.2.4. Undermetalation of the Metalloproteome. Nutrient metal starvation is thought to result in undermetalation of some or all of the proteome. This would result if the bioavailable pool of a particular metal is insufficient to metalate all cognate metalloproteome sites quantitatively, and is of course a prediction of the set-point metallostasis model, where the free energy of (mis)metalation is positive ($+\Delta\Delta G$) (Figure 8B). The extent to which the metalloproteome is metalated, i.e., the fraction of metal sites that are occupied at any point in time, is unknown. However, robust global chemoproteomics strategies have been developed that are capable of quantifying a *change* in metal site occupancy, at least for those sites that incorporate cystine thiolate ligation. The experiment is based on the simple premise that metal coordinating thiol ligands will be protected from reaction with an electrophilic probe, and become far more reactive if the metal is lost from the coordination complex (Figure 9), and is a "metals-focused" extension of the general concept of activity-based protein profiling.[182] This workflow leverages a rich history of cysteine thiol-reactive probes, which are available in distinct isotopomers, e.g., "heavy" and "light" versions which allows implementation of an isotope dilution-based strategy to detect a change in reactivity for all peptides in a proteome in a single experiment; when coupled to a parallel experiment that quantifies a change in peptide abundance, a normalized change in cysteine reactivity to be measured.

This experiment has been used to track the maturation of Fe−S cluster-containing proteins across the *E. coli* proteome through the strategic use of a collection of deletion strains that are predicted to stall or interrupt this process at a specific stage, either early or later, and monitoring metalation status in each case.[184] In another application, an isotopic tandem orthogonal proteolysis-activity-based protein profiling (isoTOP-ABPP) workflow was used to show that the antibiotic holomycin, a dithiolopyrrolone, functions by inducing widespread metal depletion of the *E. coli* proteome[183,185] upon reduction by cytoplasmic low molecular weight thiols[186] to the dithiol form. Two enzymes among several, including fumarase A, which harbors an Fe−S cluster, and carbonic anhydrase II, which is a Zn^{II} enzyme (Section 4.3.4), were projected to be undermetalated upon holomycin treatment.[183] Indeed, holomycin induces broad spectrum zinc and iron starvation, with striking parallels to that of the antimicrobial protein, calprotectin, providing support for the idea that transition metal-starvation is an evolutionarily conserved weapon to keep microbial predators at bay. This chemoproteomics workflow is of course blind to the specific metal being probed, which must be inferred from our accumulating knowledge of the metalloproteome. In addition, a cysteine must be present in the first metal coordination shell, with metal sites that lack thiolate ligation undetected in this assay. This has motivated in part the development histidine- and carboxylate-specific probes that can be used in parallel alongside of thiol-specific probes, which when jointly deployed, may well approach full coverage of the metalation status of the metalloproteome.[184,187,188]

3. METAL SENSORS

3.1. Historical Overview

3.1.1. Protein-Based Regulatory Proteins. The efficacy of metallostasis (Figure 1) relies on a panel of sensory macromolecules that are "tuned" such that they maintain a specific bioavailable pool of metals in the bacterial cytoplasm, thus ensuring the integrity of the metalloproteome (Figure 8). Historically, these sensory molecules drive either transcriptional repression or activation of the expression of genes that encode metal uptake or efflux transporters thus allowing cells to control intracellular metal levels. The first efflux regulators were

https://doi.org/10.1021/acs.chemrev.4c00264
Chem. Rev. 2024, 124, 13574−13659

identified during the characterization of metal and metalloid ions resistance genes found in bacteria, in both clinical isolates and in soil or water isolates from areas polluted with these "heavy" metal species.[189,190] These resistance determinants were often plasmid-borne or present in other mobile genetic elements,[191−193] in contrast to the previously characterized chromosomally encoded transport systems for phosphate (Pho) and potassium (K), which were regulated by two component systems.[194,195] The initial interest in these heavy metal resistance determinants was primarily to understand the remarkable chemistry of the biological transformation of toxic metals and metalloids into nontoxic or less toxic species.[189,190]

The idea that a site-specific DNA binding protein might regulate transcription of resistance genes by reversible binding of a metal first emerged by identifying potential metal binding sites in these DNA binding proteins.[196] Direct validation of this hypothesis quickly followed and led to the concept of a "metalloregulatory" protein.[135] The first metalloregulatory protein so-designated was the mercuric ion resistance regulator, MerR, from the transposons Tn501 from *P. aeruginosa* and Tn21 from *Shigella flexneri* R100 plasmid.[135,191,192] While this seminal work focused mostly on DNA recognition and the mechanism of transcriptional regulation, these authors noted the presence of a potential metal binding motif, later shown to be critical for imparting metal selectivity (*vide infra*).[135] Soon thereafter, quantitative DNA binding experiments were used to demonstrate that Hg^{II} triggered both a modest change in affinity and a significant remodeling of the DNA promoter structure, converting a weak promoter into a strong one (Figure 6A, *bottom*).[197] MerR thus became the founding member of the best characterized family of metal-responsive transcription activators (Section 3.2.3).

This discovery was followed by the identification of other transcriptional repressors that responded to arsenic ions (ArsR)[198] or zinc (SmtB) toxicity,[130,199] both of which became founding members of the first and most diverse superfamily of metal- and metalloid-responsive repressors (Section 3.2.2). Shortly thereafter, the discovery of the copper-inducible repressor of a copper ATPase (CopY) from *Enterococcus hirae*,[200] revealed that a metalloregulatory protein could be a member of a protein family better known to elicit a response to small organic molecules, including antibiotics (Section 3.2.5).[201] A tetracycline repressor (TetR) family member was then shown to be responsible for regulating Zn^{II} efflux in *S. pneumoniae*.[202] Finally, Cu^{I}-responsive efflux regulation described initially in *M. tuberculosis* led to the discovery of CsoR (copper-sensitive operon repressor),[203] a founding member of the CsoR/RcnR[204] protein family that harnesses a unique DNA-binding fold consisting of a tetrameric antiparallel four-helix bundle architecture (Section 3.2.4).

The discovery and early biochemical characterization of metal efflux regulators occurred alongside the identification of the repressor of iron uptake, derived from the study of the molecular mechanism of regulation of siderophore-mediated iron assimilation.[132,205] The characterization of *E. coli* Fur (ferrous iron uptake repressor) as a negative regulator of the expression of siderophore-mediated iron assimilation under conditions of replete cellular Fe validated an earlier proposal that Fur was a metal (Fe^{II}) binding protein that would be "activated" to bind DNA upon metal coordination.[206] It was not until later that metal binding properties were studied *in vitro* which ultimately led to the discovery of myriad Fur family proteins that sense other transition metal ions[207] or oxidative stressors[208,209] (Section 3.2.6). The discovery of the founding members of the other two protein families of uptake regulators came with the study of the regulation diphtheria toxin expression in *Corynebacterium diphtheriae* (DtxR)[210−212] (Section 3.2.7) and nickel uptake regulation in *E. coli* (NikR)[213,214] (Section 3.2.8). Various members of another DNA-binding family (Rrf2), initially connected to iron uptake in rhizobia,[215] were later shown to regulate iron−sulfur cluster status or to sense diverse reactive oxygen, nitrogen and electrophile stressors (Section 3.2.9).[216] In the case of Rrf2, this category of metalloregulator is connected both with the regulation of iron uptake and the crucial role of metals in sensing reactive small molecules. Similarly, the observation that GntR/FadR proteins require metalation for binding organic inducers allows us to include this family as putative metalloregulators (Section 3.2.10).[217] Other uptake regulators were then described in well-characterized protein families that responded primarily to organic molecules, such as the zinc uptake regulator of *S. pneumoniae* (AdcR), from the multiple antibiotic resistance regulator superfamily (MarR)[218,219] (Section 3.2.11), zinc efflux activator of *S. pneumoniae* (SczA), from the tetracycline repressor family (TetR)[202,220] (Section 3.2.12), and the molybdenum uptake regulator of *E. coli* (ModE) from the lysine uptake regulator family (LysR)[221] (Section 3.2.13).

3.1.2. RNA-Based Regulation of Metallostasis. Although single pairs of protein-based efflux and uptake metallosensors are sometimes sufficient to control cellular metallostasis (Figures 6 and 8), RNA-based regulatory mechanisms continue to emerge that generally allow bacteria to expand or otherwise fine-tune the range of bioavailable metal (Section 2.2.2). The first example of this was the discovery of a small *trans*-acting regulatory RNA, *E. coli* RyhB, that significantly extends Fur-based regulation of metal starvation responses by down-regulating translation of mRNA transcripts of nonessential iron-containing proteins via an imperfect base pairing model.[222,223] This canonical form of "Fe sparing" makes Fur in many organisms a global regulator.

While these RyhB-like sRNA molecules clearly function in the regulation of metallostasis, these "off"-switches do not recognize a metal ion directly, and their cellular specificity derives entirely from the metal specificity of metalloregulatory protein that controls their expression. RNA-based regulation of metallostasis expanded significantly with the discovery of metal-sensing riboswitches, termed metalloriboswitches.[150] These generally (but not always) function as "on"-switches under conditions of metal toxicity and are highly structured regulatory RNA segments found within the 5′ noncoding or untranslated region (UTR) of mRNAs that often encode metal transporters. The binding of a metal (or a metal complex) to the riboswitch aptamer alters the folding of the RNA such that transcriptional "stop" and/or translational "off" signals are disrupted, thus leading to expression of the immediately adjacent gene (an "on" switch). These riboswitch elements are considered *cis*-acting RNAs, since they regulate transcription or translation within the same mRNA. While the first metalloriboswitch was a Mg^{II} sensor that turned "off" the expression of a Mg^{II} uptake transporter,[150] subsequent work showed that metalloriboswitches have evolved to sense Ni/Co,[224] Mn,[225,226] and other metallocofactors such as vitamin B_{12}.[227] Only recently was it shown that Ni/Co riboswitches respond primarily to iron bioavailability in cells.[228] This observation reinforces the idea that numerous other metals or metal complexes might be monitored in cells by harnessing the chemical selectivity of as yet undiscovered or "orphan"

https://doi.org/10.1021/acs.chemrev.4c00264
Chem. Rev. 2024, 124, 13574−13659

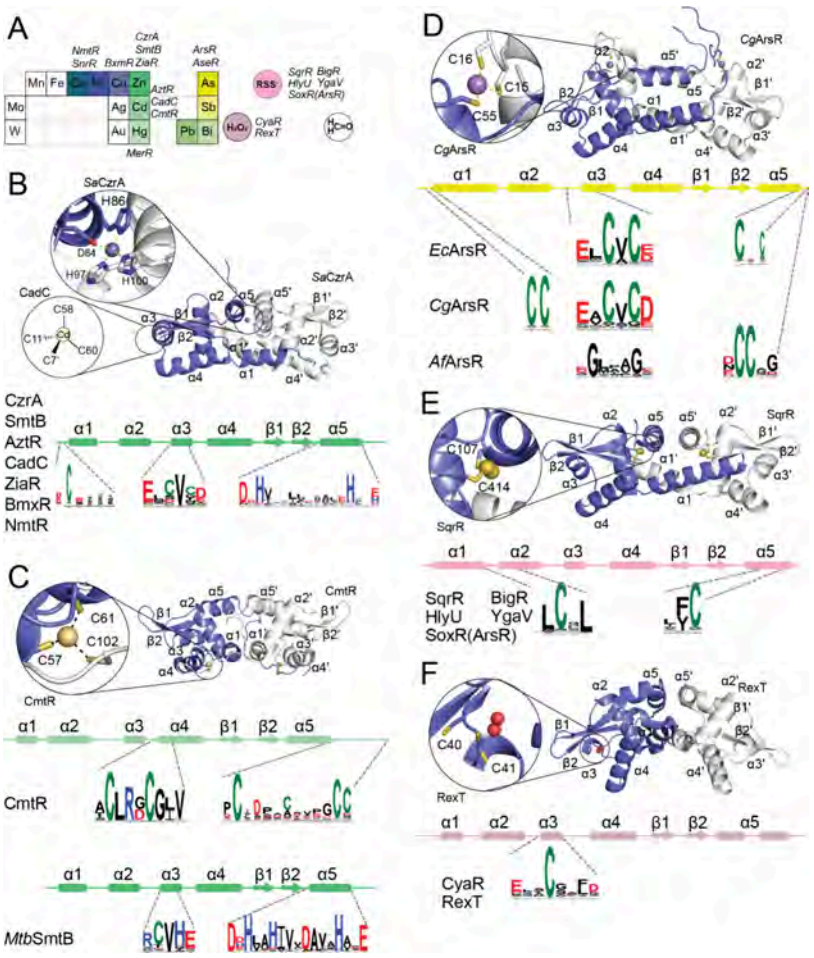

Figure 10. ArsR family proteins. A) Abbreviated periodic table showing the metals and reactive species (shaded) known to be sensed by ArsR proteins. The four-letter designations for individual proteins that perform the function listed in the nearby box are shown. B) Ribbon representation of *Sa*CzrA protein (PDB 2M30)[265] with a close-up view of the Zn^{II} binding site. An additional close-up shows the coordination of Cd^{II} present in *Sa*CadC.[266] Conserved primary structural features of different metalloregulator ArsR proteins with the different metal binding sites indicated in the text. C) Ribbon representation of *Cg*ArsR (6J0E)[248] with close-up view of the of the arsenic binding site. Conserved primary structural features of different arsenic-binding proteins (*Ec*ArsR, *Cg*ArsR, and *Af*ArsR). D) Ribbon representation of persulfide (RSSH) sensing *Rc*SqrR (6O8N)[267] with a close-up view of the polysulfide bridge formed upon reaction of the dithiol site with a thiol persulfide. Conserved primary structural features of different persulfide (RSSH) sensing ArsR. E) Ribbon representation of *No*RexT (7TXN)[258] with a close-up view of the H_2O_2 binding site. Conserved primary structural features of different RexT homologues are shown.

riboswitches to prevent the toxic accumulation of a specific analyte.[229] Although evolved to sense metals or metal-complexes directly, the set-point or sensitivity of these riboswitches to bioavailable metal may not fully align with the set-point of the analogous protein-based sensors given the complexity of the regulatory response involved (Section 3.3).

3.1.3. Biotechnological Applications. Finally, we discuss how the selectivity of some of these molecular switches has been leveraged in downstream synthetic biology and biotechnology applications, as biosensors (Section 3.4). The key component of any biosensor is the sensory module itself, tasked with selective detection of a target analyte, which is coupled to a reporter module that produces a detectable output. Among the myriad of possible sensory "parts", the metalloregulators discussed here have emerged as the "gold standard" for metal detection, due mainly to their metal sensitivity and selectivity.[230−232] Historically, the first applications of metalloregulators as biosensors were based on engineering living bacteria, where a regulated promoter was positioned upstream of a reporter gene, with strategic modifications of the bacterial chassis allowing for the desired intracellular bioaccumulation and sensitivity.[233−235] Later, this simple genetic circuity was adapted to cell-free platforms, which permits the development of field-deployable devices.[19] Synthetic biology continues to push the engineering and discovery of novel transcription factors and metalloregulator proteins in particular, enhancing both our fundamental knowledge of these molecular switches and application of metallosensors as biotechnologically useful tools.[236]

3.2. Families of Metalloregulatory Proteins

3.2.1. Overview. Metallosensors can be functionally subdivided into two broad groups of regulatory proteins. One group mediates the up-regulation of metal efflux systems upon metal binding in response to metal toxicity generally via transcriptional derepression or activation mechanisms. The second group consists of metalloregulators that down-regulate metal uptake systems via transcriptional corepression in response to cognate metal binding (Figure 6). The affinity for different metals generally follows the Irving−Williams series of stability constants for divalent metal ions (Figure 7).[144] Metal responsiveness is dictated by the set-point, K_d^S (Figure 8). the

https://doi.org/10.1021/acs.chemrev.4c00264
Chem. Rev. 2024, 124, 13574−13659

ligand set and metal coordination number and geometry, where formation of the "right" coordination geometry upon metal binding is a key feature of metal-mediated allosteric inhibition or activation of DNA operator binding.[120,141,237−240]

Among the more than 20 structural classes of "one-component" (Section 2.2.2) transcriptional regulatory systems in prokaryotes, no fewer than 12 of these structural families harbor metallosensors. Most metallosensors are "helix-turn-helix" or "winged helix" superfamily proteins proposed to be monophyletic, with the prominent exception of the CsoR protein family, proposed to have evolved from a four-helix-bundle RNA-binding protein.[203,241,242] In addition, most of these 12 structural classes also harbor representatives that control the adaptive response to cellular reactive oxygen species (ROS), e.g., superoxide and peroxides, reactive nitrogen species (RNS), e.g., GSNO and NOx, reactive electrophile species (RES), e.g., formaldehyde, quinones and the recently described reactive sulfur species (RSS), e.g., thiol persulfides or more generally "supersulfides."[243,244]

We review how sequence diversity in each structural family can be represented by clusters of closely related sequences[239,245,246] and interpreted in terms of a conserved metal binding or sensory motif, thereby defining the cognate inducer with greater confidence. Specific characteristics of the functions of genes that colocalize with a metallosensor gene (genomic neighborhood) can further improve the robustness of these predictions. This is because nature has employed a "mix-and-match" approach in the evolution of metal-sensing operons or regulons in a specific organism, likely aided by horizontal gene transfer[247] and subsequent convergent evolution.[248] This implies that a sensor derived from a particular structural family may have evolved to sense a distinct inducer (metal or reactive molecule), dictated by the specific characteristics, e.g., a specific range in metal bioavailability (Figure 8) or type of small molecule stressor specific to that organism or "chassis" encoding it. Alternatively, a collection of sensors from distinct structural families may have evolved to regulate the same gene in different organisms. For example, *M. tuberculosis*, *E. coli* and *E. hirae* encode essentially the same Cu^{I}-specific P_{1B-1}-type ATPase efflux transporter (Section 5.3) whose Cu^{I}-inducible transcription is regulated by three structurally distinct Cu^{I}-sensing metallosensors, CsoR,[203] CueR (a MerR family member),[249] and CopY,[200] respectively. The common feature is that each Cu^{I} sensor employs a low-coordination number Cys-rich Cu^{I} coordination complex with a characteristic K_d^S (Figure 8A), but which triggers very different mechanisms of metalloregulation of transcription (Figure 6A).

On the other hand, crosstalk and mismetalation (Section 2.2.3) also play critical functions in metalloregulators, which brings into question the very idea that each regulator has evolved to sense a single cognate metal.[250] For example, metal binding to *S. pneumoniae* CopY elicits a distinct transcriptional response dependent upon the bound metal; here, Zn^{II} acts as a corepressor and Cu^{I} functions as an allosteric inhibitor of DNA binding (Figure 6A) allowing the expression of Cu^{I}-specific P_{1B-1}-type ATPase effluxer specifically under conditions of Cu^{I} toxicity.[251] In *Salmonella*, acute Zn^{II} toxicity transcriptionally induces a Co^{II} toxicity response orchestrated by the Co/Ni sensor, RcnR, while conversely, acute Co^{II} toxicity triggers a Zn^{II} toxicity response regulated by the Zn^{II} efflux activator ZntR, leading also to repression of the Zur regulon.[121] Mis-metalation of Fur by Mn^{II} under conditions of Mn^{II} toxicity, in contrast, is detrimental to cell viability, and is avoided by proper tuning of the coordinated responses of the Mn^{II}-sensing repressor and Fur to distinct ranges of cellular metal activity (Figure 8A).[252] Here we review the impact of metal promiscuity and crosstalk in the context of structural and sequence determinants of metal specificity and allosteric connectivity for four classes of metal efflux regulators (ArsR, MerR, CopY, and CsoR), four families of uptake regulators (Fur, DtxR, NikR, and Rrf2) and finally, four families within which metallosensors are significantly underrepresented (TetR, MarR, LysR and GntR).

3.2.2. ArsR. Members of the arsenic repressor (ArsR) superfamily sense a wide range of stimuli (Figure 10A) and feature a compact homodimeric "winged helical" DNA binding fold, characterized by a core α1-α2-α3-α4-β1-β2-α5 secondary structure, where the dimer is formed by the quartet of α2 and α5 helices from each subunit (Figure 10B). Some ArsR proteins harbor extensions on either or both N- and C-terminal sides of this core motif, generally denoted the α0 and α6 helices, respectively.[120,253] The helix-turn-helix (HTH) motif that mediates DNA-binding is located at the α3-α4 segment that engages successive DNA major grooves, with a degenerate tetrapeptide sequence in α4 that enforces specificity for a particular DNA operator sequence.[254] The β1-β2 wing extends from the periphery of the dimer and may mediate interactions with the immediately adjacent "outer" minor grooves. Early work on ArsR family proteins suggested that the >3000 distinct members of this family were mostly metal ion or metalloid-specific regulators.[255−257] This is clearly no longer the case.[120,247] A number of ArsRs have been recently characterized and shown to respond to redox-active small molecules[258−260] or lack inducer binding sites altogether (Figure 10A).[261−263] ArsR superfamily sequence relationships were recently evaluated using a sequence similarity network (SSN) analysis of ≈168,000 unique entries from the Pfam and Interpro data sets.[245,264]

3.2.2.1. Metal-Sensing ArsRs. The largest cluster of sequences[245,264] contains the vast majority of described metalloregulators to date, that sense either biologically relevant transition metals, e.g., Cu^{I}, Zn^{II}, Ni^{II} or Co^{II} and toxic heavy metals, including Cd^{II} or Pb^{II}. Collectively, these sequences share a conserved metal binding site conforming to a $DxHx_{10}Hx_2(H/E)$ motif in the α5 helix that defines an interfacial site between the two subunits of the dimer, and an additional metal binding site harboring a CxC motif in the α3 helix (Figure 10B). Interestingly, the Zn^{II} sensors *Sa*CzrA,[131] *Bs*CzrA,[255] *Syn*ZiaR[268] and *Tt*SmtB[130] that sense Zn^{II} with significant specificity both *in vivo* and *In vitro*,[269] share the same $DxHx_{10}Hx_2(H/E)$ motif with the Ni^{II} sensor *Mtb*NmtR; however, NmtR completes an octahedral coordination complex by recruiting the N-terminal His-Gly sequence.[238,270] On the other hand, Cd^{II} and Pb^{II} responsive regulators *Lm*CadC[271] and *Sa*CadC[272,273] rely largely upon the α3 CxC motif and two N-terminal Cys as the primary allosteric site, denoted α3N, for negative regulation of DNA binding (Figure 6A, *top*) since the α5 $DxHx_{10}Hx_2(H/E)$ motif is either not present[274] or allosterically uncoupled (silent).[266,275] While this Cys-rich site retains a certain degree of selectivity for soft transition metal ions Cd^{II} and Pb^{II} over Zn^{II}, the *In vitro* metal selectivity is not as high as the paradigm Pb^{II} sensors from the MerR superfamily (*vide infra*).[269] Other characterized ArsR family metallosensors that contain allosterically *active* α3N and α5 sites are known to have relaxed metal selectivity. One example here is cyanobacterial BmxR, whose regulon is inducible by both monovalent (Cu^{I}/Ag^{I}) and divalent (Zn^{II}/Cd^{II}) ions in *O. brevis*.[276] Additionally, cyanobacterial AztR[277] responds to Zn^{II}/Pb^{II}/Cd^{II} by engaging

https://doi.org/10.1021/acs.chemrev.4c00264
Chem. Rev. 2024, 124, 13574−13659

metal donors in a modified α3N site only, while mycobacterial KmtR[278] responds to $Zn^{II}/Co^{II}/Ni^{II}$ by binding metal to a His-rich site that resembles, but is not identical to, the α5 $DxHx_{10}Hx_2(H/E)$ motif found in a canonical Zn^{II} sensor.

3.2.2.2. Other Non-α5 or α3N Metal-Sensing ArsRs. There are a number of other metal-sensing repressors from the ArsR family that differ from those described above. The regulon of the Zn^{II}-responsive efflux repressor mycobacterial SmtB includes *zur* (Section 3.2.6) which suggests a mutually reinforcing response to zinc toxicity (Section 5.3.3).[279,280] The Cd^{II} sensor CmtR from *Mycobacterium tuberculosis* and *Streptomyces coelicolor* employ a distinct metal binding site containing two metal coordinating cysteines derived from the DNA binding helix α4 and a Cys from the C-terminal flexible tail (Figure 10C).[281,282] The Ni^{II} sensor SrnR from *Streptomyces griseus*[263] is representative of a group of candidate Ni^{II}-specific regulators that depend on a Ni^{II}-binding partner protein (SrnQ) to elicit a transcriptional response.[283,284] The Hg^{II} resistance regulator from the Gram-positive bacterium *Streptomyces lividans*[285] is present in a divergently transcribed operon that has been replaced by a canonical MerR family regulator in other bacteria.[286] This sensor has more than six cysteine residues in different structural elements and several other putative metal binding sites; however, the bioinorganic chemistry of this system has not yet been examined.

3.2.2.3. As^{III} and Organoarsenical Sensors. The canonical As^{III} sensors harbor a C-(V/A)-C motif in the α3 helix coincident to that described above, which donates two of the three As^{III} ligands, adopting a trigonal planar coordination geometry (Figure 10D). This is the dominant As^{III}-sensing regulator, with an additional Cys present in either close proximity to this motif[287] or in the C-terminal region.[255] Two distinct As^{III} sensing sites described for As^{III} sensors are represented by *Acidithiobacillus ferrooxidans* ArsR[288] and *Corynebacterium glutamicum* ArsR (Figure 10D).[289] *Af*ArsR and another ArsR in *Agrobacterium tumefaciens*[290,291] feature a CCx_5C motif in the α5 helix that defines a C-terminal As^{III} binding site.[292,293] The As^{III} selectivity over Hg^{II} of this protein has been recently interrogated with a combination of different spectroscopic techniques that confirm that As^{III} binds in a rigid trigonal pyramidal geometry compared to an rather undefined geometry with Hg^{II}.[294] On the other hand, the *Cg*ArsR As^{III} binding site engages a Cys from the canonical C-(V/A)-C motif and two N-terminal Cys from the other subunit within the dimer (Figure 10D).[289] The common feature is that each of these three As^{III} sensing ArsRs utilizes three cysteine residues at spatially distinct locations within the same three-dimensional structure, suggesting that the ArsRs must have arisen independently during evolution.[266,288,289] It is important to note that while the coordination of As^{III} by the canonical As-sensing ArsR has only been characterized by EXAFS,[295] the other two As^{III} sites have been resolved by crystallography.[248]

3.2.2.4. Redox-Active Small Molecule ArsR Sensors. The remainder of the biochemically characterized ArsR family sensors are not metal ion or metalloid-sensing regulators, but instead use cysteine thiolate chemistry enabled by a precisely tuned pK_a, nucleophilicity and topology to specifically sense either RSS or ROS (Figure 10E).[245,267] All known RSS or supersulfide sensors are characterized by a pair of cysteines in the α2 and α5 helices which form an intraprotomer polysulfide bridge when incubated with a sulfane sulfur (sulfur-bonded sulfur) donor.[245,267,296,297] The paradigmatic RSS-sensing ArsR is SqrR from the purple bacterium *Rhodobacter capsulatus*.[259] X-ray crystal structures of four distinct oxidation states reveal that the two sensing Cys lie quite far apart from one other, forming a cavity that restricts solvent accessibility and disulfide bond formation, which would occur with an oxygen-derived ROS.[267] This in turn promotes the formation of a polysulfide bridge linking the two cysteines. RSS-specificity was shown not only in vitro but also in cell culture,[298] as in the case of *Vibrio cholerae* HlyU, an SqrR homologue, which regulates the expression of exotoxins necessary for bacterial colonization of the gut in response to endogenously generated persulfides.[245] SqrR homologues have also been found in other human pathogens,[296,299] plant pathogens[260] and sulfur-oxidizing bacteria.[300] On the other hand, cyanobacterial RexT is H_2O_2-specific sensor, which reacts instead with two vicinal Cys residues in the α3 helix (Figure 10F).[258] The formation of disulfide bridges between the vicinal Cys residues is the mechanism by which transcription of downstream H_2O_2-detoxifying genes is allosterically regulated. It remains unclear, however, if crosstalk with other oxidants occurs in RexT. Overall, nonmetal sensing ArsR proteins appear to exhibit exquisite chemical inducer specificity afforded by the distinct structural environment of the dithiol pair.

3.2.2.5. Allostery. The picture that emerges from a gallery of different ArsR family structures is that the sensing sites are widely distributed throughout this simple molecular scaffold, which in turns triggers a change in structure and/or conformational dynamics that inhibits DNA binding by several orders of magnitude ($\Delta G_c \approx +3-6$ kcal/mol; Figure 6A-B).[265−267,270,301] This large allosteric coupling free energy comes from distinct metal, metalloid and reactive species-specific sensing sites, which implies that each of these sites must be connected in some way to the DNA-binding helices to drive allosteric inhibition of DNA binding. This remarkable feature is unique to ArsR family sensors among all of the metalloregulatory protein families discussed here. The allosteric plasticity of this simple molecular scaffold has obvious implications for evolvability of new biological outcomes, which in one case, the Zn^{II} sensor *Sa*CzrA, appears to arise from a redistribution of internal dynamics important for DNA operator binding.[139] The extent to which this allosteric mechanism is a general feature of ArsR family regulators is unknown, but we believe likely, given the sheer number of structurally distinct sensing sites that have emerged on this simple homodimeric scaffold.[139]

3.2.3. MerR. MerR proteins, like ArsR proteins, sense a wide range of metal and chemical inducers (Figure 11A). They are homodimers organized as two symmetry-related signaling and DNA-binding domains linked by a long α-helical coiled coil derived from the α5 helix (Figure 11B).[302,303] Each DNA-binding domain is formed by the N-terminal region of each protomer which conforms to a winged helix-turn-helix motif with an α1-α2-β1-β2-α3-α4 topology (Figure 11B). The inducer binding signaling domain typically involves residues from the C-terminal region of one protomer and the N-terminal region of the α5 helix of the other protomer.[304−306] The diversity of signals collectively detected by MerR sensors may well be broader than that of the ArsR family as they not only form coordination complexes with monovalent and divalent metal ions, e.g., mercury (Hg),[135,307,308] cadmium (Cd),[309,310] lead,[237,311] cobalt,[312] zinc,[313] iron,[314] nickel,[315] gold (Au^{I})[304,316] and copper,[317] but also respond to oxidative stressors,[305,318] carbonyl and nitrosative stressors,[319,320] and lipophilic drug molecules[306,321] (Figure 11A). In general, the affinity of MerR sensors for their target operators is not significantly changed by binding the cognate inducer, i.e., the apoprotein may function as

https://doi.org/10.1021/acs.chemrev.4c00264
Chem. Rev. 2024, 124, 13574−13659

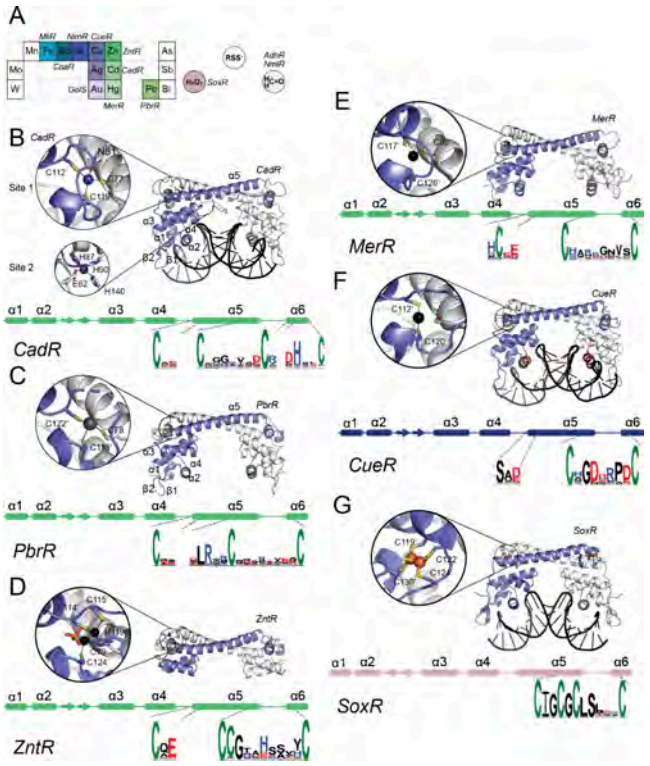

Figure 11. MerR family proteins. A) Abbreviated periodic table showing the metals and reactive species (shaded) known to be sensed by MerR proteins. The four-letter designations for individual proteins that perform the function listed in the nearby box are shown. B) Ribbon representation of CadR protein (6JGX)[309] with close up view of the Cd metal binding sites, denoted site 1 and site 2. Conserved primary structural features of different metalloregulator MerR proteins with metal binding sites with Cd binding preference. C) Ribbon representation *Rm*PbrR (5GPE)[237] with a close-up view of the of the Pb^{II} binding site. Conserved primary structural features of different MerR proteins with Pb and Cd metal binding preference. D) Ribbon representation *Ec*ZntrR (1Q08)[317] with a close-up view of the of the Zn binding site showing two Zn metal ions. Conserved primary structural features of different MerR proteins with Zn metal binding preference. E) Ribbon representation *Pa*MerR (5CRL)[308] with a close-up view of the Hg binding site. Conserved primary structural features of different MerR proteins with Hg metal binding preference. F) Ribbon representation *Ec*CueR (PDB 1Q05)[317] an activation complex with operator DNA with close up view of the of the Cu^{I} binding site. Conserved primary structural features of different MerR proteins with Cu^{I} metal binding preference. G) Ribbon representation of the peroxide sensing *Ex*SoxR (2ZHG)[305] in complex with operator DNA with close up view of the [2Fe-2S] site. Conserved primary structural features of different ROS sensitive MerR proteins.

a weak repressor of a weak promoter. On the contrary, inducer binding drives a concerted change in both the conformation of the homodimer and DNA promoter to which it is bound, eliciting a transcriptional activation response via recruitment of RNA polymerase to what is now a strong promoter.[253,321,322] Canonical MerR activators bind to their DNA operators embedded in a suboptimal promoter with the −35 and −10 promoter elements separated by 19−20 bp instead of the optimal ≈17 bp distance.[197,313] Signal perception is linked to DNA underwinding, thus moving the −35 and −10 promoter elements to same side of the DNA duplex and allowing productive engagement of RNA polymerase, and transcription initiation (Figure 6A, *bottom*).

3.2.3.1. Pb^{II}- and Cd^{II}-Sensing MerRs. Early studies of a number of canonical metal-sensing MerRs revealed that a major determinant of metal selectivity was the specific arrangement of residues (usually Cys or His) in the inducer-binding sites largely localized to a metal binding loop (MBL),[323] with a preferred coordination geometry for a monovalent vs a divalent metal ion.[149] Insights that have emerged more recently suggest a far more nuanced picture. For example, while most MerRs contain a single metal binding site in the MBL, the Cd^{II} efflux regulator from *Pseudomonas putida* CadR features two Cd^{II} binding sites, as inferred from the crystal structure of the different metalated forms (Figure 11B).[309] One site is formed by Cys in the MBL and a Cys from the N-terminal region of the dimerization (α5) helix, an arrangement shared with other divalent metal ion MerR sensors, with the second site a histidine-rich site positioned between the dimerization helix, the H-T-H motif and the C-terminal tail (Figure 11B).[309] Cd^{II} binding to the MBL site facilitates the assembly of His-rich site and the presence of this second site in turn enhances the metal affinity of the MBL site significantly, i.e., the binding of Cd^{II} in CadR is positively cooperative. CadR is the most specific, naturally occurring Cd^{II}-sensor reported to date, as the *cadR* promoter is induced only by cadmium, and this may be traced to this two-site intraprotomer cooperativity.[324] Other Cd^{II}-sensing proteins, such as CadR from *P. aeruginosa* and *E. coli*,[310] do not conserve this second Cd^{II} site, and instead rely exclusively on a *P. putida*-like Cys-thiolate-rich MBL site for regulation.

The Pb^{II} sensor PbrR from *Cupriavidus metallidurans* is representative of a group of MerRs that form a trigonal-pyramidal coordination complex with three conserved Cys, with two derived from the MBL and one from a Cys in the N-terminal region of the dimerization helix (Figure 11C).[311] The crystal structure of PbrR suggests that the Pb^{II}-selectivity of this switch may be traced to the coordination geometry itself, where fourth coordination position is occupied by the stereochemically active lone pair of electrons on the Pb^{II} ion. *Cm*PbrR, like Cd^{II}-sensing CadRs, harbors the same asparagine residue (N81; Figure 11B) that functions as the fourth metal ligand in CadRs,[309,310] but is excluded from the first coordination shell in *Cm*PbrR by the Pb^{II} lone pair. These characteristics precisely parallel previous findings for the ArsR family Pb^{II}/Cd^{II} sensor CadC.[325,326] It is interesting to note that although this three-coordinate Pb^{II}-pyramidyl structure may well be a common feature of Pb^{II}-responsive regulators, the presence of four Cys residues in the metal binding site of CadC negatively impacts Pb^{II} specificity over Cd^{II} or Zn^{II}.

3.2.3.2. MerR Family Zn^{II} Sensor. The canonical Zn^{II} efflux regulator (Figure 6) *Ec*ZntR is characterized by a conserved CCx_3Hx_4C motif in the MBL and a Cys in the N-terminal region of the α5 helix, which collectively create a binuclear Zn^{II} cluster in which the two Zn^{II} ions adopt approximately tetrahedral coordination geometries (Figure 11D).[317] *Ec*ZntR responds to intracellular spikes of Zn^{II} in the nanomolar concentration range[327] but also responds to acute phase Cd^{II} and Pb^{II} toxicity as well.[328] This suggests that the zinc selectivity of ZntR may be quite modest in *E. coli*.[329] In *Salmonella*, however, ZntR appears quite selective, at least relative to other biologically required metals, Mn^{II}, Fe^{II}, Co^{II}, Ni^{II} and Cu^{I}.[121] ZntR plays a key role specifically in *Brucella abortus* Zn^{II} homeostasis.[330] On the other hand, *A. tumefaciens* ZntR responds primarily to Cd^{II} toxicity, eliciting a comparable response to Zn^{II} and Co^{II},[331] while in *Serratia marcescens*, ZntR appears to regulate a Pb^{II} toxicity response.[332] Thus, the true cytoplasmic metal inducer of a ZntR

https://doi.org/10.1021/acs.chemrev.4c00264
Chem. Rev. 2024, 124, 13574−13659

may well be dependent upon the composition of the intracellular "buffering" milieu, which thus impacts its set-point K_d^S for a specific metal (Figure 8), perhaps in response to its environmental niche in which an organism resides. This degree of metal-sensing promiscuity across a collection of closely related ZntRs in a cell is not only anticipated but may well be beneficial, since it is well documented that the P_{1B-2} ATPase, ZntA, can efficiently transport a range of divalent soft transition metal ions, including Zn^{II}, Cd^{II}, Pb^{II} and Hg^{II} by adopting a range of coordination geometries in the transmembrane metal binding site (Section 5.3.1).[250] In fact, this modest selectivity of *Ec*ZntR has been exploited in the selection of engineered ZntR mutants capable of detecting xenobiotics[329,333,334] that are subsequently leveraged in the design of whole cell biosensors (Section 3.4).

3.2.3.3. Hg^{II}-Selective MerRs. The founding member of the MerR superfamily is plasmid-derived *Ec*MerR[135] and all share three conserved cysteines, two in the MBL and one in the N-terminal region of the α5 dimerization helix (Figure 11E). The Hg^{II} site is trigonal planar as revealed by ^{199}Hg NMR spectroscopy[335,336] and EXAFS,[337] and later confirmed by X-ray crystallography of both Gram negative[308] and Gram positive[307] Hg^{II}-sensing MerRs. This tricoordinate HgS_3 site in MerR remains the only naturally occurring Hg^{II} complex of its kind, beyond *de novo* designed three-helix bundle peptides.[338] The selectivity and sensitivity of this Hg^{II} specific switch is noteworthy, with ≈100-fold discrimination of Hg^{II} over other metal ions.[197,339,340] This property may well be traced to several His and Cys residues beyond the first coordination shell that have been implicated in driving a significant structural rearrangement in the homodimer which buries the *tris*-thiolate Hg^{II} site.[308] However, these ideas are difficult to rationalize on the basis of early extensive mutagenesis studies.[341] In any case, directed evolution of Hg^{II}-sensing MerR to create a Cd^{II}-specific sensor has been achieved through the introduction of mutations distributed throughout the molecular scaffold.[342]

3.2.3.4. The Monovalent "Coinage Metal" Sensors. The coinage metal sensors of the MerR family are exemplified by the Cu^I sensor *E. coli* CueR, which provides resistance against copper toxicity, and the gold resistance regulator from *Salmonella*, GolS (Figure 11F). Cu^I coordination by CueR involves formation of a linear *bis*-thiolato coordination complex formed by two Cys from the MBL. Selectivity for Cu^I is mediated by a negative design element, a conserved Ser in the α5 helix, required to exclude divalent metal ions,[317,343,344] as well as the somewhat shorter length of the MBL relative to divalent metal sensors (Figure 11F).[317] For example, the number of residues between the two Cys ligands in the MBL appear to impact discrimination between Hg^{II} and Cu^I.[307] GolS binds Au^I with the same coordination geometry as Cu^I-sensing CueR[316] and can be phylogenetically distinguished from CueR only on the basis of differences in the N-terminal region that appears to confer Au^I specificity[316] while modulating regulator-DNA operator specificity.[345,346] Thus, it is not surprising that *Ec*CueR is responsive to Cu^I but can also detect Ag^I and Au^I *in vivo* and *in vitro*.[302,317,339]

3.2.3.5. Unconventional Metal-Sensing MerR Proteins. There are several MerR family regulators that do not appear to conform precisely to this classical paradigm.[303] For example, *Synechocystis* CoaR harbors an additional domain that is required for CoaR to respond to intermediates of the B_{12} biosynthetic pathway.[312] MliR from the marine Bacteroidetes *Bizionia argentinensis* has been reported to function as both an iron-dependent activator and repressor of genes linked to bacterial survival under Fe-replete conditions so as to avoid Fe-overload.[314] Similarly, the *Haemophilus influenza* nickel-responsive MerR-like regulator (NimR) is the only described MerR that responds to Ni^{II} and regulates the expression of genes encoding a Ni^{II} uptake system.[315] This is in contrast to most MerR regulators, which generally elicit a detoxification response to a specific inducer.

3.2.3.6. Redox-Sensing MerRs. Three phylogenetically distinct groups of MerR sensors respond to redox-active small molecules. The superoxide sensor, *E. coli* SoxR, is among the best characterized of these subfamilies.[347−349] Each SoxR protomer harbors a CIGCGCLSxxC motif in the MBL that coordinates a sensory [2Fe−2S] cluster and mediates a response to superoxide anion, nitric oxide and redox cycling agents (Figure 11G).[305] Oxidation or nitrosation of the Fe−S centers induces a conformational change in the homodimer that renders SoxR-regulated promoters permissive for open complex formation in front of its only target gene, *soxS*, which encodes a global redox resistance regulator. It is interesting to note that in contrast to most other metal-binding MerRs the [2Fe-2S] clusters are completely solvent exposed,[305] a finding consistent with a role in cellular monitoring of small redox-active compounds. SoxR is an excellent illustration of evolutionary "plasticity" of the MBL in MerR proteins and how that plasticity can be tuned to perform a distinct function. Unlike *E. coli* and related enteric bacteria, however, the majority of SoxR regulons in *P. aeruginosa* and *Streptomyces coelicolor* lack the genes typically involved in O_2^- detoxification.[350,351] Thus, it is not yet clear that all SoxRs are superoxide anion sensors, which suggests that other redox active small molecules could have a more significant role to play in these organisms.

NmlR, first identified in *Neisseria gonorrheae*,[352] also activates transcription in response to both oxidative and nitrosative stresses, with the structure and mechanism of regulation described for the *H. influenza* homologue.[319] Oxidation of a conserved Cys pair in the MBL changes the protein conformation allowing transcriptional derepression and/or activation of the expression of a genes encoding alcohol dehydrogenase family enzymes.[319] A recent report suggests *Streptococcus pneumoniae* could also harness this chemistry to respond to strong electrophiles such as HClO.[353] AdhR, on the other hand, is a *Bacillus subtilis* aldehyde-activated sensor that is representative of the third group of redox active regulators that regulates the expression of genes encoding enzymes that reduce aldehydes or repair aldehyde derived posttranslational modifications.[354] More recently, it has been shown that polysulfane compounds induce AdhR-regulated genes.[355] Altogether these observations suggest that AdhRs and NmlR proteins may function as promiscuous redox or electrophile sensors in cells.

3.2.4. CsoR. CsoR family proteins exhibit high pairwise sequence similarities and adopt a disc-shaped, dimer-of-dimers D_2-symmetric tetrameric architecture consisting of four α-helical ≈90-residue protomers (Figure 12B).[356] Members of the CsoR family collectively detect a wide range of transition metal- and small molecule inducers, with an inducer footprint that is at present far smaller than that of the ArsR and MerR families (Figure 12A). The founding CsoR family members are the Cu^I sensor[357] from *Mycobacterium tuberculosis*[203] and the Ni^{II}/Co^{II} sensor RcnR from *E. coli*.[358] Since that time, other CsoR family members have been reported, including a second mycobacterial Cu^I sensor, RicR,[359] the Ni^{II} sensor InrS from *Synechocystis*,[360] the formaldehyde-sensing repressor FrmR from *E. coli*,[361,362] and the thiol persulfide sensor CstR, now functionally

https://doi.org/10.1021/acs.chemrev.4c00264
Chem. Rev. 2024, 124, 13574−13659

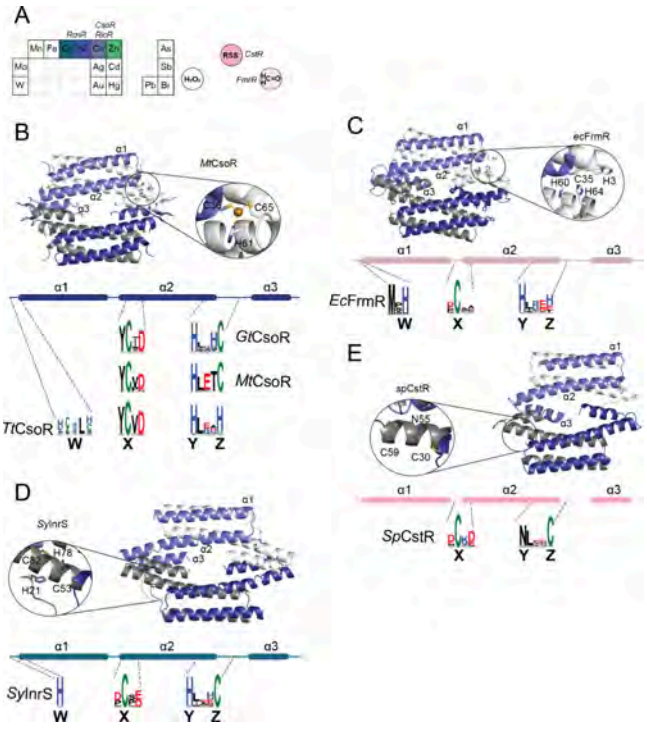

Figure 12. CsoR family proteins. A) Abbreviated periodic table showing the metals and reactive species (shaded) known to be sensed by CsoR proteins. The four-letter designations for individual proteins that perform the function listed in the nearby box are shown. B) Ribbon representation of *Mt*CsoR tetramer protein (2HH7)[203] with close up view of the Cu metal binding site. Conserved primary structural features of CsoR homologues proteins denoted in the text. C) Ribbon representation of the formaldehyde sensitive *SeFrmR* protein (5LCY)[362] with close up view of the metal binding site. Conserved primary structural features of FmrR homologues. D) Ribbon representation of the nickel activated *Sy*InrS protein (5FMN)[365] with a close-up view of the metal binding site. Conserved primary structural features of InrS proteins are shown. E) Ribbon representation of the persulfide (RSSH) sensitive *Sp*CstR protein (7MQ2)[239] with close-up view of the reduced cysteines of the RSS-reactive site. Conserved primary structural features of different CstR like proteins.

characterized in *S. pneumoniae*,[239] *S. mitis*,[239] *Staphylococcus aureus*[363] and *Enterococcus faecalis*.[364] Inducer specificity by CsoR-family repressors was originally described in the context of a simple "W-X-Y-Z" motif using the *Mt*CsoR Cu^{I} chelate as a template,[203] where the first coordination shell ligands around a subunit-bridging, trigonally coordinated Cu^{I} define the X (Cys36), Y (His61') and Z (Cys65') residue positions (Figure 12B).[204] This conceptually simple perspective on inducer specificity has proven remarkably resilient, but cannot fully explain how inducer promiscuity is avoided, particularly when considering specificity toward reactive species such as persulfides[239] and formaldehyde.[362] A recently published SSN analysis significantly extends these initial ideas, providing new insights into inducer specificity in this very large superfamily of transcriptional repressors.[239]

3.2.4.1. Cu^{I} Sensors. There are three distinct types of Cu^{I}-sensing CsoR-family repressors exemplified by *Bs*CsoR,[366] *Mt*CsoR,[203] and *Tt*CsoR (Figure 12B).[367] The reported SSN[239] coupled with a phylogenetic analysis suggests that copper specificity within this family of repressors may have arisen multiple times during evolution.[366] Copper specificity has generally been assessed by determining an affinity $\geq 10^{-18}$ M^{-1} using Cu^{I} specific chelators as competitor ligands,[203,357,368−370] although the selectivity for Cu^{I} over other transition metal ions has been determined in only for a few cases.[203,371] Nearly all functionally characterized *bona fide* CsoR-like Cu^{I} sensors are related to *Bs*CsoR[357,359,370] which conserve the three cognate Cu^{I} binding residues that form a C−H−C (Cys-His-Cys) "X-Y-Z" motif and lack an N-terminal metal binding residue "W", thus denoted x−C−H-C. Two structures of this group are *Sl*CsoR[357,372] and *Gt*CsoR,[366] obtained in the apo and Cu^{I}-bound states, respectively. A comparison between the apo- and Cu^{I}-bound states suggests a mechanism of allosteric connectivity where the metal binding event induces a kink in the α2 helix, which leads to a rearrangement of surface electrostatic potential distribution, thus driving DNA dissociation and transcriptional derepression of Cu^{I}-resistance genes.[372,373]

The x−C−H-C motif is also present in *Mt*CsoR which exhibits high specificity for Cu^{I}.[203] *Mt*CsoR and the related sequences only present in actinomycetes are characterized by a ≈30-residue, poorly conserved C-terminal tail not found in other CsoRs.[203,374] The only structure available for this subgroup is the Cu^{I}-bound form of *Mt*CsoR.[203] While structural details of the apo form are missing for this groups of Cu^{I} sensors, ion mobility mass spectrometry studies on this protein suggest that metal binding subtly alters the shape of the tetramer to a more hydrodynamically compact structure[375] which may lead to changes in the surface electrostatic potential distribution similar to that observed for *Sl*CsoR.[372,373] Moreover, the ϵ-face of Cu^{I}-coordinated His ligand interacts with residues in the second coordination shell including nearly invariant Tyr and Glu residues that are energetically linked to Cu^{I}-mediated allosteric inhibition of DNA binding, suggesting a path for allosteric connectivity.[203]

In *T. thermophilus* CsoR one of the Cu^{I}-coordinating Cys is replaced by a His, thus defining a x−C−H-H metal-binding motif (Figure 12B).[367] Although the Cu^{I} specificity of this switch has not yet been unequivocally evaluated, residues in the second coordination shell are conserved, as are the neighboring genes found in all three Cu^{I}-specific clusters (a P_{1B-1} CopA efflux pump and a CopZ metallochaperone); these features are consistent with a Cu^{I}-specific sensing function.[239] Studies designed to examine the impact of this Cys-to-His substitution concluded that the histidine positively impacts DNA-binding affinity and Cu^{I}-responsiveness of this sensor.[367] Metal displacement studies on different *Sl*CsoR mutants suggest that a His in this metal-ligating position may impact the kinetics of Ni^{II} displacement of bound Cu^{I} ions.[371] Thus, substitution of the second Cys may enhance the promiscuity of this subgroup of Cu^{I} sensors.

3.2.4.2. Ni^{II}/Co^{II} Sensors and the Formaldehyde Sensor. The Ni^{II}/Co^{II}-sensing repressor RcnR is readily distinguished from Cu^{I}-sensing CsoRs proteins by conservation of a H−C−H-H "W-X-Y-Z" motif.[204,376] RcnRs are most closely related to the formaldehyde (HCHO)-sensing FrmR,[362,377] which harbor a P (Pro)−C-H-x "W-X-Y-Z" motif, as exemplified by *Ec*FrmR and *Se*FrmR (Figure 12C). A very high level of pairwise similarity is consistent with the relative ease with which inducer specificity can be relaxed or switched in an FrmR by simple reintroduction of the Z-position His residue found in RcnRs.[362] The Ni/Co specific transcriptional response of RcnR has been extensively characterized in *lacZ*-reporter assays and EXAFS studies to identify subtle differences in Ni^{II} vs Co^{II} coordination modes in RcnR.[376,378] For example, the N-terminal His donor appears critical for Co^{II}-induced DNA dissociation but not for Ni^{II}.[376]

https://doi.org/10.1021/acs.chemrev.4c00264
Chem. Rev. 2024, 124, 13574−13659

While detailed spectroscopic studies have led to atomic-level models of the different holo RcnR species that define residues beyond the "W-X-Y-Z" motif, the lack of a structure hinders our understanding of the allosteric mechanism of transcriptional derepression by RcnR.[204,376,379] On the other hand, allostery in FrmR is driven by a methylene bridge formed between the Cys (C) and the Pro (P) in the "P−C−H-x" motif after the Cys-thiolate attacks HCHO; this chemistry appears to lead to a rearrangement of the surface electrostatic potential distribution that impairs DNA recognition.[361]

Two additional groups of Ni^{II}/Co^{II} specific clusters are exemplified by cyanobacterial InrS[119] and *Leptospirillum ferriphilum* NcrB.[380] The Ni/Co specificity of InrS over Cu^{I} and Zn^{II} has been evaluated both *in vivo* and *In vitro*, revealing that the affinity of InrS for these other transition metal ions is sufficiently low, i.e., an insufficiently negative $\Delta\Delta G$ relative to Ni^{II} (Figure 8), which prevents induction of the expression of genes encoding Ni^{II} transporters as a result of mismetalation (Figure 12D).[381] Unlike RcnR, the Ni^{II} coordination complex in InrS may well be four-coordinate square planar, which would provide some intrinsic specificity for Ni^{II} (Figure 12D). Moreover, InrS is the only Ni/Co specific sensor crystallized to date and is thus far unique among CsoR-family members in that it has been shown to repress the expression of genes encoding Ni^{II} efflux transporters, while promoting the expression of Ni^{II} uptake genes.[119] These functional characteristics of InrS permitted a detailed study of the relationship between intracellular metal bioavailability and metal sensor metal affinity in *Synechocystis* cells that provides critical support for our current understanding of the metallostasis set point model (Figure 8A).[119] The Ni^{II}/Co^{II} specificity of NcrB and NreA has been inferred from their regulation of nickel resistance determinants;[380,382] however, detailed biochemical and structural studies are needed to evaluate the extent and molecular basis of metal selectivity in these repressors, and what features distinguish them from an RcnR or an InrS.

3.2.4.3. RSS Sensors. Candidate thiol persulfide (RSSH) sensors constitute the largest group of sequences from the CsoR superfamily. The most well-studied groups of CstR (CsoR-like sulfurtransferase repressor) proteins is represented by the founding member *S. aureus* CstR found largely in Gram-positive organisms (Firmicutes).[363,383] The structure of pneumococcal CstR reveals that the two Cys found on opposite subunits within the dimer unit are characterized by long intersubunit Sγ-Sγ distances (7−9 Å), mediated in part by a "wedge' residue N55, which defines a x-C-**N**-C "W-X-Y-Z" motif (Figure 12E). This structure provides a rationale for the observed low Cu^{I} binding affinity and enhanced nucleophilicity that prevents crosstalk with the copper sensor CsoR in the same *S. aureus* cytoplasm.[239] A mass spectrometry-based kinetic profiling method performed with a variety of oxidants, including cysteine persulfide (CSSH),[384] reveals a striking asymmetry of *trans*-persulfidation within each CstR dimer unit within the tetramer, with one side of the dimer reacting and ultimately closing to a cross-linked product far faster than the opposite side of the dimer.[239] Although reactivity profiles of even closely related CstRs are distinct from one another, a per- or polysulfidated monomer is formed rapidly, on pathway, in all cases. This suggests that the key feature that controls RSS specificity is the enhanced nucleophilicity of the attacking (N-terminal) Cys, which is distinct from persulfide sensors of the ArsR family, e.g., SqrR, which Cys nucleophilicity is lower (Section 3.2.2.4). CstR, unlike SqrR, reacts rapidly with H_2O_2 *In vitro* to form the disulfide-cross-linked species, but sluggishly with GSSG.[239]

The lack of a characterized H_2O_2-specific CsoR-family sensor prevents a detailed side-by-side evaluation of the oxidant specificity of a *bona fide* RSS and ROS sensor, limiting our understanding of inducer specificity in this structural class of repressors. It is interesting to note, however, that these regulators can function cooperatively with other transcriptional regulators that respond to related sulfur-containing species. For example, it was shown *Bl*YrkD that is encoded in an operon alongside a two-component system that has been proposed to respond to extracellular H_2S.[383] The largely uncharacterized *S. coelicolor* CsoR (CstR)[385] and a mycobacterial protein, *Mt*Rv1766[203] also harbor two conserved Cys of a CstR, adopting a x-C-x-C "W-X-Y-Z" motif; a functional role in RSS sensing is consistent with a genomic neighborhood that encodes for distinct sulfide or sulfite detoxification enzymes.[239] These sensors do not conserve the wedge Asn (N) residue, which suggests that these proteins may well perform oxidative chemistry with a distinct profile of sulfur-containing donors, as yet unknown.

3.2.5. CopY. The copper-specific metallosensor CopY (Figure 13A) is a member of the methicillin and β-lactam

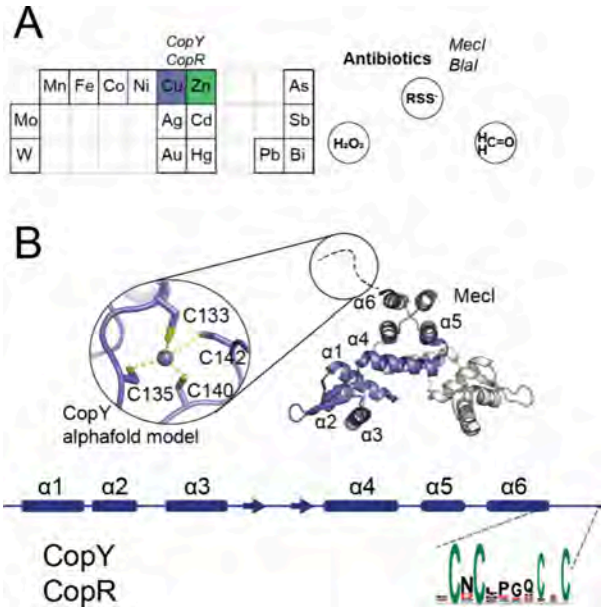

Figure 13. CopY family proteins. A) Abbreviated periodic table showing the metals and reactive species (shaded) known to be sensed by CopY proteins. The four-letter designations for individual proteins that perform the function listed in the nearby box are shown. B) Ribbon representation of antibiotic sensing *Sa*MecI dimer protein (1OKR)[397] with close up view of an Alphafold2-modeled Cu^{I} metal binding site from CopY. Conserved primary structural features of CopY metal binding homologues are shown.

repressor (MecI/BlaI) family as a result of its high sequence similarity in the N-terminal DNA binding domain and an identical cognate DNA operator sequence.[386] The DNA-binding domain adopts a canonical winged-helical domain like that found in ArsR, MerR and MarR repressor families, as determined by NMR spectroscopy.[387] The C-terminal domain functions as both the regulatory and the dimerization domain and is of unknown structure.[388] CopYs differ from MecI and BlaI by the presence of a C-terminal unstructured extension

https://doi.org/10.1021/acs.chemrev.4c00264
Chem. Rev. 2024, 124, 13574−13659

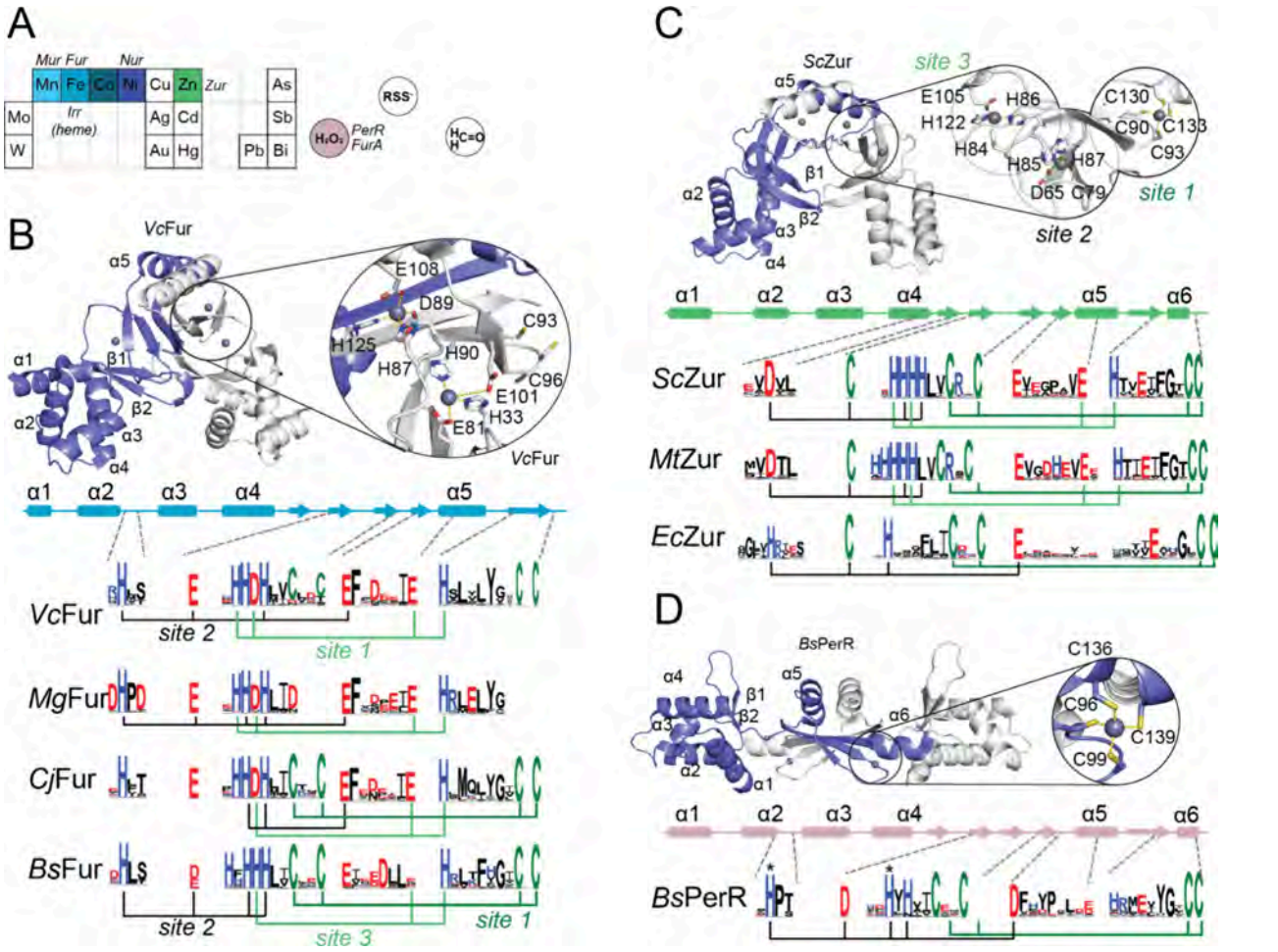

Figure 14. Fur family proteins. A) Abbreviated periodic table showing the metals and reactive species (shaded) known to be sensed by Fur proteins. The four-letter designations for individual proteins that perform the function listed in the nearby box are shown. B) Ribbon representation of *Vc*Fur (2W57)[416] with close-up view of the metal binding sites. Conserved primary structural features of different Fur proteins with the different metal binding sites indicated in brackets are shown. C) Ribbon representation of *Sc*Zur (3MWM)[414] with a close-up view of the metal binding sites. Conserved primary structural features of different Zur proteins with the different metal binding sites indicated in brackets. D) Ribbon representation of *Bs*PerR (2FE3)[417] with a close-up view of the structural metal binding site only. Conserved primary structural features of different PerR proteins with the different metal binding sites indicated in brackets.

appended to the C-terminal domain that harbors a conserved $CXCX_4CXC$ motif, or less frequently, a single CXC motif that is known to coordinate Cu^I or Zn^{II} in distinct coordination geometries and stoichiometries (Figure 13B).[389] CopYs regulate Cu^I efflux via P_{1B-1} ATPase CopA and the oxidative stress response in a small number of bacterial pathogens from closely related Firmicutes, derived from the *Lactococcus, Streptococcus* and *Enterococcus spp.*[200,390−392] CopY-type regulators are experimentally validated copper sensors in *E. hirae*,[200] *Enterococcus faecium*,[393] *L. lactis* IL1403,[391] *Streptococcus mutans*,[386] *Streptococcus pneumoniae*,[390] *Streptococcus pyogenes*,[176] *Streptococcus suis*[394] and *Streptococcus gordonii*.[395]

Remarkably, CopYs bind both Cu^I and Zn^{II} with opposite functional outputs. A single Zn^{II} per dimer is coordinated tetrahedrally to the CxC-containing CopY, and is an allosteric activator of DNA binding required for full repression of the *cop* operon in the absence of Cu^I stress; as Cu^I levels in the cell rise, two Cu^I displace the single Zn^{II} to form an $S_4{-}Cu_2$ cluster that impairs DNA binding.[251] Ion mobility mass spectrometry and SAXS of *Sp*CopY reveals that $S_4{-}Cu_2$ cluster formation leads to conformational instability and protein aggregation, possibly favoring DNA dissociation.[251,396] The distinct functional output of Zn^{II} vs Cu^I is a unique feature of CopYs, which allow the organism to exploit repressor metal promiscuity to facilitate bacterial survival to copper and zinc toxicity. While the impact of Cu regulation on the crosstalk between Zn and Mn has been investigated in other CopY-encoding bacteria,[176] it remains unclear whether the mechanistic proposal described for *Sp*CopY characterizes other members of this group of repressors.

3.2.6. Fur. The ubiquitous Fur family proteins have evolved to sense all first-row, late *d*-block divalent metal ions with the exception of Cu^{II}, and one specific reactive oxygen species, hydrogen peroxide (Figure 14A). Fe^{II}-sensing Fur and namesake of the family is a global regulator that integrates the control of metallostasis of Mn^{II} vs Fe, in particular, with other oxidative stressors. This is because Fe^{II} in the presence of even small amounts of H_2O_2 results in the generation of the biomolecule-damaging hydroxyl radical (OH•) via Fenton chemistry which becomes catalytic in the presence of cellular reductants, and catastrophic for cellular function. All Fur superfamily proteins are homodimers (some are tetrameric) where each protomer is characterized by an N-terminal winged helix-turn-helix DNA-binding domain and a C-terminal dimerization domain that are connected by a flexible hinge region. This "hinge" occurs just N-

https://doi.org/10.1021/acs.chemrev.4c00264
Chem. Rev. 2024, 124, 13574−13659

terminal to a conserved $HHxHx_2Cx_2C$ motif formally located in the C-terminal domain in the vicinity of the β2 and β3 strands (Figure 14B).[398,399] In general, one or more His in the HHxH motif are ligands to the metalloregulatory sites (sites 2 and 3; site 3 is not present in all Furs), with the Cx_2C motif forming the N-terminal half of a tetrathiolate (S_4) site 1, paired with another Cx_2C sequence at or very close to the C-terminus of each protomer (Figure 14B-D). Site 1 is a structural site which is nearly always occupied by Zn^{II}, whose integrity stabilizes the dimer. Although site 1 can form a [2Fe-2S] cluster that is reported to play a role in iron sensing in cells, the significance or generality of this finding among Fur-family proteins is not yet clear.[400]

Fur family members harbor one (site 2) or two (sites 2, 3) metalloregulatory sites (Figure 14B) whose affinity for cognate metal is tuned so as to be maximally responsive to intracellular changes in bioavailable metal (Figure 8). When site 3 is present, this allows a "graded" or fine-tuned response to cellular metal status, which generally expands the range of metal concentrations over which the sensor is responsive.[401,402] Fur proteins in general bind to a palindromic A/T-rich sequence found in the promoters of regulated genes using a metal cofactor as a corepressor (Figure 6A, *middle*).[205] Metal coordination in the regulatory site causes a change in the structure and dynamics of the repressor that promotes and stabilizes its interaction with DNA,[403] although the details if allostery in most Fur proteins remain unclear.[399,404]

The Fur family, like the MerR and CsoR families, provides an excellent illustration of how transition metal selectivity can be tuned by evolving a single primary metal sensing site (site 2) to adopt distinct coordination numbers and geometries optimized to mediate a metal-selective allosteric response (Figure 14B-D). Indeed, the presence of several Fur family proteins in the same organism is rather common, consistent with the idea that they can function independently of one another, while possessing a sufficient degree of specificity for their cognate coregulatory metal as predicated by the set-point model (Figure 8). However, crosstalk among Fur paralogs has been observed, for example in the biosynthesis, efflux and uptake of the broad-spectrum metallophore staphylopine in *S. aureus*, which are cooperatively regulated by both Fur and Zur.[405,406] Similarly, there are several examples of partially overlapping regulons,[208,399,407] suggesting a tight interconnectivity between metal balance and the resistance to oxidative stress. Indeed, Fur mismetalation may allow Fur to function as a signaling "hub" that globally integrates control of metallostasis and a response to other stresses.[399,401,408−411] Indeed, a regulatory function for apo-Fur has been demonstrated[412] reinforcing the idea that every differentially ligated state of Fur may drive a distinct regulatory output. This is in fact a central tenet of the ability of Fur proteins to orchestrate a graded response to increasing degrees of cellular metal limitation, where differentially metal-ligated states differentially repress the expression of downstream genes as metal levels incrementally fall in the cell.[252,413−415]

3.2.6.1. Fe^{II}-Sensing Fur. Fur proteins that function as Fe^{II} sensors have been described in many pathogenic and non-pathogenic Gram-positive[418] and Gram-negative bacteria.[409,410,419−425] Early structural work on *Pa*Fur[426] and *Vc*Fur[416] revealed that Fe^{II} and other divalent metals could allosterically activate DNA binding by altering the metalation status of one or both of the two regulatory sites observed (Figure 14B). These two Fur proteins, like *Mg*Fur, appear to lack what is now regarded as the canonical S_4 structural site 1, like that found in *Cj*Fur and *Bs*Fur, or that site if present, is simply devoid of metal (Figure 14B). It is the case that the double Cx_2C sequence motif of a canonical S_4 site 1 is present in most Fur sequences, which when metalated with Zn^{II}, behaves as an apoprotein (not activated to bind DNA).[252] Regardless, the conservation and interdigitated nature of the residues that form coordination bonds to one or the other regulatory site (site 1 in these structures corresponds to site 3 in other Furs with the S_4 site) allows for a significant degree of plasticity in the coordination chemistry. Indeed, the identity of the donor ligands and the coordination geometry in each site differs among the X-ray structures solved with the same or different divalent metals, e.g., Zn^{II} in *Pa*Fur,[426] *Cj*Fur[404] and *Vc*Fur;[416] and Mn^{II} in *Mg*Fur.[425] Moreover, the regulatory impact of two observed metal sites may well differ among individual Fe^{II}-sensing Furs. For example, in *Vc*Fur, metal occupancy of site 2 only by Mn^{II}, Zn^{II} and Fe^{II},[416] but not Ni^{II},[427] promotes DNA binding regardless the identity of the metal in site 1 (site 3). In contrast, *Mg*Fur site 1 (site 3) has been shown to be essential for DNA binding and site 2 was proposed to be only fine-tune DNA binding affinity.[425] How distinct Fe^{II}-sensing Furs are wired for distinct allosteric connectivities is not yet understood but remains an interesting unresolved question.

3.2.6.2. Zn^{II}-Sensing Zur Proteins. The zinc uptake regulator (Zur) is a ubiquitous Fur-family metalloregulator that represses transcription of the genes that encode proteins involved in Zn^{II} homeostasis, including high affinity transporters that mediate zinc uptake, metal allocation, low zinc paralogs and other physiological processes, depending upon the organism (Sections 4-5).[428−430] *Ec*Zur,[431] *Bs*Zur[413] and *Ab*Zur[432] harbor only two Zn^{II} sites per protomer corresponding to the canonical S_4 structural site 1 and a regulatory site 2, while *Mt*Zur[433] and *Sc*Zur[414] each contain three sites per protomer, adding site 3, the presence of which is proposed to allow for the "graded" zinc deficiency response.[413,414] It is remarkable in fact, that the central stretch of four consecutive His residues in *Mt*Zur[433] and *Sc*Zur[414] alternate by forming coordination bonds to site 2 and site 3, on opposite sides of the same β-strand. In all cases, the Zn^{II} ions are tetrahedrally coordinated (Figure 14C). Zur proteins are readily distinguished from Fur proteins by the presence of a Cys in the N-terminal region of the β2 strand, which roughly defines the hinge point between the N- and C-terminal domains which plays a key role in allostery;[432] however, it remains unclear the extent to which these differences in sequence can easily explain the differences in metal binding preferences, particularly in those regulatory sites that impact DNA binding. While some Zur proteins bind DNA only in the presence of Zn^{II} ions,[330,434,435] others showed Zur−DNA binding in the presence of Zn^{II}, Mn^{II}, and Cd^{II}, which again suggests that the cellular milieu enforces a metal specificity profile (Figure 8) that cannot be recapitulated by simple *In vitro* experiments.[436]

Recent work reveals that some Zur proteins harbor a pair of regulatory Zn^{II} sites distinct from the central $HHxHx_2Cx_2C$ motif (*vide supra*) that stabilizes an oligomeric assembly of three or more Zur dimers on the promoters of genes encoding cognate metal *efflux* transporters, leading to RNA polymerase recruitment and activation of transcription when metal levels become very high.[437−440] This regulatory mechanism thus integrates repression of uptake transporters and up-regulation of efflux transporters over a very large range of metal activity using a single regulator, allowing for a coordinated cellular response to extreme metal toxicity.

https://doi.org/10.1021/acs.chemrev.4c00264
Chem. Rev. 2024, 124, 13574−13659

3.2.6.3. Hydrogen Peroxide Sensor PerR. PerR is the master regulator of peroxide stress in many Gram-positive organisms and is functionally equivalent to the thiol-containing OxyR (Section 3.2.13) encoded by most Gram-negative bacteria, with only a few exceptions.[441,442] PerR is an Fe^{II} binding protein that forms a six-coordinate Fe^{II} structure with five protein-derived ligands (site 2) and an open coordination site that accommodates the binding of H_2O_2. The first structure of a PerR protein solved by X-ray crystallography corresponded to apo-PerR-Zn from *B. subtilis*, in which the structural S_4 site 1 was occupied by Zn^{II} (Figure 14D).[417] When peroxide binds to the regulatory Fe^{II} complex, metal-catalyzed oxidation triggers the incorporation of one atom of oxygen into one of the His in site 2 (either H36 of H91 in *Bs*PerR sequence,[443] labeled with a star in Figure 14D).[444−447] Histidine oxidation weakens the affinity of PerR for Fe^{II} and thus dissociates from the DNA with the loss of its corepressor. The structural changes induced in PerR upon loss of the regulatory remain unresolved, although it seems unlikely that the loss of the metal creates a "splayed out, open" conformation (Figure 14D).[417] The PerR regulatory site binds Fe^{II} and Mn^{II} and both function as corepressors; however, only Fe^{II} can carry out the oxidative chemistry. Thus, the functional responsiveness of PerR to peroxide stress is tuned to the cellular Mn^{II}:Fe^{II} ratio, which is in part governed by Fe^{II}-sensing Fur.[443] The mechanism underlying the peroxide selectivity by PerR relative to Fur remains incompletely understood, but replacement of E108 in β2 by Asp as found in PerRs to create E108D *Bs*Fur makes it sensitive to H_2O_2.[448]

3.2.6.4. Other Fur Regulatory Proteins. There are a number of Fur family regulators that integrate responses to other transition metal ions, including Mur[449−451] and Nur,[452,453] both of which appear to sense Mn^{II}, and Irr, which is a heme-based sensor.[454,455] Although microbial physiology studies suggest metal or metallocofactor-specific responses, there are significant data that show that metalation with various metals can promote DNA binding *In vitro*. These observations reinforce the idea that our understanding of metal specificity in Fur proteins remains limited, and must be developed beyond the simple model of a single cognate metal corepressor.

3.2.7. DtxR. DtxR (Diphtheria toxin repressor) family proteins form a phylogenetically conserved group of Fe^{II}-and Mn^{II}-regulated repressors prevalent largely in GC-rich Gram-positive bacteria and archaea, evolutionarily distinct from, but functionally analogous to, Fur family proteins (Figure 15A).[456,457] DtxR family of proteins are characterized by an N-terminal DNA-binding domain, an interfacial domain which contains two metal-binding sites, and a third C-terminal SH3 (Src homology 3)-like domain not present in all DtxR family crystal structures.[458,459] The second domain is comprised of three helices, organized as a pair of three-helix bundles from each protomer and is thus responsible for homodimerization and regulatory metal site binding. SH3-like domains are structurally like eukaryotic SH3 domains, which mediate protein−protein interactions in many signaling proteins,[460,461] but have no detectable sequence similarity with them.

3.2.7.1. Fe^{II}-Sensing IdeR/DtxR. IdeR (Iron-dependent repressor) regulates the expression of genes that encode proteins involved in the acquisition and storage of iron. These include siderophore production and transport, iron transporters, ferritins and bacterioferritins, as well as proteins involved in iron−sulfur cluster assembly and metabolic enzymes that harbor Fe cofactors.[211,458,459,463−465] While Fe^{II}−IdeR represses iron uptake, it activates the expression of iron storage genes.[463] IdeR/

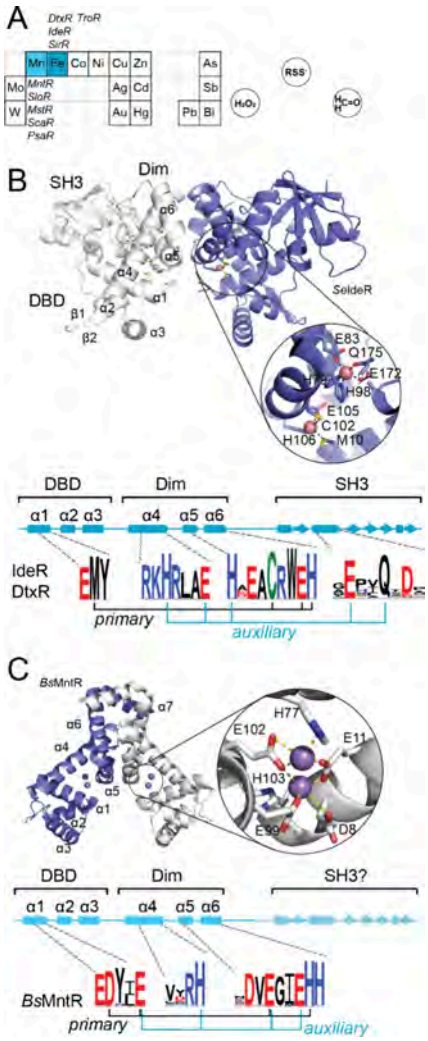

Figure 15. DtxR family proteins. A) Abbreviated periodic table showing the metals and reactive species known to be sensed by DtxR family are colored. The four-letter designations for individual proteins that perform the function listed in the nearby box are shown. B) Ribbon representation of *Se*IdeR protein (7B1 V)[459] with a close-up view of the primary metal binding site and auxiliary site. Conserved primary structural features of different IdeR proteins with the different metal binding sites indicated in brackets. C) Ribbon representation of *Bs*MntR (1ON1)[462] with a close-up view of the primary and auxiliary metal binding sites shown. Conserved primary structural features of different MntR proteins with the different metal binding sites indicated in brackets.

DtxR proteins play other roles beyond controlling iron homeostasis and in *M. tuberculosis* and *C. diphtheriae* are required for full virulence;[456,463] in the actinomycete *Streptomyces avermitilis*, IdeR regulates morphology and cellular metabolism.[465] While several IdeR homologues are known to respond specifically to Fe^{II},[465−467] *Cd*DtxR responded equally well to Fe^{II} and Mn^{II} when expressed in *Bacillus subtilis* (an organism that employs Fur to sense iron).[468] Reconciling *in vivo* selectivity for Fe^{II} with *in vitro* promiscuity remains a challenge.[212,459,469] For example, the binding of DtxR to the Tox operator *In vitro* is activated by a range of divalent metal ions, including Co^{II}, Fe^{II}, Mn^{II} and Ni^{II}, whereas Zn^{II} shows only weak activation.[470] Each IdeR subunit contains two metal-binding sites, each adopting octahedral coordination geometries, with the so-designated "primary" site characterized by

https://doi.org/10.1021/acs.chemrev.4c00264
Chem. Rev. 2024, 124, 13574−13659

a larger impact on IdeR activity; however, both primary and "auxiliary" sites must be occupied for full IdeR activity, and the auxiliary site has higher metal binding affinity (Figure 15B).[469,471−473] In both metal binding sites, the metal coordination sphere is completed by a water ligand (not visible in all structures, but likely always present).[458] To date only one structure of a bacterial IdeR protein activated by its physiological effector Fe^{II} is available.[459] However, structures of fully metalated, full-length bacterial DtxR/IdeR proteins show the same metal-binding sites and coordination geometry regardless whether a cognate or noncognate metal is used.[458,459,474] Selectivity for Fe^{II} over Mn^{II} may be enhanced by the presence of two sulfur ligands (M10 and C102) in the primary Fe^{II} site, since the corresponding MntR Mn^{II}-sensing site contains an aspartate or asparagine in place of M10 and a glutamate in place of C102 (Figure 15C). Introducing the IdeR-specific metal ligands to an MntR protein and *vice versa* switches or broadens the metal responsiveness of the respective variant in cells.[468] While IdeR can bind Mn^{II} it does not strongly activate DNA binding, as it is likely not bound to the primary site.[469,473] On the other hand, crosstalk with Zn^{II} homeostasis has been noted.[475] It has been proposed that due to the high Zn^{II} binding affinity to the primary site, only the auxiliary site would be filled with Fe^{II} *in vivo* with the other bound by a noncognate metal, most likely Zn^{II}; if true, this scenario is precisely analogous to what has been described for sites 1 and 2 in Fur proteins (*vide supra*).[458]

3.2.7.2. Mn^{II}-Sensing MntR. Structural and functional studies of Mn^{II}-specific DtxR family sensors are more limited that of the Fe^{II} responsive DtxR family proteins. Most of what we know about the metal selectivity of a Mn^{II}-sensing DtxR protein comes from *Bs*MntR. *Bs*MntR forms noncognate metal complexes with Fe^{II}, Zn^{II} and Co^{II}, that are mononuclear, rather than binuclear Mn^{II} complex, and do not allosterically activate DNA operator binding (Figure 15C).[462,476] Early structural work on *Bs*MntR revealed that the metal-binding pocket was substantially distinct from that of DtxR, with the two metal binding sites physically closer, sharing two bridging ligands, and including two water molecules, allow for heptacoordination of the Mn^{II} ions (Figure 15C).[462] Other Mn^{II} sensing DtxR family proteins such as *S. pneumoniae* PsaR are also known employ two regulatory metal sites to activate DNA binding, with Zn^{II} in the primary site and Mn^{II} in the auxiliary site.[477] A more recent study of the *Deinococcus radiodurans* Mn^{II} sensor DR2539 revealed additional metal binding sites and new insights into DNA operator recognition by these Mn^{II} sensors.[478] Other Mn^{II}-dependent transcriptional repressors from the DtxR family have been described to have an impact on pathogen virulence (Figure 15A).[456,477,479−482] This is an exciting area of future study since Mn^{II}-specific DtxRs are found broadly in Gram-positive and Gram-negative bacteria.[458]

3.2.8. NikR. NikR proteins are obligate homotetramers with a central C-terminal metal-binding domain (MBD) connected by flexible linkers to two peripheral N-terminal DNA-binding domains (DBDs) that adopt a ribbon-helix-helix fold.[483] NikR proteins sense the bioavailability of nickel only, which allosterically activates high affinity DNA binding and complex formation with the promoters of regulated genes (Figure 16A). While *H. pylori* NikR has been shown to act as both a repressor and as an activator of diverse genes that share a weak consensus in their promotor sequences,[484] *E. coli* and *Pyrococcus horikoshii* NikRs are known only to repress Ni^{II}-specific ABC-type importers under Ni^{II}-replete conditions.[213,485] The nearly 30 high resolution crystal structures of NikRs in various allosteric

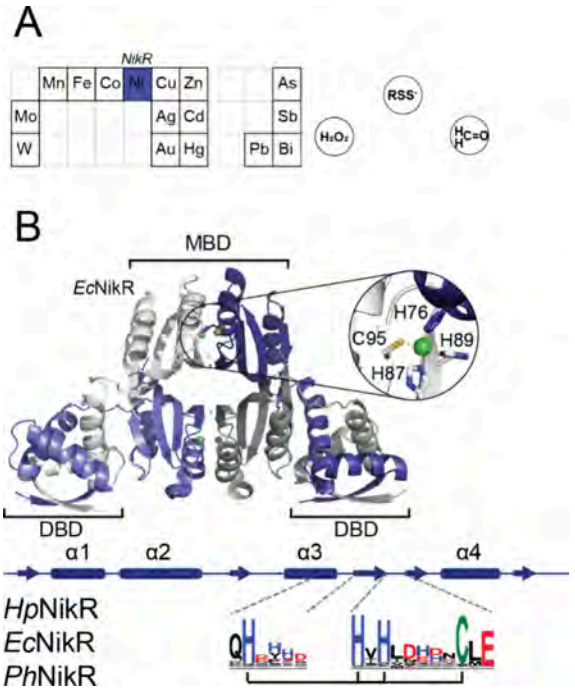

Figure 16. NikR family proteins. A) Abbreviated periodic table showing the metals and reactive species known to be sensed by NikR (shaded). B) Ribbon representation of *Ec*NikR (2HZV)[134] with close-up view of the Ni^{II} coordination complex. Conserved primary structural features of different NikR proteins with the primary metal binding site indicated by the brackets.

states reveal four symmetry-related conserved square planar His_3Cys Ni^{II} coordination complexes per tetramer that promotes a conformational change to a closed conformation competent for DNA binding (Figure 16B; Figure 6A).[134,214,485−490] This coordination geometry allows for picomolar affinity for Ni^{II} as measured by chelator competition assays.[491,492] Since NikR also binds other divalent metals, the biological Ni^{II} selectivity arises here from a precise control of allosteric coupling to DNA binding (Figure 8A) and K_d^S (Figure 8B). Noncognate metal ions Zn^{II} and Co^{II} bind with different affinities and stoichiometries, and form non-native coordination geometries and ligand sets that do not support a metal-mediated allosteric response.[491,493] A recent study suggests that Ni^{II}-specific binding couples an allosteric network of residues at an interface between the DNA binding and metal binding domains (Figure 16B), which in turn, appears to result in an increase in protein rigidity, locking NikR in a DNA binding-active conformation.[490]

NikR thus provides an exceptional illustration of the importance of metal coordination geometry as a key feature of cognate metal sensing by a metalloregulatory protein, since if mis-metalation occurs, it does so without triggering a transcriptional response. It is interesting to note that while there is no evidence of regulatory crosstalk with other metal ions, *Hp*NikR also responds to changes in pH which is consistent with its role as a global regulator in that organism. Here, NikR binds DNA with high affinity in the acidic environment *H. pylori* encounters in the human stomach, even in the absence of nickel.[494,495] Both nickel and lower pH activate *Hp*NikR to bind to the *ureA* promoter with similar affinities and locations on the DNA,[495] but the mechanism of allosteric regulation of DNA binding by acidity remains unknown.

https://doi.org/10.1021/acs.chemrev.4c00264
Chem. Rev. 2024, 124, 13574−13659

3.2.9. Rrf2. Rrf2 repressors are dimers consisting of an N-terminal DNA-binding "winged helical" domain composed of five helices and two β-strands, and a C-terminal helical dimerization domain dominated by a long helix, and thus superficially resemble MerR-family activators (Section 3.2.3).[216,496−498] The two domains are connected by an unstructured linker where the inducers and cofactors are bound. Rrf2 family repressors regulate sulfate reduction (Rrf2),[499] iron−sulfur cluster biogenesis (IscR),[216,500] cysteine metabolism (CymR),[496,501,502] iron homeostasis (RirA),[215,503,504] catechol iron uptake-coupled quinone detoxification (SifR),[246] redox balance/oxidative stress (RsrR,[497,505] HypR,[506] SaiR[507]), and the sensing of NO and reactive nitrogen species via a [4Fe-4S] cluster (NsrR) (Figure 17A).[498,508,509]

Functionally characterized members of the Rrf2 family can be broadly divided into two groups. One group utilizes an Fe−S cluster as the sensory module,[510] while the other contains one or a pair of Cys residues that sense reactive oxygen or reactive electrophile species.[507] The prototypical Rrf2-family repressor is proteobacterial IscR, an Fe−S cluster regulator that contains a 2Fe−2S cluster ligated by three Cys and one His and controls the biogenesis of Fe−S clusters in cells.[216,500,511] The chemical nature of the Fe−S cluster differs depending on the small molecule inducer. While RsrR harnesses the same IscR-like 2Fe−2S cluster as a sensory module for redox sensing (Figure 17B),[509] RirA[512] and NsrR[513] utilize a 4Fe−4S cluster to detect iron limitation and nitric oxide, respectively (Figure 17C). The cluster coordination chemistry appears to be remarkably variable. *Ec*IscR is unique,[500] while RsrR uses one His, one Glu, and two Cys as cluster ligands (Figure 17B).[497] RirA utilizes three Cys as cluster ligands,[503] while NsrR employs three Cys and one Asp as cluster ligands (Figure 17C).[498] Studies on *Tp*IscR reveal that different homologues of IscR employ different ligand sets, despite what is likely the same function in surveilling the Fe−S status of the organism (Figure 17B). It is important to note that while many biochemical studies provide support for the disparate structure of these Fe−S clusters in Rrf2 proteins, crystallographic structures have only been reported for holo-NsrR[498] and RsrR.[497]

The diversity in allosteric mechanisms of the Fe−S-containing members of Rrf2 family proteins is also of high interest. While IscR binds DNA in the apo-form and activates transcription,[514] Fe−S cluster formation in IscR, RsrR, NsrR and RirA leads to high-affinity DNA binding and repression, with subsequent chemistry leading to DNA operator dissociation and transcriptional derepression.[216,497,503,509,513] For example, in RirA, oxidation of the cluster by molecular oxygen leads to cluster disassembly and DNA dissociation, which allows RirA to function as a redox sensor.[504] In contrast, the one electron oxidation of the Fe−S cluster in RsrR leads to a ring-flip of the conserved Trp9 that appears necessary and sufficient to induce DNA dissociation; this allows RsrR to elicit specific transcriptional responses to cellular redox imbalance (Figure 17B).[497] Similarly, NsrR utilizes the 4Fe−4S cluster as a NO-sensing module; here, NO displaces Asp8 as a cluster ligand, destabilizing the cluster and thus leading to DNA dissociation (Figure 17C).[498,513]

The chemistry and allosteric mechanisms of Rrf2 proteins that do not coordinate an Fe−S cluster is comparatively less well understood, complicated by the fact the degree of Cys conservation in the sensory module is rather low. However, most characterized thiol-reactive proteins harbor at least one reactive Cys, modification of which modulates DNA binding affinity (Figure 17D). In the case of *Sa*CymR, the reactive Cys is in the wHTH domain itself, and not in the sensory module; here, H_2O_2-promoted sulfenylation has been proposed to trigger DNA dissociation (Figure 17D).[515] This Cys however is not conserved among other CymR proteins that are also thought to be redox sensors.[496,501,502] *Ba*SaiR also responds to H_2O_2 likely through a similar mechanism,[507] while *Sa*HypR appears to react

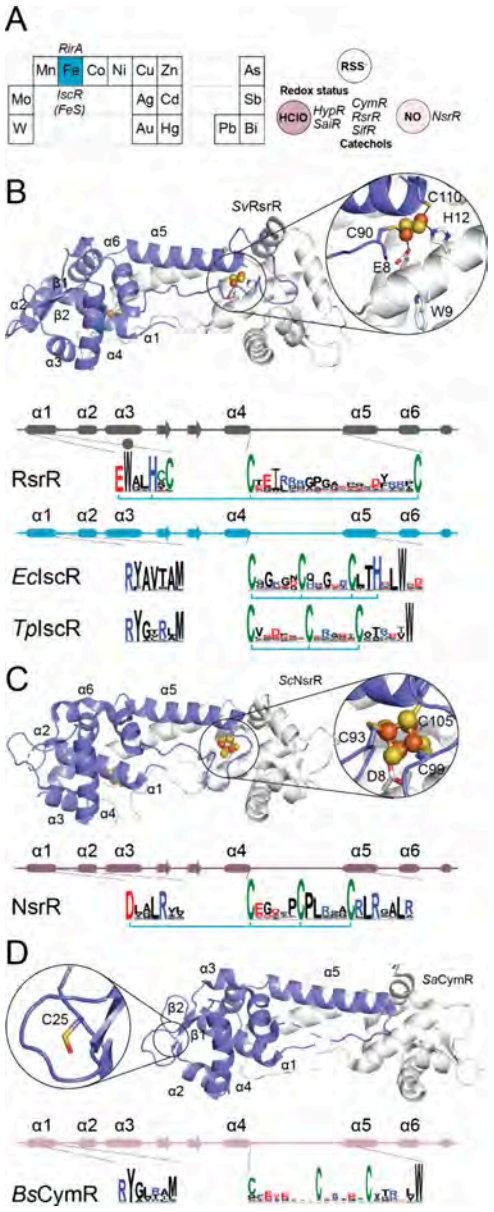

Figure 17. Rrf2 family proteins A) Abbreviated periodic table showing the metals and reactive species known to be sensed by Rrf2 family are colored. The four-letter designations for individual proteins that perform the function listed in the nearby box are shown. B) Ribbon representation of *Sv*RsrR (6Y42), with a close-up view of the [2Fe-2S] cluster site.[505] Conserved primary structural features of different RsrR-family proteins with the primary iron sulfur cluster site indicated by the brackets. C) Ribbon representation of *Sc*NsrR (5N07), with a close-up view of the [4Fe-4S] cluster site.[498] Conserved primary structural features of different NsrR-family proteins with the primary iron sulfur cluster site indicated by the brackets. D) Ribbon representation of *Sa*CymR (3T8T), with a close-up view of the reactive cysteine.[515] Conserved primary structural features of different CymR-family proteins that are also thought to function as redox sensors.

https://doi.org/10.1021/acs.chemrev.4c00264
Chem. Rev. 2024, 124, 13574−13659

selectively with hypochlorous acid (HClO) and does not react with H_2O_2.[506] The most recent member of this thiol-containing subgroup of Rrf2 proteins to be characterized is the streptococcal IscR-like family transcriptional repressor (SifR). SifR uses a single conserved Cys to react with quinones which are potent cellular electrophiles.[246] These quinones are thought to originate with the oxidation of simple catechols brought into the cell as chemically diverse coordinately unsaturated Fe^{III}–catecholate complexes through PiuBCDA. *S. pneumoniae* does not encode Fur or other global Fe regulator due to relatively modest Fe quota; the SifR-regulon seems to allow *S. pneumoniae* to meet its needs for nutritional Fe while avoiding quinone toxicity.[516]

3.2.10. GntR. Many GntR superfamily proteins regulate the expression of enzymes involved in the metabolism of sugar acids,[517−519] fatty acids, amino acids and cofactors, generally orchestrating a response to the nutrient and morphological status of the organism.[520,521] They harbor an N-terminal winged helix-turn-helix DNA-binding domain and a C-terminal effector-binding and oligomerization domain often denoted FCD (FadR C-terminal domain);[518] the C-terminal domain is the differentiating feature of well-characterized bacterial regulators, including FadR, HutC, MocR, YtrA, AraR, and PlmA subfamilies.[518,522] A small number of GntR family proteins have been shown to be metal-responsive regulators, notably *M. smegmatis* GfcR, a global regulator that responds directly or indirectly to external copper stress by regulating the expression of a number of membrane-associated transporters (Figure 18A).[523] It has been proposed that ≈70% of GntR proteins maintain a conserved, high binding site for Zn^{II}.[217] This metal binding site is buried at the bottom of a solvent accessible cavity, where it facilitates the binding of small organic acids that harbor a carboxylate group in a way that is required for transcriptional regulation (Figure 18B).[217,524−526] The small molecule effector that induces allosteric regulation of DNA binding has only been identified for a handful of sugar-sensing GntR proteins, namely GntR from *B. subtilis* (*D*-gluconate), LldR from *Corynebacterium glutamicum* (L-lactate),[525] GguR from *Polaromonas sp.* (5-keto-4-deoxy-*D*-glucarate/galactarate),[527] and DgoR (*D*-galactonate),[528] ExuR (*D*-galacturonate and *D*-glucuronate) and UxuR (*D*-glucuronate and *D*-fructuronate) from *E. coli*.[529] The extent to which metal binding is regulatory in this family of proteins or functions simply a structural cofactor that enables molecular recognition of the cognate small molecule effector remains an open question, and a subject for future studies given the ubiquitous nature of this protein superfamily in bacteria.[519]

3.2.11. MarR. MarR proteins are triangularly shaped homodimers that share a winged-helical DNA-binding domain connected to a DNA-distal all-α-helical dimerization domain. Members of this protein superfamily share the same winged-helical DNA-binding fold of ArsRs but harbor an additional C-terminal (α6) helix positioned in the dimer interface that dramatically alters the quaternary structure of the homodimer relative to ArsR family repressors (Figure 19A-B).[530−532] Canonical MarRs that repress the expression of drug efflux pumps may bind antibiotics or other small organic molecules leading to the transcriptional depression of the genes associated with an adaptive response to antibiotic stress, e.g., efflux systems.[533] Individual MarR members have been shown to bind a diverse range of ligands at a cleft between the dimerization and DNA-binding domain,[534−543] as well as to different sites on the dimer;[537,544−546] likewise, oxidation-sensing cysteine residues are also found in distinct positions within the dimer (Figure 19A).[547−556] This functional diversity of biological outcome and inducer recognition among MarR proteins stands in striking contrast to a relatively common derepression mechanism where either ligand binding or cysteine oxidation leads to DNA dissociation (i.e., allosteric inhibition, $\Delta Gc > 0$; Figure 6B).[532,557−559] It has been argued that the ancestral role of MarR family proteins was to maintain physiological homeostasis by sensing and derepressing the expression of genes encoding efflux pumps for both toxic metabolites as well as unnatural xenobiotics.[560] The structural versatility required to accommodate binding of a broad range of ligands to different sites coupled with the wide distribution of oxidation-sensing Cys residues and low overall sequence similarity among MarR regulators, collectively suggest a model where ligand binding induces a conformational change in the homodimer that cannot be explained by a single sensing site and accompanying pathway of allosteric communication. MarR proteins are thus reminiscent of ArsR-family repressors in this regard (*vide supra*).[139]

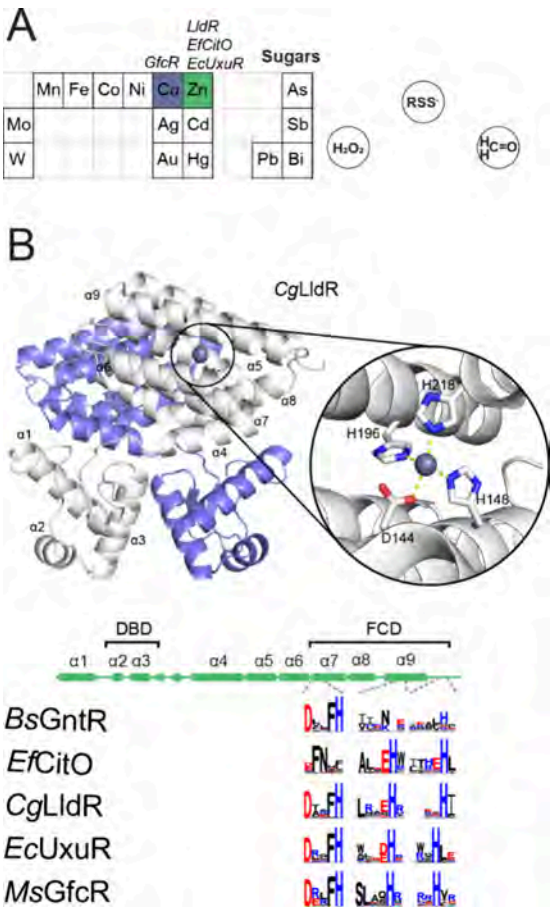

Figure 18. GntR family proteins. A) Abbreviated periodic table showing the metals and reactive species known to be sensed by GntR family are colored. The four-letter designations for individual proteins that perform the function listed in the nearby box are shown. B) Ribbon representation of *Cg*LldR protein (2DI3)[525] with a close-up view of the primary Zn^{II} binding site. Conserved primary structural features of different GntR proteins with the disinct metal sites indicated in the text.

3.2.11.1. Zn^{II}-Sensing MarRs. Zn^{II}-sensing MarRs are the only characterized metalloregulatory proteins from this very large superfamily, while also constituting an exception to the rule of allosteric *inhibition* of DNA binding as a general feature of MarR proteins. MarR family metallosensors are thus far restricted to regulators of Zn^{II} uptake,[561−563] exemplified by

https://doi.org/10.1021/acs.chemrev.4c00264
Chem. Rev. 2024, 124, 13574−13659

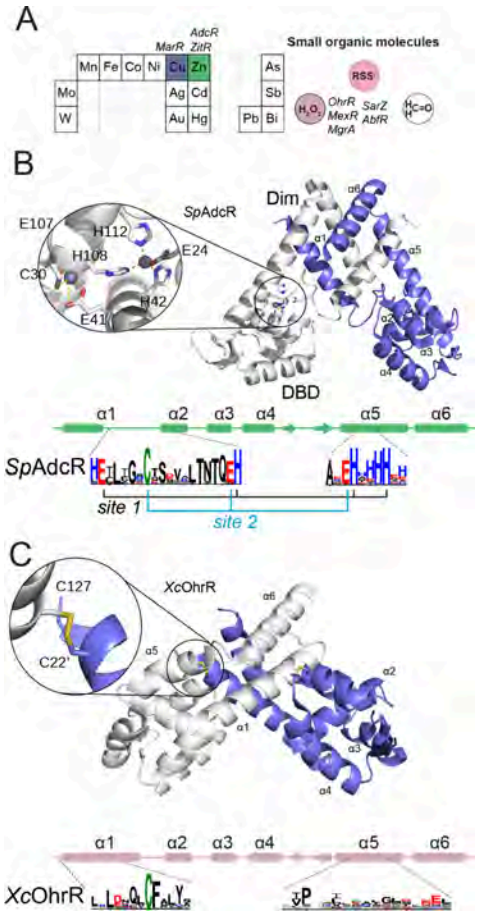

Figure 19. MarR family proteins. A) Abbreviated periodic table showing the metals and reactive species (shaded) known to be sensed by MarR proteins. The four-letter designations for individual proteins that perform the function listed in the nearby box are shown. Ribbon representation and conserved primary structural features of B) *Sp*AdcR protein (3TGN)[218] with a close-up view of the two Zn^{II} binding sites indicated by brackets; C) *Xc*OhrR protein (2PFB)[553] with a close-up view of the disulfide cross-link that results from ROS sensing.

AdcR (adhesin competence regulator) from *S. pneumoniae* and closely related *Streptococcus* and *Lactococcus* sp. exemplified by *L. lactis* ZitR (Figure 19B).[141,563−569] AdcR and ZitR possess two physically proximate pseudotetrahedral Zn^{II} binding sites that bind Zn^{II} with very different affinities.[133,218] A detailed structural study of *Ll*ZitR showed that the binding to Zn^{II} occurs sequentially with a graded effect on the DNA binding affinity.[568] Zn^{II} is an allosteric *activator* of DNA operator binding, in strong contrast to all other members of the MarR superfamily, consistent with its biological function as uptake repressor at high intracellular Zn^{II}. It is interesting to note that Zn^{II} coordination sites employ ligands from an unstructured region between the first two α-helices that for all other MarR regulators is part of a longer α2 helix (Figure 19B−C). All characterized metalloregulators of this family have been shown to bind DNA only in the metal-bound form and they all share this unstructured region, which is characterized by enhanced flexibility in the subns time scale in AdcR in the apo-state.[141,218,566−569] It has been proposed that introduction of this dynamic element during the course of MarR protein family evolution may have enabled allosteric *activation* in this molecular scaffold where metals bind as a corepressors (Figure 6A, *middle*).[141] The extent to which this allosteric activation model characterizes other metal-sensing MarR proteins yet to be characterized is unknown.[570]

3.2.11.2. Oxidation-Sensing MarRs. In many MarRs, cysteine oxidation is known to occur in distinct sites on the molecular scaffold, dependent on the nature of the stressor (Figure 19C). While SarZ, MgrA, AbfR and OhrR share a conserved cysteine in the N-terminal DNA binding domain that can become sulfenylated,[547,549,551,553,556] the identity of the nonconserved resolving Cys, as well as the Cys pair for other cysteine-based regulators from the MarR family differ.[534,571] Alternatively a resolving Cys may not be present at all, with *S*-thiolation or mixed disulfide formation with an abundant low molecule weight thiol the regulatory switch for DNA binding.[550] In any case, while the degree of crosstalk among different reactive species that signal through MarRs has not been fully elucidated, it is interesting to note that OhrR and MexR have been shown to perform chemistry with sulfane sulfur donors, including thiol persulfides in *P. aureuginosa*.[552,572] Furthermore, *Ec*MarR has been shown to respond to increased levels of Cu^{II},[534,573] which results in Cys oxidation and disulfide bond formation to create tetramers that have lost the ability to bind DNA. The extent to which this Cu^{II}-dependent regulatory modelas proxy for localized bursts of oxidative stress, functions in other MarRsrequires further study.

3.2.12. TetR. The tetracycline repressor (TetR) family, like the MarR family described above, is widely associated with antibiotic resistance and the regulation of genes encoding small molecule exporters.[574] TetRs, however, play a far more widespread regulatory role in metabolism, controlling the expression of genes involved in central carbon metabolism, antibiotic production, quorum sensing, and many other aspects of prokaryotic physiology. There are more than 700,000 proteins identified as TetRs to date and more than 500 high-resolution structures have been deposited in the Protein Databank (PDB). Canonical TetRs are all-α-helical proteins that function as ligand-mediated, homodimeric repressors, where each subunit harbors an N-terminal, three-helix bundle (α1−α3) within which is the helix-turn-helix (HTH) DNA binding motif. The HTH motif is followed by a large C-terminal regulatory domain (α4−α9) that incorporates a number of independently evolved ligand binding cavities that are readily accessible from the side, front, or top of the homodimer.[574,575]

While many TetRs function as repressors that provide cellular resistance against hydrophobic antibiotics and detergents, the few metalloregulator proteins and inorganic sensors described to date have distinct allosteric mechanisms of transcriptional control (Figure 20A). On the one hand, the large hydrophobic inducer-binding pocket in a canonical TetR regulator has been repurposed by the heme-regulated transporter regulator from *L. lactis* (HrtR) to bind heme tightly and induce DNA dissociation leading to transcriptional derepression of a heme-efflux system.[576,577] On the other hand, Cys thiol-based TetR sensors have been described that react with a wide variety of small molecule electrophiles. For example, *E. coli N*-ethylmaleimide reductase repressor (NemR) utilizes a cysteine-lysine sulfenamide thiol switch to sense HClO;[578] furthermore, a recent report suggests that an *Enterobacter* sp. protein may be induced by binding of organoarsenic compounds and chromium to a three Cys site.[579] *S. aureus* glucose-induced biofilm accessory protein A (GbaA) utilizes a dithiol pair to respond to oxidative and electrophile stress, however, the identity of the *in vivo* inducer is as yet unknown.[580,581] While there are no TetRs reported to date that can be induced by persulfides, a recent

https://doi.org/10.1021/acs.chemrev.4c00264
Chem. Rev. 2024, 124, 13574−13659

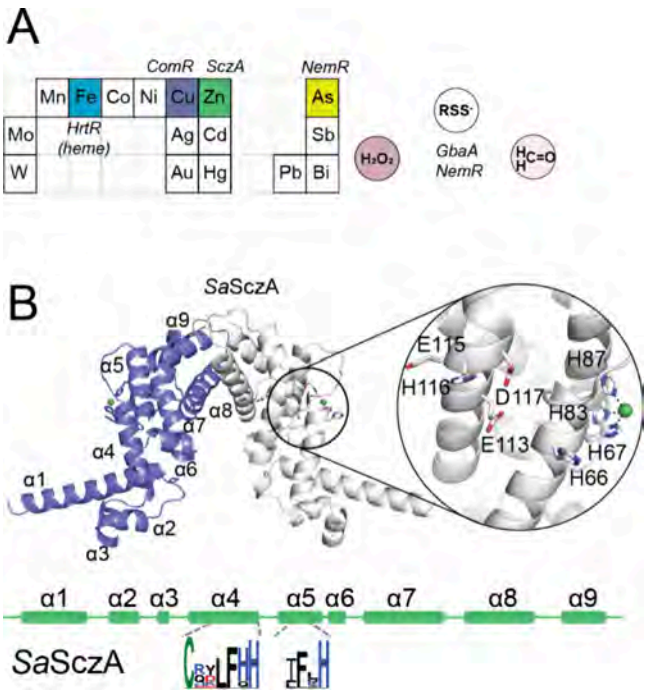

Figure 20. TetR family proteins. A) Abbreviated periodic table showing the metals and reactive species known to be sensed by TetR family are colored. The four-letter designations for individual proteins that perform the function listed in the nearby box are shown. B) Ribbon representation of *Sa*SczA protein (3KKC) with a close-up view of the primary Zn^{II} metal binding site region.[220] Conserved primary structural features of different TetR proteins with distinct metal sites.

report suggests that a TetR encoded in *Gordonia sp*. regulates biodesulfurization processes in the presence of organosulfur compounds.[582] While the objective of this singular study was to evaluate this sensor in an eventual application for the removal of sulfur in petroleum fractions, the reported results suggest that this regulator may react with sulfane sulfur-containing oxidants.

The clearest example of a TetR-family metallosensor is the transcriptional activator of the *S. pneumoniae* Zn^{II} efflux system, SczA, and related activators from other streptcocci (Figure 20B).[583] SczA activates the expression of the gene encoding the Zn^{II} efflux transporter, CzcD, upon metal binding to two pairs of metal sites per dimer, one with a tetrahedral coordination geometry and one with an octahedral geometry.[220] It is interesting to note that the crystal structure available from an SczA homologue was crystallized with Ni^{II} (likely obtained from the purification buffer). The identification of the true cognate metal inducer requires detailed studies of metal affinities[584] and a thorough characterization of the transcriptional response in cells.[220] Although the mechanism of transcriptional activation of SczA is not yet fully understood, this likely involves recruitment of RNA polymerase to SczA-regulated promoters in a Zn^{II}-dependent fashion. In any case, the community has taken full advantage of the ease with which metal-dependent transcriptional activation can be obtained with SczA, in both synthetic biology and routine molecular biology applications.[585] The footprint of TetR family inorganic sensors might not be restricted to heme and Zn^{II}, as a putative Cu-responsive TetR has been identified as ComR in *Escherichia coli*.[586,587] Although ComR is involved in the Cu stress response in some way, direct Cu^{I} or Cu^{II} binding by ComR has not yet been reported.

3.2.13. LysR. The LysR-type transcriptional regulators (LTTR) are named for the lysine repressor, LysR, which regulates lysine biosynthesis and is representative of the largest family of transcriptional regulators in prokaryotes.[588] LTTRs are involved in the transcriptional regulation of genes involved in central metabolism, amino acid biosynthesis, cell division, fermentation, photosynthesis, nitrogen fixation, oxidative stress, quorum sensing, motility, transport of Na^{I}, symbiosis, and virulence.[588] Members of this family possess the same two domain-based molecular architecture of other regulators discussed here, i.e., GntR and TetR, an N-terminal all-helical DNA binding domain and C-terminal globular ligand binding domain. While most characterized LysR members respond to effector molecules such as amino acids or intermediate metabolites, some members can be described as metal-loregulators, since they are involved in regulation of inorganic species uptake (ModE)[589,590] or harness thiol chemistry analogous to that described above for dithiol sensors that sense H_2O_2 (OxyR)[221,591] and/or persulfides (LasR)[592] (Figure 21A).

E. coli OxyR is the prototypical redox-responsive LTTR that mediates transcriptional activation of an oxidative stress regulon in response to nanomolar hydrogen peroxide.[593−595] OxyR exploits cysteine sulfenylation chemistry to affect transcriptional activation of the expression of target genes. OxyR can also respond to superoxide and nitrosative stresses, although these functions are presumed to be ancillary to its primary role as H_2O_2 sensor.[589,590] Crystallographic evidence for the H_2O_2-sensing mechanism of *Corynebacterium glutamicum* OxyR (Figure 21B) identified key residues for the peroxidatic reduction of H_2O_2 and the formation of a disulfide bond that triggers a transcriptional response by altering the OxyR interacton for the promoter region.[596] Similarly, the quorum sensing master regulator from *Pseudomonas aeruginosa* PAO1 LasR binds to its target DNA and activates transcription upon modification by a sulfur-based oxidant, e.g., a thiol persulfide, which first forms a C188 persulfide or polysulfide moiety, ultimately resulting in a pentasulfide linkage between Cys201 and Cys203.[592] However, in this case, installation of this modification does not impact the affinity of LasR for its target DNA operator, but makes it several-fold more effective in activating transcription in both *In vitro* and *in vivo* assays. Since the identities of the reactive Cys residues in the peroxide sensor OxyR and the sulfane sulfur sensor LasR are similar, the structural mechanism of oxidant specificity remains unresolved.

Metallosensors identified for this family are limited thus far to the sensing of the oxyanion molybdate (Mo^{VI}) by ModE, which represses the transcription of Mo^{VI} uptake system in *E. coli* and other bacteria.[221,591] Crystal structures of both apo- and molybdate-bound forms of ModE[597] reveal that the molybdate binding to the C-terminal domain alters the relative orientation of the N-terminal DNA binding domains from each protomer, allosterically activating the ModE homodimer to bind DNA (Figure 21C). The C-terminal regulatory domain of ModE is actually two subdomains, each corresponding to a Mop sequence similarity region. The first Mop subdomain harbors the molybdate binding site, where R128, S126 (SARN segment), S166, and K183, with the assistance of T163 and A184, form the binding pocket for the oxyanion. ModE shares the conservation of two cysteines separated by 8−13 residues in the C-terminal domain with OxyR/LasR, which enable the formation of a disulfide bridge in response to oxidants in these regulators.

https://doi.org/10.1021/acs.chemrev.4c00264
Chem. Rev. 2024, 124, 13574−13659

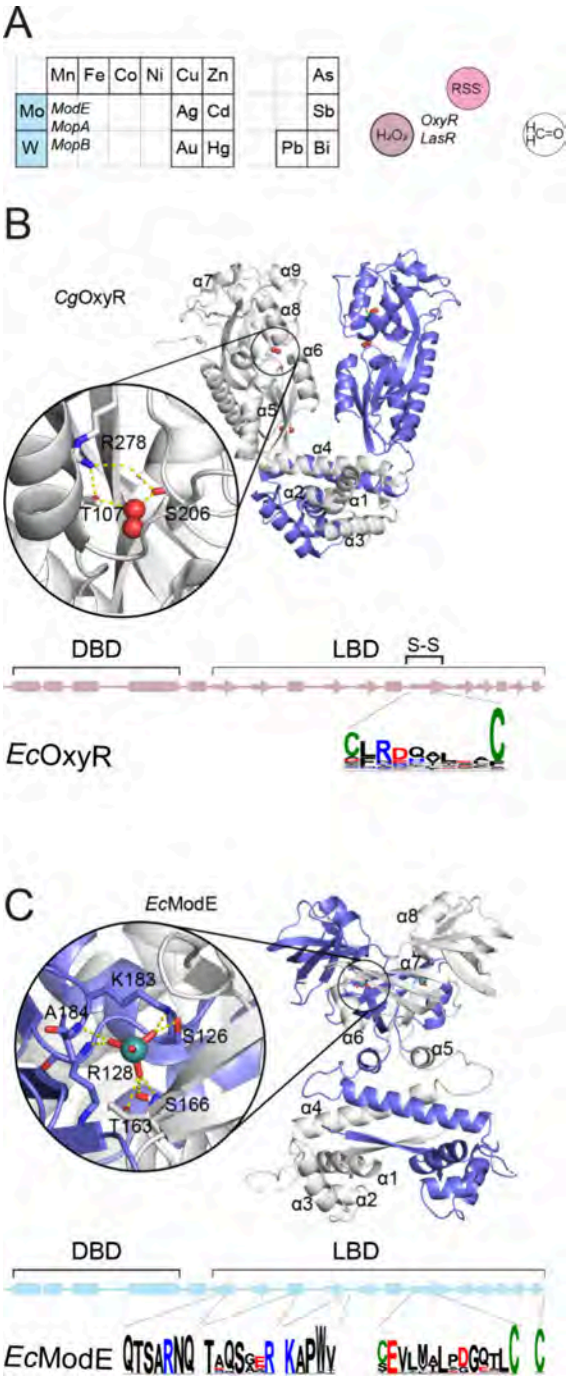

Figure 21. LysR family proteins. A) Abbreviated periodic table showing the metals and reactive species (shaded) known to be sensed by LysR proteins. The four-letter designations for individual proteins that perform the function listed in the nearby box are shown. B) Ribbon representation of *Cg*OxyR (6G4R) with a close up view of the H_2O_2 binding site. Conserved primary structural features of different regulator LysR proteins with the different ligand binding sites indicated in the text.[596] C) Ribbon representation of *Ec*ModE (107L) with a close-up view of the molybdate binding site shown.[221]

While no LTTR is as yet known to bind transition metals directly,[588] the remarkable diversity of the family, the difficulties identifying the cognate effector and the clear role of dithiol chemistry suggest that it is possible that metalloregulatory LysR activators may yet be discovered or evolved for the development of novel biosensors for metal ion monitoring.

3.3. RNA-Based Metalloregulators

3.3.1. Overview. Metalloriboswitches,[598] are highly structured, chameleon-like regulatory RNA domains found within the 5′ noncoding or untranslated region (UTR) of protein-coding mRNAs. The binding of a ligand, a specific metal, metal complex or other inorganic anion, to the aptamer domain alters the folding of the RNA, and thus expression of a downstream gene. More than 55 distinct classes of natural riboswitches have been discovered in the past 20 years. The discoveries of inorganic element-sensing riboswitches have revealed that RNAs harness the power of supramolecular chemistry, functional dynamics and coordinate-covalent bonding to achieve a metal selectivity profile that rivals that of metalloregulatory proteins, albeit sometimes with lower sensitivities (K_d^S; Figure 8).[229,599] While some extant riboswitches might be direct descendants of the RNA-based sensors and switches that may have been present in ancient organisms before the emergence of proteins,[229] in existing bacteria they are often paired with a metalloregulatory protein, endowing an organism with the ability to expand the range of metal bioavailability that is sensed, as dictated by their often weaker affinities (Figure 8A). More work is needed to provide support this conclusion, however.

Inorganic riboswitches thus far described are known to sense transition metal ions,[226,228,600−602] fluoride anion[603] and other ions including the alkali metals Li^I and Na^I, and the alkaline earth metals Mg^{II} and Ca^{II} (Figure 22A).[150,226,604] Here we aim to discuss molecular insights into metalloriboswitch metal selectivity from atomic structures, and how the physiological "division of labor" between these RNA elements and metalloregulatory proteins might be orchestrated. It should be noted that the metalloriboswitches thus far characterized represent only a small fraction of the ≈10,000 riboswitches that have been proposed to exist in modern organisms;[229,599] thus, this picture of metal selectivity and specificity may well change as new insights emerge. An interesting observation is that small organic molecule-sensing riboswitch pairs are capable of functioning as canonical logic gates in cells;[605] the extent to which metalloriboswitches function in this way, perhaps in concert with protein partners, is not yet known.

3.3.2. B_{12}- and Moco-Sensing Riboswitches. The adenosylcobalamin (AdoCbl) riboswitch represents the first high-resolution structure of a transition metal or organometallic cofactor bound to a riboswitch.[227] Here, AdoCbl recognition is accomplished largely through shape complementarity between the RNA and the ligand, thus highlighting the role that supramolecular chemistry plays in molecular recognition (Figure 22B). More recent studies show that the cobalamin-sensing riboswitch RNAs as a class is capable of sensing and responding to multiple derivatives of vitamin B_{12}, collectively termed corrinoids.[608] The exquisite corrinoid specificity of these RNAs is achieved by shape complementarity that is highly sensitive to distinct conformational features of individual B_{12} variants.

The mechanism of metallocofactor recognition of corrinoids shares similarities to Moco (molybdenum cofactor)-sensing RNA motifs known to respond to Mo- and W (tungsten)-containing compounds broadly identified in γ-Proteobacteria, δ-Proteobacteria, Clostridia, Actinobacteria, Deinococcus-Thermus species and environmental DNA samples.[600] Interestingly, the Moco-sensing RNA motifs are present downstream of the operator-promoter regions of genes regulated by molybdate-bound ModE (Figure 21), including the high affinity molybdate transporter, *modABCD*.[221] Both protein-based and RNA-based

https://doi.org/10.1021/acs.chemrev.4c00264
Chem. Rev. 2024, 124, 13574−13659

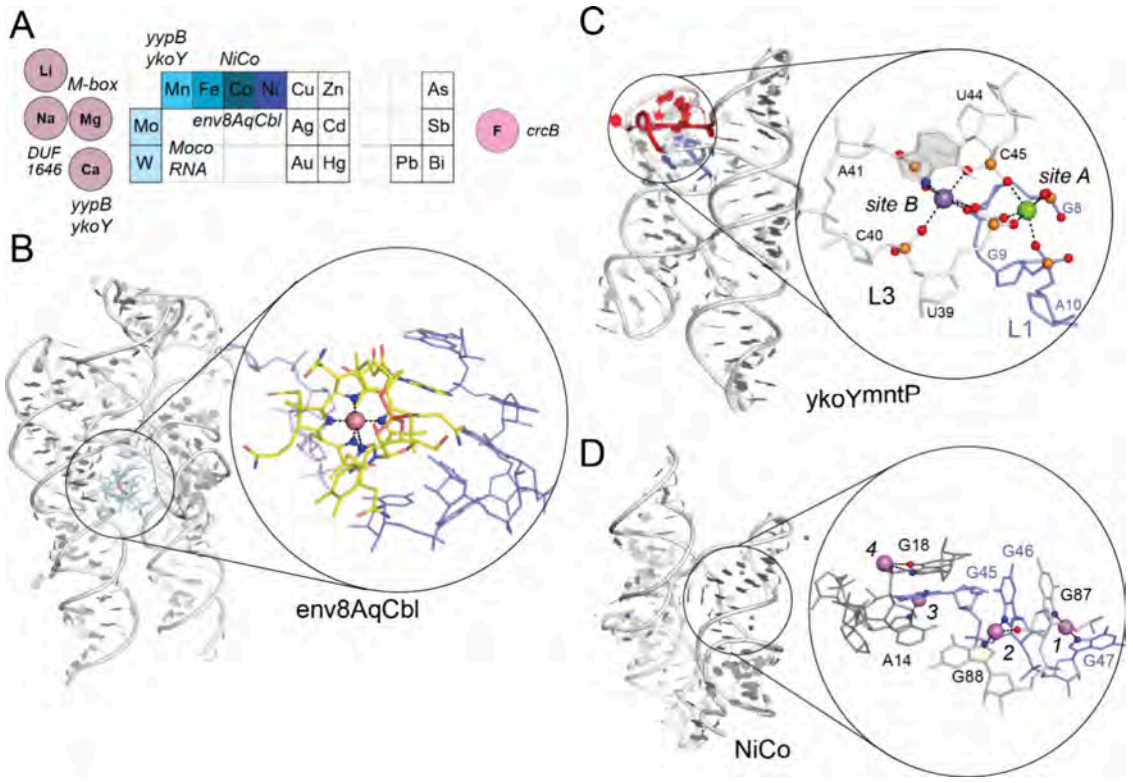

Figure 22. RNA-based metalloregulators. A) Abbreviated periodic table showing the metals and other elements (shaded) known to be sensed by inorganic riboswitches. The designations for individual RNAs that perform the function are listed near the box shown. B) Structure of cobalamin riboswitch in marine metagenome with close up view of the aquo-adenosylcobalamin binding site (4GMA).[227] C) Structure of Mn^{II}-sensing riboswitch from *Lactococcus lactis* (*Ll ykoY*) bound to Mg^{II} (site A) and the Mn^{II} (site B) (4Y1I).[606] D) Structure of NiCo riboswitch from *Erysipelotrichaceae* bacterium with a closeup view of the four Co sites (4RUM).[224] Metal site 4 was later shown to play no regulatory role and is not occupied in solution studies.[607]

regulatory mechanism collectively ensure sufficient molybdate supply to biosynthesize Moco, an "expensive" cofactor. This highly conserved RNA, of unknown structure, effectively discriminates against closely related analogues of Moco, which is also triggered by the analogous tungsten cofactor (Tuco). Although clearly connected to cellular metallostasis, corrinoid and Moco sensing is dictated by specific interactions with the organic cofactor rather than specific contacts with the metal ion itself. This mode of molecular recognition also contrasts with most metalloriboswitches, which combine the influence of supramolecular chemistry and "soft" ligand (nitrogen) coordination chemistry to create coordination complexes that bind transition metals selectively while outcompeting cell-abundant Mg^{II}, required to fold these complex polyanionic and globular RNA structures. This is highlighted by the crystal structures of the Mn^{II}-sensing (Figure 22C)[609] and Ni^{II}/Co^{II}-sensing riboswitches (Figure 22D).[224]

3.3.3. Mn^{II}/Ca^{II}-Sensing Riboswitches. The discovery of a Mn^{II}-sensing riboswitch was driven by genetic experiments first carried out in *Salmonella*,[225] but the chemical selectivity remained speculative until the structure of the *E. coli yybP-ykoY* orphan riboswitch in complex with both Mg^{II} and Mn^{II} was reported in 2015 (Figure 22C).[609] The Mn^{II} coordination chemistry in this structure suggests that that metal selectivity is achieved largely by a single "soft" coordination bond to the N7 of an invariant adenosine (A41), as the only inner-sphere Mn^{II} contact (Figure 22C). Indeed, when A41 is substituted by U41, the structure contains only Mg^{II} ions. On the other hand, the slow (millisecond) conformational dynamics of the Mn^{II}-sensing *yybP-ykoY* aptamer RNA revealed by single-molecule fluorescence energy transfer (smFRET) spectroscopy suggests that conformational selection, i.e., where Mn^{II} "selects" a Mg^{II}-stabilized "closed" conformation of the RNA, is an important component of metal ion selectivity.[610,611] These findings reveal how these highly structured and complex RNA motifs harness the conformational ensemble to stabilize distinct ligand-bound forms of the RNA, thus enhancing the affinity of what would otherwise be weak coordinate-covalent bonds.

A follow-up study of distinct *yybP-ykoY* mRNA sequences posited that the selectively of this RNA for Mn^{II} could be traced to the structure of the Mn^{II} chelate itself, which resembles the heptacoordinated Mn^{II} complex in the Mn^{II}-sensing protein repressor, *B. subtilis* MntR (Figure 15C).[612] However, the long coordination bonds and relatively modest resolution of the Mn^{II}-bound *yybP-ykoY* riboswitch structure casts doubt on this conclusion. What is more significant from this work is that the *yybP-ykoY* riboswitch Mn^{II} binding affinity (in a background of physiological Mg^{II}) is at least 10-fold weaker than the reported affinity of the Mn^{II}-sensing repressor MntR, a finding that parallels analogous experiments in *S. pneumoniae* with the Mn^{II}-sensing repressor PsaR and the *yybP-ykoY* riboswitch RNA.[226,477] These physiological studies are consistent with a model where riboswitches sense higher bioavailable concentration of Mn^{II} than is sensed by their counterpart protein metalloregulators, and thus likely function as a fail-safe "on" signal to prevent Mn^{II} toxicity by high cellular Mn^{II}.[226]

Interestingly, the *S. pneumoniae yybP-ykoY* riboswitch RNA that regulates *mgtA* expression binds and responds to Ca^{II} in the

https://doi.org/10.1021/acs.chemrev.4c00264
Chem. Rev. 2024, 124, 13574−13659

presence of millimolar Mg^{II}, stabilizing a compact state that elicits the same transcriptional response *in vitro* with *E. coli* RNA polymerase.[226] However, Ca^{II} is not as strong an inducer of *mgtA* transcription *in vivo* as Mn^{II}, and the extent to which Ca^{II} efflux by MgtA is beneficial for this respiratory pathogen during an infection is not known. Nonetheless, MgtA is most closely related to the P_{2A}-type ATPase, human SPCA1, known to efflux both Mn^{II} and Ca^{II} (Section 5.3.1.1) with the coordination structures of these two metal complexes now known (see Figure 54, below). Thus, while the metal selectivity of the riboswitch appears to match that of the regulated efflux pump, the functional significance of Ca^{II} binding by this riboswitch in bacteria is not yet fully understood.

3.3.4. Ni^{II}/Co^{II}- or Fe^{II}-Sensing Riboswitches. The NiCo riboswitch was originally discovered and functionally characterized in *Clostridium botulinum* and *Erysipelotrichaceae bacterium (Eba)* cultured in the presence of Co^{II}.[224] This riboswitch is found in the 5′ UTR of the *czcABC* mRNA in these organisms, which encodes a periplasm-spanning metal efflux "gun" in Gram-negative bacteria, and is generally considered to mediate resistance against Cd^{II}, Zn^{II} and Co^{II} (*czc*) toxicity.[613,614] Thus, these initial findings were broadly consistent with a regulatory scenario that is analogous to the *yybP-ykoY* riboswitch described above (Section 3.3.3).

However, one puzzling feature of this initial work is that the binding affinity for Ni^{II} and Co^{II} ions are in the low micromolar range,[224] which is significantly less sensitive than the corresponding Ni^{II}- and Co^{II}-sensing metalloregulatory proteins that have affinities in the (sub)-nanomolar range of bioavailable metal (Figure 8A).[204,270,615,616] Indeed, more recent studies reveal that this NiCo class of metal-responsive riboswitches is overrepresented in obligate anaerobes and has recently been shown to exhibit a robust response to Fe^{II} (but not Fe^{III}), a conclusion reached through use of a fluorescent-sensing derivative of the NiCo riboswitch.[228] Iron responsiveness was initially missed because cells were cultured aerobically, where Fe^{II} is rapidly oxidized to insoluble Fe^{III}.[224] An RNA-based fluorescent sensor based on the NiCo RNA aptamer to detect bioavailable Fe levels in *E. coli* cells suggests that the K_d is actually tuned to known bioavailable Fe^{II} pools buffered in the low μM range (Figure 8A).[228] It has therefore been proposed that *czcD* riboswitches primarily respond to physiological Fe^{II} to mitigate iron toxicity, rather than Co^{II} and Ni^{II}.[228,602] The transition metal selectivity of the NiCo riboswitch remains unsettled and more work is clearly warranted here.

In any case, the structure of the Co^{II}-bound NiCo riboswitch reveals four Co^{II} binding sites that likely nucleate formation of a four-way junction stabilized by a network of contacts that may explain how cooperative binding of Co^{II} ions to adjacent sites might be achieved (Figure 22D).[224,607] This structure reveals at least seven inner sphere Co^{II} coordination bonds with nucleobase nitrogen atoms, while the supramolecular chemistry of the folded RNA drives a cooperative metal binding that must contribute to fine-tuning of the regulatory response to these metals in cells. More comprehensive metal-binding studies of NiCo riboswithces from *Eba* and *Listeria monocytogenes* reveal a metal binding stoichiometry of three in solution, with metal site 4 (Figure 22D) playing no regulatory role, and likely an artifact of the high Co^{II} concentration used in the crystallographic experiments.[607]

3.3.5. Other Inorganic Metalloriboswitches. The first crystallographic structure of a metal-sensing RNA riboswitch of any kind was the *B. subtilis* Mg^{II}-sensing riboswitch positioned upstream of a Mg^{II} uptake transporter.[150] This ubiquitous Mg^{II}-sensing "off" riboswitch is thought to make a major contribution to cellular Mg^{II} homeostasis in most bacterial cells.[121] Consistent with this, the metal binding affinity for Mg^{II} and noncognate cations are all weak, in the millimolar range, which ensures a Mg^{II}-specific response as this is the only metal in the cell that reaches millimolar bioavailability (Figure 8A). This is the case despite that fact that the folding of this RNA could be induced *In vitro* by many different divalent metal cations.[150]

The ligand-bound structure of the *Thermotoga petrophila* fluoride-sensing riboswitch reveals that inorganic riboswitches are not necessarily restricted to positively charged metal ions. Here, the bound fluoride is encapsulated within a junctional architecture, anchored through direct coordination to three Mg^{II} ions, which in turn are octahedrally coordinated to water molecules and five inwardly pointing backbone phosphates.[617] The selectivity of this riboswitch is unparalleled as it readily discriminates against other larger halides; as such, it has been used to develop a highly specific F^- biosensor for water analysis.[618]

More recently, a new riboswitch class, exemplified by the DUF1646 motif, was characterized to selectively sense Na^I and regulate the downstream expression of sodium and calcium transporters among other genes relevant to sodium biology.[604] Interestingly, these Na^I riboswitches exhibit dissociation constants in the low mM range, and show no response to any other alkali and alkaline earth group metal. It has been proposed that bacterial cells exploit the specificity of these Na^I-specific riboswitches alongside the c-di-AMP-sensing riboswitches to coordinate gene expression in order to mount an osmotic stress response. The structure of this riboswitch is as yet unknown but promises many surprises.

3.4. Biotechnological Applications of Metalloregulatory Systems

3.4.1. Overview. The fast-growing field of synthetic biology sees biological systems as toolboxes to be deconstructed into "parts" for subsequent repurposing. In that sense, the capacity of a regulatory "circuit" that leverages the ability of the "one-component" transcriptional regulators discussed here (Section 3.2) to sense a specific metal stimulus makes them ideal sources of diverse parts. At its most basic level, a biosensor is composed of a sensory module, which selectively detects a target analyte of interest, and a reporter module that produces a detectable output (Figure 23A). Among the myriad of possible sensory parts (functional DNA, RNA, transcription factors, enzymes, antibodies) the metalloregulatory systems discussed here have emerged as the "gold standard" for rapid and sensitive metal detection, as a result of their desirable sensitivity and selectivity profiles.[230−232]

3.4.2. Utility and General Features of an Allosteric Transcription Factor. A major application of metalloregulator-based biosensors is to assess water quality, as the chemical contamination of drinking water remains a challenging analytical problem to which these biosensors might provide useful solutions. Securing global access to clean and safe drinking water is one of the main technological challenges today.[619] Benchmark technology currently used to assess water quality must be performed by experts with expensive equipment in specialized laboratories, limiting the geographical reach of water surveillance campaigns worldwide. In the last decades of the 20th century[233] biosensors have been proposed as an inexpensive, easy to use, field-deployable, and highly sensitive

https://doi.org/10.1021/acs.chemrev.4c00264
Chem. Rev. 2024, 124, 13574−13659

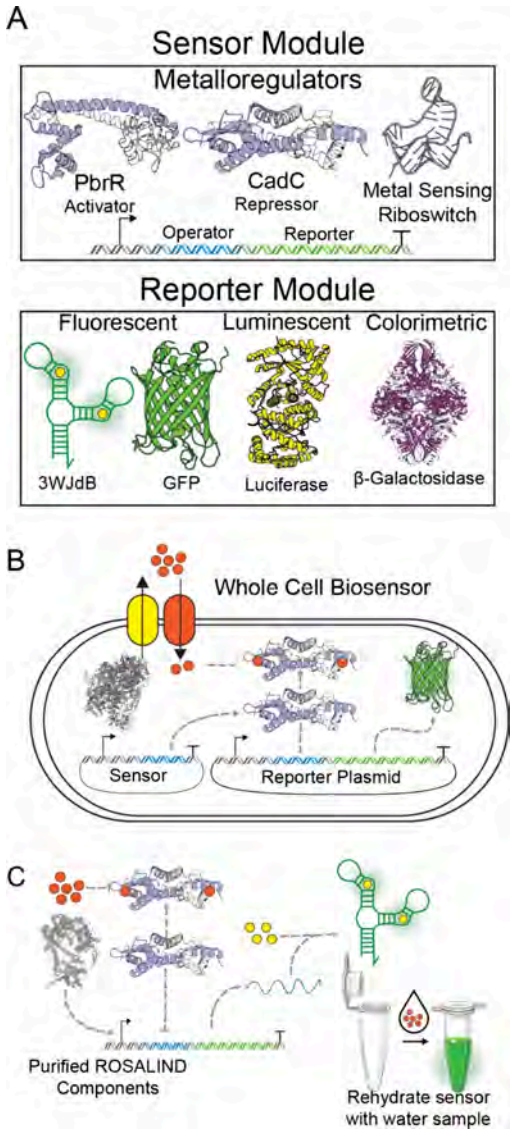

Figure 23. Transcription and transcription-translation based biosensors. A) Components of the sensor and reporter modules, these parts can be employed in both WCB and cell-free contexts. The sensor module can comprise metalloregulators from any transcription factor family that act as repressors or activators of transcription. Promotor design is an important factor in biosensor performance, correctly assembling a regulatory circuit requires defining an operator sequence (blue) and a reporter gene (green). In the case of riboswitches, circuit design must incorporate the correct features to allow for correct regulation. The reporter gene encodes can encode for a transcriptional reporter such as fluorescent aptamer or reporter proteins and enzymes in the reporter module. B) Whole cell biosensor (WCB) construction based on a two-plasmid design; one plasmid constitutively expresses the regulatory element with the reporter plasmid encoding for a reporter regulated by the metalloregulator. The inducer (orange) concentration inside the cell depends on efflux/influx systems of the selected chassis. C) Cell-free biosensors that employ the regulatory function of TFs, their minimal construction is reflected in ROSALIND biosensors that are based on *In vitro* transcription reactions. Among the advantages of cell-free biosensors are that the sensory molecule is directly exposed to the total concentration of inducer and the ease of lyophilization and reconstitution on-site of the reactions.[269]

alternative. The emerging enthusiasm for adopting metalloregulator-based biosensors derives from their innate sensibility and selectivity, and their compatibility with inexpensive, point-of-care devices compliant with current water quality regulations. Notably, the effective metal concentrations to which metalloregulators are tuned to activate a transcriptional response inside a cell (Figure 8) are in fact similar to required limits of detection in the field, even if a design is limited by an underperforming, but easily optimized, output or signal detection strategy.[620,621] This makes applications of whole cell biosensors to biological engineering and industrial biotechnology rather straightforward. On the other hand, a major challenge of cell-free approaches is that metal selectivities of the metallosensors tend to be reinforced by the cellular milieu, i.e., the buffering molecules in cells (Section 2.2; Figure 8). This has to be taken into account in the design of such cell-free devices.[19]

Although well-characterized metalloregulators have the advantage of a well-defined metal selectivity profile, metal promiscuity[250] if present can also be leveraged to create sensors for arrays of metals where the limit of detection of each metal ion matches the desired application.[622] Moreover, an attractive feature of working with bacterial transcription factors is access to naturally occurring sensors for potentially any natural product of interest through genome mining approaches (Figure 24A, below). Improved bioinformatics tools have more robust annotation of candidate allosteric transcription factors (aTFs) in genomes[623] and have recently been used to predict a cognate DNA operator(s) suitable for circuit design.[624] Multiple databases are available to explore well-characterized transcription factors and their regulons, including regulonDB,[625] SwissRegulon[626] and GroovDB.[627] Now, thanks to decades of research into the components that make them, metal-sensing biosensor platforms are closer than ever to mainstream application in the field.[628]

3.4.3. Whole Cell Biosensors. The simplest whole cell biosensor (WCB) functions as a traditional reporter assay (Figure 23B). Here, a synthetic regulon or "circuit" is constructed with a regulatory factor, e.g., a metalloregulator, that controls the expression of a reporter gene positioned downstream of a DNA operator/promoter region. Growth of this strain containing the gene circuit in the presence of an inducer activates transcription of the reporter gene, producing a detectable signal, as long as the inducer exceed a specified concentration, which defines the limit of detection (LOD) or sensitivity of the circuit. WCBs offer many advantages, including the low cost of growing small quantities of bacterial culture and access to a range of configurable and orthogonal output signal detection modalities, including luminescence, fluorescence and colorimetric approaches. Additionally, these circuits can be tailored for any specific application by expanding the toolbox to include amplification circuits, logic computations, signal integration[630,631] and rapid allosteric transcription factor library screening.

The development of WCBs specific for metal ions and metalloids began almost immediately with the description of the regulatory element of the *ars* operon,[198,632,633] and indeed, biosensors employing ArsR continue to emerge.[235,634,635] A typical *ars* operon contains a regulatory gene, *arsR*, and genes encoding for an arsenate reductase and an arsenite efflux pump (namely, *asrA*, *arsB* and *arsC*) that collectively mediate As^{III} resistance (Section 3.2.2). A number of improvements to arsenic biosensors have been reported that highlight advantages of employing WCBs. On the one hand, the choice of strain or "chassis" was demonstrated to be a major factor in determining As^{III} sensitivity[636] because the WCB signal ultimately depends on the bioavailability of the inducer in that cell, and thus how it is

https://doi.org/10.1021/acs.chemrev.4c00264
Chem. Rev. 2024, 124, 13574−13659

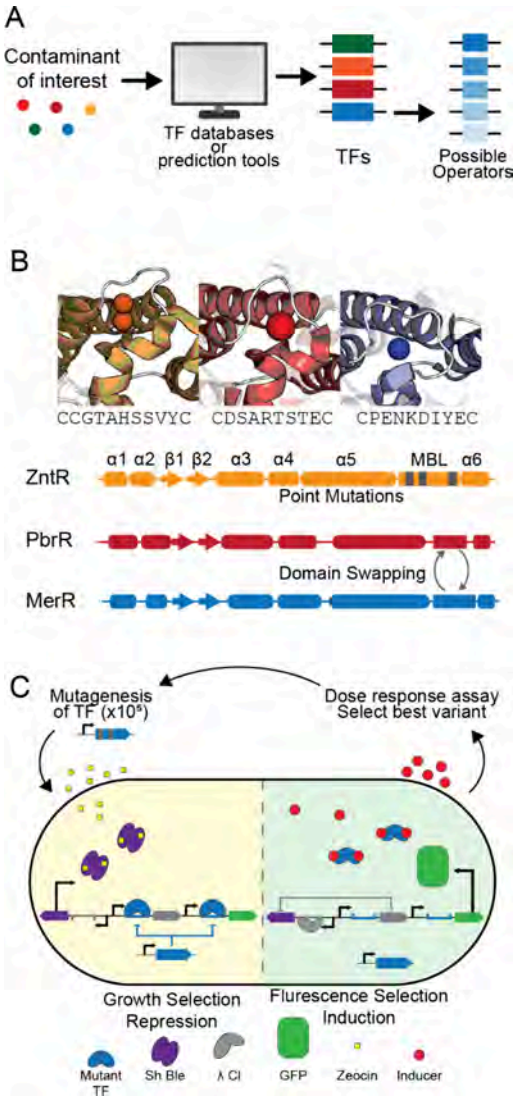

Figure 24. Transcription factor sourcing and tuning. A) Novel genome mining tools assisted with operator and inducer predictions software complement the existing transcription factor databases to extract novel TFs for novel biosensor development. B) Rational design of metalloregulator mutants is based on prior knowledge of its regulation mechanism. In the case of the MerR family, in depth studies of its metal preference led to different design strategies such as exchanging metal binding domains and points mutations in key residues. C) Example of an established directed evolution scheme (SELIS) with dual selection optimized for transcription factor evolution, starting from a library of random TF mutants assessing their repression and induction capabilities.[629]

"tuned" to detect the analyte.[637] On the other hand, strategic choice of reporter[638] and gene circuitry design[621,639] has permitted significant gains in performance relative to previous designs. The first generation As sensors were based on ArsRs that harbor the canonical As^{III} α3 coordination site (Section 3.2.2); however, this biosensor is limited to the detection of soluble As^{III} species and cannot detect other As speciation. To expand the repertoire of detection of As species, biosensors based on ArsRs containing other As^{III} sensing sites, e.g., *Af*ArsR and *Cg*ArsR, were found to specifically enhance detection of organoarsenicals for example,[640] highly relevant due to their widespread use as herbicides. In an effort to detect arsenate (AsO_4; As^V) directly, a *Paracoccus sp.* ArsRC fusion protein containing an arsenate reduction domain linked to an As^{III}-sensing ArsR regulatory domain resulted in improved detection of As^V.[641] Metal promiscuity can also be leveraged, as in *Sa*CadC,[642] while aTFs from different metallosensor families can be employed in parallel to construct biosensor arrays suitable for quantitation of many heavy metal contaminants simultaneously.[230,622] Moreover, these sensor arrays combined with DNA logic circuits may also permit the design of tools able to compensate for the lack of selectivity of a given metal if other sensors predictably respond to interferences.[19] MerR family activators (Section 3.2.3) are particularly relevant in this regard, since some exhibit a relatively high selectivity for a specific metal analyte, e.g., for Pb^{II} with *Cm*PbrR,[643] Cu^I with *Pp*CueR,[644] and Au^I with *St*GolS.[645]

A significant strength of the WCB approach is that the anticipated biosensor metal selectivity profile is well predicted by extensive studies that provide the foundation for the set-point model, which aims to reflect metal sensitivity in cells (Section 2.2). A major limitation of WCBs is that bacterial cultures must be maintained and continuously cultured over multiple generations under antibiotic selection, which could result in the accumulation of mutations that ultimately disrupt WCB performance. Field deployment is further limited by the need to transport sophisticated equipment to the field and the use of biocontainment protocols to prevent the release of engineered microorganisms into the environment.[230,646]

3.4.4. Cell-Free Biosensors. *In vitro* or cell-free biosensor systems do not suffer from the same limitations of a WCB and have emerged in the past decade as a means to circumvent the use of living bacterial cells. While cell-free reactions with metalloregulatory proteins were developed soon after their discovery,[340] the output signal of initial designs proved insufficient. A number of strategies have been introduced to transduce, and more importantly, amplify output signals from transcription factors *In vitro*, which has catalyzed further development of these platforms.[647−649] Some leverage structural changes that occur in the metalloregulator upon ligand binding or couple DNA binding to an electrochemical signal.[650] Other strategies couple transcription factors with the wealth of established DNA signal detection platforms such as strand displacement amplification (SDA)[648] or nicked DNA template-assisted signal transduction (NAST).[647] These emerging strategies have largely been developed with nonmetal-sensing transcription factors and have been thoroughly reviewed elsewhere.[231] Exploring these strategies with metalloregulatory proteins represents a promising avenue for the future development of novel metal biosensing platforms.

In vitro cell-free transcription systems, like WCBs, leverage metalloregulators as metal detectors that elicit a transcriptional response that leads to an amplified signal. The ROSALIND platform[269] employs apo-repressors as transcription factors from different structural families (Section 3.2) to sense a wide array of metal and organic contaminants in water (Figure 23C). The platform consists of only a few purified components. These include a linear DNA template with a bacteriophage T7 RNA polymerase promoter and a DNA operator sequence that binds the transcription factor of choice, each separated by a spacer. These elements regulate the transcription of an RNA aptamer (three-way junction dimeric broccoli, 3WJdB) that when bound to an organic dye, produces a fluorescent signal. This work showed that with appropriate promoter design an aTF can regulate transcription of even the highly processive phage T7 RNA polymerase. The modularity of ROSALIND has permitted

https://doi.org/10.1021/acs.chemrev.4c00264
Chem. Rev. 2024, 124, 13574−13659

the development of transcriptional circuits controlled not only by metallosensors, including SmtB (Zn^{II}), CsoR (Cu/Zn^{II}) and CadC (Pb^{II}/Cd^{II}), but also those capable of detecting small organic molecules, such as TetR (tetracycline), MphR (erythromycin) and QacR (benzalkonium chloride).[269]

While ROSALIND is limited to the use of well-characterized apo-repressors, cell extract-based *In vitro* transcription-translation (Tx-Tl) systems permit the development of biosensors with the whole array of possible aTFs[622,651,652] and orthogonal regulatory elements, including riboswitches (Section 3.4),[653] since both protein- and RNA-based "parts" make use of the same *endogenous* RNA polymerase. The use of riboswitches in this way has thus far has been limited to Tx-Tl systems, and as yet only for the detection of nonmetal analytes such as fluoride anion.[653] We believe that riboswitches are a particularly unexplored area for metal biosensor development given our considerable knowledge base[598,602,654] and the comparative ease with which they can be engineered relative to protein-based factors.[655] Cell extracts also allow the use of metabolic engineering to integrate the signal from a target molecule for which a transcription factor is currently unknown.[656,657] Major limitations of the use of cell extracts arises from a generally slow "turn-on" response as a result of inconsistent manufacturing[658,659] and storage[660] of the extracts that does not allow for robust calibration required by a quantitative biosensor.

3.4.5. Engineering and Evolution of aTFs for Biosensor Applications. Currently, the construction of a biosensor based on a metalloregulator begins by defining a target metal contaminant of interest for detection. Then, the choice of a metalloregulator is made by consulting available databases that are populated with well-characterized and annotated transcriptional regulators. These databases are continuously updated, allowing the user to create a "short list" of strong candidate metalloregulators with the desired inducer specificity profile and operator DNA sequence. Candidate combinations are then evaluated using homologues of well-characterized metalloregulators to identify one that is best suited for the desired application.[661] Even then, metal binding site promiscuity and a lack of sensitivity can limit the use of naturally occurring metalloregulators for a particular application.

A key aspect of transcription factors is their tunability.[662] Rational (targeted) engineering of transcription factors has been explored as a means to improve sensibility, metal specificity and/or expand the repertoire of analytes to be detected. MerR family members have been the subject of many engineering efforts from different perspectives, facilitated by the fact that these are largely "single-site" regulators, in which metal specificity is determined, at least part, by the specific nature of the metal binding loop (MBL) (Section 3.2.3). For example, the mutation of a highly conserved serine residue in the MBL of monovalent metal specific regulators to a cysteine, based on its presence in divalent metal regulators, resulted in variants capable of sensing both Hg^{II} as well as the monovalent coinage metals (Figure 24B).[304] In another study, *Ec*ZntR metal promiscuity was further enhanced by introduction of targeted mutations in the MBL, resulting in variants with and ability to sense both Hg^{II} and Cd^{II}.[333,663,664] Other studies that simply "swapped" MBLs among MerRs with different metal selectivity profiles, however, have met with limited or unpredictable success,[665] which reinforces the idea that transition metal selectivity in MerRs is not solely determined by the first coordination shell, but also by the physical presentation of the MBL in the context of the protein scaffold. This conclusion has been reinforced by findings with a dual selection, directed evolution campaign carried out with *Cm*PbrR.[666] Two very distinct PbrR variants were obtained with improved selectivity of Pb^{II} over Zn^{II}. One variant harbored a C134R substitution in the MBL, while the other variant featured two substitutions (N64A/L68S) far from the MBL. These findings are consistent with the conclusion that predicting selectivity from sequence information alone remains a challenge in the biosensor design field (Figure 24B).

More recently, other selection schemes have been implemented to improve analyte inducibility and thus the biosensor response using *Ec*ArsR as a model.[639,652,667] Other robust dual selection schemes easily tailored to sensor evolution, e.g., SELIS (Figure 24C),[629,668,669] have been used to introduce novel organic ligand selectivity into a previously ligand-promiscuous transcription factor. This scheme has not yet been applied to metalloregulators and represents a promising avenue to evolve metalloregulators with virtually any desired metal selectivity profile. Although metalloregulator engineering and rational or targeted mutagenesis campaigns geared toward biosensor applications have provided valuable new information on how transition metal selectivity emerges, we believe nonguided design paths such as directed evolution or more recent "ligand-aware" artificial intelligence tools may ultimately emerge as the new standard approach for biosensor development.[670−672]

4. METALLOPROTEOME PARALOGS

4.1. Overview

Metal sensors control the expression of the genes that encode proteins that allow an organism to maintain homeostasis while mounting an adaptive response to either metal limitation or metal toxicity. In the following two sections, we consider two specific adaptive responses to perturbation of the extracellular metal availability that highlight the remarkable versatility of the adaptive response in prokaryotes. These include the expression and characterization of metalloenzyme paralogs and cambialistic metalloenzymes recently described (Section 4) and specific mechanistic features, recently uncovered, of metal delivery to downstream protein clients and trafficking of metals across bacterial membranes, including intracellular organelles (see Section 5).[673,674]

4.1.1. Metalloenzyme Paralogs vs Cambialism. The general concept of a metalloenzyme paralog derives from a comparative genomics analysis of distinct species,[675] where a particular metabolic pathway, while clearly present in two organisms, appears to lack one or more enzymes in that pathway, e.g., a "pathway hole", and yet the pathway remains fully functional.[676] Thus, there must be a workaround. In one case, a distinct enzyme has evolved via convergent evolution, or "nonorthologous displacement," that catalyzes exactly the same reaction.[677,678] In another case, an enzyme has evolved that catalyzes a different reaction that eliminates the requirement for one or more other reactions within the same pathway, establishing an "alternative route."[679] Metalloenzyme paralogs are a specialized type of nonorthologous displacement where an enzyme evolves to catalyze the same reaction as an obligatory Zn^{II}-dependent enzyme, for example, but is characterized by a relaxed metal cofactor specificity profile or uses no metal at all. If distinct genes encoding the conventional or "housekeeping" vs paralogous enzymes are present in the same genome, they may well be differentially regulated by metal nutrient status of the growth conditions. An early example of this was in fact GTP cyclohydrolase-I (Section 4.3.3). Known enzyme paralogs often

https://doi.org/10.1021/acs.chemrev.4c00264
Chem. Rev. 2024, 124, 13574−13659

catalyze what might be considered "permissive" chemistry, where the metal cofactor does not undergo a change in oxidation state, e.g., in hydrolytic enzymes or other kinds of Lewis acid catalysts.

Cambialism, in contrast, defines the specialized case where the same metalloenzyme can be metalated with distinct metal cofactors without a significant loss of catalytic activity.[680] This might occur in response, at least in part, to nutrient metal availability,[7,681,682] a strategy that may well be more widespread than previously anticipated.[683] Remarkably, the work summarized here on the superoxide dismutases (SODs) and ribonucleotide reductases (RNRs) reveal that cambialism and more generally metalloenzyme paralogs have evolved in enzymes that catalyze more "restrictive" chemistry, where a change in oxidation state and even access to high-valent intermediates, is involved. Here, Mn^{II}/Fe^{II} cambialism is superimposed on paralogism, where one member of a series of paralogous enzymes exhibits the distinct property of cambialism.

4.1.2. Expression of Metalloprotein Paralogs in the Metal Limitation Response. Although Zn and Fe are essential nutrients for growth, bacteria often colonize Zn- and Fe-deplete environments.[684,685] Pathogenic bacteria are particularly susceptible to transition metal starvation by the action of metal scavengers including calprotectin (CP) and related S100 proteins. CP often induces components of the Zur and Fur regulons, which is hypothesized to result in collateral undermetalation of the proteome (Section 3.2.6; Figure 8B).[10,686] In the specific case of zinc starvation, bacterial cells upregulate the expression of protein paralogs of obligatory Zn^{II}-dependent enzymes that function in key physiological pathways.[687,688] These paralogs include ribosomal proteins, global transcriptional regulators, enzymes of central carbon metabolism, one-carbon metabolism and carbon fixation, and perform tRNA modification and aminoacylation, nucleotide (purine, pyrimidine and pyridine) biosynthesis, heme biosynthesis, amino acid biosynthesis and bacterial cell wall remodeling.[689] In the case of the Zn^{II} enzymes, the regulation of the expression of these paralogs is believed to be a form of "Zn sparing" that mobilizes Zn^{II} for other functions,[687] conserving a severely restricted nutrient for essential processes.

We classify the functional characteristics of currently known paralogs into two distinct groups (Figure 25A): (1) paralogs that have lost metal coordinating residues and may or may not dispense of the need for metal altogether (Category 1), and (2) paralogs that are metal-promiscuous and require a metal for catalysis but may or may not retain function with Zn^{II} (Category 2). As discussed above, enzyme paralogs can arise as a result of convergent evolution, in which structurally distinct solutions to the same reaction chemistry evolve (Figure 25B). Each category exhibits distinct mechanistic features in adaptation to low Zn so that metabolic flux through a major biosynthetic pathway can be preserved. Here, we exploit one genomic region of the *P. aeruginosa* Zur regulon to illustrate these general principles (Figure 25C). This region of the genome harbors two distinct Zur-boxes that regulate the expression of different sets of genes (an operon). The first divergently transcribed operon encodes for two proteins of unknown function, two candidate COG0523-family putative Zn metallochaperones, the DksA2 paralog, and a TonB transporter component that may be involved in Zn uptake across the outer membrane in this Gram-negative bacterium, through the outer membrane porin ZnuD. The second divergently transcribed operon encodes the paralogs FolEIB, PyrC2, AmiA, and a γ-class carbonic anhydrase. Finally,

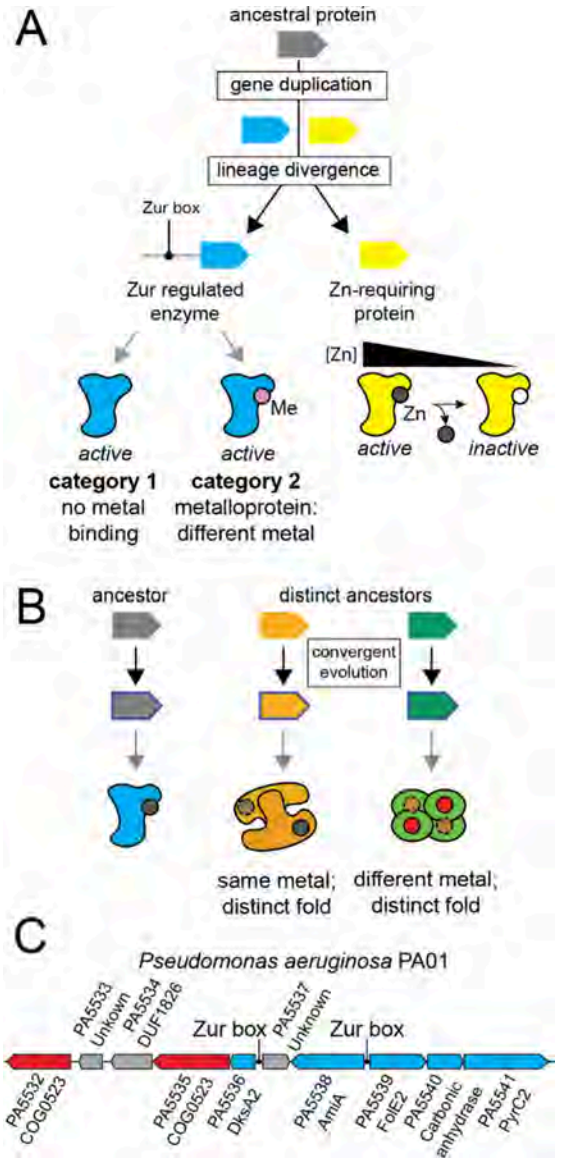

Figure 25. Conceptual framework defining the different categories of Zur-regulated paralogs of Zn-requiring enzymes that catalyze the same reaction, as an example. A) Gene duplication and divergent evolution leads to extant Zn-requiring and non-Zn-requiring enzymes. At higher intracellular Zn (gray spheres) concentrations, the canonical enzyme (yellow) can acquire Zn while the paralog (cyan) is repressed by Zn-bound Zur. When Zn levels drop in the cell and the canonical enzyme is inactivated via loss of Zn, a Zur-regulated paralog is expressed where it functions in the absence of any metal (category 1), or with an alternative metal to Zn (purple sphere, category 2). B) Enzyme paralogs can also arise as a result of convergent evolution in which structurally distinct solutions to the same reaction chemistry evolve, where the Zn enzyme (cyan) might be subject to inactivation via loss of Zn; the others may be regulated by Zur (not shown). C) Part of the *P. aeruginosa* Zur regulon comprised of two divergently transcribed operons is shown, with locus tags (gene IDs; PAxxxx) and inferred functional assignments. Two known Zur boxes are indicated.[690] Genes that encode paralogs as defined here are shaded cyan, COG0523-family candidate Zn metallochaperones shaded red,[691] and genes of unknown function are shaded gray.

the intriguing cases of two cambialistic enzymes, superoxide dismutase (SOD) and ribonucleotide reductase Ib (RNRs), are discussed.

https://doi.org/10.1021/acs.chemrev.4c00264
Chem. Rev. 2024, 124, 13574−13659

4.2. Category 1: Metal-Independent Paralogs

4.2.1. Ribosomal C− Paralogs. A classic example of Zur-regulated paralogs comes from the modification of a structural, not a catalytic, Zn binding site.[692,693] This is exemplified in the Zn sparing phenomenon of Zur-regulated, nonenzymatic ribosomal protein paralogs. These paralogs lack 4 conserved cysteines that form a pair of CxxC Zn binding motifs (called "C−" ribosomal proteins) present in their Zn binding counterparts ("C+,").[687,692] The model organism *E. coli* encodes two C+ ribosomal proteins, L31 and L36, encoded by the genes *rpmE* and *rpmJ*, respectively, and two C− paralogs L31B and L36B, encoded by the genes *ykgM* and *ykgO* (Figure 26A).[694] *E. coli* Zur achieves upregulation of L31 through a "repression of a repressor" mechanism. Zur regulated L31B, expressed in zinc-deficient conditions, in turn represses L31 expression by binding to its mRNA 5′ UTR. In the presence of sufficient zinc, the C+ ribosomal protein is expressed while the C− paralogue is repressed.[695] This allows the organism to deploy this significant new intracellular pool of bioavailable Zn for other crucial processes as ribosomes are among the most abundant molecular assemblies in the cell.[694] Across the bacterial kingdom there exists a large diversity of C− paralogs, with seven identified thus far in Zur regulons; some organisms encode for no C− paralogs while others possess up to six.[430] These paralogs are sprinkled throughout the mature ribosome, spanning both large and small subunits inside and out, and are generally incorporated into both intermediate and late 50S ribosomal assembly intermediates, but not early ones;[696] the significance of this finding is unknown.

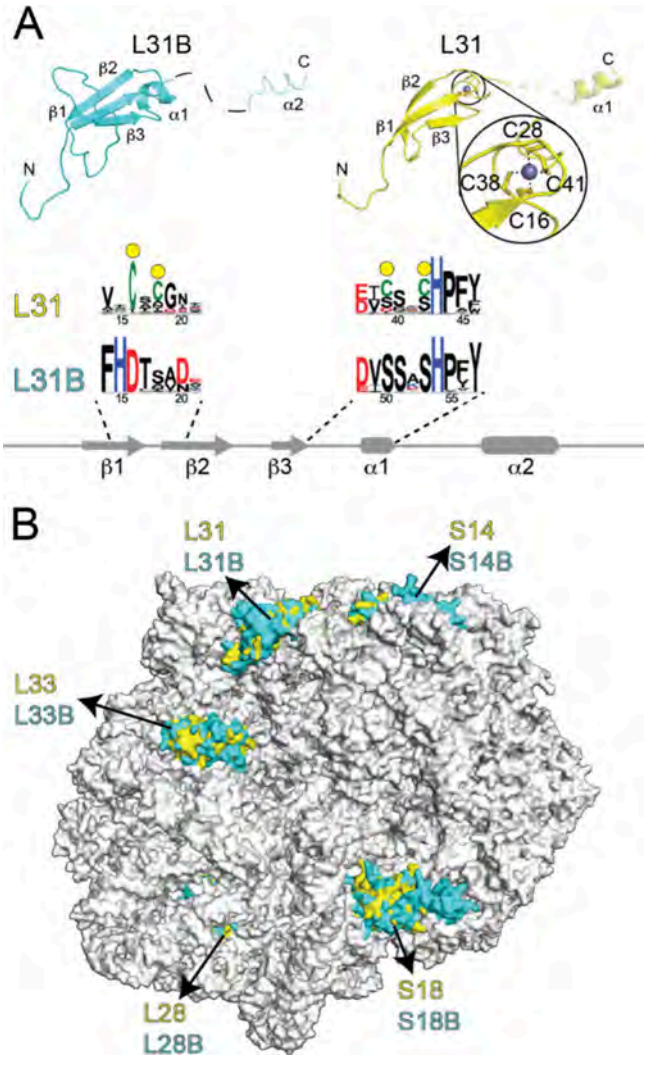

Figure 26. C− ribosomal protein paralogs. A) Ribbon representations of *M. smegmatis* L31 and the low-zinc paralog, L31B.[697,698] Conserved features of C+ vsC− subunits with Zn-binding Cys residues labeled highlighted with a yellow sphere. B) Space-fill model of the *M. smegmatis* 70S ribosome shaded gray with the indicated ribosomal subunits highlighted in yellow and cyan (PDB: 5O61 C+ ribosome and 6DZI C− ribosome[697,698]). The five C+ subunits (yellow) associated with Zur-regulated C− paralogs (cyan) are shown.

Structurally, the C− proteins not only lack the Zn binding Cys residues, considered essential for their C+ counterpart function, but also contain insertions, extensions, and divergent sequences. Both C+ and C− ribosomes from *M. smegmatis* have been structurally characterized[697,698] and these ribosomes have been evaluated for functional differences (Figure 26B). Specific C− insertions protect the ribosome active site by inhibiting the efficacy of antibiotics.[699] C− and C+ ribosomes appear to have similar elongation rates and error rates, and may be more active under Zn-limiting conditions.[700] However, C− ribosomes exhibit distinct translation profiles and are characterized by slower translation initiation rates relative to C+ ribosomes.[700,701] The extent to which C− subunits confer additional features on the ribosome remains to be fully evaluated, but an exciting hypothesis is that ribosome remodeling during Zn limitation may selectively upregulate the translation of cellular transcripts that enable physiological adaptation to nutrient limited conditions.

4.2.2. DksA/DksA2. The stringent response is induced by general nutrient starvation resulting in hyperphosphorylation of nucleotides which signals an alleviation mechanism(s) that involves a global change in gene expression patterns ultimately leading to stasis or quiescence.[702] Major signaling molecules in the bacterial stringent response are the alarmones guanosine pentaphosphate (guanosine 5′-triphosphate, 3′-diphosphate; pppGpp), and guanosine tetraphosphate (guanosine 5′-diphosphate, 3′-diphosphate; ppGpp), collectively referred to as (p)ppGpp. These are synthesized from GTP or GDP, respectively, and ATP, as the source of 3′-pyrophosphate moiety. These alarmones severely deplete cellular GTP pools, and function either by inhibiting enzymatic activity directly by binding to a GTP or GDP binding site in competition with this substrate or "signal" within the transcriptional machinery itself.[703,704] The stringent response is also dependent on specialized proteins, including DksA.[705] DksA is a broadly conserved RNA polymerase regulatory factor and is present in most bacterial species,[706] with the prominent exception of Firmicutes. DksA2 is a paralog that is found in Zur regulons of β- and γ-proteobacteria[688] and has been most extensively characterized in *P. aeruginosa*. *Pa*DksA2 shares 34% sequence identity with *Pa*DksA, and both proteins adopt nearly identical folds (Figure 27A). Moreover, during the evolution of *Salmonella* from an environmental bacterium to a vertebrate enteric pathogen, a number of virulence genes were genomically colocalized into an ancestral DksA regulon, highlighting an important role of DksA as a pathogenicity regulator.[707]

Although DksA is constitutively expressed, it is known to function only when (p)ppGpp and/or ROS/RNS are abundant in cells.[708,709] Under these conditions, DksA binds directly to RNA polymerase and differentially regulates transcription from selected promoters of genes encoding proteins involved in translation or amino acid biosynthesis and uptake.[706,710,711] The

https://doi.org/10.1021/acs.chemrev.4c00264
Chem. Rev. 2024, 124, 13574−13659

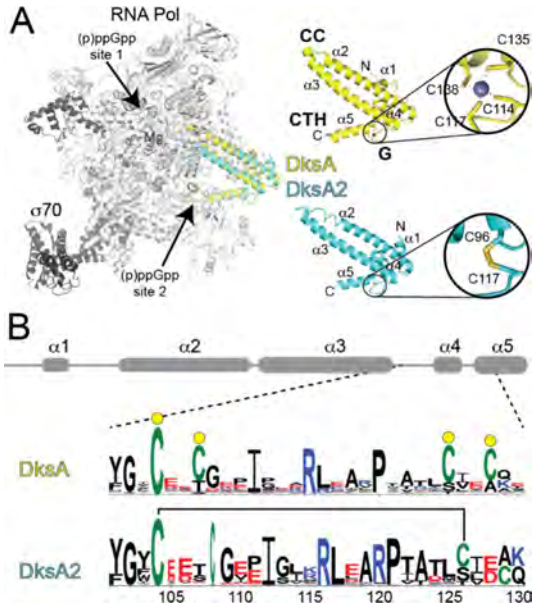

Figure 27. DksA transcription factor. A) Ribbon representation of the RNAP−DksA binary complex (PBD: 5W1T). Motifs of RNAP (domains in white and σ70 in black) binding (p)ppGpp are indicated with an arrow.[709] *Right*, ribbon structures of *E. coli* DksA (yellow, PDB: 1TI1)[710] and *P. aeruginosa* DksA2 (cyan, PDB: 4IJJ),[715] and the DksA Zn ion shown as a gray sphere. The globular (G), coiled-coil (CC), and C-terminal helix (CTH) domains are highlighted. Tetrathiolate Zn binding site of *E. coli* DksA with Zn coordinating Cys residues labeled and shown in stick, with the Zn ion shown as a gray sphere. Analogous metal binding site region of *P. aeruginosa* DksA2, with the two conserved Cys that from a disulfide bridge labeled and shown in stick representation. B) Conserved primary structural features of the global transcriptional regulator DksA and DksA2, centered only on the DksA metal binding region. DksA Zn-binding residues are labeled in yellow and highlighted with a yellow sphere and the DksA2 disulfide bridge is labeled with a bracket.

combination of DksA and (p)ppGpp in the stringent response inhibits ribosome production, thereby decreasing amino acid consumption by translation and increasing amino acid biosynthesis, as global efforts to restore nutrient balance in the organism. In fact, RelA, the synthase that synthesizes (p)ppGpp binds to the ribosome directly, particularly those ribosomes that harbor an unacylated tRNA in the A-site, which occurs as a result of amino acid starvation, further stimulating the cellular production of (p)ppGpp. The DksA-dependent regulatory profile that is independent of (p)ppGpp and connected to ROS/RNS stress down-regulates both the ribosome biogenesis machinery and amino acid biosynthesis, while also promoting redox buffering and repair of biomolecules, thus resulting in broad cellular resistance to these conditions.[708,712]

DksA is a small protein with an N-terminal globular domain (NTD), an extended coiled-coil (CC) domain, and a C-terminal α-helix (CTH) (Figure 27A, *right*).[710] The NTD is linked to the CTH by a tetrathiolate, tetrahedral Zn^{II} binding site.[713,714] Substitution of the Zn^{II} coordinating Cys residues disrupts DksA activity in cells.[711,715,716] The four Zn-coordinating Cys residues have been shown to be susceptible to oxidation by various reactive oxygen and reactive nitrogen species (ROS and RNS) which enhances global DksA-mediated transcriptional inhibition.[708,716] Reaction with ROS and RNS species results in the release of Zn, and treatment with reducing agent after oxidation results in nearly full restoration of DksA secondary structure. These findings suggest that the primary role of Zn is not that of a structural cofactor, but rather as a sensor of redox stress. This oxidation event also leads to potent transcriptional inhibition in the absence of (p)ppGpp, consistent with its assignment as a regulatory metal site that tunes ROS and RNS sensing by DksA.[712]

*Pa*DksA2 possesses only two cysteines of the four Zn-coordinating Cys present in DksA (C96 and C117), which are precisely analogous to the redox-sensing cysteines C114 and C135 in *Ec*DksA (Figure 27B). Loss of two or three Zn coordinating cysteines (some DksA2 paralogs possess only one of the four Cys observed in *Ec*DksA) would of course abolish Zn binding in the cell, and thus would effectively "spare" this Zn for another purpose.[715] In *P. aeruginosa* the Δ*dksA* strain exhibits a growth phenotype on Zn-replete minimal media since Zur will repress the expression of *dksA2* under these conditions.[716] As expected, this phenotype is suppressed under low Zn, where *dksA2* is upregulated. Indeed, DksA2 has been shown to functionally complement DksA *in vivo* and *In vitro* to varying degrees.[708,716] Additionally, a *P. aeruginosa* strain that expresses only DksA (a Δ*dksA2* strain) exhibits inhibited growth on Zn-deplete minimal media, clearly indicative of a disruption of DksA function specifically under conditions of low Zn.

A consensus model holds that DksA becomes undermetalated under zinc limiting conditions which results in an increased sensitivity to ROS/RNS and an impaired alarmone-dependent adaptive response. Under these conditions DksA2 is upregulated, thus restoring the stringent response. Zn coordination by DksA may attenuate its redox-sensing activity, reserving the redox-sensing Cys pair to respond only under conditions of chronic ROS stress, where cellular reductant pools become depleted.[708] Consistent with this, the Zn-free DksA2 is 50-fold more reactive toward H_2O_2 *In vitro* and oxidation-induced transcriptional repression is far more sensitive to low H_2O_2 in cells expressing only DksA2 vs cells expressing only DksA.[708] Kinetics studies reveal that the Zn-bound DksA requires significantly higher ROS to enhance transcriptional repression since the major cellular reducing thiol glutathione (GSH) preferentially scavenges ROS under these conditions; in striking contrast, DksA2 is a far better ROS scavenger than GSH itself.[708] This results in reduced survival in macrophage models of infection of bacterial cells that express only DksA2 compared to those expressing only DksA, as (p)ppGpp-independent transcription inhibition occurs at lower ROS levels. Taken together, dispensing of the Zn binding site in DksA2 is a remarkably complex evolutionary adaptation that appears to integrate the bacterial adaptive response to Zn restriction and chronic ROS exposure that may well be coincident in the infected host.

4.3. Category 2: Metal-Promiscuous Paralogs

4.3.1. QueD/QueD2. Transfer RNA (tRNA) modifications are widespread in all kingdoms of life and are regarded as global regulators of translational capacity and important markers of nutritional status.[717,718] Queuosine (Q) is a hypermodified, 7-deazaguanosine incorporated into the 34th or "wobble" position of the anticodon loop of four specific tRNAs (Asn, Asp, Tyr and His) that decode synonymous NA**C** and NA**U** (N = A, U, C or G) codons.[719] Q-tRNAs bind more tightly to the translating ribosome, although the effects vary widely. The Q modification in eukaryotic cells impacts the decoding of NA**U** codons while decreasing amino acid misincorporation, thus affecting translation accuracy and speed.[720] The loss of Q results in weaker codon-anticodon pairing of NAU codons (called Q-decoded

https://doi.org/10.1021/acs.chemrev.4c00264
Chem. Rev. 2024, 124, 13574−13659

codons) which can also lead to ribosome stalling in these cells.[720−726] The effects of Q loss in bacteria may well be more complex, and strongly growth condition-dependent, but can lead to biased translation and proteome remodeling, particularly under the combined effects of nutritional stress and antibiotic stress.[727,728] This has led to the concept of "modification-tunable transcripts (MoTTs)"[717,727] which drives a global adaptive response in bacteria, potentially enhancing virulence or endowing an organism some other growth advantage in the infected host.[727]

Only bacteria possess the ability to *de novo* synthesize queuosine-tRNA from GTP, with higher eukaryotes dependent on the salvage of queuine (the nucleobase) from the microbiota.[92] The Q-tRNA biosynthesis pathway is complex and depends on no fewer than seven enzymes that require transition metals as cofactors.[729−735] Nutrient metal starvation negatively impacts flux through the queuosine-tRNA biosynthetic pathway in *Acinetobacter baumannii* while giving rise to a more pleiotropic response in *E. coli*.[9,736] The committed step in the Q-tRNA biosynthesis pathway is performed by a 6-carboxytetrahydropterin (CPH_4) synthase, QueD[737] or a QueD paralog termed QueD2.[688] Bacteria either encode a housekeeping QueD or a QueD2 that becomes cell-abundant under conditions of Zn^{II} restriction,[738] or alternatively encode both a constitutively expressed QueD and a Zur-regulated QueD2. Mutant strains of different organisms lacking the housekeeping enzyme could be complemented by over-expression of a paralog, revealing a conserved function.[9,739]

Both QueD and QueD2 are obligate metalloenzymes, with QueD copurifying and structurally characterized with tightly bound Zn^{II}.[729,740] Recent work reveals that both QueD and QueD2 are rather metal-promiscuous, with each possessing comparable specific activities with Mn^{II}, Fe^{II} and Zn^{II}. Each is a member of the tunnel fold (T-fold) superfamily characterized by an oligomeric assembly state that forms a central β-barrel that resembles a tunnel. This family consists of two $\beta_{2n}\alpha_n$ rings ($n \geq 2$) that join in a head-to-head fashion, with the symmetry-related active sites bridging the two rings. QueD possesses a conserved Cx_3HGH motif containing the essential catalytic nucleophile, Cys27 in *Ec*QueD and two His (His31 and His33) that coordinate the Zn^{II} (Figure 28A).[740] An additional conserved residue, His16, contributes the third protein-derived ligand, with two water molecules or two oxygen atoms from the substrate, intermediates or product completing the five-coordinate trigonal bipyramidal Zn^{II} site.

The QueD2 paralog exhibits very low (<20%) sequence identity relative to the housekeeping QueD and harbors a one-residue insertion in the catalytic Cx_3HGH motif of QueD to create the Cx_4HGH motif of QueD2. A recent structure of QueD2 from *Acinetobacter baumannii* reveals a distinct octameric assembly state (two stacked tetrameric rings) relative to the *E. coli* QueD hexamer.[9] In contrast to QueD, there are two high occupancy Zn^{II} binding sites in the structure of *Ab*QueD2 (Figure 28B). One corresponds roughly to the active site of *Ec*QueD (site 1), with the second site (site 2) more peripheral and solvent exposed, some ≈14 Å away and coordinated by the active site nucleophile, Cys23, an invariant Cys specific to QueD2s, Cys18 (this is a His in the other major cluster of QueD2 sequences), and two other poorly conserved residues derived from an adjacent subunit within a tetrameric ring. The inserted amino acid in the QueD2 Cx_4HGH motif displaces the Cys nucleophile far from the catalytic site, while shifting the metal coordinating HGH motif (His28 and His30 in *Ab*QueD2)

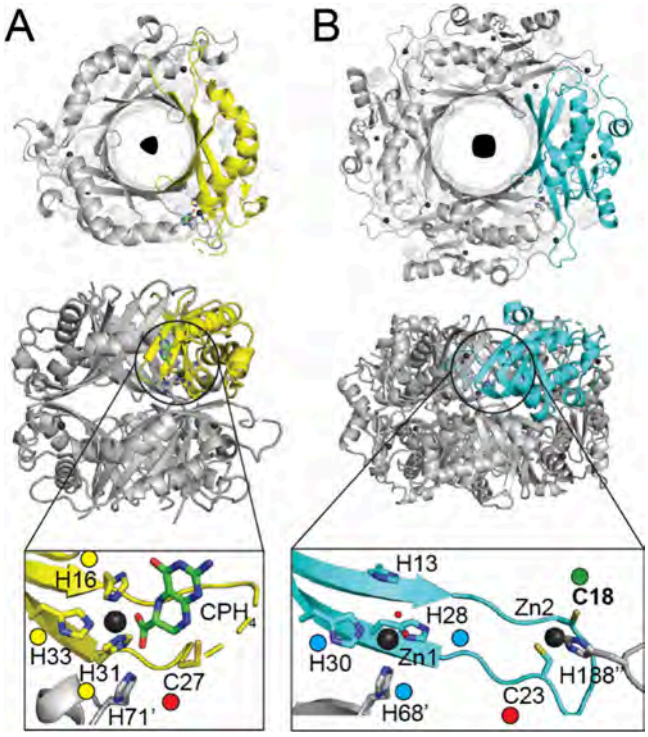

Figure 28. 6-carboxy-5,6,7,8-tetrahydropterin (CPH_4) synthase QueD. A) Top-down (*left*) and side (*right*) views of the ribbon structure of the hexameric *E. coli* QueD (yellow, PDB: 4NTM).[740] A single protomer is colored, the remaining protomers are shaded gray, with the Zn ions (black) shown. The product 6-carboxy-5,6,7,8-tetrahydropterin (CPH_4) binding site is highlighted. Close up view of the *E. coli* QueD Zn binding site with conserved catalytic and metal binding residues labeled and shown in stick (highlighted by the yellow circles), and the Zn ion represented by a black sphere. The catalytic nucleophile, C27, is highlighted with a red circle. The sepiapterin-like intermediate is shown as green CPK stick. B) Top-down (*top*) and side (*middle*) views of the ribbon structure the octameric *A. baumannii* QueD2 (cyan, PDB: 7 V0F).[9] Close up view of the *A. baumannii* QueD2 Zn binding sites 1 and 2 (*bottom*) with conserved catalytic (C23, red; H68′, blue circle) and metal binding residues labeled (blue circles) and shown in stick, with water molecules shown as small red spheres coordinated to Zn1, and the Zn ion represented by a black sphere. C18 (green circle) is uniquely conserved in QueD2 genes as either a Cys or a His.

further into the β2 strand relative to *Ec*QueD.[9] In addition, His13 in *Ab*QueD2 (analogous to metal ligand His16 in *Ec*QueD) does not coordinate the Zn^{II} and instead incorporates His 68'', analogous to His71'' in *Ec*QueD, one of the catalytic bases in the second half of the reaction.[740] Activity assays reveal that as expected, Zn^{II} binding to site 2 inhibits turnover by QueD2, which suggests that the active site 1 may well be conformationally "plastic" or dynamically heterogeneous and must "fold" to accommodate substrate, in striking contrast to the housekeeping enzyme QueD.[9]

What then is the function of metal site 2 in this low-zinc paralog QueD2? K_{Zn} for this site is quite weak and it is unlikely to be occupied under conditions of zinc starvation or even under zinc-replete conditions (+$\Delta\Delta G$ for metalation; Figure 8B). The conserved site 2 ligand, Cys18 in *Ab*QueD2, inhibits the rate of Zn^{II} dissociation, consistent with a function as a "trap" of exchange-labile metal in coordinately plastic first coordination shell.[9] Even more significantly, *Ab*QueD2 possesses an ≈100-fold higher catalytic activity when bound to Fe^{II} in a way that is not dependent upon Cys18. How this high activity with Fe^{II} is

https://doi.org/10.1021/acs.chemrev.4c00264
Chem. Rev. 2024, 124, 13574−13659

accomplished is unknown, but suggests a significant alteration in the active site structure that specifically facilitates the second step of this two-step reaction, the release of acetaldehyde.[9] In any case, these features make it possible for an organism expressing a QueD2 to adapt quickly to niches where Zn^{II} is deplete and Fe^{II} remains replete. This complex, multifaceted evolutionary adaptation to metal restriction, from metal "retention" to classical Zn sparing, represents a response that can be tuned to any flavor of metal starvation.[9]

4.3.2. PyrC/PyrC2. All members of the amidohydrolase superfamily share similar catalytic functions, enabling the reversible ring formation/opening of cyclic amides.[741] PyrC is a dihydroorotase (DHOase) that catalyzes the reversible interconversion of carbamoyl aspartate (CAA) and dihydroorotate (DHO) and functions in the third step of *de novo* pyrimidine biosynthesis, just downstream of the committed step catalyzed by another Zn-metalloenzyme, aspartate transcarbamoylase.[742] As such, PyrC is an essential enzyme.[743−745] Historically, bacterial DHOases can be grouped into two classes and a representative member of each has been structurally characterized. These are the 45 kDa class I PyrC enzymes largely found in Gram-positive bacteria, e.g., *Bacillus anthracis* (Figure 29A)[746,747] while the 38 kDa class II enzymes are generally found in Gram-negative bacteria, including the prototypical enzyme from *Escherichia coli* (Figure 29B).[748,749] They require a divalent metal ion for enzymatic activity, thought to be Zn^{II} in the cell; Zn^{II} and Co^{II} typically exhibit maximal activity while other divalent metals result in inhibition.[749−752] While both enzyme classes harbor a nearly isostructural binuclear Zn^{II} site where each Zn^{II} exhibits a trigonal bipyramidal geometry containing four His and an Asp, the sixth ligand is an Asp in class I PyrC and a post-translationally modified carboxylated Lys in class II DHOases.[746−749]

The Zur-regulated paralog PyrC2 is structurally uncharacterized, but is found in Zur regulons of Gram-negative bacteria, e.g., *P. aeruginosa* (Figure 25C) and *B. cenocepacia*. In these organisms, the housekeeping PyrC is a class II enzyme that is not regulated by Zur or Zn starvation. *P. aeruginosa* PyrC2 is distinct from *P. aeruginosa* PyrC, with just 10% sequence identity, but notably exhibits 30% sequence identity to the class I *B. anthracis* PyrC. Furthermore, *P. aeruginosa* PyrC2 has lost the most N-terminal of the Zn1-coordinating His residues, which is replaced by a Gln that is conserved in other Zur-regulated PyrCs (Figure 29D).[688] Interestingly, the structure of Gram-negative *Porphyromonas gingivalis* PyrC, a third DHOase denoted class III (Figure 29C), reveals features of both class I (sequence similarity and an N-terminal extension) and class II (a carboxylated Lys as a bridging ligand, instead of an Asp) enzymes. We view this structure as an excellent model for Zur-regulated PyrC2 given the high (50%) sequence identity and the presence of the same site 1 Gln substitution that is found in the *P. aeruginosa* PyrC2 paralog. This suggests that class III PyrCs may well contain other paralogs that may function better under Zn-limited conditions, as yet unknown. PyrC may be undermetalated under conditions of low Zn, thereby necessitating the upregulation of PyrC2 to maintain flux through this pathway; however, the ability of a Δ*pyrC2* strain to grow in Zn-limited conditions has not yet been evaluated. The difference between class I and II coordination spheres might relax the metal preference of PyrC2 allowing Mn^{II} to bind, for example,[753] or alter Zn affinities or kinetic labilities. Alternatively, the upregulation of PyrC2 simply forces metabolite flux toward pyrimidine biosynthesis by mass action in this reversible enzyme.

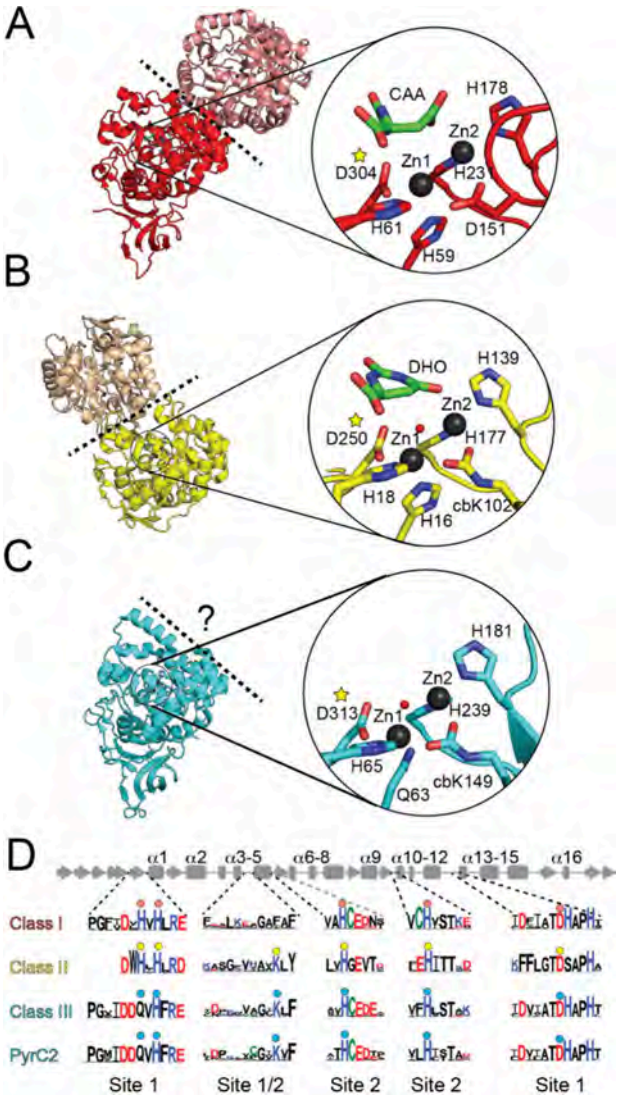

Figure 29. Binuclear zinc metalloenzyme dihydroorotase PyrC. A) Ribbon representation of the structure of *B. anthracis* PyrC (4YIW)[747] with the dimerization interface indicated by the dashed line, and the CAA-bound Zn binding site (close up) with Zn binding residues labeled and shown in stick, the CAA substrate shown in green stick, and Zn ions shown as black spheres. B) Ribbon representation of the structure of *E. coli* PyrC (1XGE)[754] with the dimerization interface indicated by the dashed line, and the DHO-bound Zn binding site (close up) with Zn binding residues labeled and shown in stick, the DHO substrate shown in green stick, water molecules shown as red spheres, and Zn ions shown as black spheres. C) Ribbon representation of the structure of *P. gingivalis* PyrC (PDB: 2GWN) with the putative dimerization interface based on homology to *B. subtilis* PyrC indicated by the dashed line, and the Zn binding site (close up) with Zn binding residues labeled and shown as sticks, water molecules shown as red spheres, and Zn ions shown as black spheres. D) Conserved primary structural features of PyrCs belonging to class I (represented by *B. anthracis* enzyme), class II (represented by *E. coli* enzyme), and class III (represented by *P. gingivalis* enzyme), jointly with PyrC2 (represented by *P. aeruginosa*) comparing the different Zn coordinating residues in each class. Class I Zn coordinating residues are highlighted in red, class II Zn binding residues are highlighted in yellow, and class III residues are highlighted in cyan, with the ligands corresponding to metal sites 1 and 2 indicated.

https://doi.org/10.1021/acs.chemrev.4c00264
Chem. Rev. 2024, 124, 13574−13659

4.3.3. FolE1A/FolE1B. GTP cyclohydrolase-IA (GCYH-IA; FolEIA or simply FolE) is a Zn^{II} metalloenzyme that catalyzes the conversion of GTP to 7,8-dihydroneopterin triphosphate (H_2NTP). H_2NTP is the first intermediate in the *de novo* biosynthesis of tetrahydrofolate (THF, folate) in all kingdoms of life; in bacteria, H_2NTP is a true metabolic branch point, serving as the substrate for QueD/QueD2 in the biosynthesis of the queuosine-tRNA (Section 4.3.2).[755] FolEIB (GCYH-IB; also known as FolE2), in contrast, has been described as a metal-cambialistic paralog that can catalyze the same reactions when metalated with Zn^{II} or another divalent metal.[677,678] Genes encoding FolEIB, like QueD2, are not exclusive to Zur regulons and in some organisms, e.g., *Staphylococcus aureus*, only *folEIB* is present. Like QueD/QueD2, both FolEIA and FolEIB are members of the T-fold superfamily,[678] and are characterized by very low pairwise sequence identity and distinct oligomeric assembly states, *i.e*, dimer of pentamers vs a dimer of dimers double ring-shaped architectures in FolEIA and FolEIB, respectively (Figure 30A,B). As apoproteins, both FolEIA and FolEIB are inactive and activity can only be observed by metalation of the active site as revealed by mutagenesis and enzymatic activity assays.[678,756]

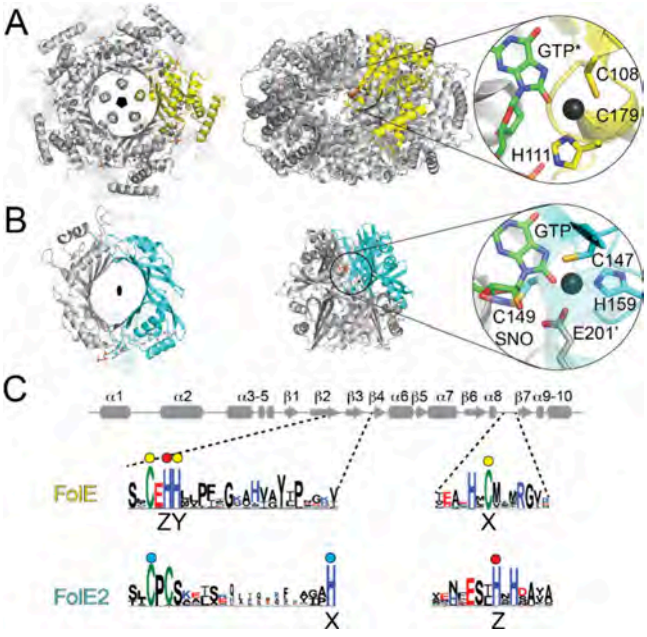

Figure 30. GTP cyclohydrolase I, FolE. A) Top-view (*left*) and side view (*middle*) of the ribbon representation of the decameric *T. thermophilus* FolE (1WUR)[764] with a single protomer shaded in yellow ribbon, with the remaining protomers shaded gray. Active site region (close up) with Zn binding residues labeled and highlighted in yellow stick, the catalytic intermediate mimic 8-oxo-GTP* shown in green stick, and the Zn ions shown as black spheres. B) Top-view (*left*) and the side view (*middle*) of the ribbon representation of the tetrameric *N. gonorrheae* FolE2 (3D2O) with a single protomer shaded in cyan ribbon, with the remaining protomers shaded gray. Active site region (close up) with Zn binding residues labeled and highlighted in cyan stick, the catalytic intermediate mimic 8-oxo-GTP is labeled as GTP* and shown in cyan stick, and the Zn ions shown as black spheres. S-nitrosated C149 is also shown in *Ng*FolE2. C) Conserved primary structural features of FolE and FolE2 in the active site region. The active site acid (which donates a proton) is labeled Z, while X and Y are metal ligands along with a conserved Cys. Note that the FolE2 Y (not shown in this region) and X coordinating ligands (panel B) and the Z functional groups in the primary structure of *T. thermophilus* FolE and *N. gonorrheae* FolE2 are significantly displaced from one another.[4]

Both enzymes coordinate Zn^{II} in a distorted tetrahedral geometry as revealed by the structures of *E. coli* FolEIA and the *Neisseria gonorrheae* FolEIB (Figure 30A,B), with three protein-derived ligands and a mimic of the first catalytic intermediate, 8-oxo-GTP (GTP*) coordinated to the metal.[756,757] This open coordination site in the absence of substrate analog is filled by OH^-, which is poised to attack the electrophilic C8, which itself is activated by a nearby His (Z residue; Figure 30C). FolEIA features a $Cys_2His\text{-}OH^-$ coordination site while in FolEIB, one of the Cys (C179 in FolEIA; the Y ligand) is replaced with a glutamate (E201') from a protomer in the opposite dimer in this dimer-of-dimers architecture, thus creating a "harder" coordination site.[4] While FolEIA is thought to be an obligatory Zn^{II} enzyme and clearly copurifies with Zn^{II}, this has not been rigorously established. In contrast, FolEIB enzymes from *B. subtilis, Cupriavidus metallidurans* and *N. gonorrheae* generally have lower activity when metalated by Zn^{II}, significant activity with Mn^{II}, Fe^{II} and Co^{II} and low activity with Ni^{II}, all trends consistent with the observed change in the first coordination shell in FolEIB vs FolEIA.[678,758] Interestingly, some FolEIB enzymes are reported to be active with Mg^{II}, to an extent on par with that of Co^{II}, which is puzzling given the presence of clearly "softer" ligands in both FolEIB coordination shells.

Both FolEIA and FolEIB catalysis feature classic Lewis acid chemistry and proton transfer-catalyzed ring-opening and ring-closing rearrangements, involving several pentacoordinate-metal intermediates, with the release of formate and H_2NTP. Interestingly, inspection of the active site regions of both FolEIA and FolEIB suggests the possibility that posttranslational modification of one or more residues might have a regulatory role. Indeed, *Ng*FolEIB, as purified, features additional electron density on the nonliganding cysteines, C149 (Figure 30B) assigned as an *S*-nitrosated Cys essentially positioned "on top" of the active site.[759] Mutation of this Cys to Ala or Ser largely inactivates the enzyme, which suggests that *S*-nitrosation may be a protective mechanism that preserves FolEIB activity under conditions of nitrosative stress. The evolution of FolEIB in bacteria may be reflective of a GCYH that evolved under the influence of dual stressors, oxidative/nitrosative stress and Zn^{II} limitation, reminiscent of DskA2 vs DksA (Section 4.2.2).[715]

In any case, the significant activity of FolEIB with divalent metal ions other than Zn^{II} uncovers a clear evolutionary adaptation for bacterial survival under conditions of Zn starvation, given the universality of one-carbon (1C) metabolism in all cells.[760,761] Indeed, this adaptation may well have several regulatory layers, since in *B. subtilis*, the housekeeping enzyme FolEIA is reported to be a target of the COG0523 superfamily metallochaperone, ZagA (Section 5.1.4).[761] ZagA is reported to sustain folate biosynthesis under conditions where *folEIB* is not expressed, as part of the graded response to increasing degrees of cellular zinc limitation.[761,762] A putative protein−protein interaction between ZagA and FolEIA appears to be stimulated by the alarmone and purine derivative ZTP (5′-aminoimidazole-4-carboxamide-1-β-D-ribofuranosyl-5′-triphosphate; AICAR triphosphate),[763] which accumulates in cells under conditions of folate deficiency.[758] Mechanistically how ZagA impacts FolE catalytic activity is not yet known since FolEIA binds Zn^{II} essentially irreversibly and may well be kinetically trapped, since it is difficult to remove with chelators and thiol modifying agents (Section 5.1.4).[758]

https://doi.org/10.1021/acs.chemrev.4c00264
Chem. Rev. 2024, 124, 13574−13659

4.3.4. Carbonic Anhydrases. Carbonic anhydrase (CA) is the prototypical zinc metalloenzyme that catalyzes the reversible hydration of gaseous CO_2 to bicarbonate anion, HCO_3^-, and a proton (H^+). CAs therefore play a crucial role in equilibrating CO_2 and bicarbonate inside the cell. The central importance of CAs in global carbon capture, pH regulation, pyrimidine biosynthesis and in providing a universally employed substrate for all biotin-dependent carboxylation reactions[765] underscores the remarkable evolutionary diversity of CAs. Indeed, there are now eight known gene families that encode structurally divergent classes of CAs: the α-, β-, γ-, δ-, ζ-, η-, θ-, and ι-CAs.[766,767] All human CAs the α-class enzymes, where at least 12 active isozymes have been described that differ in oligomeric assembly state, subcellular localization, tissue expression, and kinetic properties while all sharing Zn^{II} as an essential cofactor.[768] In bacteria, the major structural classes are the α, β and γ enzymes while the ι-CA is present in marine diatoms.[769] Bacterial α-CAs are generally are generally periplasmic (in Gram-negative organisms) and function as monomers or dimers, while employing Zn^{II} as the Lewis acid cofactor in a His_3-H_2O motif like the mammalian CAs (Figure 31A). β-CAs are typically dimers, tetramers or octamers that are also obligate Zn^{II} metalloenzymes that coordinate Zn^{II} with two Cys, one His and an open coordination site (Figure 31B). β-CAs often exhibit strongly pH-dependent activity in which an Asp is recruited into the open coordination site at high pH, thus abolishing turnover. γ-CAs are adopt a trimeric left-handed β-helical architecture and utilize the same His_3-H_2O motif as α-CAs (Figure 31C), but are reported to be Fe^{II}-dependent enzymes that are also active with Zn^{II} and Co^{II}. One ι-CA has been reported to prefer Mn^{II} over Zn^{II}, although the extent to which this is broadly the case is not known.[770]

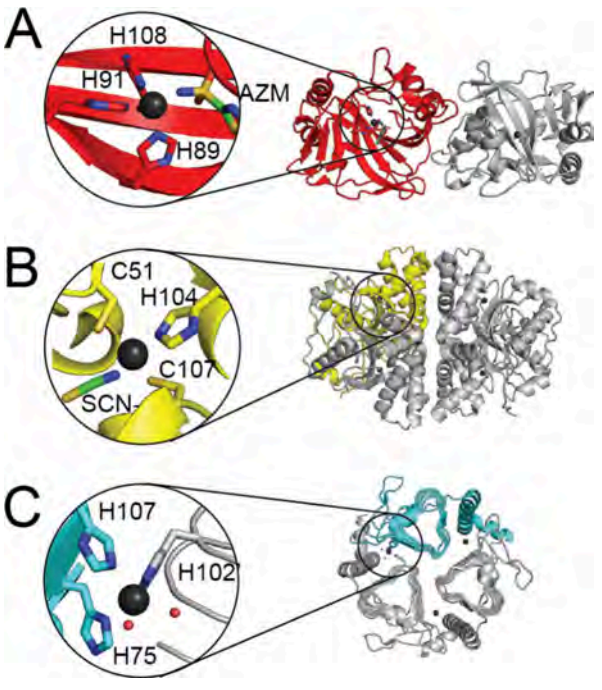

Figure 31. Carbonic anhydrases likely arose via convergent evolution. A) Ribbon representation of the homodimeric α-carbonic anhydrase (4X5S)[773] with the highlighted monomer labeled in red and other protomer colored gray. α-carbonic anhydrase active site (close up, *left*) with Zn binding residues shown as red sticks, Zn ion as a black sphere, and the acetazolamide (AZM) inhibitor shown as green sticks. B) Ribbon representation of the tetrameric β-carbonic anhydrase (2A5V)[774] with the highlighted monomer labeled in yellow and additional protomers colored gray. β-carbonic anhydrase active site (close up; *left*) with Zn binding residues shown as yellow sticks, Zn ion as a black sphere, and SCN^- molecule shown as green sticks. C) Ribbon representation of the trimeric γ-carbonic anhydrase (3KWC)[775] with the highlighted monomer labeled in cyan and additional protomers colored gray. γ-carbonic anhydrase active site (close up; *left*) with Zn binding residues shown as cyan sticks, Zn ion as a black sphere, and water molecules as red spheres.

Most bacteria encode more than one CA, often but not always derived from all three major classes (cytoplasmically localized β- and γ-class enzymes feature prominently in clinically relevant pathogens), with some regulated by nutrient stressors. In the few instances where it has been documented that cellular expression of a CA changes with Zn^{II} restriction[738] and/or represents a *bona fide* Zur target (as in *P. aeruginosa*) these enzymes tend to belong to the β- and γ-classes, with bacterial pathogens often encoding multiple β-CAs with apparently nonredundant functions.[690,738,769] We believe that Zur-regulated expression of a γ-CA may represent a case of Zn-sparing, since this enzyme is reported to be metal-promiscuous with Fe^{II} the preferred metal cofactor when prepared under anaerobic conditions.[771,772] An in depth study of metal preferences across the different families of CAs and, in particular, in the case of Zur-regulated γ-CAs is clearly warranted to correctly identify how this essential metabolism has adapted to microenvironmental niches poor in nutrient metal availability.

4.3.5. Cambialistic Superoxide Dismutases. The superoxide dismutases (SODs) detoxify superoxide, a reactive oxygen anion radical produced in all organisms exposed to oxygen particularly during aerobic metabolism. Superoxide is also employed by the mammalian immune system in response to infection.[776] The ubiquity of SODs across the tree of life illustrates their biological importance in an oxygenated world, and are particularly important as part of the host−pathogen interface.[777] Typically, SODs are classified in families according to their metal cofactor, and are grouped into three different structural classes: the copper and zinc or Cu-only SODs, the nickel SODs, and the manganese (Mn), iron (Fe) or cambialistic Fe/Mn SODs.[778] Each metal cofactor results in a metal active site with a distinct redox potential and architecture. SOD subfamilies also diverge in distribution, subcellular location, quaternary structure and specific mechanism.[778] Nonetheless, in general they achieve catalysis via a ping-pong mechanism, in which the metal center oscillates between oxidized and reduced states that differ by one electron.[779] As such, the general SOD mechanism consists of two half-reactions, where substrate oxidation produces O_2 and a reduced metal site, and substrate reduction produces H_2O_2 and the oxidized metal site.

The differential expression of SODs with different metal requirements by the same organism can be considered a canonical metal sparing mechanism to ensure organism survival during metal nutrient limitation and the oxidative burst.[777] A highly conserved regulatory mechanism, originally described in *E. coli*, consists of a global regulator, the Fe^{II} sensor Fur, a small RNA, RyhB, and two genes encoding distinct Mn- and Fe-SODs, *sodA* and *sodB*, respectively. When Fe is replete, Fur represses transcription of *sodA* and *ryhB*, which lowers the stability of the *sodB* mRNA, thus leading to the production of Fe-SOD. Under conditions of Fe starvation, Fur dissociates from its operator, leading to transcriptional derepression of *sodA* and *ryhB*, allowing for high cellular levels of Mn^{II}−SOD.[780] This mode of regulation has also been described in *Azotobacter vinelandii*,[781]

https://doi.org/10.1021/acs.chemrev.4c00264
Chem. Rev. 2024, 124, 13574−13659

Bacillus subtilis[782] and *Helicobacter pylori*[783] with global regulators from the same regulator family and SODs with distinct metal preferences.

Another regulatory mechanism first described in *Streptomyces coelicolor* involves the inverse regulation of the expression of *sodF* (Fe-containing) and *sodN* (Ni-containing) by the nickel-specific repressor Nur, a Fur-family regulator.[784] In nickel-replete conditions, Nur represses *sodF* transcription, while inducing *sodN* expression indirectly. The *sodF* gene produces a stable small-sized RNA species (s-SodF) of ≈90 nucleotides that harbors an anti-*sodN* sequence complementary to the 5′ end of *sodN* mRNA through the ribosome binding site. Therefore, Nur activates *sodN* expression by inhibiting the synthesis of the *sodF* mRNA, from which inhibitory s-SodF RNA is generated forgoing the need for another small RNA to acts as a mediator.[784] SODs of different metal selectivity are thus differentially expressed according to cellular metal nutrient bioavailability.

In contrast to metal-specific SODs, there are other SODs that are genuinely cambialistic (camSOD)[785] or metal-interchangeable. Here, a SOD may be characterized by distinct metal binding affinities for Fe vs Mn yet possess identical specific activities when cofactored by either metal.[7] These SODs, denoted SodFMs, will be differentially metalated with Fe or Mn depending on which metal is present and bioavailable. Notably, *S. aureus* camSOD (Figure 32A) allows superoxide detoxification during host-imposed Mn starvation by calprotectin (CP), which functions in place of the Mn-dependent SodA (Figure 32B) and is presumably not effectively metalated under these conditions (Section 2.2.2).[181,786] This is an excellent illustration of Mn^{II}-sparing, also found for at least one glycolytic enzyme in the same organism under the conditions of CP-mediated nutrient limitation.[6]

The evolutionary diversity of extant SODs is thought to arise in part from a series of gene duplication events, later selected during the earth's geological changes, e.g., the great oxygenation event, or as an adaptation of pathogens to host-imposed stresses, including nutritional immunity and ROS exposure.[181,787] Determining the metal preference of a metalloprotein in general remains a difficult task, and in the case of SODs, these preferences have been shown to depend not only on the first coordination shell of metal binding residues but is also impacted by the identity of specific second sphere residues (Figure 32C).[787] In addition, discoveries such as the Cu-only SODs from an opportunistic fungal pathogen that dispose of the requirement for Zn altogether within a canonical Cu/Zn-dependent SOD fold, and which are strongly induced under conditions of Fe-starvation, highlights a potential of still uncovered regulatory and structural diversity within the superoxide dismutases.[788−790] Recently, a comprehensive sequence and phylogenetic analysis has been shown to improve the ability to predict the preferred metal cofactor in a SOD, which enhances our understanding of the catalytic diversity present in this family.[680] This study proposes that redox tuning[791] allowed the SodFM subfamily to exquisitely fine-tune their metal preference along a continuum of Mn:Fe preferences as a result of very subtle structural changes in the active site. Indeed, cambialism may not simply be a feature that has evolved multiple independent times, but may also be under positive selection in nature to allow a bacterial pathogen to circumvent host-derived nutritional immunity during an infection.[181,680]

4.3.6. Ribonucleotide Reductases. The ribonucleotide reductases (RNRs) catalyze the 2′-dehydroxylation of a ribonucleotide substrate thus providing the only *de novo* route to 2′-deoxyribonucleotide building blocks for DNA synthesis.[8,793] RNRs are typically composed of two types of subunits: a catalytic R1 subunit and a small radical-generating subunit R2. R2 comprises a core four-helix bundle that harbors the metal cofactor, and four additional auxiliary helices that participate in the interaction with the other subunits (Figure 33A). Ribonucleotide reduction typically requires a metal cofactor and an oxidant in the R2 subunit (encoded by *nrdF*) that ultimately oxidizes an active site cysteine side chain in the R1 subunit to create a thiyl radical; this allows for radical activation of an otherwise inert C−H bond in the ribose ring of the substrate bound to R1.[8] The mechanism by which the metal cofactor generates the radical to initiate this chemically challenging reduction reaction varies substantially among the three classes of RNRs. While class II requires an adenosylcobalamin cofactor and class III, a [4Fe-4S]-activating enzyme, all class I enzymes harbor a bimetallic metal site defined in the core four-helix bundle that also encodes for an aromatic residue which participates in electron transfer (Y105 in *E. coli* NrdF) (Figure 33).[8] A metal-free class Ie enzyme constitutes a possible exception within class 1 which lacks the metal-ligating glutamates (highlighted in blue in Figure 33B) and instead

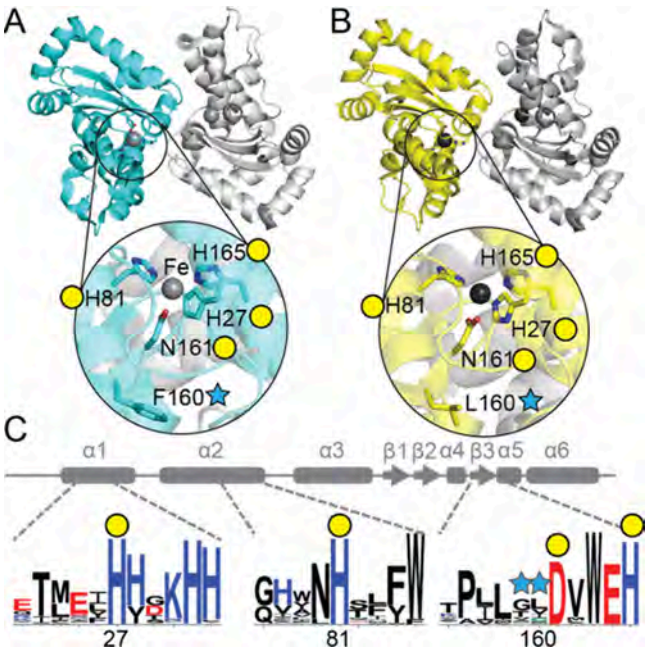

Figure 32. Superoxide Dismutases. A) Ribbon representation of the dimeric cambialistic superoxide dismutase SodM (camSOD) from *S. aureus* (6EX4)[792] with the highlighted monomer shaded cyan. The active site (close-up) with identical metal binding residues shown as sticks and highlighted in yellow. Fe is a gray sphere. A cyan star highlights an identified residue responsible for determining metal preference. B) Ribbon representation of the dimeric Mn^{II}-dependent superoxide dismutase SodA (MnSOD) from *S. aureus* (5N56)[792] with the highlighted monomer labeled in yellow. The active site (close-up) shows the Mn binding residues in sticks and highlighted in yellow. Mn is a black sphere. A cyan star highlights an identified residue responsible for determining metal preference. C) Conserved features of SODs that encompass both metal selective and cambialistic enzymes. While each has a high degree of identity and highly conserved metal binding residues (highlighted in yellow), certain key residue positions have been identified as determinants in metal preference (highlighted with cyan stars). Their identity can modulate its metal preference from Mn- or Fe-selective to cambialistic.

https://doi.org/10.1021/acs.chemrev.4c00264
Chem. Rev. 2024, 124, 13574−13659

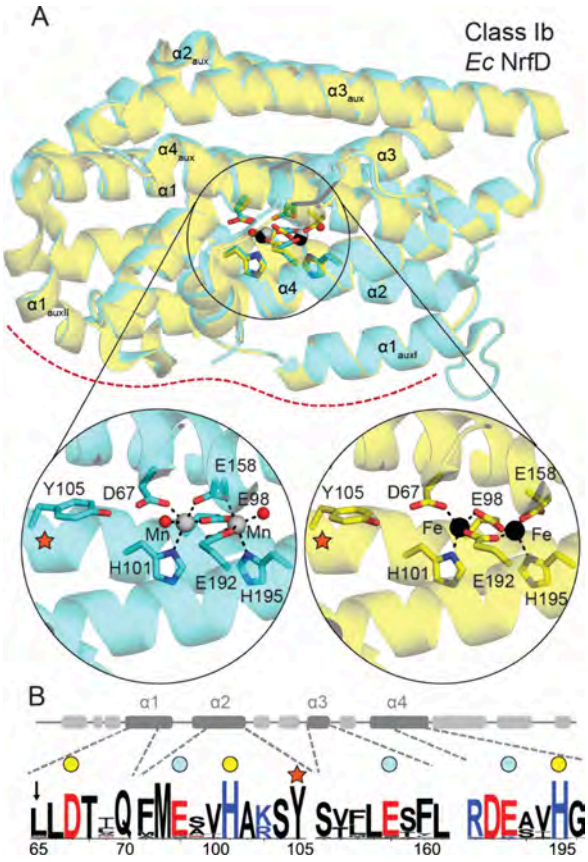

Figure 33. Ribonucleotide reductases. A) Ribbon representation of the R2 subunit of the ribonucleotide reductase NrdF from *E. coli* in the Mn_2-form in cyan (3N37) and Fe_2-form in yellow (3N38).[795] A close-up view of the active site with metal binding residues shown as sticks. Fe is a black sphere, Mn is a gray sphere, and the red spheres represent water molecules. An orange star highlights the tyrosine residue that will become a tyrosyl radical upon metal oxidation. The interface with the catalytic R1 subunit is indicated with a red dashed line. C) Conserved features of class Ib R2 subunit that encompass metal binding residues highlighted with circles, while the tyrosyl radical is highlighted with a star. Residues conserved among all class I enzymes are highlighted in yellow while the residues absent in the metal free class Ie activase are highlighted in cyan. The residue that has been shown to impact metal preference in *B. anthracis* R2 is indicated with a black arrow.

requires a specialized NrdI activating enzyme.[8,794] The metal requirement and metal specificities of the R2 subunits have been shown to differ among the class I subclasses, with class Ib of particular note here, since class Ib R2 enzyme is truly cambialistic, forming active enzymes with both dinuclear Fe/Fe and Mn/Mn cofactors (Figure 33).[795]

The physiological conditions that drive iron or manganese loading in class Ib enzymes remain long-standing questions in the field.[683,796] One possibility is that metalation is primarily determined by the specific characteristics of the growth environment where the bioavailability of Fe^{II}, which can be significantly modulated by collateral oxidative stress, vs Mn^{II} may well dictate metal occupancy of a single expressed class Ib enzyme, thus enhancing bacterial survival.[7] It has been proposed that use of Mn^{II} by bacterial subclass Ib, Ic and Id RNRs, which contrasts with the exclusive use of iron by the eukaryotic Ia enzymes, may help to protect certain pathogens against iron deprivation imposed by their hosts. In *E. coli*, for example, the class Ib NrdF protein is not expressed under conditions of metal-replete aerobic growth but is induced under iron limitation and oxidative stress. In contrast to the class Ia diferric tyrosyl radical (Fe^{III}_2-Y•) cofactor, which can self-assemble and mature from Fe^{II}_2-NrdF and molecular O_2, generation of the Mn^{III}_2-Y• cofactor in the class Ib enzyme requires the reduced form of a flavoprotein, $NrdI_{hq}$, and O_2 to create superoxide anion for active site assembly and oxidative maturation.[795] Indeed, structures of the NrdI-NrdF complexes have been known for a number of years now.[795] This may not be generally true for all class Ib enzymes, since in *Bacillus cereus*, for example, the NrdF–NrdI complex is not strongly affected by the nature of the bound metal in the NrdF subunit.[797] Furthermore, *Bacillus anthracis* class Ib R2 subunit intrinsically selects manganese over iron, under both aerobic and anoxic conditions, when the metal-free protein is subjected to incubation with equimolar Mn^{II} and Fe^{II} in a crystallographic soaking experiment.[798] These findings are at face value in opposition to expectations from the Irving-Williams series (Figure 8). Interestingly, introduction of a substitution of a second coordination sphere residue (highlighted with an arrow in Figure 33B) in *B. anthracis* NrdF only subtly changes the site 1 metal coordination geometry and yet impacts spontaneous metalation of the protein to form a predominant heterodinuclear Mn/Fe cofactor under aerobic conditions and a Mn/Mn metal center under anoxic conditions.[798] There is clearly much more to learn about the general principles of metal selectivity in cells, particularly in class 1b RNR activating enzymes.

5. METAL TRAFFICKING TO SPECIFIC CLIENTS AND COMPARTMENTS

A second major regulatory outcome of metalloregulation of gene expression by metal sensor proteins is the expression of proteins that traffic or allocate transition metals to a specific recipient protein or cellular compartment (Figure 1). Seminal work on copper chaperones found in all domains of life provides the framework for much of this discussion.[799,800] These early studies showed that a metallochaperone forms a ligand-exchange *labile* coordination complex with a specific metal and exploits the specificity of protein–protein interactions to transfer the metal to an acceptor or client protein (Figure 34, *top*). Here, we discuss more recently published work on a distinct class of soluble, NTP-hydrolysis powered metallochaperones involved in metalloenzyme maturation.[688,691,801] We also discuss recent structural and biological work on metal transporters, some from the P-type ATPase superfamily,[802,803] as historical clients of the

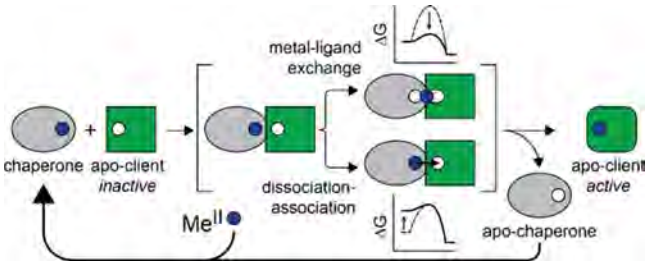

Figure 34. Conceptual framework for thermodynamically favorable metal transfer from a donor protein to an acceptor client protein. *Top*, metallochaperone-client protein interaction lowers the kinetic barrier to metal transfer via intermolecular metal–ligand exchange. *Bottom*, metallochaperone-client protein interaction reduces the thermodynamic stability of the metallochaperone-metal complex, enabling transfer by increasing the favorability of the transfer reaction.

https://doi.org/10.1021/acs.chemrev.4c00264
Chem. Rev. 2024, 124, 13574–13659

copper chaperones,[804,805] that are paired with an accessory protein(s) that may have metallochaperone-like features, or possess intrinsic metallochaperone activity itself.[792] Although chemical and structural mechanisms that underscore the processes we describe here are, in some cases, not yet known, these biological studies establish a foundation for future studies.

One prevailing model of metallochaperone function holds that the association between a metalated donor and an apoprotein acceptor occurs such that the donor metal complex is in close physical proximity to the empty client metal binding site, allowing client metal ligands to invade the first coordination shell of the donor metal complex, and initiate a ligand exchange process.[804,806,807] This framework exploits the fact that late *3d*-block divalent transition metal complexes formed with biological ligands, even complexes of considerable thermodynamic stability and metal association constants of 10^{10} to $\geq 10^{20}$ M^{-1}, are kinetically exchange-labile,[808] particularly so if a higher coordination number complex can be transiently formed during the metal transfer process (Figure 34, *top*).[809,810] Alternatively, protein−protein docking disrupts or alters the first coordination shell of the donor, independent of intermolecular metal ligand exchange, lowering the metal affinity, thereby enhancing the kinetics and thermodynamics of metal transfer (Figure 34, *bottom*).

The rates and mechanism by which metals are exchanged between donor and acceptor remains understudied, but must be dictated in part by their position along a continuum of divalent metal stability constants with simple organic ligands, known as the Irving-Williams series (Figure 7).[157] We posit that for high affinity metals, notably Cu^{II} (and Cu^{I}), Zn^{II} and Ni^{II}, affinities are so tight so as to render metal dissociation rates (off-rates), even if increased by the presence of metal-buffering small molecules, far too slow to be relevant during intermolecular metal transfer (Figure 34, *top*). A metal−ligand exchange process effectively lowers the kinetic barrier to the metal movement as long as the thermodynamic gradient from donor to acceptor is favorable.[805] This arrangement also effectively prevents deleterious "off-pathway" reactions by highly competitive metals (Figure 7) where inappropriate metal dissociation might drive noncognate mis-metalation of the proteome (Section 2.2.3), particularly problematic for metalloenzymes that require weaker binding metals for activity.[168,811] In contrast, metal dissociation rates into solvent for those weaker binding metals, including Mn^{II} and Fe^{II} on the *left* side of this series (Figure 7), can be sufficiently rapid to be captured by both metal-buffering small molecules and ultimately the recipient acceptor protein, particularly if an open or solvent-accessible coordination site is available on the metal bound to the donor protein.

5.1. Soluble Nucleotide-Dependent Metallochaperones

5.1.1. Overview. Enzymes associated with the superfamily of P-loop G3E GTPases and other closely related NTPases are the principal nucleotide-dependent metallochaperones (NMC) in all kingdoms of life (Figure 35A).[688,691,801] These GTPases (G-proteins) use the energy of GTP hydrolysis to facilitate metal transfer or another step in the metalloenzyme maturation cycle, shown specifically for a metal transfer reaction (Figure 35B).[56,812−815] G-proteins are characterized by several short, conserved G-loops that are responsible for GTP binding and hydrolysis and are denoted G1-G5, from N- to C-terminus (Figure 36A,B).[816] Loop G1 encompasses the canonical P-loop or Walker A motif and recognizes the α- and β-phosphates. G2

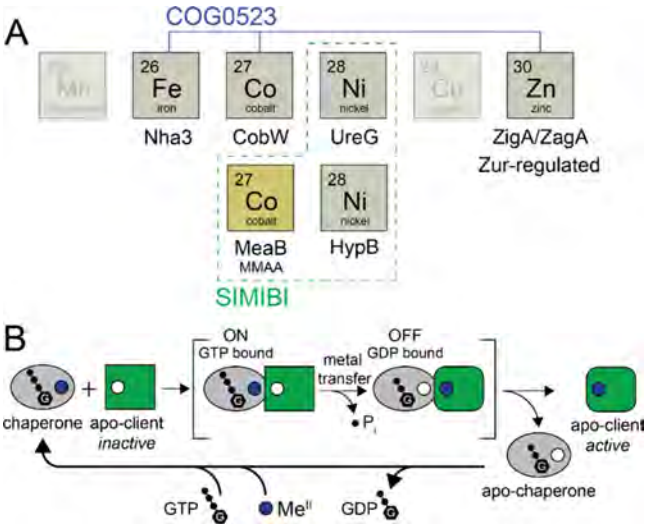

Figure 35. Nucleotide-dependent metallochaperones. A) Known members of the small P-loop G3E superfamily of NTPases that are known or thought to be involved in metallocofactor maturation. SIMIBI, signal recognition particle, MinD, and BioD; COG0523, cluster of orthologous groups 0523. The Co MeaB square is shaded differently to emphasize that MeaB functions as an accessory protein for ATR (Section 5.1.3). B) Nucleotide-dependent metallochaperone model, which proposes that GDP hydrolysis and dissociation of P_i are just upstream or coincident with metal transfer to the client.

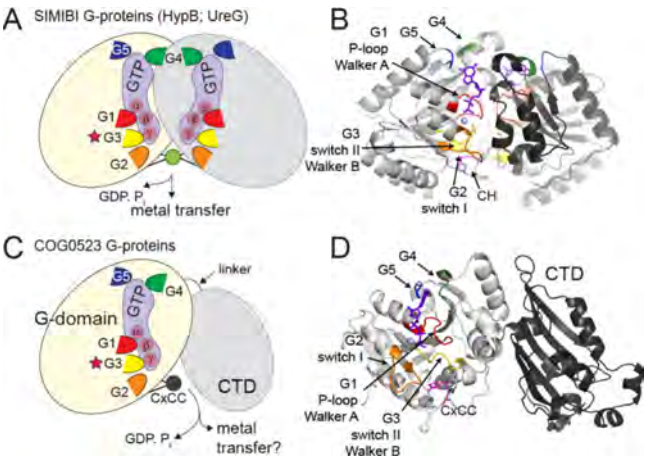

Figure 36. Conceptual and structural comparisons between representative SIMIBI class and COG0523 subfamily metallochaperones. A) Cartoon representation of SIMIBI G-proteins. The five G-loops are shaded as in panel B: G1, red; G2, orange; G3, yellow; G4, green; G5, blue. The GTP is purple with the three 5′ phosphate groups shaded red. The metal to be transferred is shaded green. B) Ribbon representation of *Helicobacter pylori* HypB (4LPS), with the five G-loops shaded as in panel A. C) Cartoon representation of a canonical COG0523 protein, colored as in panel A, with Zn^{II} shaded black. CxCC (C, Cys; x, any amino acid) is the high affinity metal binding site of COG0523 enzymes.[820] D) AlphaFold2 model of *Acinetobacter baumannii* ZigA from Model Archive showing GTP and Zn^{II} positioned as in the crystal structure of *Methanococcus janaschii* HypB (PDB 2HF8) (panel B).[820] Conserved motifs are indicated on the structure, shaded red, orange, yellow, green, and blue for G1-G5 respectively. Mg^{II} ion, gray sphere; Zn^{II} ion black sphere; GTP, purple stick.

(switch 1/switch I) and G3 (Walker B or switch 2/switch II) stabilize the β- and γ-phosphates on the bound nucleotide and donate ligands to the Mg^{II} coordinated by these phosphates

https://doi.org/10.1021/acs.chemrev.4c00264
Chem. Rev. 2024, 124, 13574−13659

(Figure 36A). The Mg^{II} activates a water molecule for GTP hydrolysis. The G3E family gets its name from a Glu (E) in the G3 motif, **E**xxG instead of the canonical **D**xxG.[817] The glutamate directly participates in coordinating the Mg^{II} ion, whereas the more typical aspartate makes a water-mediated contact to the metal ion.[817] The G4 (often NKxD, where N, Asn, K, Lys; D, Asp) and G5 loops influence nucleotide specificity and release, respectively, via interactions with the nucleobase; G5, in particular, exhibits higher sequence variability than the other G-loops.[801]

The G2 and G3 loops are conformationally plastic and function as molecular switches that drive a change in structure and/or dynamics within and likely beyond the G-domain upon GTP hydrolysis. The conformation of the G2 loop in particular defines the active ON (GTP-bound) and inactive or relaxed OFF (GDP-bound) states;[818,819] conformational switching by one or more G-domain "switches" upon GTP hydrolysis is likely the key structural trigger that orchestrates NMC function in a metallochaperone cycle (Figure 35B).

5.1.2. SIMIBI Proteins Involved in Ni^{II}-Enzyme Biogenesis. UreG and HypB are examples of extensively characterized G3E GTPases that utilize their G-domains to catalyze Ni^{II} insertion into urease and [NiFe]-hydrogenase, respectively (Figure 37).[819,821,822] This metalloenzyme specificity is not absolute, since UreG can substitute for HypB in the maturation of [NiFe]-hydrogenase, with the accessory protein UreE a key player that links the two metalloenzyme maturation pathways in some bacterial cells (Figure 37).[823,824] Both UreG and HypB are members of the SIMIBI (signal recognition particle, MinD, and BioD) class of ATPases and GTPases[825] that are regulated by reversible dimerization stabilized by NTP binding that is linked to formation of a metal coordination site that is destined to be transferred to a client enzyme (Figure 38A,B).[819,826] In the GTPases, the GTP is sandwiched into two symmetry-related binding sites at the protomer interface of the dimer in the ON or GTP-bound state. In the case of UreG, this creates a subunit-bridging Ni^{II} site that is coordinated by an invariant **Cys**-Pro-**His** sequence from opposite protomers and positioned between the G2 and G3 loops in the primary structure, to form an approximately square planar Cys_2-His_2 coordination complex (Figure 38A),[821] mutagenesis of which abolishes urease maturation.[827] Zn^{II} can also bind to this site, but the binding is weaker.[162] These general features also characterize HypB, except that the subunit-bridging coordination chemistry is distinct, involving two invariant Cys, one of which is part of an **Cys**-His motif positioned between the G2 and G3 loops,[691] and another embedded in the G3/switch II motif itself (Figure 38B).[819,824,828] This suggests a conformational "gating" mechanism in HypB where GTP hydrolysis signals to the Ni^{II} binding site through G3, thus initiating metal transfer to HypA, which itself later inserts Ni^{II} into [NiFe]-hydrogenase (Figure 37, *top*).[829] There is evidence to suggest that the His in the Cys-**His** motif in HypB (Figure 38B) toggles on and off the Ni^{II} as a function of nucleotide status as an important aspect of the gating process, but more needs to be done here.[828]

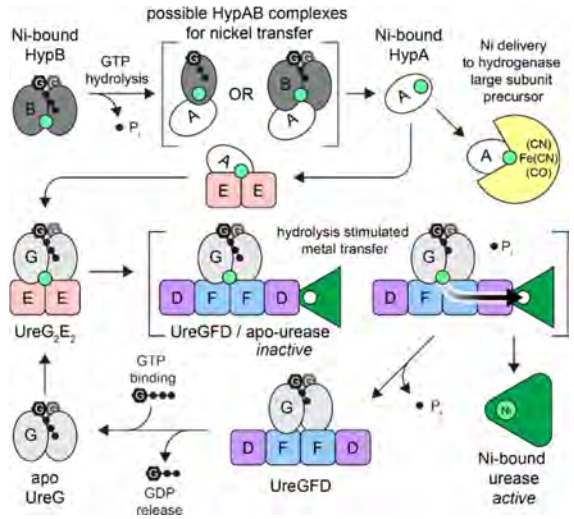

Figure 37. Schematic illustration of the maturation of bacterial [NiFe]-hydrogenase and urease. UreE (labeled E; shaded pink) is thought to bridge the two metalation pathways, capable of accepting Ni^{II} from HypA and UreG as indicated.[824]

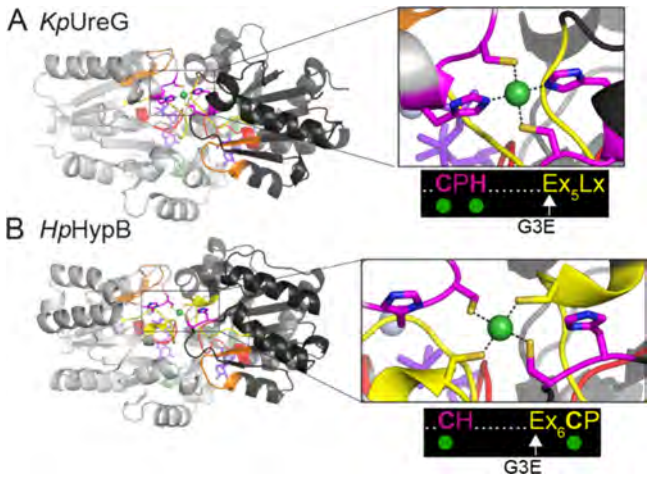

Figure 38. Structural features of the UreG and HypB homodimers. A) Ribbon structure of the *Kp*UreG dimer (gray, black subunits) with G-loops shaded as in Figure 36 and the intersubunit Ni^{II} coordination sphere shown in magenta stick. Ni^{II}, cyan. GTP, purple stick. *Inset*, Close-up of the Ni^{II} coordination sphere with an abbreviated primary structure representation with Ni^{II} ligands (cyan circles) and the E residue as the namesake of the G3E superfamily indicated. B) Ribbon diagram of the *Hp*HypB dimer, shaded as in panel A. *Inset*, close-up of the Ni^{II} coordination site, with the Cys residue drawn from the G3 loop (yellow) and CH sequence (magenta) shown.

5.1.2.1. Urease Maturation. There has been considerable progress in our mechanistic understanding of UreG-dependent urease maturation in both *Klebsiella pneumoniae* and in the gut pathogen *Helicobacter pylori* (Figure 37, *bottom*).[824,828,830] Urease hydrolyzes urea into carbon dioxide and ammonia[831] and allows *H. pylori* to thrive in the acidic environment of the stomach, where it portends an increased risk of peptic ulcers and gastric cancer.[832] Urease adopts a C3-symmetric trimer of trimers ($\alpha\beta\gamma$) architecture (Figure 39A), harboring a buried binuclear Ni_2 active site (Figure 39B) featuring a bridging carbamylated Lys (Figure 39C), with all metal ligands derived from the α-subunit. Urease maturation involves the participation of four accessory proteins that form a urease activation complex that ultimately moves Ni^{II} from UreG to UreB (*H. pylori* designation) via the obligatory intermediacy of UreF and UreD (UreH in other organisms) (Figure 37, *bottom*). Early work established that UreG, UreF and UreD form a 2-fold symmetric $UreG_2F_2D_2$ complex in which the UreG dimer fits snugly between an approximately linear UreD-UreF−UreF'-UreD' complex with $UreG_2$ docked opposite the $UreF_2$ core,

https://doi.org/10.1021/acs.chemrev.4c00264
Chem. Rev. 2024, 124, 13574−13659

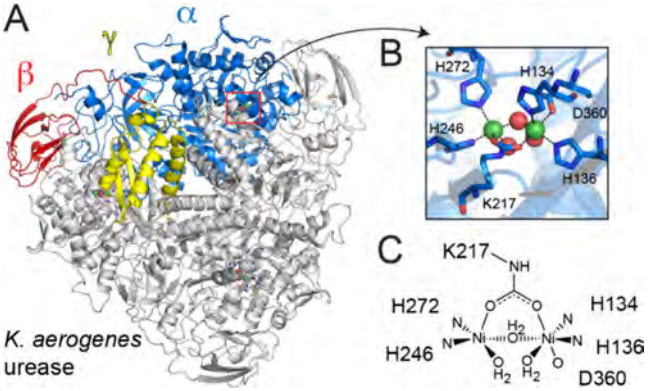

Figure 39. Structure of *K. aerogenes* urease (1FWJ).[824] A) Ribbon representation of the trimer or trimers architecture, with one $\alpha\beta\gamma$ heterotrimer shaded blue, red and yellow, respectively. B) Metal coordination structure of the binuclear Ni_2 active site. C) chemical representation of the coordination structure, featuring a bridging carbamylated Lys.

positioning the subunit-bridging Ni^{II} ion at the $UreG_2F_2$ interface (Figure 40A).[830]

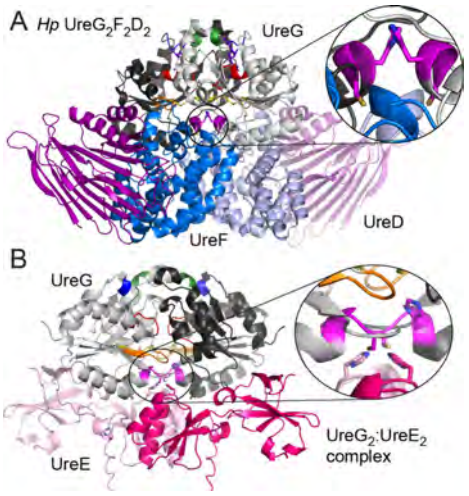

Figure 40. Urease maturation intermediates. A) The 2-fold symmetric *H. pylori* $UreG_2F_2D_2$ complex (4HI0), with the UreG G-loops of the homodimeric UreG shaded as in Figure 38A. G1-G5 loops are colored red, orange, yellow, green, and blue, respectively; GDP, colored purple, and the CPH Ni-binding motif colored magenta. UreF subunits are colored light and dark blue, and UreD subunits are colored light and dark purple. B) An Alphafold2 model of the $UreG_2$•$UreE_2$ complex (ModelArchive ma-41ctj), which functions upstream of the complex in panel A.

Functionally upstream of UreG is UreE, and it is the $UreG_2$-GTP form that productively engages Ni^{II}-bound $UreE_2$ and accepts the metal, leading to dissociation of UreE following Ni^{II} transfer (Figure 40B). The GTP-bound form $UreG_2$ is then incorporated into the $UreG_2F_2D_2$ complex (Figure 40A). Assembly of this metal transfer intermediate alters the structure of the terminal UreD subunit in such a way that this allows $UreG_2F_2D_2$ complex to engage a single protomer of the apo-urease trimer, with a single UreD subunit of UreDF heterodimer necessary and sufficient to bind a urease trimer, primarily via interactions with UreB (Figure 41).[833] Remarkably, formation this UreFD-urease complex results in the formation of an

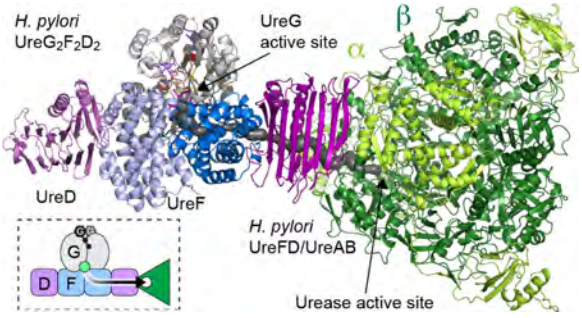

Figure 41. Model of a single $UreG_2F_2D_2$ complex (colored as in Figure 40A) bound to one of the three urease heterotrimers (green), based on overlaying the cryo-EM structure of *H. pylori* urease in complex with UreFD (8HC1)[833] and the crystal structure of *H. pylori* $UreG_2F_2D_2$ complex (4HI0). This results in formation of an extended tunnel (dark gray), as identified by the Pymol plugin Caver 3.0.3,[834] that connects the UreG active site (magenta) with the urease active site.[833] The schematic model from Figure 37 is shown in the lower left.

extended ≈100 Å tunnel that links the UreG-Ni^{II} binding domain with the empty urease active site, thus suggesting a plausible pathway of Ni^{II} movement from UreG to urease (Figure 41). Critically, mutations that disrupt the $UreG_2F_2D_2$ complex or the UreFD interface abolish urease activation in cells and *In vitro*, respectively.[830,833] In addition, mutations that compromise the integrity of the tunnel negatively impact urease maturation *In vitro*.[833]

This remarkable tunnel serves to enhance the exquisite metal specificity of urease maturation that must be dictated by the metal specificity of the $UreE_2G_2$ complex itself, while also chaperoning this highly competitive Ni^{II} (Figure 7) into the active site, so as to avoid off-pathway mis-metalation by this toxic metal ion. Mechanistically, GTP hydrolysis is known to induce a conformational switch in the G2 loop and **Cys**-Pro-**His** Ni^{II}-binding motif in UreG (Figure 38A),[821] and perhaps only as part of the activation complex, may weaken the Ni^{II} affinity and allow for dissociation of Ni^{II} into the vestibule (Figure 34, *bottom*).[833] How the integrity of metalation of client proteins dependent on other G-protein metallochaperones (Section 5.1.4) is not yet known, and this is an area worthy of significant future study.

5.1.3. SIMIBI Proteins: MeaB and Maturation of B_{12}-Cofactored Enzymes. Although the work described above for HypB and UreG is consistent with the metallochaperone model (Figure 35B), both function upstream of the actual apoenzyme metalation event and neither directly interacts with the client enzyme itself. In the maturation of the adenosylcobalamin (AdoCbl; B_{12})-dependent enzyme, methylmalonyl-CoA mutase (MCM), the SIMIBI family G-protein MeaB (MMAA in humans) also requires the energy of GTP hydrolysis to drive metallocofactor insertion into MCM. However, MeaB (MMAA) functions not to deliver metallocofactor cargo (AdoCbl) directly, but instead uses the energy of GTP hydrolysis to close a "wedge" between the two subdomains of MCM, after another enzyme, adenosyltransferase (ATR; MMAB in humans[835,836]) inserts the cofactor into an "open" form stabilized by the MeaB-GTP dimer (Figure 42A).[816,837] ATR has two roles, one of which is to adenylate cob(II)alamin using ATP to make AdoCbl, followed by transfer of AdoCbl to the cobalamin (Cbl)-binding domain of MCM. Thus, MeaB (MMAA) leverages the energy of GTP hydrolysis to gate AdoCbl insertion into the active site of MCM, while also

https://doi.org/10.1021/acs.chemrev.4c00264
Chem. Rev. 2024, 124, 13574−13659

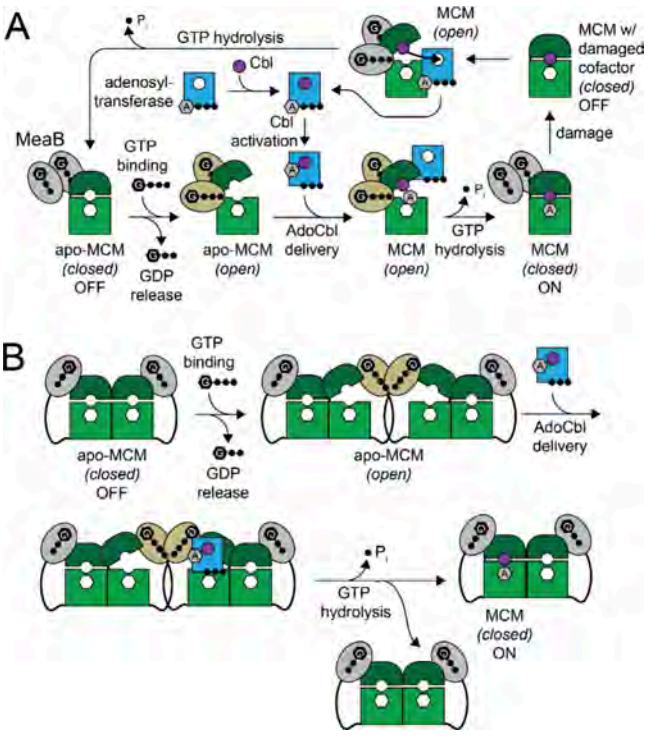

Figure 42. MeaB and adenosyltransferase (ATR)-dependent maturation of MCM. MeaB is shaded gray (GDP-bound OFF state) or bronze (GTP-bound ON state), ATR, blue and MCM, green, with the Cbl-binding domain of MCM shaded dark green.[841] A) Model for a typical system in which MCM and MeaB are different polypeptide chains. GTP binding activates MeaB to recruit cofactor-loaded ATR to an "open" conformation of the mutase; GTP hydrolysis inactivates MeaB (OFF), leading to a "closed" conformation. Cofactor damage leads to the recruitment of GTP-bound MeaB and ATR, leading to release of the damaged cofactor. B) Model for maturation of a fused (IcmF) system, which requires GTP dependent dimerization of two peripheral MeaB protomers within a filamentous oligomer to create a conformation that is active for maturation.[841]

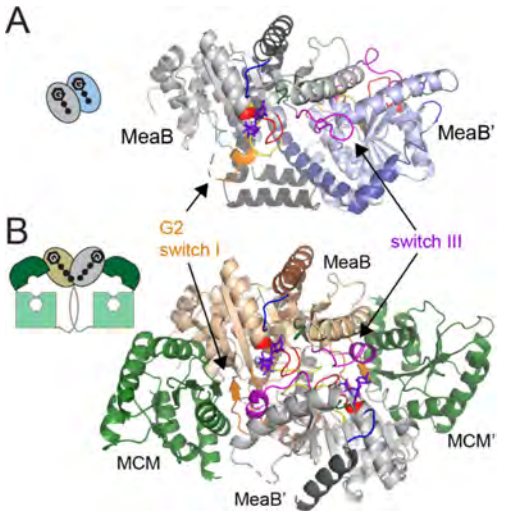

Figure 43. Conformational change in MeaB in moving from the "inactive" GDP-bound conformation to the "active" GMPPCP-bound state enabled by the stable interacion with the Cbl-binding domain of MCM. A) GDP-bound conformation (2QM7).[842] B) The active conformation compared to a cartoon model of a dimer interface that must be formed in the filament form of IcmF.[841] This structure is that of the soluble MCM^{Cbl}-MeaB 2:2 complex (8DPB).[837] The two MeaB subunits on the *left* are oriented in exactly the same way in panels A and B, allowing visualization of the large movement of the MeaB' subunit (*right*) in the "active" relative to "inactive" states. The G2 switch I (orange) and the switch III (magenta) regions are highlighted in each structure, with the G-loops shaded as above. The bound nucleotide is in stick (purple).

stimulating removal of damaged cofactor from inactive MCM (Figure 42A).[816,838]

5.1.3.1. Standalone MeaB. Initial structures of dimeric MeaB in the apo-, product GDP- substrate GMPPNP-bound states were rather similar (Figure 43A), with the nucleotides of each protomer far apart, thus inconsistent with the dimer structures of HypB and UreG (Figure 36A,B). Further, a functionally critical switch III loop, a mobile loop that is very close to G3 and unique to MeaB, was exposed to solvent. MMAA mutant alleles in this region are associated with human disease-causing mutations in methylmalonic aciduria, an inborn error of metabolism[99] making these findings puzzling. A more recent structure of a high affinity ($K_d \leq 100$ nM) 1:1 complex between MeaB and the Cbl-binding domain of an MCM, solved in the presence of GMPPCP, reveals a completely different dimer conformation, where the two nucleotides are now quite close to one another, sandwiched at the dimer interface, with the switch III loop now engaged in direct interactions with the nucleotide of the opposite protomer of MeaB, effectively burying the bound GTP (Figure 43B). The G2-loop (switch I), disordered in the "inactive" conformation,[816] becomes ordered in this complex, forming a β-strand that hydrogen-bonds with a β-strand in MCM, establishing much of the intermolecular interface. This conformation of MeaB is thought to be representative of the "active" state.[837]

The binding of MCM stimulates the GTPase activity of MeaB dramatically, and thus the client functions as a GTPase activating protein (GAP), a finding nicely explained by the structure of the complex.[839] Consistent with this, switch III mutants effectively uncouple GTP hydrolysis from cofactor transfer from ATR, in that significant cofactor transfer occurs in the presence of a nonhydrolyzable GTP analog, GMPPNP; in addition, these mutants suppress the GAP function of MCM, giving rise to elevated MCM-independent GTPase activity. As expected, switch III mutants are impaired for the ability to offload damaged cofactor,[816,837] notably cobalamin(II), which results from the loss of the 5′-deoxyadenosyl moiety.[816]

5.1.3.2. Fused MeaB. Studies of another bacterial B_{12} enzyme maturation system provides new insights into *how* GTP hydrolysis gates AdoCbl transfer to the mutase. IcmF from *Cupriavidas metallodurans* is an AdoCbl-dependent isobutyryl-CoA mutase fused (IcmF), in which the MeaB domain exists as an independent domain of the target enzyme, which itself harbors two domains, an N-terminal TIM barrel-shaped substrate binding domain and a C-terminal Rossman fold AdoCbl-binding domain (Figure 42B).[840] The AdoCbl cofactor is situated at the interface between these two subdomains. IcmF is a homodimer, with the substrate-binding domain forming most of the dimer interface, placing the two G-domains on the periphery of the dimer (Figure 42B).[840] A key aspect of these structures was that the apo- and holo (cofactor-bound)-IcmF dimers were found to adopt "open" and "closed" states, which are representative of a structure ready to accept cofactor from ATR and the catalytically competent and cofactored state,

https://doi.org/10.1021/acs.chemrev.4c00264
Chem. Rev. 2024, 124, 13574−13659

respectively, a finding that parallels subsequent work in human MMUT-MMAA complex.[840]

These IcmF structures proved puzzling, however, in that it seemed impossible to form an obligatory G-protein dimer like that described above (Figure 43B)[816,837] furthermore, the switch III region was again fully solvent-exposed.[837] This conundrum of the "inactive" dimeric IcmF was ultimately solved when it was shown that in the presence of GMPPCP, IcmF oligomerizes into filamentous chains, thus creating the "active" MeaB-like dimer between IcmF dimers within the filament (Figure 43B).[841] This form is capable of recruiting ATR, and once one of the two immediately adjacent ICM active sites is metalated, GTP hydrolysis closes the "gate", and metalated and catalytically active IcmF dissociates (Figure 42B).[840] Both the identity of the G-nucleotide and the chemical integrity of AdoCbl cofactor impact the oligomeric state equilibrium, albeit to distinct degrees, consistent with their functional importance.[841] The "open" state of IcmF is also readily visible in these structures and distinct from that of the "closed" state.[841]

5.1.4. COG0523 Proteins. Detailed studies like those described above of SIMIBI GTPases provide significant context for our understanding of other poorly understood NMCs. Cluster of orthologous groups (COG) 0523 proteins are a distinct subfamily of the G3E P-loop NTPases that are associated with the biosynthesis of vitamin B_{12}, the maturation of the Fe-dependent nitrile hydratase and a large diversity of other proteins that are often, but not always, regulated by Zur and thus become cell-abundant under conditions extreme zinc starvation (Figure 35).[146,688,843−845] COG0523 enzymes are conserved in all kingdoms of life, from bacteria to plants to higher vertebrates, and many are connected to the cellular zinc limitation response.[56,691,814,846] Unlike SIMBI family proteins, COG0523 proteins may function as monomers and harbor an N-terminal G-domain of ≈240 residues and a C-terminal candidate protein−protein interaction domain connected to the G-domain by a variable length linker (Figure 36C,D). The only known COG0523 crystallographic structures, of *E. coli* YjiA show a C-terminal domain consisting of an antiparallel β-sheet flanked on one side by a pair of α-helices, in a β1-α1-β5-β2-β3-β4-α2 topology (Figure 44A).[818,847] Alphafold2-based modeling suggests that many families of COG0523 proteins follow the same pattern (Figure 44B), while others have additional elements of secondary structure inserted between the β4 and β5 strands (Figure 44C), and some have an additional β-strand N-terminal to β1 (Figure 44D). These features in the CTD may impact target protein specificity but this is not yet known. The extent to which the G-domain and the C-terminal domain stably interact with one another is also unknown and may well change as a function of G-nucleotide status. Although some COG0523 proteins have been reported to weakly self-associate,[125,848] the functional importance of this is not known nor are there general trends in oligomerization state that are dependent on G-nucleotide status across the COG0523 subfamily; in any case, the C-terminal domain of *Ec*YjiA docks against the G-domain in a way that would seem to inhibit dimerization in a UreG or HypB-like fashion, at least in the conformational state.[120]

5.1.4.1. Coordination Chemistry. The key distinguishing feature of the G-domains of COG0523 proteins relative to SIMIBI proteins is the presence of an N(G/S)CϕCC (N, Asn; G/S, Gly/Ser; C, Cys; ϕ, hydrophobic) motif on a loop that is positioned between the G2 and G3 loop motifs that has long been thought to serve as a high affinity ($K_{Zn} \approx 10^{10}-10^{11}$ M^{-1}) coordination site for cognate metal (Figure 36).[688] A superposition of one subunit of the Mg^{II}•GTP-bound HypB and an Alphafold2 model of *A. baumannii* ZigA (Zur-induced GTPase A) G-domain reveals that the Ni^{II} transfer site in HypB is nearly precisely coincident with the CICC motif in this Zur-regulated COG0523 enzyme (Figure 45).[820] Recent X-ray absorption spectroscopy (XAS) studies of *A. bauammnii* ZigA reveal that all three Cys residues contribute to a S_3(O/N) Zn^{II} coordination complex in the G-nucleotide-free form, with the identity of the fourth ligand as yet unknown.[820] The structure of this chelate remains S_3(N/O) in the GTPγS-bound ON and GDP-bound states OFF states, although these spectra will be somewhat insensitive to a change in the nature of the lighter donor atom in this complex.[820] This chelate structure is in contrast to an early crystallographic study of Zn^{II}-soaked *Ec*YjiA, which suggested a Zn^{II} binding site composed of the second Cys in the CϕCC motif and two acidic residues derived from the G2 loop region, not conserved in *Ab*ZigA.[691] *Ec*YjiA, of unknown biological function, and *Ab*ZigA, which clearly plays an important role in the adaptive response to transition metal starvation[125,738] are only distantly related to one another.[691] The GTPase activity both *Ab*ZigA, the same enzyme from *Staphylococcus aureus* (*Sa*ZigA) and another *E. coli* COG0523 enzyme of unknown

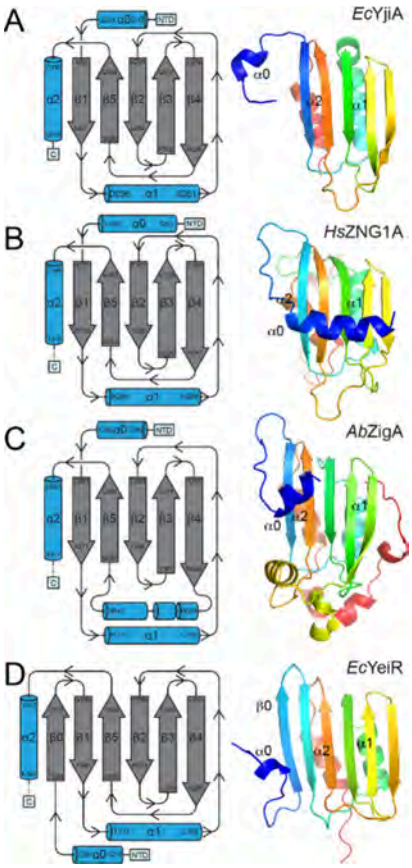

Figure 44. Secondary structural schematics (*left*) of the tertiary structure (A) or AlphaFold2 model (B-D) (*right*) of the C-terminal domains (CTDs) of selected COG0523 family members. A) *E. coli* YjiA (PDB 4IXN),[818] B) human ZNG1A (Q9BRT8)[56] C) *A. baumannii* ZigA (ModelArchive ma-zam5h),[820] and D) *E. coli* YeiR (P33030).[848] *Left*, α-helices, blue cylinders; β-strands, gray arrows, with the residue numbers from each primary structure that define the 2° structure boundaries indicated. NTD, N-terminal G-domain upstream. *Right*, the ribbon is colored from blue to red, starting with the α0 helix (front), then the most N-terminal β-strand, β1 through to the C-terminal α2 helix (back, opposite the β1 and β5 strands).

https://doi.org/10.1021/acs.chemrev.4c00264
Chem. Rev. 2024, 124, 13574−13659

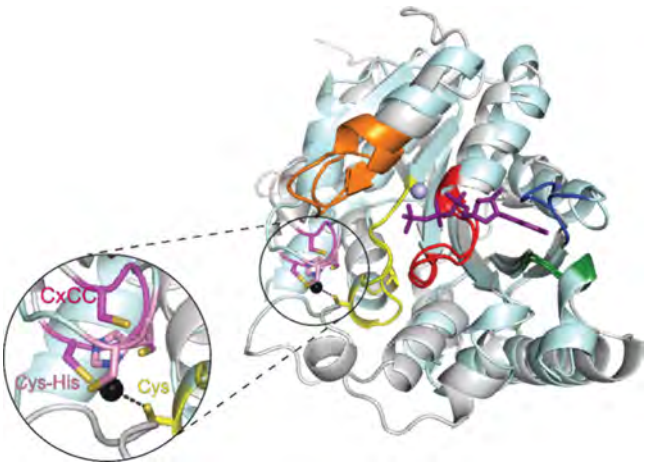

Figure 45. Superposition of one subunit of the *Mj*HypB in the GTP-bound ON state (2HF8, cyan)[820] and the G-domain of the AlphaFold2 model of *A. baumannii* ZigA (ModelArchive ma-zam5h, light gray). The G-loops are colored as above, with G1-G5 colored red, orange, yellow, green, and blue, respectively; GMPNP colored purple, CxCC motif colored magenta, and the CH Ni^{II}-binding motif colored pink.

(HDX-MS) to investigate the ligand-free, Zn^{II} bound, Mg^{II}•GTPγS−Zn^{II} substrate and Mg^{II}•GDP-Zn^{II} product states (Figure 47).[820] These and other findings reveal that Zn^{II}

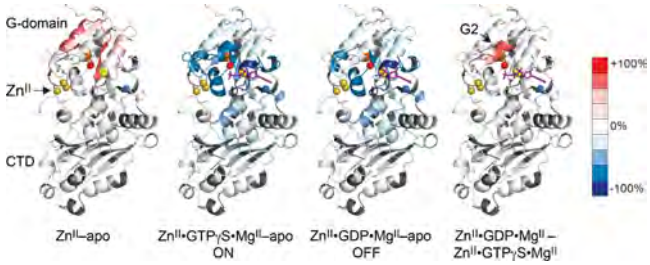

Figure 47. Ribbon representation (Alphafold2 model) of the results of probing various allosteric states of the bacterial Zn^{II} metallochaperone, *A. baumannii* ZigA, by hydrogen−deuterium exchange-mass spectrometry (HDX-MS) relative to a common apo (ligand-free) reference state.[820] ON-state, GTP bound; OFF-state, GDP bound. The Zn^{II}-coordinating Cys S^{γ} atoms are.indicated (yellow spheres). The ribbon in each case is colored according to% change in deuterium uptake (see scale, right). See text for details.

function, *Ec*YeiR, are both modestly (up to ≈5-fold) stimulated by Zn^{II} binding to a high affinity site; in both ZigAs, this stimulation is ablated in a triple serine substitution mutant, CICC to SISS, which selectively eliminates high affinity Zn^{II} coordination to S_3(N/O) site.[848,849] Although both *Ec*YeiR and *Ec*YjiA bind Zn^{II} with equilibrium affinity comparable to that ZigA, the Zn^{II} affinity in neither case is appreciably increased by GTP binding, in contrast to *Ab*ZigA (see below).[146,820] Most COG0523 enzymes connected in some way to zinc homeostasis harbor one or more secondary Zn^{II} sites of lower affinity whose functions are unknown.[56,848,849]

5.1.4.2. Structure and Dynamics of G-Nucleotide Binding. A near total lack of high-resolution structure and dynamics insights for COG0523 enzymes and how these molecular switches change from the "spring-loaded"[850] GTP-bound ON state to the "relaxed" GDP-bound OFF state, continues to severely limit our understanding of these enzymes. Insights from a family of bacterial GTPases that regulate ribosome biogenesis under conditions of nutrient limitation[850] reveal that in the Mg^{II}•GMPPCP[818]-bound ON state, the G2 helix and the G3 loop are fully folded to engage the terminal γ-phosphate; upon nucleotide hydrolysis, the G2 helix is destabilized and becomes highly dynamic (Figure 46).[850] Recent studies of *Ab*ZigA employed hydrogen−deuterium exchange mass spectrometry coordination by the CxCC motif slightly destabilizes the G-domain, while subsequent addition of either substrate analog GTPγS and product GDP induce significant stabilization of a metastable or fluxional G-domain (Figure 47); analogous findings may well characterize the closely related Fe^{II}-dependent nitrile hydratase activator protein.[843] Quantitative metal binding studies reveal that both Mg^{II}•GDP and Mg^{II}•GTPγS enhance the Zn^{II} binding affinity, with the effect far greater for Mg^{II}•GTPγS, by ≈10-fold;[820] these findings of significant positive linkage between substrate Mg^{II}•GTPγS and Zn^{II} binding, also observed by Co^{II}-bound CobW.[851] A significantly reduced Zn^{II} affinity of the Mg^{II}•GDP-bound OFF state may well provide a (shallow) thermodynamic driving force for metalation of a client protein (Figure 48A), exactly in line with thermodynamic gradients previously observed in sequential Cu^{I} trafficking reactions,[805] and analogous to protein−protein interaction affinity gradients recently observed in [4Fe-4S] cluster enzyme maturation.[852] The HDX-MS reveal unfolding of the G2 loop specifically upon GTP hydrolysis, which impacts the stability of selected other regions of *Ab*ZigA, extending into the CTD (Figure 48B).[820] This long-range communication of nucleotide status in the G-domain to other regions of the protein is canonical long-range allostery, and a hallmark of G-proteins in general.

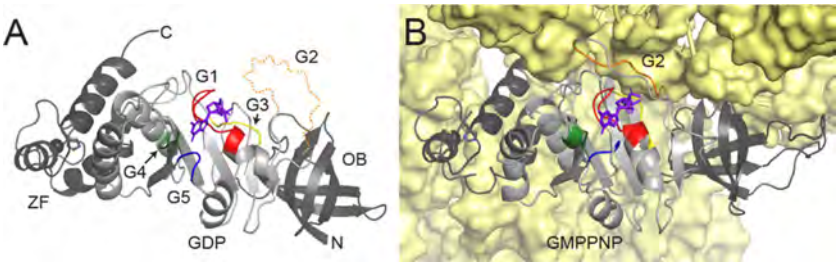

Figure 46. A depiction of a structural changes in the small GTPase involved in ribosome biogenesis, *Staphylococcus aureus* RsgA. A) GDP-bound OFF state. The G-loops are labeled and shaded as above; note that the G2 loop is disordered in this structure and not observed in the crystal structure (pdb 6ZHM).[850] The structure of the alarmone (ppGpp)-bound state (pdb 6ZHL) is similar, with a disordered G2 loop.[850] The immediately adjacent oligonucleotide-oligosaccharide (OB)-fold (OB) and ZF (zinc finger) domains are shown in dark gray. B) GMPPNP-bound ON state of *Escherichia coli* RsgA bound to the 30S ribosomal subunit (pdb 7NAR).[853]

https://doi.org/10.1021/acs.chemrev.4c00264
Chem. Rev. 2024, 124, 13574−13659

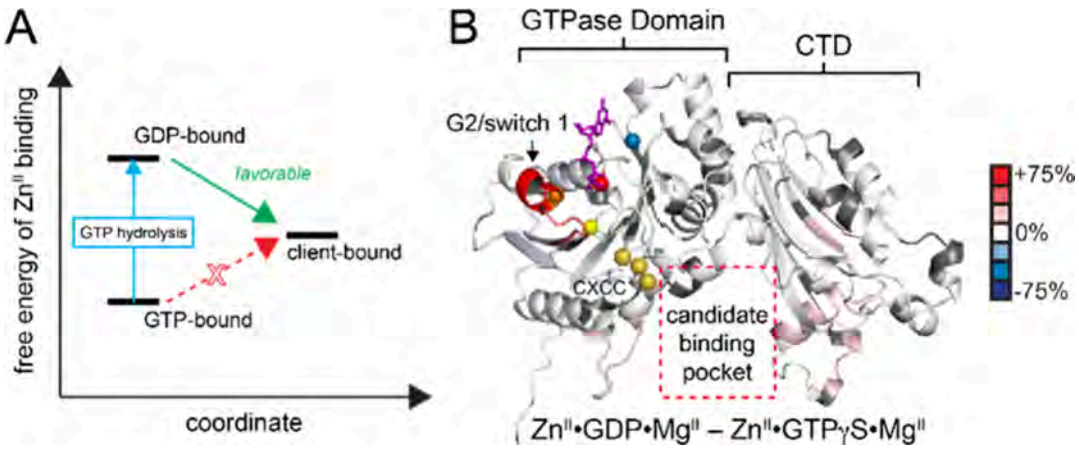

Figure 48. Thermodynamic model for favorable metal transfer that is linked to GTP hydrolysis by a nucleotide-dependent metallochaperone.[820,851] Here, the ON- or substrate GTP-bound state of the metallochaperone has a higher affinity for the metal to be transferred relative to the OFF or product GDP-bound state, as experimentally verified for CobW and *A. baumannii* ZigA. If the recipient client protein has an affinity between these two extremes, the metal will move thermodynamically "downhill" to the client (green arrow), with concomitant dissociation of the chaperone-client protein complex. (B) Depiction of the structural and/or dynamic changes originating with the G2/switch 1 region, as experimentally determined for *A. baumannii* ZigA by HDX-MS, which is destabilized in the OFF state. These changes in structure or dynamics propagate to the other regions of the G-domain and the C-terminal domain (pink ribbon). The approximate positions of the G1, G2, G2 and G4 loops are indicated by the red, orange, yellow and blue Cα spheres, respectively. The Sγ atoms of the high affinity Zn^{II} site shown as dark yellow spheres. Scale bar:% change in deuterium uptake in the GDP•Zn^{II} state relative to the GTPγS•Zn^{II} state, colored onto the ribbon AlphaFold2 model of ZigA.

5.1.4.3. Client Proteins and Mechanistic Insights. Unlike the SIMIBI GTPases, there are few insights into metalation clients of bacterial COG0523 proteins, with the exceptions of authentic CobW[146] and the Fe-dependent nitrile hydratase activator protein Nha3.[843] The acquisition of Co^{II} by the corrin component of vitamin B_{12} occurs in cells via one of two distinct pathways, designated as the early or late Co^{II} insertion pathways. In the late insertion pathway, Co^{II} is accessed by the COG0523-family metallochaperone CobW and incorporated into hydrogenobyrinic acid a,c-diamide (HBAD), as part of a HBAD-CobNST chelatase complex, to form Co^{II}–HBAD, in what is also known as the metallochaperone-dependent pathway.[146,851] This reaction is calculated to be unfavorable if the Co^{II} is derived from bioavailable Co^{II} pool based on an idealized metal pool in *Salmonella* (Figure 8A) but is calculated to become thermodynamically favorable only when Co^{II} is bound to the product Mg^{II}•GDP-CobW complex (Figure 48A).[851] There is as yet no published biochemical evidence that CobW activates CobNST directly, and the involvement of intermediary protein cannot yet be ruled out.

Limited biochemical data on the Fe-dependent $\alpha_2\beta_2$ heterotetrameric nitrile hydratase maturation factor Nha3 support a model in which the folded α-subunit forms a complex with Nha3; Fe^{II} binding to Nha3 followed by GTP binding then stimulates GTP hydrolysis and Fe^{II} transfer to the α-subunit.[843,844] Following transfer, Fe^{II}-α is proposed to engage the β subunit and via subunit swapping with apo-GDP Nha3, which then drives formation of the mature $\alpha_2\beta_2$ heterotetramer (Figure 49A).[844] Maturation of the Co^{II}-dependent nitrile hydratase also involves a subunit swapping step and may require ATPase activity for metallocofactor insertion, but shows no requirement for a COG0523 metallochaperone.[854−856] The GTPase activity of Nha3 is required to obtain active nitrile hydratase in cells.[857] This work on Fe-dependent nitrile hydratase raises many questions, but a molecular switch in Nha3 from the ON to the OFF state might be anticipated to modulate the stability of the Fe^{II}-α complex, so that subunit swapping can occur. The catalytic Fe^{II} site in Fe^{II}-dependent

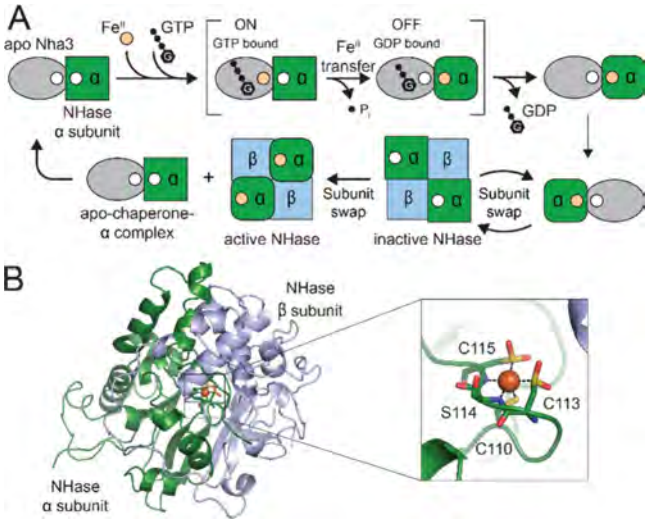

Figure 49. A) Proposed activation mechanism of bacterial Fe-dependent nitrile hydratase (NHase) in which Fe^{II} is transferred from the COG0523 metallochaperone, Nha3.[844] Once the α-subunit is loaded with metal, this facilitates dissociation of the OFF-state chaperone and subunit swapping into an "immature" $\alpha_2\beta_2$ tetramer via an as yet unknown mechanism. B) Ribbon representation of the structure of an $\alpha\beta$ heterodimer of mature Fe^{III} nitrile hydratase from *Rhodococcus erythropolis* AJ270 (2QDY), with the alpha subunit shaded green and the beta subunit shaded blue.[861]

nitrile hydratase is buried at the $\alpha-\beta$ subunit interface;[192] the same is true of the Co^{II}-dependent enzyme (Figure 49B).[858] However, it remains unclear as yet why nitrile hydratase activation requires a *specific* metallochaperone, and molecular details of cofactor biogenesis remain largely lacking. One possibility is that the metallochaperone coordinates maturation of the cofactor beyond insertion of the metal, including selective oxidation of the two coordinating cysteines in the first coordination shell;[859] arguing against this is the finding that in at least one case, the α-subunit alone has significant catalytic

https://doi.org/10.1021/acs.chemrev.4c00264
Chem. Rev. 2024, 124, 13574−13659

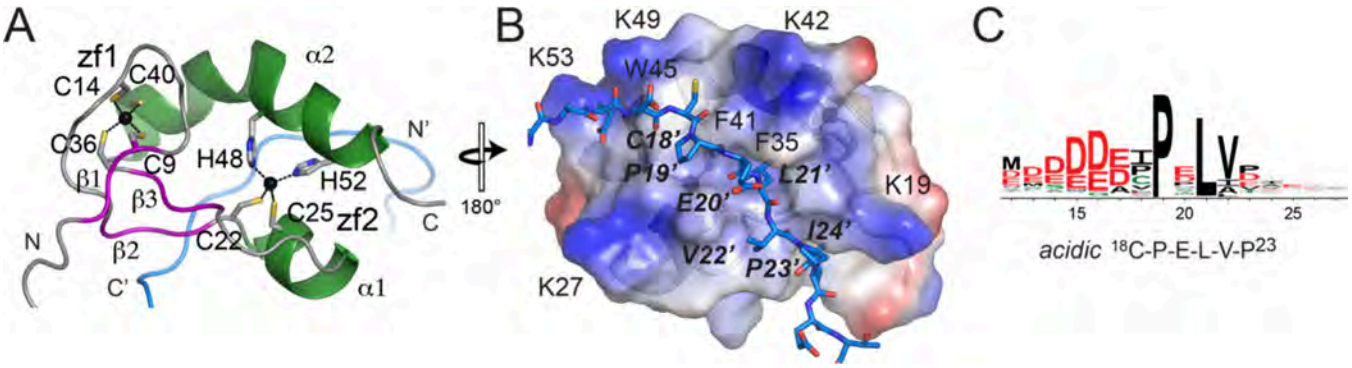

Figure 50. Solution structure of the major site of interaction between eukaryotic ZNG1 and METAP1.[56] A) Ribbon representation of the structure of the N-terminal tail of ZNG1 (blue) bound to METAP1 ZF domain (PDB 7SEK). B) Same structure as in panel A, with the N-terminal tail of ZNG1 shown in stick (residue numbers in bold italic) and the ZF domain shown in spacefill colored as an electrostatic surface rendering. C) Conserved features of all ZNG1 N-terminal METAP1-interacting motif, with the sequence of the vertebrate ZNG1 shown below the weblogo.[56]

activity and harbors a fully post-translationally modified metal site.[860]

There are no known metalloenzyme clients for any bacterial Zur-regulated COG0523 protein, although the functional characterization of *B. subtilis* ZagA and its connection to sustaining folate biosynthesis and one-carbon (1C) metabolism under conditions of Zn^{II} restriction has been reported.[761] FolE catalyzes the rate-determining step in bacterial folate biosynthesis and is an obligatory Zn^{II}-dependent enzyme.[862] When Zn^{II} levels become scarce, Zur regulates the expression of ZagA and if this fails, a Zn^{II}-independent paralog, FolEB, which uses other divalent cations for activity, in an effort to sustain folate biosynthesis under these conditions (Section 4.3.3).[762] The simplest mechanistic model is that ZagA and apo-FolE physically interact in a way that is modulated by G-nucleotide status of ZagA, but this is not yet known. Attempts to obtain a preparation of metal-free apo-FolE from Zn^{II}-bound FolE purified from *E. coli* has generally met with limited success, consistent with the idea that the Zn^{II} bound to subunit interface in the folded decameric FolE oligomer may not be in equilibrium with the bioavailable Zn^{II} pool.[863] Thus, other models may well be required to explain the metallochaperone activity of ZagA. It is the case that ZagA binds and hydrolyzes the alarmone, 5-amino 4-imidazole carboxamide riboside 5′-triphosphate (ZTP), which accumulates in cells under 1C folate deficiency,[198] the functional significance of which is remains unknown.[761]

The previously noted strong evolutionary similarity of bacterial ZigA/ZagA to the mycobacterial Mrf (MPY recruitment factor) deserves comment.[691] Mrf binds to the 30S subunit of the ribosome and loads mycobacterial factor Y (MPY) onto the 70S ribosome to induce ribosome inactivation under conditions of Zn^{II} deficiency.[697] This suggests the possibility that some COG0523 proteins function by physically associating with the ribosome. Here, Zn^{II} might be installed into an obligatory Zn^{II}-dependent protein(s) by ZigA cotranslationally, into the nascent unfolded chain, thus avoiding kinetic or thermodynamic trapping of the metal into a holoprotein once folded.[864,865] Indeed, *Mycobacterium smegmatis*, the soil saprophyte of *M. tuberculosis*, encodes both ZigA and Mrf, and both are regulated by Zur; this may allow the organism to fine-tune control of ribosome function and metalloproteome maintenance under conditions of nutrient Zn^{II} restriction. Ribosome profiling[866] in a Δ*zigA* strain grown under conditions of Zn^{II} deficiency would provide strong support for a cotranslational metal insertion model that is stimulated by ZigA, for example.

5.1.4.4. Eukaryotic COG0523 Proteins. Landmark studies published in 2022 establish that a eukaryotic COG0523 protein, named ZNG1 for Zn-regulated GTPase metalloprotein activator 1, fulfills all the criteria that one would anticipate of a metallochaperone for methionine aminopeptidase-1 (METAP1) in vertebrates and the yeast *Saccharomyces cerevisiae*, a finding recapitulated recently in plants.[56,814,846] METAP1 is a cell-abundant binuclear Zn^{II} enzyme that associates with the translating ribosome, cleaving the N-terminal methionine (Met) in over 50% of the nascent polypeptide chains.[867] This activity is critical to cell physiology since the identity of the N-terminal residue in a mature protein can dictate organellar destination in eukaryotic cells. There is as yet no evidence that bacterial or archaeal methionine aminopeptidase is dependent upon a COG0523 for metalation under conditions of metal restriction, although this is clearly worthy of investigation.

METAP1 and ZNG1 form a complex mediated in part by a conserved N-terminal CPxLxP (C, Cys; P, Pro; L, leucine; x, any amino acid) sequence motif in ZNG1 not present in bacterial homologues, and an N-terminal Cys_6His_2 cross-brace zinc finger (ZF) structure in METAP1 (Figure 50A).[56] The NMR solution structure of the complex reveals a core $\beta\beta\alpha\beta\alpha$, cross-brace fold with a 1,3,2 antiparallel β-sheet arrangement, in which the outer β2 strand hydrogen bonds with the ZNG1-derived peptide (Figure 50B). This structure fully explains the sequence conservation of the METAP1 interacting motif in ZNG1, from lower eukaryotes to plants and animals across millions of years of evolution, conforming the general sequence "$[D/E]_n\psi$PxLVp (Figure 50C).[56] These studies suggest that GTP hydrolysis by ZNG1 simulates metalation of the empty METAP1 active site above that which could be obtained with GMPPNP or the OFF-state product GDP, consistent with the mechanistic model shown (Figure 51A).

Although structures of the complex are lacking, an Alphafold2 model (Figure 51B) places the CXCC motif of ZNG1 in close proximity to the active site of METAP1, seemingly poised to undertake a sequence of ligand exchange reactions and metal transfer down a thermodynamic gradient (see Figure 34, *top*). In fact, some METAP1 structures incorporate a "third" metal binding site, positioned just above the binuclear active-site cluster, coordinated by a series of conserved residues, a subset of which function in substrate binding and catalysis (Figure 51C).[868] One hypothesis is that these residues play multiple

https://doi.org/10.1021/acs.chemrev.4c00264
Chem. Rev. 2024, 124, 13574−13659

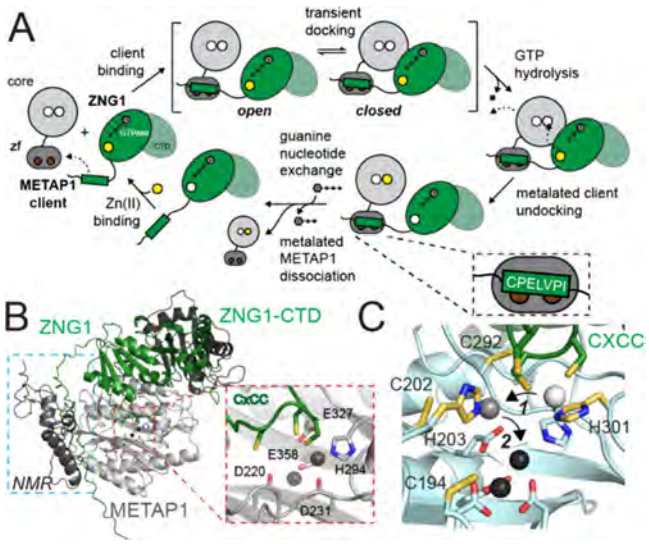

Figure 51. A mechanistic model of ZNG1 function.[56] A) Cartoon depiction of the catalytic cycle illustrating one round of metal insertion. B) An AlphaFold2 model of the complex between human ZNG1 (green) and human METAP1 (gray). The region of the model that corresponds to the NMR solution structure is boxed (cyan; *NMR*). A close-up of the interfacial region of highlighting the close juxtaposition of the native binuclear Zn^{II} center (black) with its ligands indicated and the CXCC motif of ZNG1 (green ribbon). C) A potential metal−ligand exchange pathway that connects the Zn^{II} bound to the CXCC motif of ZNG1 (white), through a "third" metal site (gray) and the binuclear active site of METAP1 (black). The residues highlighted (yellow stick) are conserved in METAP1 sequences and thus may function to guide the metal into the (empty) active site via a sequential metal ligand-exchange process.

roles, one of which is to initiate ligand exchange with the metallochaperone. However, the nature of the driving force for metalation (Figure 34) awaits further study. The K_{Zn} values for isolated ZNG1 and METAP1 are very similar in the absence of G-nucleotide; furthermore, Zn^{II} slightly inhibits the GTPase activity of ZNG1, like in *Ec*YjiA, its closest bacterial homologue;[691] addition of Zn_2 METAP (with the active sites empty) to Zn^{II}-ZNG1 restores the GTPase activity to that of apoprotein, as expected if metal moves from donor ZNG1 to client.

It is interesting to note that the N-terminal ZF domain of METAP1 is also required for association with the translating ribosome, via the C-terminus of the β-subunit of the nascent polypeptide-associated complex (NAC). NAC is analogous to bacterial trigger factor, which is anchored near ribosome exit tunnel on what is considered a "universal" ribosome docking site.[865] This suggests a model, not yet tested, in which the β-NAC peptide and the N-terminal tail of ZNG1 are in competition with one another and given increased cellular expression of ZNG1 under conditions of Zn^{II} limitation,[56] may help to ensure that inactive metal-free METAP1 does not readily associate with the ribosome. Alternatively, the metalation status of METAP1 may regulate ribosome binding in some way.

Finally, of the hundreds of zinc metalloenzymes present in even a simple eukaryotic cell,[869] why does METAP1 require what may be a dedicated metallochaperone under conditions of nutritional zinc deficiency? One possibility is that cotranslational processing of the nascent chain by a highly cell-abundant enzyme is simply "too big to fail". Indeed, cell abundant proteins in specialized cells often have their own specialized protein chaperone as a means to maintain proteostasis, exactly parallel to metallostasis (Figure 1). These ideas are in line with metalloproteomics experiments in *Saccharomyces cerevisiae*, which reveal that 20 cell-abundant Zn^{II} metalloenzymes, if fully metalated, account for ≥90% of the zinc quota in the cell, one of which is methionine aminopeptidase.[869] It will be interesting to discover the extent to which cells use this or other approaches to prioritize utilization of Zn^{II} under conditions of metal nutrient limitation.

5.2. Copper Storage Proteins and Metal Allocation

5.2.1. Overview of Copper Toxicity. Cu is an essential micronutrient required as a cofactor for various cuproenzymes in nearly all forms of aerobic life. Copper homeostasis, like the homeostasis of other transition metals,[120] is tightly controlled by the combined action of transcriptional regulators that sense copper levels (Section 3), efflux pumps, storage proteins and metallochaperones, the latter of which allocate Cu to partner proteins without dissociation into solvent.[807,870−872] It is worth noting that the number of cuproenzymes that are resident in cytoplasm tends to be quite small (or zero) in nearly all organisms, with cell-abundant cuproproteins sequestered in intracellular membrane vesicles, e.g., thylakoids, intracytoplasmic membrane structures,[873] e.g., for particulate methane monooxygenase (pMMO),[112] or simply embedded in the plasma membrane with active sites facing out. As such, Cu present in the cytoplasm may be recognized as toxic. A major mechanism of bacterial resistance to Cu toxicity is cytoplasmic efflux of Cu^{I} via one or more P_{1B}- type ATPase exporters, e.g., CopA or CopB (Section 5.3.2). These transporters function alongside a cytoplasmic Cu^{I} metallochaperone that plays a role in buffering cytoplasmic Cu^{I} to very low concentrations (Figure 8) and is capable of delivering Cu^{I} directly to an exporter for efflux[874,875] and in some cases, to the Cu^{I}-sensing transcriptional repressor that orchestrates the adaptive response Cu toxicity (Figure 34).[876−878]

In Gram-negative bacteria, the fate of this periplasmic Cu^{I} differs depending on the organism, but includes oxidation by a multicopper oxidase (MCO) to the less toxic Cu^{II},[879−882] sequestration by periplasmic Cu^{I}/Cu^{II} binding proteins,[883−885] and capture by CusF and efflux via the periplasm-spanning CusABC system.[886,887] More recently, a novel membrane-anchored and surface-exposed Cu binding lipoprotein, CopL, from methicillin-resistant *Staphylococcus aureus* (MRSA), was shown to provide hyper-resistance against Cu toxicity in clinically relevant MRSA strains; this activity is independent of the virulence-associated CopB efflux pump, but whose function is dependent on Cu^{I} binding to a novel Cu^{I}-binding architecture.[170,888,889] This suggests that extracytoplasmic Cu sequestration may be important mode of resistance to copper toxicity. Within the cytoplasm, Cu^{I} coordination and sequestration represents another mode of bacterial resistance to copper toxicity, and in some cases, but not all, the genes that encode these proteins are regulated by a Cu-sensing repressor. These include a mycobacterial metallothionein, MymT,[359,890] CutC found in some Firmicutes,[891] a CopZ,[876] and more recently, proteins termed copper storage proteins (Csp) discussed here.[892,893]

5.2.2. Copper Storage Protein Structure. Csps are a family of closely related cysteine thiolate-rich four-helix bundle proteins that form homotetramers that are capable of binding up to 80 Cu^{I} per tetramer.[894] The inner surface of this tube-like structure harbors ≈13−20 cysteines, and often a cluster of

https://doi.org/10.1021/acs.chemrev.4c00264
Chem. Rev. 2024, 124, 13574−13659

histidine residues at the open end or "mouth" of each four-helix bundle (Figure 52). Though first discovered as a soluble,

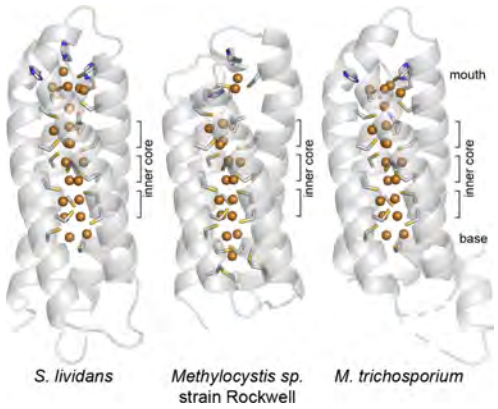

Figure 52. Crystallographic structures of one protomer of tetrameric copper storage protein (Csp) from the organisms indicated. *Left*, *Streptomyces lividans* Csp3 (6EK9);[896] *center*, *Methylocystis sp.* strain Rockwell Csp3 (6ZIF); and *right*, *Methylosinus trichosporium* OB3b Csp3 (5ARN). Cu^{I} ions (copper spheres) and Cu^{I}-ligating residues are shown in stick. The tri-tetrad inner core of 12 Cu^{I} ions is common to all Csps, with the base and mouth regions variable.

periplasmic binding protein (Csp1/Csp2) in methanotrophs and proposed to function in the metalation of pMMO, the cytoplasmic Csp3 is now considered the far more prevalent Csp, and has now been identified in at least ten different bacterial phyla.[892] Csp3-like proteins differ slightly in Cu^{I}-binding stoichiometries, but all contain a common core of three tetrameric Cu-binding clusters (which collectively bind 12 Cu), with the additional coordination chemistry variable above or below this cluster (Figure 52). Csp3s bind Cu^{I} with high equilibrium affinities ($K_{Cu} \approx 10^{16}$ M^{-1}) to multiple classes of sites that vary slightly in affinity. Although the details differ for different Csp3s, the kinetics of Cu^{I} binding are generally quite fast but only for an initial phase, with the kinetics of Cu^{I} removal by a high affinity Cu(I) chelator very slow, beyond the first couple mol equivalents of Cu^{I}.[894,895]

5.2.3. Copper Storage Protein Function. Despite their discovery some 10 years ago, the functional role(s) of Csp3 in bacterial cells remain largely enigmatic. These Cu^{I} binding properties are potentially consistent with a role in Cu storage under Cu-replete or Cu-toxic conditions,[897] or as part of an "anticipatory" Cu-toxicity response, when cells are chronically metal-starved, and thus particularly vulnerable to mismetalation mediated by even modest Cu toxicity (see Section 5.3.2).[174] There is also some evidence to suggest that Csp3 can function as a cushion for very high levels of Cu^{I} in some specialized cases, e.g., where the ability of cells to efflux Cu^{I} is compromised (in a Δ*copA* strain).[898] However, *csp3* expression, unlike the primary Cu^{I} toxicity regulon discussed above, is rarely regulated by Cu stress.

There is recent evidence in support of the original proposal[893] that Csp3 functions as a copper chaperone to mediate Cu^{I} delivery to a client enzyme, in *Bacillus subtilis*.[899] Here, it was demonstrated the Cu^{I}-loaded Csp3 is capable of metalating a Cu-requiring endospore-resident multicopper oxidase CotA, a laccase, which is one just two known Cu-requiring enzymes in *B. subtilis*. Importantly, *B. subtilis* Csp3 does not protect cells from Cu intoxication and thus must play some other role. Both CotA and Csp3 are upregulated during late stages of spore formation[900] and appear to protect spores against hydrogen peroxide and UV light via production of a melanin-like molecule. Csp3 stimulates the extent of CotA metalation, albeit over very long time points (hours), as evidenced by activity assays, and a soluble Cu^{I} chaperone CopZ does not function in this assay, consistent but not confirmatory of a specific protein−protein interaction.[899] The extent to which Csp3s broadly function in metalloenzyme maturation is unknown.

5.3. Metal Ion Transport and Supramolecular Assemblies

We next describe recent biologically focused discoveries in transition metal transport in bacterial cells that highlight the involvement of accessory proteins that function as part of supramolecular efflux assemblies to facilitate metal transport across a membrane. These transporters and cognate accessory proteins may function as membrane-associated metallochaperones, in the regulation of transport, or in the metalation of metalloenzymes. The major metal transporter discussed here are a poorly understood subclass of the P-type (phosphorylation-type) ATPase efflux pumps,[901] notably those derived from the P_{1B-6} subclass of transporters. We place these discoveries in the context of a discussion of new structural advances in our understanding of the metal selectivity and transport mechanisms of P-type ATPases.

5.3.1. P-Type ATPases. P-type ATPases are conserved across all kingdoms of life and collectively mediate the movement of metals, protons and lipids across biological membranes from the cytoplasm to the extracellular space or an extracytoplasmic compartment or organelle.[901] All P-type ATPases possess three domains, a transmembrane domain (TM) composed of six to eight membrane-spanning α-helices that comprise the transport channel, an ATP-binding domain composed of nucleotide (N) binding and phosphorylation (P) subdomains, and an actuator domain (A) that allosterically signals a change in the phosphorylation status in the P domain to the TM domain to allow for transport. Metal transport is well-modeled by the alternating states Post-Albers cycle[902] which involves two distinct conformational states, an inward-facing E1 state and an outward-facing E2 state. The E1 state has high affinity for the cognate metal(s) and binds and hydrolyzes ATP; formation of the phosphoenzyme intermediate on an Asp residue in the P subdomain is coincident with formation of the low-metal binding affinity E2 (E2P) state, which then releases P_i (E2) and ultimately relaxes to the E1 state (Figure 53). Transient phosphorylation drives significant conformational changes in the membrane-spanning domain of transporter required for transport against a concentration gradient.[903,904] These changes in transporter domain ultimately expose the metal egress pathway on the opposite side of the membrane, thus allowing for vectorial or unidirectional transfer across the membrane. Some P-type ATPases including the P_{1B}-type subfamily, contain ancillary domains, often metal binding domains (MBDs), or other regulatory domains that can modulate or gate transport activity (Figure 54, *top*).

5.3.1.1. P_{2A}-Type Ca^{II} and Ca^{II}/Mn^{II} Transporters. Metal-transporting P-type ATPases typically form intramembrane metal sites derived from the TM4 and TM6 helices in the core TM domain, with the identity of these metal-binding residues strongly impacting the metal specificity (or promiscuity) of the transporter.[905] This is true for both the paradigm sarco(endo)-plasmic reticulum calcium ATPase (SERCA) pumps and related transporters from the P_{2A} subclass that function in the ER and *cis*-Golgi in vertebrates, as well as the "heavy metal" transporting

https://doi.org/10.1021/acs.chemrev.4c00264
Chem. Rev. 2024, 124, 13574−13659

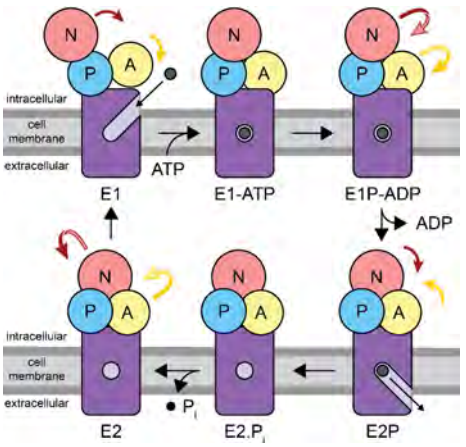

Figure 53. Metal transport is well-modeled by the alternating states Post-Albers cycle[902] which involves two distinct conformational states, an inward-facing E1 state and an outward-facing E2 state. The E1 state has high affinity for the cognate metal(s) and binds and hydrolyzes ATP; formation of the phosphoenzyme intermediate on an Asp residue in the phosphorylation subdomain is coincident with formation of the low-metal binding affinity E2 (E2P) state, which then releases P_i (E2) and ultimately transitions to the E1 state.

P_{1B}-type transporters described below (*vide infra*) (Figure 54). Of particular interest regarding metal specificity of P_{2A} ATPases is a suite of cryo-EM structures of the secretory-pathway Ca^{II}-ATPases (SPCA1), long known to transport Mn^{II} as well,[906] which function both to metalate key metalloenzymes in this compartment and beyond, including those associated with *O*-linked glycosylation, while also mediating Mn^{II} detoxification in neuronal tissues by actively pumping cytosolic Mn^{II} into the secretory pathway (Figure 55).[907]

These cryo-EM structures provide high resolution snapshots of all intermediates in a complete transport cycle and nicely illustrate the large amplitude conformational transitions of one domain relative to another that occur as a function of metal binding and phosphorylation status of the P-domain (Figure 55).[907] Pertinent to the discussion here, these structures provide unprecedented insights into the relaxed metal specificity of SPCA1 relative to SERCA enzymes, which are strictly Ca^{II} transporters (Figure 54, *bottom*) (see Section 3.3.3).[908] In SPCA1, Mn^{II} was found to bind to the same metal binding site II as Ca^{II}, but more tightly in forming a lower coordination number square pyramidal complex that results in residues on TM6, in particular D742, moving closer to those ligands derived from TM4, which donates three main-chain carbonyl oxygens to the

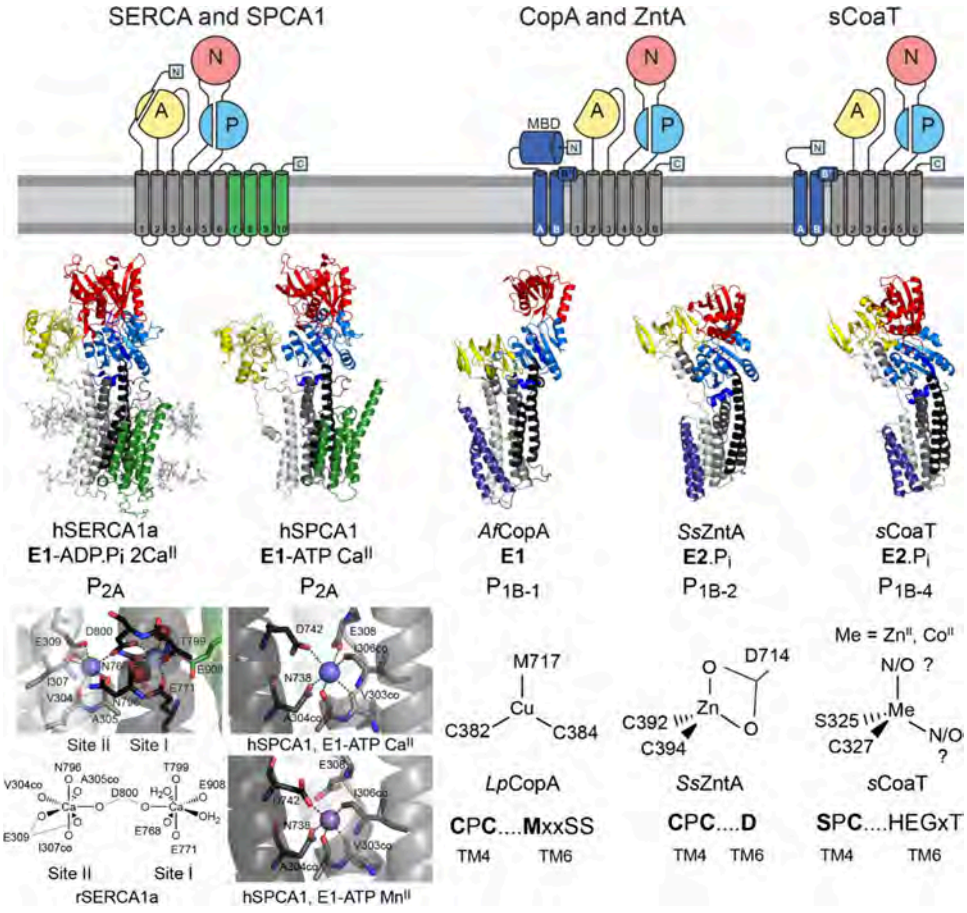

Figure 54. P-type ATPase transporter structures derived from the P_2 and P_1 subfamilies. Schematic representations (*top*) are color-coded as shown in the ribbon diagram of each strucure (*middle*). ADP-AlF_4^--bound human (h) SERCA1a (PDB 5XA8), AMPPCP-bound hSPCA1 (8IWR), ligand-free *Af* CopA (7R0H), AlF_4^--bound *Ss*ZntA (4UMW), BeF_3^--bound *s*CoaT (7QC0). The Post-Albers conformational state is indicated in each case, as well as ligands resolved in each structure. *Bottom*, coordination chemistry of each transporter as determined by X-ray crystallography (rSERCA; 1SU4) or cryo-EM (hSPCA1; 8IWR, Ca^{II} bound; 7YAJ, Mn^{II} bound) or via X-ray absorption spectroscopy and mutagenesis studies (others). The minimal sequence motif characteristic of each subfamily is shown below the metal coordination domain model for the three P_{1B} transporters, positioned on TM4 or TM6 helices, as indicated.[909] The structures of P_{1B-3}, P_{1B-5}, P_{1B-6} and P_{1B-7} transporters are not yet known.

https://doi.org/10.1021/acs.chemrev.4c00264
Chem. Rev. 2024, 124, 13574−13659

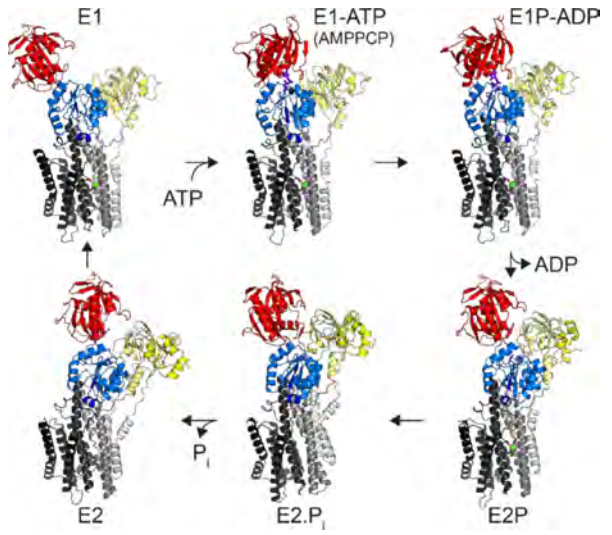

Figure 55. A suite of cryo-EM structures of the secretory-pathway Ca^{II}-ATPases (hSPCA1) which pump Ca^{II} and Mn^{II} into the *trans*-Golgi lumen.[907] The domains of the transporter are colored as in Figure 55. Ca^{II} ions, green; ATP, ADP and P_i, purple stick. New insights into the mechanism of Ca^{II} release obtained from inspection of the Ca^{II}-bound E2P conformation, prior to hydrolysis of the covalent phosphate ester (E2.P_i) and P_i dissociation (E2), were derived from this work.

metal.[908] In the E2-P_i modeled complex that contains no metal, those residues that coordinate the Ca^{II} or Mn^{II} move far apart, allowing for metal release into the *trans*-Golgi lumen in eukaryotic cells. In addition, SPCA1 lacks the second metal site found in SERCA (metal site I), which may help enforce Mn^{II} transport activity by SPCA1 relative to SERCA (Figure 54, *bottom*).

5.3.1.2. P_{1B}-Type Transporters. It is generally accepted that P_{1B}-ATPases conform to seven distinct structural subclasses, denoted P_{1B-1}-P_{1B-7}, all of which transport "heavy" metals (Figure 56).[901,910] Many P_{1B} transporters differ significantly from the P_{2A} transporters discussed above in that they have evolved MBDs appended to either the N-terminus or C-terminus on the core transporter structure (Figure 54, *right*). These MBDs often, but not always, provide hints as to the metal selectivity of the pump itself, and in the case of the P_{1B-1}-P_{1B-3} transporters that transport Cu^{I} and Zn^{II}, are in direct communication with the cytoplasmic environment.[911] Their metal affinities are tuned to the bioavailable "pool" of each metal. Cu^{I}-transporting P_{1B-1} ATPases nearly always harbor an N-terminal domain (or multiple repeated isostructural domains) that adopt a ferredoxin-like or cupredoxin fold, that accepts metal from an isostructural copper metallochaperone (Figure 34), likely via a metal ligand exchange intermediate.[804,807,875,912] These domains are not required for transport activity, and may well be regulatory;[911] indeed, recent structural studies suggests that that the Cu^{I} chaperone has direct access to the high-affinity metal binding site in the membrane, where an intermediate Met residue mediates metal dissociation.[913]

Like the P_{2A} transporters discussed above, the metal specificity of a P_{1B}-ATPase is also impacted by conserved signature sequences present in transmembrane segments 4, 5, and 6 (TM4, TM5, and TM6; numbered such that the first two helices in the P_{1B} transporters not found in P_{2A} transporters are labeled TM_A and TM_B[901]) (Figure 54, *top*; Figure 56). The short TM4 sequence **CPC** is characteristic of both P_{1B-1} and P_{1B-2} transporters, widely accepted to transport Cu^{I} and $Zn^{II}/Cd^{II}/Pb^{II}$, respectively, but each differs on the basis of residues in TM6 (Figure 56). In P_{1B-1} transporters, a Met in the TM6 is part of a **M**xxSS sequence coordination bond to the TM Cu^{I} site in the E1 state to complete a trigonal planar **CPC**. . .**M** chelate (Figure 54, *bottom*).[914] In P_{1B-2} transporters, a bidentate Asp completes a distorted tetrahedral complex in the E1 state, except for the Pb^{II} enzyme, which excludes one the O ligands of Asp replacing it with its "stereochemically active" lone pair (Figure 54, *bottom*).[915,916]

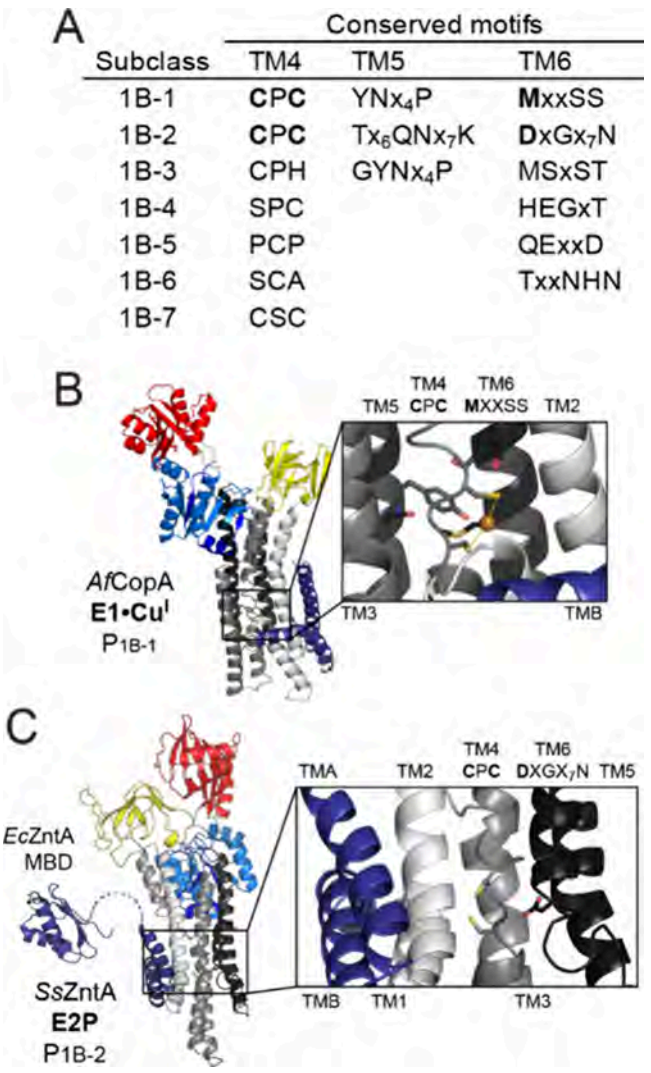

Figure 56. Primary structure determinants of P_{1B}-type ATPase transporters that impact their transition metal specificity profiles. A) Primary structure motifs in the TM4, TM5 and TM6 that impact metal specificity of P1B subclass ATPases. B) Ribbon structure of *Af* CopA in the E1•Cu^{I} state (7R0H). *Inset*, metal binding site region with the metal ligands and the Tyr-Asn sequence from TM5 shown in stick.[913] C) Ribbon structure of *S. sonnei* ZntA in the E2P state (4UMV), with the structure of the *Ec*ZntA metal binding domain also shown (1MWZ). *Inset*, metal binding site region with the four known metal ligands shown in stick.[918]

A number of high-resolution P_{1B}-type ATPase structures have now been solved to date in various conformations within the Post-Albers catalytic cycle (Figure 54, *middle*). These include the P_{1B-1} Cu^{I}-specific CopA from *Archaeoglobus fulgidus* in the Cu^{I}-free E1 state (Figure 54, *middle*), Cu^{I}-specific CopA from *Legionella pneumophilia* in the Cu^{I}-free E2•P_i and E2 states, ZntA, a P_{1B-2}-subclass Zn^{II} transporter from *Shigella sonnei*, in

https://doi.org/10.1021/acs.chemrev.4c00264
Chem. Rev. 2024, 124, 13574−13659

the metal-free E2P and E2-P_i states (Figure 54, *middle*).[913,917,918] Each structure was used to inform the coordination chemistry confirmed by X-ray absorption spectroscopy and other methods (Figure 54, *bottom*). More recently, the structure of a canonical P_{1B-4}-type enzyme has been solved, *Sulfitobacter sp.* NAS14−1 *s*CoaT, in the metal-free E1 state, as representative of the simplest member of the entire P-type ATPase superfamily[259,910] and which lacks ancillary MBDs altogether (Figure 54, *top*).[909] P_{1B-4}-subclass ATPases were originally proposed to be Co^{II}-specific transporters,[919] but may well be characterized by a relaxed metal specificity profile;[920,921] in at least three cases, they have been shown to be Fe^{II}-efflux transporters in bacterial cells.[920,922−924] Here, Fe^{II} transport is coupled to the H_2O_2 stress response and the expression is regulated by PerR or Fur (Section 3). These are extremely interesting transporters from a therapeutic perspective, since although they were functionally characterized first in the model organisms *B. subtilis* (PfeT), P_{1B-4} ATPases are present in many bacterial pathogens, including *Mycobacterium tuberculosis* (CtpD),[921] Group A *Streptococcus* (PmtA),[923−925] and *Listeria monocytogenes* (FrvA).[920]

5.3.2. Ferrous Iron Transport into Bacterial Ferrosomes. Given its abundance in the metalloproteome and the extremely low solubility of Fe^{III} in aerobic environments, iron is considered a precious metal nutrient for nearly all cells. As a result, most cells go to extraordinary lengths to scavenge and if possible, store, this metal nutrient, to protect from subsequent Fe starvation. Ferrous iron, Fe^{II}, is the oxidation state that is bioavailable in the cytoplasm and dominates extracellularly in oxygen-deplete anaerobic and acidic environments of the stomach, for example. Unlike Fe^{III}, Fe^{II} is highly soluble and exchange labile, and recent work reveals that Fe^{II} is bioavailable in these specific niches and recognized to play an important role in nutritional immunity against invading pathogens.[926−928]

5.3.2.1. Overview. It has long been known that one way to obtain a "pool" of bioavailable Fe^{II} required for protein metalation in bacterial cells is to store it in intracellular compartments, notably heme-based bacterioferritins, ferritins, or in mini-ferritins, derived from the superfamily of DNA-binding proteins from starved cells (Dps), all of which are protein-coated biomineralized compartments of Fe^{II} and Fe^{III}. However, iron storage in these compartments is dependent upon the availability of oxygen, and therefore cannot function efficiently in an anoxic environment. The only other known strategy available to protect bacteria from iron intoxication is to efflux the metal from the cytoplasm, via ferrous ion transporters. Their structures and transport mechanisms have been reviewed recently,[929,930] and we focus on one here.

5.3.2.2. Ferrosomes and P_{1B-6} ATPase Transporters. There is considerable excitement around the P_{1B-6} subclass of transporters, given the fact that up until recently they were poorly characterized as to both metal transport specificity and function in cells (Figure 56A). A preliminary genomics analysis suggested that these transporters might transport Fe^{II}, given an occasional genomic colocalization with *feoB*, known to encode the primary bacterial ferrous ion uptake transporter FeoAB.[910,931] Remarkably, this prediction turns out to be true, although only in part. Seminal work from the Komeili group published in 2010 revealed that lipid-encased electron dense particles exist in the anaerobic bacterium *Desulfovibrio magneticus*, long studied as a model organism for the formation of "bullet-shaped" magnetosomes, which biomineralize Fe as magnetite (Fe_3O_4) in a membrane-encased "organelle" organized into long chains that use geomagnetic fields for direction sensing.[932,933] In that work, the presence of another electron-dense particle rich in Fe and phosphate and surrounded by a lipid membrane was noted, and whose biogenesis was clearly distinct from that of magnetosomes.[933]

In more recent studies, these authors further characterized these amorphous granules as specifically enriched in Fe and phosphate in what are now known as ferrosome organelles (ferrosomes), and identified a three-gene cluster arranged into a putative operon responsible for their formation as encoding ferrosome-associated (Fez) proteins (Figure 57A,B).[674] Core

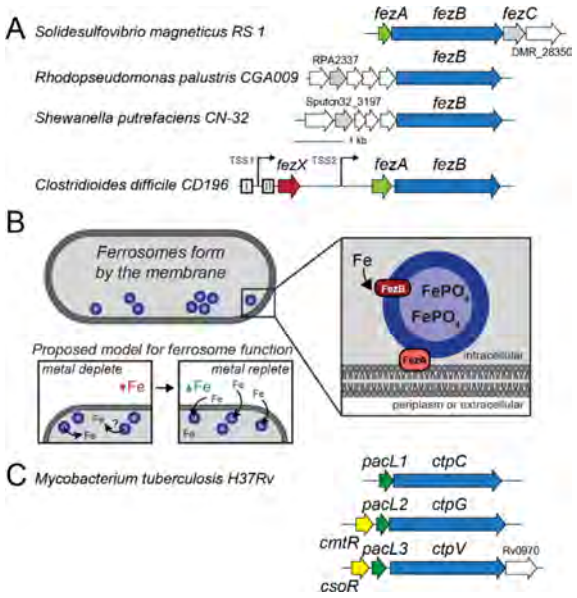

Figure 57. P-type ATPase transporter genomic localization and transporter function. A) Genomic organization of the *fez* operon regions in selected organisms. Fur boxes and two transcription start sites (TSS) are indicated on the *C. difficile* genome.[673,674,934] B) Ferrosome function in *C. difficile*. Ferrosomes assemble at or near the plasma membrane. Fe^{II} is driven into the interior of the ferrosome by the P_{1B-6}-class transporter, FezB. The function of FezA (DUF1610) is unknown but may assist in deforming the plasma membrane to facilitate ferrosome biogenesis, or play some other role in activating Fe^{II} transport. C) Three distinct P_{1B}-type transporters in *M. tuberculosis* that function as part of metal efflux platforms and incorporate a PacL*n* (DUF1490) homologue.[935]

components of this operon are FezA, a predicted α-helical transmembrane membrane protein (DUF6110) and FezB, a P_{1B-6}-ATPase transporter, as well as a third small protein denoted FezC or FezX, depending on the organism, of unknown function. P_{1B-6}-ATPases harbor a characteristic **S**PC motif in TM4 and a TxxNHN motif in TM6, which may well impact metal specificity (Figure 56A). Purification of ferrosomes from bacterial cells reveal that both FezA and FezB are greatly enriched in these electron-dense granules, with no detectable FezX.[673] Thus, although biochemical experiments are not yet available, FezB is clearly an Fe^{II} transporter, but is tasked with moving metal across an *intracellular* membrane, a remarkable finding given that bacteria are not broadly assumed to harbor intracellular membrane-encased organelles.

Ferrosomes have now been imaged by energy-dispersive X-ray spectroscopy (EDS) and characterized in the Gram-positive, spore-forming, intestinal anaerobe and human pathogen, *Clostridioides difficile*. They have been shown to play an integral

https://doi.org/10.1021/acs.chemrev.4c00264
Chem. Rev. 2024, 124, 13574−13659

role in iron homeostasis in this organism and defense against nutritional immunity mediated by CP stress during an infection.[673] In *C. difficile*, ferrosomes function in iron storage, and the expression of *fezX* and *fezAB* is regulated by Fur and inducible by the metal chelator dipyridyl, often used to starve cells for Fe. These genes are constitutively expressed in a Δ*fur* strain and appear to protect *C. difficile* from Fe toxicity during an acute switch from a Fe-deplete to an Fe-replete growth conditions (Figure 57B).[673] High-resolution tomographic imaging of *C. difficile* engineered to constitutively express *fezAB* suggests that although these compartments are clearly cytoplasmic, ferrosome clusters are frequently found adjacent to the cell membrane, for reasons that are not yet clear (Figure 57B). Heterologous expression of *fezXAB*, but not *fezAB* alone, in *B. subtilis*, reveals that despite the fact that FezX cannot be detected in these organelles isolated from *C. difficile*, it is required for their assembly, at least in this heterologous host organism.[673] CP induces the transcription of *fezXAB* in cell culture and in infected animals and it appears that FezB and the inhibitory impact of CP in nutritional immunity and function most acutely during colonization of the gastrointestinal tract during infections.

These comprehensive studies establish a new paradigm for membrane-encased organelles or compartments in bacteria, but also raise many important questions that bear on P_{1B}-type ATPase function, assembly and mechanism like other work described below (Section 5.3.4),[935] The biological function of the DUF6110 protein FezA is completely unknown. Does it function as a novel ferrosome-membrane-associated metallochaperone or scavenger of cytoplasmic Fe^{II} funneled to FezB, as a regulator of FezB transport activity, a membrane bilayer remodeling protein, or a canonical protein chaperone that enables assembly of active and folded FezB in the membrane? FezX (29 amino acids), on the other hand, is perhaps reminiscent of small proteins (<50 residues) that regulate bacterial Mn^{II} homeostasis,[936] whose functions are only beginning to gain some clarity.[937] How does FezX, not found in all *fez* operons, impact this process in *C. difficile*? Detailed biochemical reconstitution and cell biological studies will be required to address these exciting questions, answers to which to greatly enhance our understanding of P_{1B-6}-ATPase transporters.

5.3.3. Membrane Efflux Platforms. A prevailing view in the P-type ATPase field is that these transporters tend to function independently, with the exception of soluble cytoplasmic metallochaperones most strongly associated with the P_{1B-1}-type Cu^{I} chaperones, which deliver metal to the transport site.[799,913,938] The work on bacterial FezA-FezB described above suggests that this need not be in the case. In fact, it is interesting to consider the singular example of a membrane-anchored metallochaperone, CupA, and its cognate P_{1B-1}-ATPase CopA in the Gram-positive respiratory pathogen *Streptococccus pneumoniae* in this context.[939] CupA was shown to be required for the cellular copper resistance, and a heterologous CopZ-like chaperone which adopts a distinct fold could not substitute for CupA in cells; further, membrane anchoring was required for resistance against copper toxicity.[912] It is not yet known if and how *S. pneumoniae* CupA and CopA physically interact, or form a stable complex in the membrane, but this is of course the expectation.[940]

5.3.3.1. DUF1490 Proteins Impact P_{1B} ATPase Function. *Mycobacterium tuberculosis* encodes seven P_{1B}-type ATPases encoded by *ctpA-D*, *ctpG*, *ctpJ* and *ctpV* that mediate comprehensive resistance to transition metal toxicity in the hostile intracellular environment of the phagolysosome.[941] These include at least three Cu^{I}-specific transporters (CtpA, CtpB and CtpV), with CtpV, regulated by the Cu^{I}-sensing repressor CsoR (Section 3), required for full virulence of the organism.[203,374,942] Interestingly, the genes encoding CtpC, CtpG and CtpV are each immediately downstream of a gene encoding a DUF1490 protein (Figure 57C), found in a genomic arrangement that is reminiscent of *fezAB* in *D. magneticus* and *C. difficile*; in fact, DUF1490 and DUF6110 (*fezA*) proteins are distantly related to one another in that both are predicted to be α-helical membrane proteins with a C-terminal tail.[935] Boudehen et al. have extensively functionally characterized the DUF1490 immediately in front of CtpC, a P_{1B-6}-like ATPase transporter that harbors a canonical P_{1B-1}- and P_{1B-2} CPC motif in the TM4 associated with Cu^{I} an Zn^{II} transporters (Figure 54, *bottom*), but contains a canonical P_{1B-6}-class TxxNHN motif in TM6 (Figure 56A), consistent with a global SSN analysis that places these CPC enzymes in their own cluster of closely related sequences.[910] The expression of *pacL1-ctpC* is induced specifically by zinc toxicity in both liquid cultures and infected macrophages, with the identity of the zinc-sensing efflux repressor not yet known.[935,943] These authors establish that this DUF1490, renamed PacL1, for P-ATPase-associated chaperone-like protein 1, binds Zn^{II} via a C-terminal "DLHDHDH" metal binding motif, and may function as a metallochaperone for CtpC at high cellular Zn^{II} toxicity.[935] Furthermore, PacL1 is also required under conditions of modest Zn^{II} toxicity in a way that is independent of its metal binding function where it plays a role as a scaffold to stabilize CtpC in the plasma membrane. A strain harboring a deletion of *pacL1-ctpC* is sensitive to zinc toxicity while single *pacL1*- or *ctpC*-complemented strains fail to rescue this growth phenotype; this is consistent with a model in which PacL1 and CtpC are both required to efficiently efflux Zn^{II} from the cytoplasm.[935]

Light microscopy-based imaging reveals that CtpC and PacL1 physically interact and form high molecular weight complexes in the mycobacterial membrane that the authors dub "metal efflux platforms"[935] that enhance resistance to metal poisoning. Such membrane microdomains like these, which impact enzyme activity, may be more common in bacterial membranes than previously believed.[937,944] Although more work needs to be done, orthologs PacL2, encoded in front of CtpG and containing a single D-E (Asp-Glu) sequence, and PacL3, in front of CtpV and harboring a "DDGHDH" sequence in its C-terminal metal-binding motif (Figure 57C) are partially redundant when expressed at high intracellular levels. This is a function of their conserved motifs in the protein chaperone-specific regions of these proteins rich in Glu/Ala repeats are reminiscent of the canonical protein chaperone GroEL1.[935] These Glu/Ala motifs mediate a physical interaction with CtpC in these membrane microdomains.[935] Biochemical reconstitution experiments and structural studies of a PacL1-CtpC complex will be required to significantly extend these studies.

5.3.4. Extracellular Metalation of Manganese Metalloenzymes. A final frontier in metalloprotein metalation is the metalation of exoenzymes, which include those enzymes secreted into the extracellular milieu as well as those that are integral membrane proteins whose active sites face outward, relative to the cytoplasm. There are a number of reports of P_{1B}-type ATPases that exhibit metal efflux rates that are too slow to be effective in resisting the effects of cellular metal toxicity, and thus must play some other role. One potential role is in metalation of extracytoplasmic enzymes.[945,946] This becomes

https://doi.org/10.1021/acs.chemrev.4c00264
Chem. Rev. 2024, 124, 13574−13659

particularly critical for weakly binding metals, including Mn^{II} and Fe^{II}, which may be outcompeted by extracellular Zn^{II} or Cu^{II}, which generally bind much more tightly to proteins (Section 2.2.2).[157] Seminal work by Robinson and co-workers showed that the twin-arginine translocation (Tat)-dependent secretion system, which exports folded metalloproteins, could be used to ensure cognate metalation by a Mn^{II}-metalloenzyme;[157] however, the Tat system only functions for soluble proteins and not integral membrane proteins or those anchored in the plasma membrane with their active sites facing out. This suggests the strong possibility that metalation with Mn^{II} might be dependent on a specific efflux transporter.

5.3.4.1. TerC Proteins Function in Exoenzyme Metalation. TerC proteins are a subgroup of the lysine transporter superfamily, and were originally described as mediating cellular resistance to tellurite oxide anion (TeO_3^{2-}) in extremophiles,[947] via a mechanism connected to cell envelope stress,[948] but more recently linked to Mn^{II} homeostasis in both *B. subtilis* and *E. coli*.[949−951] These apparently conflicting accounts have now been reconciled by recent findings that reveal that TerC proteins function during protein export via the generalized secretory pathway that is dependent on the SecYEG holotranslocon, activated by the SecA ATPase, that collectively define a core component of the secretosome (Figure 58).[952] *B. subtilis*

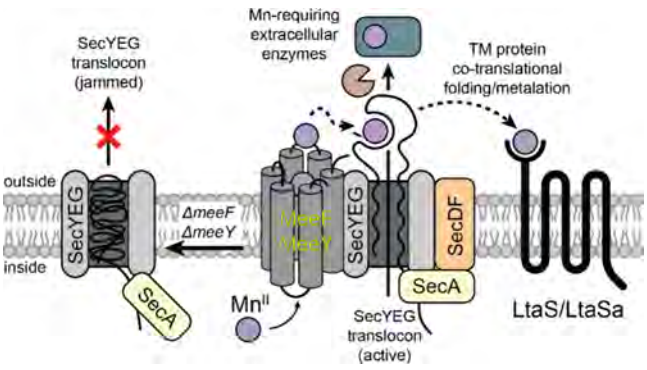

Figure 58. *B. subtilis* TerC proteins MeeF/MeeY physically associate with the SecYEG translocon-secretosome where the mediate the extracellular metalation of Mn^{II}-requiring soluble exoenzymes (slate square) and integral membrane proteins (represented by LtaS/LtaSa). Strains that lack both *meeY/meeF* genes result in general reduction in cellular protein secretion. Pac-man symbol (brown), Sec-associated extracellular processing enzyme. LtaS, major lipoteichoic acid (LTA) synthase; LtaSa, stress-induced LTA synthase.[952]

encodes three TerC homologues, two of which were renamed MeeF (metalation of exoenzymes with Mn) (formerly YceF) and MeeY (formerly YkoY), the latter of which is regulated by the *yybP-ykoY* Mn-sensing riboswitch in both *B. subtilis* and *E. coli* (named Alx) (Section 3.3.3). *meeF* appears to constitutively expressed in *B. subtilis* but can be upregulated further under conditions of acute cellular stress.

Remarkably, coimmunoprecipation experiments reveal a direct interaction of both TerC proteins with common components of the secretosome. This protein assembly must mediate cotranslational folding of secretosome clients since *B. subtilis* strains deficient in *both* MeeF and MeeY are strongly defective for protein secretion, independent of the metalation of a client (Figure 58). The Δ*meeF*-Δ*meeY* (FY) mutant strain can be rescued by induction of the expression of FtsH, an ATP-dependent metalloprotease that is known to clear "jammed" SecYEG translocons (Figure 58, *left*). The FY strains also secretes fewer extracellular proteases as well. Thus, TerC proteins appear to be integral components of the bacterial secretory apparatus, but also endow the secretosome with the ability to metalate exoenzymes, notably, the Mn^{II}-dependent lipoteichoic acid synthase (LtaS), the major lipotechoic acid synthase in *B. subtilis* (Figure 58, *right*). LtaS is an integral membrane protein that features an outward facing Mn^{II} active site that functions in cell wall homeostasis. These findings in *B. subtilis* appear general, since heterologous expression of TerCs from *L. monocytogenes* and *B. anthracis* in *B. subtilis* complements the FY mutant, restoring fitness and normal levels of protease and Mn^{II} secretion into the spent growth media.[952]

The mechanism of cotranslocational metalation by TerC proteins of LtaS and perhaps other clients during other stages of growth is not known, but several possibilities exist.[952] One is that of a classical metallochaperone role that requires a functional interaction that drives ligand exchange and metal transfer between a conserved metal site on the MeeF/MeeY donor[951] and the client LtaS (Figure 34). Another is that TerC proteins increase the local concentration of Mn^{II} so that it better competes with more tightly binding metals, e.g., Zn^{II}, in a way that does not require a direct physical interaction. Indeed, Zn^{II} inhibits Mn^{II}-dependent LtaS metalation in a way that is exacerbated in the FY mutant, a finding consistent with other reports of the mismetalation of Mn^{II} enzymes by Zn^{II} (Section 2.2.3). How LtaS holds on to its metal is not known, but kinetic trapping may well be involved. As this cotranslocational metal insertion system appears broadly conserved in all kingdoms of life,[952] there exists a strong motivation to identify of other TerC clients and fundamental bioinorganic chemistry features of this process.

6. CONCLUSIONS

Metalloproteins,[953] ranging from proteins that use a metal as an enzymatic cofactor to those with structural metals that stabilize the protein fold, play myriad distinct and often evolutionarily conserved roles in all kingdoms of life.[1] Since approximately one-third of a typical bacterial proteome consists of metalloproteins, cells must ensure that the metalloproteome is metalated with integrity[3] and is resistant to mismetalation or under-metalation that might occur under conditions of environmental metal toxicity or metal restriction, respectively. Metallostasis (Section 2) encompasses all those processes that maintain the integrity of the metalloproteome and its associated metabolic and regulatory functions, the complexity of which is orchestrated by the upstream "sentinels" of this process, the metallosensors (Section 3). These model regulatory proteins and RNAs exploit fundamental coordination chemistry to drive allosteric switching[18] in a wide range of molecular scaffolds[575] to induce a specific biological output of physiological or biotechnological value.[19]

Historically, our understanding of the metal (ligand) specificity and regulatory mechanisms of these sensory biomolecules has come from the study of "one molecule at a time" through application of classical approaches in bioinorganic chemistry, biophysical chemistry and structural biology (Section 3). While powerful, this approach becomes limiting in the search for general features that impact metal selectivity in a superfamily of proteins that do not necessarily share all specific features of the model protein.[241,253] The gap between detailed chemical and physical studies and bacterial phylogeny continues to close with the emergence and broad application of sophisticated

https://doi.org/10.1021/acs.chemrev.4c00264
Chem. Rev. 2024, 124, 13574−13659

comparative genomics tools, e.g., sequence similarity network (SSN) and related tools, that allows our community to exploit continuous advances in genome sequencing.[239,245,246] Machine learning approaches now make it possible to leverage reasonable quality structures of a significant number of evolutionarily related, yet biologically uncharacterized proteins, to determine the degree to which findings from a model system, on metal selectivity, for example, can be extended to the group.[954,955] Emerging advances in machine learning will continue to move the field of structural biology from a labor-intensive to high-throughput structure and dynamics prediction pipeline that will ultimately inform comparative genomics efforts to understand molecular evolution of specificity.[956] This paradigm shift, well underway, will permit new applications of metalloregulatory proteins as biotechnological "parts", while also informing new experimental strategies to develop new functionalities on these molecular scaffolds.[957] For example, high throughput selection and counter-selection strategies have led to the development of metal ion-specific DNAzymes with unprecedented metal specificity that continue to teach us how nucleic acids distinguish among various transition metal ions, while also creating reagents for applications as biosensing tools.[958]

Myriad cell-adaptive mechanisms, some newly discovered,[673,935,952,959] allow bacterial cells to maintain a metal quota that is capable of reacting to both chronic and acute metal starvation or toxicity, whatever the source. The expression of metalloprotein "paralogs", which occurs often under conditions of restriction of a specific metal,[6,680] or alternatively in distinct organisms with distinct lifestyles and access to distinct profiles of metal nutrients, is a form of metalloproteome remodeling, the footprint of which is likely far more widespread than discussed here (Section 4). Indeed, one enzyme superfamily only briefly touched upon here encompasses the ribonucleotide reductases (Section 4.3.6) required for the synthesis of DNA in all life forms.[793,960] A number of clearly distinct metallo-forms exist and have been characterized in detail in microbes, which remarkably, includes a metal-free variant of the enzyme,[8,794,961,962] which in human pathogens could retain function under conditions of host-mediated metal restriction.[963]

We also discuss new mechanistic insights into "old friends", the nucleotide-dependent metallochaperones (Section 5)[56,801,814,824] leading to a far more sophisticated understanding of enzyme metalation and transport, with many unanswered questions left for future work.[964,965] These adaptive responses, which occur in the context of an extraordinary ability of cells to "buffer" transition metal ions, enhance the resiliency of the metalloproteome while avoiding off-pathway metal toxicity.[966] They are remarkable examples of the extent to which evolution has gone to maintain the catalytic power of cellular metabolism dependent on metalloenzymes, particularly those enzymes involved in central carbon metabolism, one-carbon shuttling, scavenging of reactive oxygen species, and diverse aspects of the central dogma, when critical nutrient metals are in short supply. The implementation and development of global computational and experimental methods to map and explore the metalation status of the proteome,[62,160,184,967,968] *i.e*, metalloproteomics,[68,969] as well as workflows to better define the metal buffering components in cells,[119] promises novel insights into metalloregulation of cell biology and mechanisms of metallostasis from single cells to whole organisms in all kingdoms of life.

AUTHOR INFORMATION

Corresponding Authors

Daiana A. Capdevila − *Fundación Instituto Leloir, Instituto de Investigaciones Bioquímicas de Buenos Aires (IIBBA-CONICET), C1405 BWE Buenos Aires, Argentina;* orcid.org/0000-0002-0500-1016; Email: dcapdevila@leloir.org.ar

David P. Giedroc − *Department of Chemistry, Indiana University, Bloomington, Indiana 47405-7102, United States;* orcid.org/0000-0002-2342-1620; Email: giedroc@indiana.edu

Authors

Johnma J. Rondón − *Fundación Instituto Leloir, Instituto de Investigaciones Bioquímicas de Buenos Aires (IIBBA-CONICET), C1405 BWE Buenos Aires, Argentina*

Katherine A. Edmonds − *Department of Chemistry, Indiana University, Bloomington, Indiana 47405-7102, United States*

Joseph S. Rocchio − *Department of Chemistry, Indiana University, Bloomington, Indiana 47405-7102, United States*

Matias Villarruel Dujovne − *Fundación Instituto Leloir, Instituto de Investigaciones Bioquímicas de Buenos Aires (IIBBA-CONICET), C1405 BWE Buenos Aires, Argentina*

Complete contact information is available at: https://pubs.acs.org/10.1021/acs.chemrev.4c00264

Author Contributions

CRediT: **Daiana A. Capdevila** conceptualization, funding acquisition, visualization, writing - original draft, writing - review & editing;**Johnma J. Rondón** investigation, visualization, writing - original draft, writing - review & editing; **Katherine A. Edmonds** visualization, writing - original draft, writing - review & editing; **Joseph S. Rocchio** writing - review & editing; **Matias Villarruel Dujovne** visualization, writing - original draft, writing - review & editing; **David P. Giedroc** conceptualization, funding acquisition, visualization, writing - original draft, writing - review & editing.

Notes

The authors declare no competing financial interest.

Biographies

Daiana A. Capdevila earned her bachelor's degree in Chemistry at the University of Buenos Aires, Argentina. In 2015, she obtained her Ph.D. in Chemistry in the same institution under the supervision of Prof. Daniel Murgida. She later earned a Latin American PEW fellowship for a postdoctoral position in the Giedroc group where she studied the role of conformational dynamics in metalloregulatory proteins. In 2019, she returned to Argentina to start her own research group at the Leloir Institute Foundation in Buenos Aires. She was appointed Professor of Chemistry at the University of San Martin in 2021.

Johnma J. Rondón Guerrero earned his bachelor's degree in Biology at the Universidad de los Andes, Venezuela. He later obtained his Ph.D. in Cellular Biology at the same institution. He is currently working as a postdoctoral fellow at the Capdevila group studying the molecular evolution of the ArsR family of transcription factors in *Mycobacterium tuberculosis*.

Joseph S. Rocchio earned his undergraduate degree in Chemistry from Rensselaer Polytechnic Institute. He is currently a Ph.D. student in Chemistry at Indiana University in the Giedroc group, where he studies the biochemistry of the metal starvation response in *Acinetobacter baumannii*.

https://doi.org/10.1021/acs.chemrev.4c00264
Chem. Rev. 2024, 124, 13574−13659

Katherine A. Edmonds earned her B.S. in Chemistry at the University of Chicago. She obtained her Ph.D. in Biophysics at Harvard University under the supervision of Prof. Gerhard Wagner, where she studied protein NMR and eukaryotic translation initiation. Dr. Edmonds is a research scientist in the Giedroc group interested in transition metal homeostasis.

Matias Villarruel Dujovne earned his bachelor's degree in Chemistry at the University of Buenos Aires, Argentina. He is currently a Ph.D. student in Chemistry at the same institution while working in the Capdevila group, where he is combining the biophysical characterization of bacterial transcription factors with the development of cell-free biosensors.

David P. Giedroc earned a B.S. in Biochemistry from the Pennsylvania State University and Ph.D. in Biochemistry from the Vanderbilt University School of Medicine in 1984. Following a postdoctoral stint as an NIH postdoctoral fellow in the laboratory of the late Joseph Coleman at Yale University, he joined the faculty in the Department of Biochemistry and Biophysics at Texas A&M University in 1988. He was appointed Professor of Chemistry at Indiana University in 2007, served as Chair of Department from 2010-2015 and is currently holder of the Lilly Chemistry Alumni Chair. He was appointed Distinguished Professor of Chemistry in 2020. Prof. Giedroc is a Fellow of the AAAS, the American Academy of Microbiology, and the Royal Society of Chemistry.

ACKNOWLEDGMENTS

This work was supported by grants from the National Institutes of Health (R35 GM118157, R01 AI101171, and R01 AI178929) to D.P.G. and by Bunge & Born, Argentina, the Williams Foundations and MinCyT Argentina PICT-2021-GRF-TI-0415 and B81-CYTCH (to D.A.C.). D.A.C. is a staff member from CONICET; J.J.R. and M.V.D. are supported by a postdoctoral and a doctoral fellowship provided by CONICET, Argentina.

ABBREVIATIONS

Mn	manganese
Zn	zinc
Fe	iron
Co	cobalt
Ni	nickel
Cu	copper
Se	selenium
Mo	molybdenum
Mg	magnesium
K	potassium
Pho	phosphate
Hg	mercury
Au	gold
Cd	cadmium
As	arsenic
Pb	lead
Fe−S	iron−sulfur
Cys	cysteine
His	histidine
Asp	aspartate
Glu	glutamate
Met	methionine
Pro	proline
Trp	tryptophan
Asn	asparagine
Gly	glycine
Ser	serine
Lys	lysine
RSSH	organic persulfide
CSSH	cysteine persulfide
GSSH	glutathione persulfide
H_2S	hydrogen sulfide
ROS	reactive oxygen species
RNS	reactive nitrogen species
GSNO	*S*-Nitrosoglutathione
NO_x	nitric oxide (NO) and nitrogen dioxide (NO_2)
RES	reactive electrophile species
RSS	reactive sulfur species
Moco	molybdenum cofactor
GMPPNP	5′-Guanylyl imidodiphosphate
GMPPCP	Guanylyl 5′- (β,γ−methylenediphosphonate)
ppGpp	guanosine tetraphosphate
pppGpp	guanosine pentaphosphate
GTP	guanosine triphosphate
GDP	guanosine diphosphate
ATP	adenosine triphosphate
H_2NTP	7,8-dihydroneopterin triphosphate
THF	tetrahydrofolate
Q	queuosine
CAA	carbamoyl aspartate
DHO	dihydroorotate
EDTA	Ethylenediaminetetraacetic acid
PPRPP	Phosphoribosyl diphosphate
AMA	aspergillomarasmine A
ZTP	5-amino 4-imidazole carboxamide riboside 5′-triphosphate
GTPγS	guanosine 5′-O-[γ-thio]triphosphate
HDX-MS	hydrogen−deuterium exchange mass spectrometry
AdoCbl	adenosylcobalamin
HMW	high molecular weight
ZF	zinc finger
NTD	N-terminal domain
CC	coiled-coil
HTH	helix-turn-helix DNA binding motif
TM	transmembrane domain
MBD	metal-binding domain
DBD	DNA-binding domain
MBL	metal binding loop
FCD	FadR C-terminal domain
DNA	DNA
RNA	ribonucleic acid
mRNA	mRNA
tRNA	tRNA
5′ UTR	5′ Untranslated Region
aTFs	allosteric transcription factors
MoTTs	modification-tunable transcripts
WCB	whole cell biosensor
LOD	limit of detection
SDA	strand displacement amplification
NAST	nicked DNA template-assisted signal transduction
Tx-Tl	transcription-translation
SELIS	Seamless Enrichment of Ligand-Inducible Sensors
EXAFS	Extended X-ray Absorption Fine Structure
XAS	X-ray absorption spectroscopy
EDS	energy-dispersive X-ray spectroscopy

https://doi.org/10.1021/acs.chemrev.4c00264
Chem. Rev. 2024, 124, 13574−13659

Cryo-EM	cryogenic electron microscopy
SSN	sequence similarity network
NMR	nuclear magnetic resonance spectroscopy
SAXS	small-angle X-ray scattering
FRET	Förster resonance energy transfer
ICP-MS	inductively coupled plasma-mass spectrometry
2D-LC-ICP-MS	Two-dimensional liquid chromatography inductively coupled plasma mass spectrometry
GE-LS	polyacrylamide gel electrophoresis laser ablation
isoTOP-ABPP	isotopic tandem orthogonal proteolysis-activity-based protein profiling
K_d	dissociation equilibrium constant
pM	picomolar
nM	nanomolar
EC	Enzyme Commission
PDB	Protein Databank
CP	calprotectin
NMC	nucleotide-dependent metallochaperones
GAP	GTPase activating protein
ArsR	arsenic repressor
IdeR	Iron-dependent repressor
MerR	mercuric ion resistance regulator
CsoR	copper sensitive operon repressor
CstR	CsoR-like sulfurtransferase repressor
CopY	copper-responsive repressor
Fur	ferrous iron uptake repressor
Zur	Fur family zinc uptake regulator
DtxR	Diphtheria toxin repressor
NikR	Nickel responsive regulator of the *nik* operon
GntR	gluconate repressor
Mar	multiple antibiotic resistance repressor
TetR	Tetracycline Repressor
LysR	lysine repressor
DHOase	dihydroorotase
PyrC	pyrimidine biosynthetic enzyme dihydroorotase
QueD: 6-carboxy-5	6,7,8-tetrahydropterin synthase
DksA	RNA polymerase-binding transcription factor DksA/DnaK suppressor protein
FolE	GTP cyclohydrolase-IA (GCYH-1A)
CA	carbonic anhydrase
SODs	superoxide dismutases
camSOD	cambialistic superoxide dismutase
nsp	nonstructural protein
PTP1B	protein tyrosine phosphatase 1B
PBP2	penicillin-binding protein
MBLs	metallo-β-lactamases
SIMIBI	Signal recognition particle, MinD and BioD
ZigA	Zur-induced GTPase A
MCM	methylmalonyl-CoA mutase
MeaB	MCM accessory GTPase
UreG	urease accessory GTPase
NHase	nitrile hydratase
MPY	mycobacterial factor Y
Mrf	MPY recruitment factor
ZNG1	Zn-regulated GTPase metalloprotein activator
METAP1	methionine aminopeptidase-1
NAC	nascent polypeptide-associated complex
Csp	copper storage protein
MCO	multicopper oxidase
SERCA	sarco(endo)plasmic reticulum calcium ATPase
SPCA1	secretory-pathway Ca^{II}-ATPases

REFERENCES

(1) Andreini, C.; Cavallaro, G.; Lorenzini, S.; Rosato, A. MetalPDB: A Database of Metal Sites in Biological Macromolecular Structures. *Nucleic Acids Res.* **2012**, *41*, D312−9.

(2) Andreini, C.; Bertini, I.; Cavallaro, G.; Holliday, G. L.; Thornton, J. M. Metal Ions in Biological Catalysis: From Enzyme Databases to General Principles. *J. Biol. Inorg. Chem.* **2008**, *13*, 1205−1218.

(3) Waldron, K. J.; Rutherford, J. C.; Ford, D.; Robinson, N. J. Metalloproteins and Metal Sensing. *Nature* **2009**, *460*, 823−30.

(4) Jordan, M. R.; Dujovne, M. V.; Capdevila, D. A.; Giedroc, D. P. Metal Ion Homeostasis: Metalloenzyme Paralogs in the Bacterial Adaptative Response to Zinc Restriction. In *Comprehensive Inorganic Chemistry III*; Elsevier, 2023; pp 30−52.

(5) Radin, J. N.; Kelliher, J. L.; Solórzano, P. K. P.; Grim, K. P.; Ramezanifard, R.; Slauch, J. M.; Kehl-Fie, T. E. Metal-Independent Variants of Phosphoglycerate Mutase Promote Resistance to Nutritional Immunity and Retention of Glycolysis during Infection. *PLoS Pathog* **2019**, *15*, No. e1007971.

(6) Parraga Solorzano, P. K.; Bastille, T. S.; Radin, J. N.; Kehl-Fie, T. E. A Manganese-Independent Aldolase Enables *Staphylococcus aureus* To Resist Host-Imposed Metal Starvation. *mBio* **2023**, *14*, No. e0322322.

(7) Cotruvo, J. A., Jr.; Stubbe, J. Metallation and Mismetallation of Iron and Manganese Proteins *in vitro* and *in vivo*: The Class I Ribonucleotide Reductases as a Case Study. *Metallomics* **2012**, *4*, 1020−1036.

(8) Ruskoski, T. B.; Boal, A. K. The Periodic Table of Ribonucleotide Reductases. *J. Biol. Chem.* **2021**, *297*, 101137.

(9) Jordan, M. R.; Gonzalez-Gutierrez, G.; Trinidad, J. C.; Giedroc, D. P. Metal Retention and Replacement in QueD2 Protect Queuosine-tRNA Biosynthesis in Metal-Starved *Acinetobacter baumannii*. *Proc. Natl. Acad. Sci. U. S. A.* **2022**, *119*, No. e2213630119.

(10) Antelo, G. T.; Vila, A. J.; Giedroc, D. P.; Capdevila, D. A. Molecular Evolution of Transition Metal Bioavailability at the Host-Pathogen Interface. *Trends Microbiol* **2021**, *29*, 441−457.

(11) Zygiel, E. M.; Nolan, E. M. Transition Metal Sequestration by the Host-Defense Protein Calprotectin. *Annu. Rev. Biochem.* **2018**, *87*, 621−643.

(12) Sheldon, J. R.; Skaar, E. P. Metals as Phagocyte Antimicrobial Effectors. *Curr. Opin. Immunol* **2019**, *60*, 1−9.

(13) Liu, C.; Jursa, T.; Aschner, M.; Smith, D. R.; Mukhopadhyay, S. Up-Regulation of the Manganese Transporter SLC30A10 by Hypoxia-Inducible Factors Defines a Homeostatic Response to Manganese Toxicity. *Proc. Natl. Acad. Sci. U. S. A.* **2021**, *118*, 1−12.

(14) Banerjee, R.; Gouda, H.; Pillay, S. Redox-Linked Coordination Chemistry Directs Vitamin B12 Trafficking. *Acc. Chem. Res.* **2021**, *54*, 2003−2013.

(15) Bagheri, S.; Squitti, R.; Haertlé, T.; Siotto, M.; Saboury, A. A. Role of Copper in the Onset of Alzheimer's Disease Compared to Other Metals. *Front Aging Neurosci* **2018**, *9*, 1−15.

(16) de Bie, P.; Muller, P.; Wijmenga, C.; Klomp, L. W. J. Molecular Pathogenesis of Wilson and Menkes Disease: Correlation of Mutations with Molecular Defects and Disease Phenotypes. *J. Med. Genet* **2007**, *44*, 673−688.

(17) Rodriguez-Granillo, A.; Crespo, A.; Wittung-Stafshede, P. Conformational Dynamics of Metal-Binding Domains in Wilson Disease Protein: Molecular Insights into Selective Copper Transfer. *Biochemistry* **2009**, *48*, 5849−5863.

(18) Giedroc, D. P.; Arunkumar, A. I. Metal Sensor Proteins: Nature's Metalloregulated Allosteric Switches. *Dalton Trans* **2007**, 3107−3120.

(19) Jung, J. K.; Alam, K. K.; Verosloff, M. S.; Capdevila, D. A.; Desmau, M.; Clauer, P. R.; Lee, J. W.; Nguyen, P. Q.; Pastén, P. A.;

https://doi.org/10.1021/acs.chemrev.4c00264
Chem. Rev. 2024, 124, 13574−13659

Matiasek, S. J.; et al. Cell-Free Biosensors for Rapid Detection of Water Contaminants. *Nat. Biotechnol.* **2020**, *38*, 1451−1459.
(20) Zhang, Y.; Zheng, J. Bioinformatics of Metalloproteins and Metalloproteomes. *Molecules* **2020**, *25*, 3366.
(21) Sigel, H.; Sigel, A. The Bio-Relevant Metals of the Periodic Table of the Elements. *Zeitschrift fur Naturforschung - Sec B J. Chem. Sci.* **2019**, *74*, 461−471.
(22) Freisinger, E.; Sigel, R. K. O. The Bioinorganic Periodic Table. *Chimia (Aarau)* **2019**, *73*, 185−193.
(23) Probst, C.; Yang, J.; Krausze, J.; Hercher, T. W.; Richers, C. P.; Spatzal, T.; Kc, K.; Giles, L. J.; Rees, D. C.; et al. Mechanism of Molybdate Insertion into Pterin-Based Molybdenum Cofactors. *Nat. Chem.* **2021**, *13*, 758−765.
(24) Zhang, Y.; Gladyshev, V. N. Molybdoproteomes and Evolution of Molybdenum Utilization. *J. Mol. Biol.* **2008**, *379*, 881−899.
(25) Zupok, A.; Iobbi-Nivol, C.; Mejean, V.; Leimkühler, S. The Regulation of Moco Biosynthesis and Molybdoenzyme Gene Expression by Molybdenum and Iron in Bacteria. *Metallomics* **2019**, *11*, 1602−1624.
(26) Kang, W. Structural Insights and Mechanistic Understanding of Iron-Molybdenum Cofactor Biosynthesis by NifB in Nitrogenase Assembly Process. *Mol. Cells* **2023**, *46*, 736−742.
(27) Weber, J. N.; Minner-Meinen, R.; Behnecke, M.; Biedendieck, R.; Hansch, V. G.; Hercher, T. W.; Hertweck, C.; van den Hout, L.; Knuppel, L.; Sivov, S.; et al. Moonlighting Arabidopsis Molybdate Transporter 2 Family and GSH-Complex Formation Facilitate Molybdenum Homeostasis. *Commun. Biol.* **2023**, *6*, 801.
(28) Tejada-Jimenez, M.; Leon-Miranda, E.; Llamas, A. Chlamydomonas Reinhardtii-A Reference Microorganism for Eukaryotic Molybdenum Metabolism. *Microorganisms* **2023**, *11*, 1671.
(29) Johannes, L.; Fu, C. Y.; Schwarz, G. Molybdenum Cofactor Deficiency in Humans. *Molecules* **2022**, *27*, 6896.
(30) Hausinger, R. P. New Metal Cofactors and Recent Metallocofactor Insights. *Curr. Opin Struct Biol.* **2019**, *59*, 1−8.
(31) Daumann, L. J.; Pol, A.; Op den Camp, H. J. M.; Martinez-Gomez, N. C. A Perspective on the Role of Lanthanides in Biology: Discovery, Open Questions and Possible Applications. *Adv. Microb Physiol* **2022**, *81*, 1−24.
(32) Featherston, E. R.; Cotruvo, J. A., Jr The Biochemistry of Lanthanide Acquisition, Trafficking, and Utilization. *Biochim Biophys Acta Mol. Cell Res.* **2021**, *1868*, 118864.
(33) Mattocks, J. A.; Jung, J. J.; Lin, C. Y.; Dong, Z.; Yennawar, N. H.; Featherston, E. R.; Kang-Yun, C. S.; Hamilton, T. A.; Park, D. M.; Boal, A. K.; et al. Enhanced Rare-Earth Separation with a Metal-Sensitive Lanmodulin Dimer. *Nature* **2023**, *618*, 87−93.
(34) Zoidis, E.; Seremelis, I.; Kontopoulos, N.; Danezis, G. P. Selenium-Dependent Antioxidant Enzymes: Actions and Properties of Selenoproteins. *Antioxidants* **2018**, *7*, No. e00624-19.
(35) Santesmasses, D.; Mariotti, M.; Gladyshev, V. N. Bioinformatics of Selenoproteins. *Antioxid Redox Signal* **2020**, *33*, 525−536.
(36) Andreini, C.; Bertini, I. A Bioinformatics View of Zinc Enzymes. *J. Inorg. Biochem* **2012**, *111*, 150−156.
(37) Choi, S.; Bird, A. J. Zinc'ing Sensibly: Controlling Zinc Homeostasis at the Transcriptional Level. *Metallomics* **2014**, *6*, 1198−1215.
(38) Damon, L. J.; Ocampo, D.; Sanford, L.; Taylor, J.; Allen, M. A.; Dowell, R. D.; Palmer, A. E. Cellular Zinc Status Alters Chromatin Accessibility and Binding of Transcription Factor p53 to Genomic Sites. *bioRxiv* **2023**. DOI: 10.1101/2023.11.20.567954.
(39) Laity, J. H.; Andrews, G. K. Understanding the Mechanisms of Zinc-Sensing by Metal-Response Element Binding Transcription Factor-1 (MTF-1). *Arch. Biochem. Biophys.* **2007**, *463*, 201−210.
(40) Wang, Z.; Feng, L. S.; Matskevich, V.; Venkataraman, K.; Parasuram, P.; Laity, J. H. Solution Structure of a Zap1 Zinc-Responsive Domain Provides Insights into Metalloregulatory Transcriptional Repression in *Saccharomyces cerevisiae*. *J. Mol. Biol.* **2006**, *357*, 1167−1183.
(41) Lange, M.; Ok, K.; Shimberg, G. D.; Bursac, B.; Marko, L.; Ivanovic-Burmazovic, I.; Michel, S. L. J.; Filipovic, M. R. Direct Zinc Finger Protein Persulfidation by H_2S Is Facilitated by Zn^{2+}. *Angew. Chem., Int. Ed. Engl.* **2019**, *58*, 7997−8001.
(42) Cui, B.; Pan, Q.; Clarke, D.; Villarreal, M. O.; Umbreen, S.; Yuan, B.; Shan, W.; Jiang, J.; Loake, G. J. *S*-Nitrosylation of the Zinc Finger Protein SRG1 Regulates Plant Immunity. *Nat. Commun.* **2018**, *9*, 4226.
(43) Mely, Y.; Rocquigny, H.; Shvadchak, V.; Avilov, S.; Dong, C.; Dietrich, U.; Darlix, J.-L. Targeting the Viral Nucleocapsid Protein in Anti-HIV-1 Therapy. *Mini Rev. Med. Chem.* **2008**, *8*, 24−35.
(44) Miller Jenkins, L. M.; Ott, D. E.; Hayashi, R.; Coren, L. V.; Wang, D.; Xu, Q.; Schito, M. L.; Inman, J. K.; Appella, D. H.; Appella, E. Small-Molecule Inactivation of HIV-1 NCp7 by Repetitive Intracellular Acyl Transfer. *Nat. Chem. Biol.* **2010**, *6*, 887−889.
(45) Tedbury, P. R.; Freed, E. O. HIV-1 Gag: An Emerging Target for Antiretroviral Therapy. *Curr. Top Microbiol Immunol* **2015**, *389*, 171−201.
(46) Deshmukh, L.; Tugarinov, V.; Appella, D. H.; Clore, G. M. Targeting a Dark Excited State of HIV-1 Nucleocapsid by Antiretroviral Thioesters Revealed by NMR Spectroscopy. *Angew. Chem., Int. Ed. Engl.* **2018**, *57*, 2687−2691.
(47) Shimberg, G. D.; Pritts, J. D.; Michel, S. L. J. Iron-Sulfur Clusters in Zinc Finger Proteins. *Methods Enzymol* **2018**, *599*, 101−137.
(48) O'Brien, E.; Holt, M. E.; Thompson, M. K.; Salay, L. E.; Ehlinger, A. C.; Chazin, W. J.; Barton, J. K. The [4Fe4S] Cluster of Human DNA Primase Functions as a Redox Switch Using DNA Charge Transport. *Science* **2017**, *355*. DOI: 10.1126/science.aag1789.
(49) O'Brien, E.; Salay, L. E.; Epum, E. A.; Friedman, K. L.; Chazin, W. J.; Barton, J. K. Yeast Require Redox Switching in DNA Primase. *Proc. Natl. Acad. Sci. U. S. A.* **2018**, *115*, 13186−13191.
(50) Pritts, J. D.; Michel, S. L. J. Fe-S Clusters Masquerading as Zinc Finger Proteins. *J. Inorg. Biochem* **2022**, *230*, 111756.
(51) Shimberg, G. D.; Michalek, J. L.; Oluyadi, A. A.; Rodrigues, A. V.; Zucconi, B. E.; Neu, H. M.; Ghosh, S.; Sureschandra, K.; Wilson, G. M.; Stemmler, T. L.; Michel, S. L. J. Cleavage and Polyadenylation Specificity Factor 30: An RNA-Binding Zinc-Finger Protein with an Unexpected 2Fe-2S Cluster. *Proc. Natl. Acad. Sci. U. S. A.* **2016**, *113*, 4700−4705.
(52) White, M. F.; Dillingham, M. S. Iron-Sulphur Clusters in Nucleic Acid Processing Enzymes. *Curr. Opin Struct. Biol.* **2012**, *22*, 94−100.
(53) Khodour, Y.; Kaguni, L. S.; Stiban, J. Iron-Sulfur Clusters in Nucleic Acid Metabolism: Varying Roles of Ancient Cofactors. *Enzymes (Essen)* **2019**, *45*, 225−256.
(54) Maio, N.; Raza, M. K.; Li, Y.; Zhang, D. L.; Bollinger, J. M., Jr; Krebs, C.; Rouault, T. A. An Iron-Sulfur Cluster in the Zinc-Binding Domain of the SARS-CoV-2 Helicase Modulates Its RNA-Binding and -Unwinding Activities. *Proc. Natl. Acad. Sci. U. S. A.* **2023**, *120*, No. e2303860120.
(55) Maio, N.; Lafont, B. A. P.; Sil, D.; Li, Y.; Bollinger, J. M., Jr; Krebs, C.; Pierson, T. C.; Linehan, W. M.; Rouault, T. A. Fe-S Cofactors in the SARS-CoV-2 RNA-Dependent RNA Polymerase Are Potential Antiviral Targets. *Science* **2021**, *373*, 236−241.
(56) Weiss, A.; Murdoch, C. C.; Edmonds, K. A.; Jordan, M. R.; Monteith, A. J.; Perera, Y. R.; Rodríguez Nassif, A. M.; Petoletti, A. M.; Beavers, W. N.; Munneke, M. J.; et al. Zn-Regulated GTPase Metalloprotein Activator 1 Modulates Vertebrate Zinc Homeostasis. *Cell* **2022**, *185*, 2148−2163.
(57) Summers, M. F.; Henderson, L. E.; Chance, M. R.; South, T. L.; Blake, P. R.; Perez-Alvarado, G.; Bess, J. W.; Sowder, R. C.; Arthur, L. O.; Sagi, I.; et al. Nucleocapsid Zinc Fingers Detected in Retroviruses: EXAFS Studies of Intact Viruses and the Solution-state Structure of the Nucleocapsid Protein from HIV-1. *Protein Sci.* **1992**, *1*, 563−574.
(58) Newman, J. A.; Douangamath, A.; Yadzani, S.; Yosaatmadja, Y.; Aimon, A.; Brandão-Neto, J.; Dunnett, L.; Gorrie-stone, T.; Skyner, R.; Fearon, D.; et al. Structure, Mechanism and Crystallographic Fragment Screening of the SARS-CoV-2 NSP13 Helicase. *Nat. Commun.* **2021**, *12*, 4848.
(59) Bellomo, E.; Birla Singh, K.; Massarotti, A.; Hogstrand, C.; Maret, W. The Metal Face of Protein Tyrosine Phosphatase 1B. *Coord. Chem. Rev.* **2016**, *327*−*328*, 70−83.

(60) Bellomo, E.; Massarotti, A.; Hogstrand, C.; et al. Zinc Ions Modulate Protein Tyrosine Phosphatase 1B Activity. *Metallomics* **2014**, *6*, 1229−1239.
(61) Bellomo, E.; Abro, A.; Hogstrand, C.; Maret, W.; Domene, C. Role of Zinc and Magnesium Ions in the Modulation of Phosphoryl Transfer in Protein Tyrosine Phosphatase 1B. *J. Am. Chem. Soc.* **2018**, *140*, 4446−4454.
(62) Cheng, Y.; Wang, H.; Xu, H.; Liu, Y.; Ma, B.; Chen, X.; Zeng, X.; Wang, X.; Wang, B.; Shiau, C.; et al. Co-Evolution-Based Prediction of Metal-Binding Sites in Proteomes by Machine Learning. *Nat. Chem. Biol.* **2023**, *19*, 548−555.
(63) Durr, S. L.; Levy, A.; Rothlisberger, U. Metal3D: A General Deep Learning Framework for Accurate Metal Ion Location Prediction in Proteins. *Nat. Commun.* **2023**, *14*, 2713.
(64) Putignano, V.; Rosato, A.; Banci, L.; Andreini, C. MetalPDB in 2018: A Database of Metal Sites in Biological Macromolecular Structures. *Nucleic Acids Res.* **2018**, *46*, D459−D464.
(65) Laveglia, V.; Giachetti, A.; Sala, D.; Andreini, C.; Rosato, A. Learning to Identify Physiological and Adventitious Metal-Binding Sites in the Three-Dimensional Structures of Proteins by Following the Hints of a Deep Neural Network. *J. Chem. Inf Model* **2022**, *62*, 2951−2960.
(66) Feehan, R.; Franklin, M. W.; Slusky, J. S. G. Machine Learning Differentiates Enzymatic and Non-Enzymatic Metals in Proteins. *Nat. Commun.* **2021**, *12*, 3712.
(67) Laveglia, V.; Bazayeva, M.; Andreini, C.; Rosato, A. Hunting down Zinc(II)-Binding Sites in Proteins with Distance Matrices. *Bioinformatics* **2023**, *39*, btad653.
(68) Zhou, Y.; Li, H.; Sun, H. Metalloproteomics for Biomedical Research: Methodology and Applications. *Annu. Rev. Biochem.* **2022**, *91*, 449−473.
(69) Micelli, C.; Dai, Y.; Raustad, N.; Isberg, R. R.; Dowson, C. G.; Lloyd, A. J.; Geisinger, E.; Crow, A.; Roper, D. I. A Conserved Zinc-Binding Site in *Acinetobacter baumannii* PBP2 Required for Elongasome-Directed Bacterial Cell Shape. *Proc. Natl. Acad. Sci. U. S. A.* **2023**, *120*, No. e2215237120.
(70) Murdoch, C. C.; Skaar, E. P. Nutritional Immunity: The Battle for Nutrient Metals at the Host-Pathogen Interface. *Nat. Rev. Microbiol* **2022**, *20*, 657−670.
(71) Weinberg, E. D. Nutritional Immunity. Host's Attempt to Withhold Iron from Microbial Invaders. *JAMA* **1975**, *231*, 39−41.
(72) Kehl-Fie, T. E.; Skaar, E. P. Nutritional Immunity beyond Iron: A Role for Manganese and Zinc. *Curr. Opin Chem. Biol.* **2010**, *14*, 218−224.
(73) Lonergan, Z. R.; Nairn, B. L.; Wang, J.; Hsu, Y.-P.; Hesse, L. E.; Beavers, W. N.; Chazin, W. J.; Trinidad, J. C.; VanNieuwenhze, M. S.; Giedroc, D. P.; et al. An *Acinetobacter baumannii*, Zinc-Regulated Peptidase Maintains Cell Wall Integrity during Immune-Mediated Nutrient Sequestration. *Cell Rep* **2019**, *26*, 2009−2018.
(74) Sychantha, D.; Rotondo, C. M.; Tehrani, K.; Martin, N. I.; Wright, G. D. Aspergillomarasmine A Inhibits Metallo-Beta-Lactamases by Selectively Sequestering Zn^{2+}. *J. Biol. Chem.* **2021**, *297*, 100918.
(75) King, A. M.; Reid-Yu, S. A.; Wang, W.; King, D. T.; De Pascale, G.; Strynadka, N. C.; Walsh, T. R.; Coombes, B. K.; Wright, G. D. Aspergillomarasmine A Overcomes Metallo-Beta-Lactamase Antibiotic Resistance. *Nature* **2014**, *510*, 503−506.
(76) Bahr, G.; Gonzalez, L. J.; Vila, A. J. Metallo-Beta-Lactamases in the Age of Multidrug Resistance: From Structure and Mechanism to Evolution, Dissemination, and Inhibitor Design. *Chem. Rev.* **2021**, *121*, 7957−8094.
(77) Bahr, G.; Vitor-Horen, L.; Bethel, C. R.; Bonomo, R. A.; González, L. J.; Vila, A. J. Clinical Evolution of New Delhi Metallo-Beta-Lactamase (NDM) Optimizes Resistance under Zn(II) Deprivation. *Antimicrob. Agents Chemother.* **2018**, *62*, No. e01849-17.
(78) Gonzalez, L. J.; Bahr, G.; Gonzalez, M. M.; Bonomo, R. A.; Vila, A. J. In-Cell Kinetic Stability Is an Essential Trait in Metallo-Beta-Lactamase Evolution. *Nat. Chem. Biol.* **2023**, *19*, 1116−1126.
(79) Heffern, M. C.; Park, H. M.; Au-Yeung, H. Y.; Van De Bittner, G. C.; Ackerman, C. M.; Stahl, A.; Chang, C. J. In Vivo Bioluminescence Imaging Reveals Copper Deficiency in a Murine Model of Non-alcoholic Fatty Liver Disease. *Proc. Natl. Acad. Sci. U. S. A.* **2016**, *113*, 14219−14224.
(80) Ackerman, C. M.; Chang, C. J. Copper Signaling in the Brain and Beyond. *J. Biol. Chem.* **2018**, *293*, 4628−4635.
(81) Krishnamoorthy, L.; Cotruvo, J. A.; Chan, J.; Kaluarachchi, H.; Muchenditsi, A.; Pendyala, V. S.; Jia, S.; Aron, A. T.; Ackerman, C. M.; Wal, M. N. V.; et al. Copper Regulates Cyclic-AMP-Dependent Lipolysis. *Nat. Chem. Biol.* **2016**, *12*, 586−592.
(82) Chang, C. J. Searching for Harmony in Transition-Metal Signaling. *Nat. Chem. Biol.* **2015**, *11*, 744−7.
(83) Lutsenko, S. Dynamic and Cell-Specific Transport Networks for Intracellular Copper Ions. *J. Cell Sci.* **2021**, *134*, jcs240523.
(84) Vitaliti, A.; De Luca, A.; Rossi, L. Copper-Dependent Kinases and Their Role in Cancer Inception, Progression and Metastasis. *Biomolecules* **2022**, *12*, 1520.
(85) Lu, J.; Liu, X.; Li, X.; Li, H.; Shi, L.; Xia, X.; He, B.; Meyer, T. F.; Li, X.; Sun, H.; Yang, X. Copper Regulates the Host Innate Immune Response against Bacterial Infection via Activation of ALPK1 Kinase. *Proc. Natl. Acad. Sci. U. S. A.* **2024**, *121*, 2017.
(86) Shanbhag, V. C.; Gudekar, N.; Jasmer, K.; et al. Copper Metabolism as a Unique Vulnerability in Cancer. *Biochim Biophys Acta - Mol. Cell Res.* **2021**, *1868*, 118893.
(87) Turski, M. L.; Brady, D. C.; Kim, H. J.; Kim, B.-E.; Nose, Y.; Counter, C. M.; Winge, D. R.; Thiele, D. J. A Novel Role for Copper in Ras/Mitogen-Activated Protein Kinase Signaling. *Mol. Cell. Biol.* **2012**, *32*, 1284−1295.
(88) Brady, D. C.; Crowe, M. S.; Turski, M. L.; Hobbs, G. A.; Yao, X.; Chaikuad, A.; Knapp, S.; Xiao, K.; Campbell, S. L.; Thiele, D. J.; Counter, C. M. Copper Is Required for Oncogenic BRAF Signalling and Tumorigenesis. *Nature* **2014**, *509*, 492−496.
(89) Grasso, M.; Bond, G. J.; Kim, Y.-J.; Boyd, S.; Matson Dzebo, M.; Valenzuela, S.; Tsang, T.; Schibrowsky, N. A.; Alwan, K. B.; Blackburn, N. J.; et al. The Copper Chaperone CCS Facilitates Copper Binding to MEK1/2 to Promote Kinase Activation. *J. Biol. Chem.* **2021**, *297*, 101314.
(90) Rae, T. D.; Schmidt, P. J.; Pufahl, R. A.; Culotta, V. C.; O'Halloran, T. V. Undetectable Intracellular Free Copper: The Requirement of a Copper Chaperone for Superoxide Dismutase. *Science* **1999**, *284*, 805−808.
(91) Kim, Y.; Bond, G. J.; Tsang, T.; Posimo, J. M.; Busino, L.; Brady, D. C. Copper Chaperone ATOX1 Is Required for MAPK Signaling and Growth in BRAF Mutation-Positive Melanoma. *Metallomics* **2019**, *11*, 1430−1440.
(92) Wang, J.; Luo, C.; Shan, C.; You, Q.; Lu, J.; Elf, S.; Zhou, Y.; Wen, Y.; Vinkenborg, J. L.; Fan, J.; et al. Inhibition of Human Copper Trafficking by a Small Molecule Significantly Attenuates Cancer Cell Proliferation. *Nat. Chem.* **2015**, *7*, 968−979.
(93) Guo, J.; Cheng, J.; Zheng, N.; Zhang, X.; Dai, X.; Zhang, L.; Hu, C.; Wu, X.; Jiang, Q.; Wu, D.; et al. Copper Promotes Tumorigenesis by Activating the PDK1-AKT Oncogenic Pathway in a Copper Transporter 1 Dependent Manner. *Adv. Sci.* **2021**, *8*, 1−14.
(94) Ge, E. J.; Bush, A. I.; Casini, A.; Cobine, P. A.; Cross, J. R.; DeNicola, G. M.; Dou, Q. P.; Franz, K. J.; Gohil, V. M.; Gupta, S.; et al. Connecting Copper and Cancer: From Transition Metal Signalling to Metalloplasia. *Nat. Rev. Cancer* **2022**, *22*, 102−113.
(95) Tsang, T.; Posimo, J. M.; Gudiel, A. A.; Cicchini, M.; Feldser, D. M.; Brady, D. C. Copper Is an Essential Regulator of the Autophagic Kinases ULK1/2 to Drive Lung Adenocarcinoma. *Nat. Cell Biol.* **2020**, *22*, 412−424.
(96) Pezacki, A. T.; Matier, C. D.; Gu, X.; Kummelstedt, E.; Bond, S. E.; Torrente, L.; Jordan-Sciutto, K. L.; DeNicola, G. M.; Su, T. A.; Brady, D. C.; et al. Oxidation State-Specific Fluorescent Copper Sensors Reveal Oncogene-Driven Redox Changes That Regulate Labile Copper(II) Pools. *Proc. Natl. Acad. Sci. U. S. A.* **2022**, *119*, 1−9.

(97) Ohgami, R. S.; Campagna, D. R.; McDonald, A.; Fleming, M. D. The Steap Proteins Are Metalloreductases. *Blood* **2006**, *108*, 1388−1394.
(98) McDonald, A. G.; Tipton, K. F. Enzyme Nomenclature and Classification: The State of the Art. *FEBS J.* **2023**, *290*, 2214−2231.
(99) Gherasim, C.; Lofgren, M.; Banerjee, R. Navigating the B_{12} Road: Assimilation, Delivery, and Disorders of Cobalamin. *J. Biol. Chem.* **2013**, *288*, 13186−13193.
(100) Desguin, B.; Zhang, T.; Soumillion, P.; Hols, P.; Hu, J.; Hausinger, R. P. A Tethered Niacin-Derived Pincer Complex with a Nickel-Carbon Bond in Lactate Racemase. *Science* **2015**, *349*, 66−9.
(101) Andreini, C.; Putignano, V.; Rosato, A.; Banci, L. The Human Iron-Proteome. *Metallomics* **2018**, *10*, 1223−1231.
(102) Basler, S.; Studer, S.; Zou, Y.; Mori, T.; Ota, Y.; Camus, A.; Bunzel, H. A.; Helgeson, R. C.; Houk, K. N.; Jimenez-Oses, G.; et al. Efficient Lewis Acid Catalysis of an Abiological Reaction in a *de Novo* Protein Scaffold. *Nat. Chem.* **2021**, *13*, 231−235.
(103) Studer, S.; Hansen, D. A.; Pianowski, Z. L.; Mittl, P. R. E.; Debon, A.; Guffy, S. L.; Der, B. S.; Kuhlman, B.; Hilvert, D. Evolution of a Highly Active and Enantiospecific Metalloenzyme from Short Peptides. *Science* **2018**, *362*, 1285−1288.
(104) Koebke, K. J.; Pinter, T. B. J.; Pitts, W. C.; Pecoraro, V. L. Catalysis and Electron Transfer in *De Novo* Designed Metalloproteins. *Chem. Rev.* **2022**, *122*, 12046−12109.
(105) Van Stappen, C.; Deng, Y.; Liu, Y.; Heidari, H.; Wang, J. X.; Zhou, Y.; Ledray, A. P.; Lu, Y. Designing Artificial Metalloenzymes by Tuning of the Environment beyond the Primary Coordination Sphere. *Chem. Rev.* **2022**, *122*, 11974−12045.
(106) Jacobsen, F. E.; Kazmierczak, K. M.; Lisher, J. P.; Winkler, M. E.; Giedroc, D. P. Interplay between Manganese and Zinc Homeostasis in the Human Pathogen *Streptococcus pneumoniae*. *Metallomics* **2011**, *3*, 38−41.
(107) Aguirre, J. D.; Clark, H. M.; McIlvin, M.; Vazquez, C.; Palmere, S. L.; Grab, D. J.; Seshu, J.; Hart, P. J.; Saito, M.; Culotta, V. C. A Manganese-Rich Environment Supports Superoxide Dismutase Activity in a Lyme Disease Pathogen, *Borrelia Burgdorferi*. *J. Biol. Chem.* **2013**, *288*, 8468−8478.
(108) Jomova, K.; Makova, M.; Alomar, S. Y.; Alwasel, S. H.; Nepovimova, E.; Kuca, K.; Rhodes, C. J.; Valko, M. Essential Metals in Health and Disease. *Chem. Biol. Interact* **2022**, *367*, 110173.
(109) Outten, C. E.; O'Halloran, T. V. Femtomolar Sensitivity of Metalloregulatory Proteins Controlling Zinc Homeostasis. *Science* **2001**, *292*, 2488−2492.
(110) Lisher, J. P.; Giedroc, D. P. Manganese Acquisition and Homeostasis at the Host-Pathogen Interface. *Front Cell Infect Microbiol* **2013**, *3*, 91.
(111) Kim, B.; Karlin, K. D. Ligand-Copper(I) Primary O_2-Adducts: Design, Characterization, and Biological Significance of Cupric-Superoxides. *Acc. Chem. Res.* **2023**, *56*, 2197−2212.
(112) Koo, C. W.; Rosenzweig, A. C. Biochemistry of Aerobic Biological Methane Oxidation. *Chem. Soc. Rev.* **2021**, *50*, 3424−3436.
(113) Christianson, D. W. Structural Chemistry and Biology of Manganese Metalloenzymes. *Prog. Biophys. Mol. Biol.* **1997**, *67*, 217−252.
(114) Ragsdale, S. W. Nickel-Based Enzyme Systems. *J. Biol. Chem.* **2009**, *284*, 18571−18575.
(115) Kaluarachchi, H.; Chan Chung, K. C.; Zamble, D. B. Microbial Nickel Proteins. *Nat. Prod Rep* **2010**, *27*, 681.
(116) Reyes-Caballero, H.; Campanello, G. C.; Giedroc, D. P. Metalloregulatory Proteins: Metal Selectivity and Allosteric Switching. *Biophys Chem.* **2011**, *156*, 103−14.
(117) Foster, A. W.; Osman, D.; Robinson, N. J. Metal Preferences and Metallation. *J. Biol. Chem.* **2014**, *289*, 28095−103.
(118) Capdevila, D. A.; Wang, J.; Giedroc, D. P. Bacterial Strategies to Maintain Zinc Metallostasis at the Host-Pathogen Interface. *J. Biol. Chem.* **2016**, *291*, 20858−20868.
(119) Foster, A. W.; Pernil, R.; Patterson, C. J.; Scott, A. J. P.; Pålsson, L.-O.; Pal, R.; Cummins, I.; Chivers, P. T.; Pohl, E.; Robinson, N. J. A Tight Tunable Range for Ni(II) Sensing and Buffering in Cells. *Nat. Chem. Biol.* **2017**, *13*, 409−414.
(120) Capdevila, D. A.; Edmonds, K. A.; Giedroc, D. P. Metallochaperones and Metalloregulation in Bacteria. *Essays Biochem* **2017**, *61*, 177−200.
(121) Osman, D.; Martini, M. A.; Foster, A. W.; Chen, J.; Scott, A. J. P.; Morton, R. J.; Steed, J. W.; Lurie-Luke, E.; Huggins, T. G.; Lawrence, A. D.; et al. Bacterial Sensors Define Intracellular Free Energies for Correct Enzyme Metalation. *Nat. Chem. Biol.* **2019**, *15*, 241−249.
(122) Alchoubassi, G.; Kińska, K.; Bierla, K.; Lobinski, R.; Szpunar, J. Speciation of Essential Nutrient Trace Elements in Coconut Water. *Food Chem.* **2021**, *339*, 127680.
(123) Flis, P.; Ouerdane, L.; Grillet, L.; Curie, C.; Mari, S.; Lobinski, R. Inventory of Metal Complexes Circulating in Plant Fluids: A Reliable Method Based on HPLC Coupled with Dual Elemental and High-resolution Molecular Mass Spectrometric Detection. *New Phytologist* **2016**, *211*, 1129−1141.
(124) Basak, P.; Cabelli, D. E.; Chivers, P. T.; Farquhar, E. R.; Maroney, M. J. *In vitro* Maturation of NiSOD Reveals a Role for Cytoplasmic Histidine in Processing and Metalation. *Metallomics* **2023**, *15*, mfad054.
(125) Nairn, B. L.; Lonergan, Z. R.; Wang, J.; Braymer, J. J.; Zhang, Y.; Calcutt, M. W.; Lisher, J. P.; Gilston, B. A.; Chazin, W. J.; de Crécy-Lagard, V.; et al. The Response of *Acinetobacter baumannii* to Zinc Starvation. *Cell Host Microbe* **2016**, *19*, 826−836.
(126) O'Halloran, T. V.; Culotta, V. C. Metallochaperones, an Intracellular Shuttle Service for Metal Ions. *J. Biol. Chem.* **2000**, *275*, 25057−60.
(127) McCullagh, M.; Zeczycki, T. N.; Kariyawasam, C. S.; Durie, C. L.; Halkidis, K.; Fitzkee, N. C.; Holt, J. M.; Fenton, A. W. What Is Allosteric Regulation? Exploring the Exceptions That Prove the Rule. *J. Biol. Chem.* **2024**, *300*, 105672.
(128) Monod, J.; Wyman, J.; Changeux, J. P. On the Nature of Allosteric Transitions: A Plausible Model. *J. Mol. Biol.* **1965**, *12*, 88−118.
(129) Osman, D.; Foster, A. W.; Chen, J.; Svedaite, K.; Steed, J. W.; Lurie-Luke, E.; Huggins, T. G.; Robinson, N. J. Fine Control of Metal Concentrations Is Necessary for Cells to Discern Zinc from Cobalt. *Nat. Commun.* **2017**, *8*, 1884.
(130) Morby, A. P.; Turner, J. S.; Huckle, J. W.; Robinson, N. J. SmtB Is a Metal-Dependent Repressor of the Cyanobacterial Metallothionein Gene SmtA: Identification of a Zn-Inhibited DNA-Protein Complex. *Nucleic Acids Res.* **1993**, *21*, 921−925.
(131) Eicken, C.; Pennella, M. A.; Chen, X.; Koshlap, K. M.; VanZile, M. L.; Sacchettini, J. C.; Giedroc, D. P. A Metal-Ligand-Mediated Intersubunit Allosteric Switch in Related SmtB/ArsR Zinc Sensor Proteins. *J. Mol. Biol.* **2003**, *333*, 683−695.
(132) Hantke, K. Cloning of the Repressor Protein Gene of Iron-Regulated Systems in *Escherichia coli* K12. *Mol. Gen Genetics* **1984**, *197*, 337−341.
(133) Reyes-Caballero, H.; Guerra, A. J.; Jacobsen, F. E.; Kazmierczak, K. M.; Cowart, D.; Koppolu, U. M. K.; Scott, R. A.; Winkler, M. E.; Giedroc, D. P. The Metalloregulatory Zinc Site in *Streptococcus pneumoniae* AdcR, a Zinc-Activated MarR Family Repressor. *J. Mol. Biol.* **2010**, *403*, 197−216.
(134) Schreiter, E. R.; Wang, S. C.; Zamble, D. B.; Drennan, C. L. NikR-Operator Complex Structure and the Mechanism of Repressor Activation by Metal Ions. *Proc. Natl. Acad. Sci. U. S. A.* **2006**, *103*, 13676−13681.
(135) O'Halloran, T.; Walsh, C. Metalloregulatory DNA-Binding Protein Encoded by the MerR Gene: Isolation and Characterization. *Science* **1987**, *235*, 211−4.
(136) Foster, A. W.; Young, T. R.; Chivers, P. T.; et al. Protein Metalation in Biology. *Curr. Opin Chem. Biol.* **2022**, *66*, 102095.
(137) Foster, A. W.; Pernil, R.; Patterson, C. J.; Scott, A. J. P. P.; Pålsson, L.-O. O.; Pal, R.; Cummins, I.; Chivers, P. T.; Pohl, E.; Robinson, N. J. A Tight Tunable Range for Ni(II) Sensing and Buffering in Cells. *Nat. Chem. Biol.* **2017**, *13*, 409−414.

(138) Grossoehme, N. E.; Giedroc, D. P. Energetics of Allosteric Negative Coupling in the Zinc Sensor *S. aureus* CzrA. *J. Am. Chem. Soc.* **2009**, *131*, 17860−17870.
(139) Capdevila, D. A.; Braymer, J. J.; Edmonds, K. A.; et al. Entropy Redistribution Controls Allostery in a Metalloregulatory Protein. *Proc. Natl. Acad. Sci. U. S. A.* **2017**, *114*, 4424−4429.
(140) Capdevila, D. A.; Edmonds, K. A.; Campanello, G. C.; Wu, H.; Gonzalez-Gutierrez, G.; Giedroc, D. P. Functional Role of Solvent Entropy and Conformational Entropy of Metal Binding in a Dynamically Driven Allosteric System. *J. Am. Chem. Soc.* **2018**, *140*, 9108−9119.
(141) Capdevila, D. A.; Huerta, F.; Edmonds, K. A.; Le, M. T.; Wu, H.; Giedroc, D. P. Tuning Site-Specific Dynamics to Drive Allosteric Activation in a Pneumococcal Zinc Uptake Regulator. *Elife* **2018**, *7*, No. e37268.
(142) Martin, J. E.; Edmonds, K. A.; Bruce, K. E.; Campanello, G. C.; Eijkelkamp, B. A.; Brazel, E. B.; McDevitt, C. A.; Winkler, M. E.; Giedroc, D. P. The Zinc Efflux Activator SczA Protects *Streptococcus pneumoniae* Serotype 2 D39 from Intracellular Zinc Toxicity. *Mol. Microbiol.* **2017**, *104*, 636−651.
(143) Philips, S. J.; Canalizo-Hernandez, M.; Yildirim, I.; Schatz, G. C.; Mondragon, A.; O'Halloran, T. V. Allosteric Transcriptional Regulation via Changes in the Overall Topology of the Core Promoter. *Science* **2015**, *349*, 877−881.
(144) Irving, H.; Williams, R. J. P. Order of Stability of Metal Complexes. *Nature* **1948**, *162*, 746−747.
(145) Waldron, K. J.; Robinson, N. J. How Do Bacterial Cells Ensure That Metalloproteins Get the Correct Metal? *Nat. Rev. Microbiol* **2009**, *7*, 25−35.
(146) Young, T. R.; Martini, M. A.; Foster, A. W.; Glasfeld, A.; Osman, D.; Morton, R. J.; Deery, E.; Warren, M. J.; Robinson, N. J. Calculating Metalation in Cells Reveals CobW Acquires Co(II) for Vitamin B_{12} Biosynthesis While Related Proteins Prefer Zn(II). *Nat. Commun.* **2021**, *12*, 1195.
(147) VanZile, M. L.; Cosper, N. J.; Scott, R. A.; Giedroc, D. P. The Zinc Metalloregulatory Protein *Synechococcus* PCC7942 SmtB Binds a Single Zinc Ion per Monomer with High Affinity in a Tetrahedral Coordination Geometry. *Biochemistry* **2000**, *39*, 11818−11829.
(148) Foster, A. W.; Young, T. R.; Chivers, P. T.; Robinson, N. J. Protein Metalation in Biology. *Curr. Opin Chem. Biol.* **2022**, *66*, 102095.
(149) Ma, Z.; Jacobsen, F. E.; Giedroc, D. P. Coordination Chemistry of Bacterial Metal Transport and Sensing. *Chem. Rev.* **2009**, *109*, 4644−81.
(150) Dann, C. E.; Wakeman, C. A.; Sieling, C. L.; Baker, S. C.; Irnov, I.; Winkler, W. C. Structure and Mechanism of a Metal-Sensing Regulatory RNA. *Cell* **2007**, *130*, 878−892.
(151) Wang, D.; Hurst, T. K.; Thompson, R. B.; Fierke, C. A. Genetically Encoded Ratiometric Biosensors to Measure Intracellular Exchangeable Zinc in *Escherichia coli*. *J. Biomed. Opt* **2011**, *16*, 087011.
(152) Foster, A. W.; Clough, S. E.; Aki, Z.; Young, T. R.; Clarke, A. R.; Robinson, N. J. Metalation Calculators for *E. coli* Strain JM109 (DE3): Aerobic, Anaerobic, and Hydrogen Peroxide Exposed Cells Cultured in LB Media. *Metallomics* **2022**, *14*, mfac058.
(153) Pratt, E. P. S.; Damon, L. J.; Anson, K. J.; Palmer, A. E. Tools and Techniques for Illuminating the Cell Biology of Zinc. *Biochim Biophys Acta Mol. Cell Res.* **2021**, *1868*, 118865.
(154) Jensen, G. C.; Janis, M. K.; Jara, J.; Abbasi, N.; Zastrow, M. L. Zinc-Induced Fluorescence Turn-On in Native and Mutant Phycoerythrobilin-Binding Orange Fluorescent Proteins. *Biochemistry* **2023**, *62*, 2828−2840.
(155) Chen, J.; Wang, R.; Ma, M.; Gao, L.; Zhao, B.; Xu, M. Laser Ablation-Inductively Coupled Plasma-Mass Spectrometry (LA-ICP-MS)-Based Strategies Applied for the Analysis of Metal-Binding Protein in Biological Samples: An Update on Recent Advances. *Anal. Bioanal. Chem.* **2022**, *414*, 7023−7033.
(156) Sussulini, A.; Becker, J. S. Combination of PAGE and LA-ICP-MS as an Analytical Workflow in Metallomics: State of the Art, New Quantification Strategies, Advantages and Limitations. *Metallomics* **2011**, *3*, 1271−1279.
(157) Tottey, S.; Waldron, K. J.; Firbank, S. J.; Reale, B.; Bessant, C.; Sato, K.; Cheek, T. R.; Gray, J.; Banfield, M. J.; Dennison, C.; et al. Protein-Folding Location Can Regulate Manganese-Binding versus Copper- or Zinc-Binding. *Nature* **2008**, *455*, 1138−1142.
(158) Cvetkovic, A.; Menon, A. L.; Thorgersen, M. P.; Scott, J. W.; Poole, F. L.; Jenney, F. E.; Lancaster, W. A.; Praissman, J. L.; Shanmukh, S.; Vaccaro, B. J.; et al. Microbial Metalloproteomes Are Largely Uncharacterized. *Nature* **2010**, *466*, 779−782.
(159) Mazzotta, M. G.; McIlvin, M. R.; Moran, D. M.; Wang, D. T.; Bidle, K. D.; Lamborg, C. H.; Saito, M. A. Characterization of the Metalloproteome of Pseudoalteromonas (BB2-AT2): Biogeochemical Underpinnings for Zinc, Manganese, Cobalt, and Nickel Cycling in a Ubiquitous Marine Heterotroph. *Metallomics* **2021**, *13*, mfab060.
(160) Coverdale, J. P. C.; Polepalli, S.; Arruda, M. A. Z.; da Silva, A. B. S.; Stewart, A. J.; Blindauer, C. A. Recent Advances in Metalloproteomics. *Biomolecules* **2024**, *14*, 104.
(161) Riisom, M.; Jamieson, S. M. F.; Hartinger, C. G. Critical Evaluation of Cell Lysis Methods for Metallodrug Studies in Cancer Cells. *Metallomics* **2023**, *15*, 21−24.
(162) Focarelli, F.; Giachino, A.; Waldron, K. J. Copper Microenvironments in the Human Body Define Patterns of Copper Adaptation in Pathogenic Bacteria. *PLoS Pathog* **2022**, *18*, 1−19.
(163) Wagner, D.; Maser, J.; Lai, B.; Cai, Z.; Barry, C. E.; Höner zu Bentrup, K.; Russell, D. G.; Bermudez, L. E. Elemental Analysis of *Mycobacterium Avium* -, *Mycobacterium Tuberculosis* -, and *Mycobacterium Smegmatis* -Containing Phagosomes Indicates Pathogen-Induced Microenvironments within the Host Cell's Endosomal System. *J. Immunol* **2005**, *174*, 1491−1500.
(164) White, C.; Lee, J.; Kambe, T.; Fritsche, K.; Petris, M. J. A Role for the ATP7A Copper-Transporting ATPase in Macrophage Bactericidal Activity. *J. Biol. Chem.* **2009**, *284*, 33949−56.
(165) Tan, G.; Yang, J.; Li, T.; Zhao, J.; Sun, S.; Li, X.; Lin, C.; Li, J.; Zhou, H.; Lyu, J.; et al. Anaerobic Copper Toxicity and Iron-Sulfur Cluster Biogenesis in *Escherichia coli*. *Appl. Environ. Microbiol.* **2017**, *83*, No. e00867.
(166) Brancaccio, D.; Gallo, A.; Piccioli, M.; Novellino, E.; Ciofi-Baffoni, S.; Banci, L. [4Fe-4S] Cluster Assembly in Mitochondria and Its Impairment by Copper. *J. Am. Chem. Soc.* **2017**, *139*, 719−730.
(167) Chillappagari, S.; Seubert, A.; Trip, H.; Kuipers, O. P.; Marahiel, M. A.; Miethke, M. Copper Stress Affects Iron Homeostasis by Destabilizing Iron-Sulfur Cluster Formation in *Bacillus Subtilis*. *J. Bacteriol.* **2010**, *192*, 2512−2524.
(168) Macomber, L.; Imlay, J. A. The Iron-Sulfur Clusters of Dehydratases Are Primary Intracellular Targets of Copper Toxicity. *Proc. Natl. Acad. Sci. U. S. A.* **2009**, *106*, 8344−8349.
(169) Djoko, K. Y.; McEwan, A. G. Antimicrobial Action of Copper Is Amplified via Inhibition of Heme Biosynthesis. *ACS Chem. Biol.* **2013**, *8*, 2217−2223.
(170) Norambuena, J.; Al-Tameemi, H.; Bovermann, H.; Kim, J.; Beavers, W. N.; Skaar, E. P.; Parker, D.; Boyd, J. M. Copper Ions Inhibit Pentose Phosphate Pathway Function in *Staphylococcus aureus*. *PLoS Pathog* **2023**, *19*, No. e1011393.
(171) De Oliveira, D. M. P.; Forde, B. M.; Phan, M. D.; Steiner, B.; Zhang, B.; Zuegg, J.; El-Deeb, I. M.; Li, G.; Keller, N.; Brouwer, S.; et al. Rescuing Tetracycline Class Antibiotics for the Treatment of Multidrug-Resistant *Acinetobacter baumannii* Pulmonary Infection. *mBio* **2022**, *13*, No. e0351721.
(172) Ghssein, G.; Brutesco, C.; Ouerdane, L.; Fojcik, C.; Izaute, A.; Wang, S.; Hajjar, C.; Lobinski, R.; Lemaire, D.; Richaud, P.; et al. Biosynthesis of a Broad-Spectrum Nicotianamine-like Metallophore in *Staphylococcus aureus*. *Science* **2016**, *352*, 1105−9.
(173) Laffont, C.; Arnoux, P. The Ancient Roots of Nicotianamine: Diversity, Role, Regulation and Evolution of Nicotianamine-like Metallophores. *Metallomics* **2020**, *12*, 1480−1493.
(174) Hossain, S.; Morey, J. R.; Neville, S. L.; Ganio, K.; Radin, J. N.; Norambuena, J.; Boyd, J. M.; McDevitt, C. A.; Kehl-Fie, T. E. Host Subversion of Bacterial Metallophore Usage Drives Copper Intoxication. *mBio* **2023**, *14*, No. e0135023.

https://doi.org/10.1021/acs.chemrev.4c00264
Chem. Rev. 2024, 124, 13574−13659

(175) Tarrant, E.; Riboldi, G. P.; McIlvin, M. R.; Stevenson, J.; Barwinska-Sendra, A.; Stewart, L. J.; Saito, M. A.; Waldron, K. J. Copper Stress in *Staphylococcus aureus* Leads to Adaptive Changes in Central Carbon Metabolism. *Metallomics* **2019**, *11*, 183.
(176) Hong, Y.; Mackenzie, E. S.; Firth, S. J.; Bolton, J. R. F.; Stewart, L. J.; Waldron, K. J.; Djoko, K. Y. Mis-Regulation of Zn and Mn Homeostasis Is a Key Phenotype of Cu Stress in *Streptococcus pyogenes*. *Metallomics* **2023**, *15*, mfad064.
(177) Couñago, R. M.; Ween, M. P.; Begg, S. L.; Bajaj, M.; Zuegg, J.; O'Mara, M. L.; Cooper, M. A.; McEwan, A. G.; Paton, J. C.; Kobe, B.; et al. Imperfect Coordination Chemistry Facilitates Metal Ion Release in the Psa Permease. *Nat. Chem. Biol.* **2014**, *10*, 35−41.
(178) Neville, S. L.; Sjöhamn, J.; Watts, J. A.; MacDermott-Opeskin, H.; Fairweather, S. J.; Ganio, K.; Hulyer, A. C.; McGrath, A. P.; Hayes, A. J.; Malcolm, T. R.; et al. The Structural Basis of Bacterial Manganese Import. *Sci. Adv.* **2021**, *7*, 1−11.
(179) Martin, J. E.; Lisher, J. P.; Winkler, M. E.; Giedroc, D. P. Perturbation of Manganese Metabolism Disrupts Cell Division in *Streptococcus pneumoniae*. *Mol. Microbiol.* **2017**, *104*, 334−348.
(180) McFarland, A. L.; Bhattarai, N.; Joseph, M.; Winkler, M. E.; Martin, J. E. Cellular Mn/Zn Ratio Influences Phosphoglucomutase Activity and Capsule Production in *Streptococcus pneumoniae* D39. *J. Bacteriol.* **2021**, *203*, jb00602.
(181) Garcia, Y. M.; Barwinska-Sendra, A.; Tarrant, E.; Skaar, E. P.; Waldron, K. J.; Kehl-Fie, T. E. A Superoxide Dismutase Capable of Functioning with Iron or Manganese Promotes the Resistance of *Staphylococcus aureus* to Calprotectin and Nutritional Immunity. *PLoS Pathog* **2017**, *13*, No. e1006125.
(182) Cravatt, B. F. Activity-Based Protein Profiling - Finding General Solutions to Specific Problems. *Isr J. Chem.* **2023**, *63*, 68−95.
(183) Chan, A. N.; Chen, X.; Falco, J. A.; Bak, D. W.; Weerapana, E.; Li, B. Chemoproteomics Reveals Disruption of Metal Homeostasis and Metalloproteins by the Antibiotic Holomycin. *ACS Chem. Biol.* **2023**, *18*, 1909−1914.
(184) Bak, D. W.; Weerapana, E. Monitoring Fe-S Cluster Occupancy across the *E. coli* Proteome Using Chemoproteomics. *Nat. Chem. Biol.* **2023**, *19*, 356−366.
(185) Chan, A. N.; Shiver, A. L.; Wever, W. J.; Razvi, S. Z. A.; Traxler, M. F.; Li, B. Role for Dithiolopyrrolones in Disrupting Bacterial Metal Homeostasis. *Proc. Natl. Acad. Sci. U. S. A.* **2017**, *114*, 2717−2722.
(186) Albini, F.; Bormann, S.; Gerschel, P.; Ludwig, V. A.; Neumann, W. Dithiolopyrrolones Are Prochelators That Are Activated by Glutathione. *Chemistry* **2023**, *29*, No. e202202567.
(187) Bach, K.; Beerkens, B. L. H.; Zanon, P. R. A.; Hacker, S. M. Light-Activatable, 2,5-Disubstituted Tetrazoles for the Proteome-Wide Profiling of Aspartates and Glutamates in Living Bacteria. *ACS Cent Sci.* **2020**, *6*, 546−554.
(188) Wan, C.; Wang, Y.; Lian, C.; Chang, Q.; An, Y.; Chen, J.; Sun, J.; Hou, Z.; Yang, D.; Guo, X.; et al. Histidine-Specific Bioconjugation via Visible-Light-Promoted Thioacetal Activation. *Chem. Sci.* **2022**, *13*, 8289−8296.
(189) Summers, A. O.; Silver, S. Microbial Transformations of Metals. *Annu. Rev. Microbiol.* **1978**, *32*, 637−672.
(190) Robinson, J. B.; Tuovinen, O. H. Mechanisms of Microbial Resistance and Detoxification of Mercury and Organomercury Compounds: Physiological, Biochemical, and Genetic Analyses. *Microbiol Rev.* **1984**, *48*, 95−124.
(191) Lund, P. A.; Ford, S. J.; Brown, N. L. Transcriptional Regulation of the Mercury-Resistance Genes of Transposon Tn501. *Microbiology* **1986**, *132*, 465−480.
(192) Foster, T. J.; Brown, N. L. Identification of the MerR Gene of R100 by Using *mer-lac* Gene and Operon Fusions. *J. Bacteriol.* **1985**, *163*, 1153−1157.
(193) Foster, T. J. Plasmid-Determined Resistance to Antimicrobial Drugs and Toxic Metal Ions in Bacteria. *Microbiol Rev.* **1983**, *47*, 361−409.
(194) Silver, S.; Walderhaug, M. Gene Regulation of Plasmid- and Chromosome-Determined Inorganic Ion Transport in Bacteria. *Microbiol. Rev.* **1992**, *56*, 195.
(195) Stock, J. B.; Ninfa, A. J.; Stock, A. M. Protein Phosphorylation and Regulation of Adaptive Responses in Bacteria. *Microbiol. Rev.* **1989**, *53*, 450.
(196) Berg, J. M. Potential Metal-Binding Domains in Nucleic Acid Binding Proteins. *Science* **1986**, *232*, 485−487.
(197) O'Halloran, T. V.; Frantz, B.; Shin, M. K.; Ralston, D. M.; Wright, J. G. The MerR Heavy Metal Receptor Mediates Positive Activation in a Topologically Novel Transcription Complex. *Cell* **1989**, *56*, 119−129.
(198) Francisco, M. J. D.; Hope, C. L.; Owolabi, J. B.; Tisa, L. S.; Rosen, B. P. Identification of the Metalloregulatory Element of the Plasmid-Encoded Arsenical Resistance Operon. *Nucleic Acids Res.* **1990**, *18*, 619−624.
(199) Turner, J. S.; Glands, P. D.; Samson, A. C. R.; Robinson, N. J. Zn^{2+}-Sensing by the Cyanobacterial Metallothionein Repressor SmtB: Different Motifs Mediate Metal-Induced Protein-DNA Dissociation. *Nucleic Acids Res.* **1996**, *24*, 3714−3721.
(200) Strausak, D.; Solioz, M. CopY Is a Copper-Inducible Repressor of the *Enterococcus hirae* Copper ATPases. *J. Biol. Chem.* **1997**, *272*, 8932−6.
(201) Sala, C.; Haouz, A.; Saul, F. A.; Miras, I.; Rosenkrands, I.; Alzari, P. M.; Cole, S. T. Genome-Wide Regulon and Crystal Structure of BlaI (Rv1846c) from *Mycobacterium tuberculosis*. *Mol. Microbiol.* **2009**, *71*, 1102−1116.
(202) Kloosterman, T. G.; Van Der Kooi-Pol, M. M.; Bijlsma, J. J. E.; Kuipers, O. P. The Novel Transcriptional Regulator SczA Mediates Protection against Zn 2+ Stress by Activation of the Zn^{2+}-resistance Gene *czcD* in *Streptococcus pneumoniae*. *Mol. Microbiol.* **2007**, *65*, 1049−1063.
(203) Liu, T.; Ramesh, A.; Ma, Z.; Ward, S. K.; Zhang, L.; George, G. N.; Talaat, A. M.; Sacchettini, J. C.; Giedroc, D. P. CsoR Is a Novel *Mycobacterium tuberculosis* Copper-Sensing Transcriptional Regulator. *Nat. Chem. Biol.* **2007**, *3*, 60−68.
(204) Iwig, J. S.; Leitch, S.; Herbst, R. W.; Maroney, M. J.; Chivers, P. T Ni(II) and Co(II) Sensing by *Escherichia coli* RcnR. *J. Am. Chem. Soc.* **2008**, *130*, 7592−7606.
(205) Bagg, A.; Neilands, J. B. Molecular Mechanism of Regulation of Siderophore-Mediated Iron Assimilation. *Microbiol Rev.* **1987**, *51*, 509−518.
(206) Neilands, J. B. Microbial Iron Transport Compounds (Sidero-Chromes). *Inorg. Biochem* **1973**, *1*, 167−202.
(207) Gaballa, A.; Helmann, J. D. Identification of a Zinc-Specific Metalloregulatory Protein, Zur, Controlling Zinc Transport Operons in *Bacillus Subtilis*. *J. Bacteriol.* **1998**, *180*, 5815−5821.
(208) Fuangthong, M.; Herbig, A. F.; Bsat, N.; Helmann, J. D. Regulation of the *Bacillus subtilis* Fur and PerR Genes by PerR: Not All Members of the PerR Regulon Are Peroxide Inducible. *J. Bacteriol.* **2002**, *184*, 3276−3286.
(209) Bsat, N.; Herbig, A.; Casillas-Martinez, L.; Setlow, P.; Helmann, J. D. *Bacillus subtilis* Contains Multiple Fur Homologues: Identification of the Iron Uptake (Fur) and Peroxide Regulon (PerR) Repressors. *Mol. Microbiol.* **1998**, *29*, 189−198.
(210) White, A.; Ding, X.; VanderSpek, J. C.; Murphy, J. R.; Ringe, D. Structure of the Metal-Ion-Activated Diphtheria Toxin Repressor/Tox Operator Complex. *Nature* **1998**, *394*, 502−506.
(211) Schmitt, M. P.; Holmes, R. K. Cloning, Sequence, and Footprint Analysis of Two Promoter/Operators from *Corynebacterium diphtheriae* That Are Regulated by the Diphtheria Toxin Repressor (DtxR) and Iron. *J. Bacteriol.* **1994**, *176*, 1141−1149.
(212) Tao, X.; Murphy, J. R. Binding of the Metalloregulatory Protein DtxR to the Diphtheria Tox Operator Requires a Divalent Heavy Metal Ion and Protects the Palindromic Sequence from DNase I Digestion. *J. Biol. Chem.* **1992**, *267*, 21761−21764.
(213) Navarro, C.; Wu, L. -F; Mandrand-Berthelot, M.-A. The Nik Operon of *Escherichia coli* Encodes a Periplasmic Binding-protein-dependent Transport System for Nickel. *Mol. Microbiol.* **1993**, *9*, 1181−1191.
(214) Chivers, P. T.; Sauer, R. T. NikR Is a Ribbon-Helix-Helix DNA-Binding Protein. *Protein Sci.* **1999**, *8*, 2494−2500.

https://doi.org/10.1021/acs.chemrev.4c00264
Chem. Rev. 2024, 124, 13574−13659

(215) Todd, J. D.; Wexler, M.; Sawers, G.; Yeoman, K. H.; Poole, P. S.; Johnston, A. W. B. RirA, an Iron-Responsive Regulator in the Symbiotic Bacterium *Rhizobium leguminosarum*. *Microbiology* **2002**, *148*, 4059−4071.
(216) Rajagopalan, S.; Teter, S. J.; Zwart, P. H.; Brennan, R. G.; Phillips, K. J.; Kiley, P. J. Studies of IscR Reveal a Unique Mechanism for Metal-Dependent Regulation of DNA Binding Specificity. *Nat. Struct Mol. Biol.* **2013**, *20*, 740−747.
(217) Zheng, M.; Cooper, D. R.; Grossoehme, N. E.; Yu, M.; Hung, L. W.; Cieslik, M.; Derewenda, U.; Lesley, S. A.; Wilson, I. A.; Giedroc, D. P.; Derewenda, Z. S. Structure of *Thermotoga maritima* TM0439: Implications for the Mechanism of Bacterial GntR Transcription Regulators with Zn^{2+}-Binding FCD Domains. *Acta Crystallogr. D Biol. Crystallogr.* **2009**, *65*, 356−365.
(218) Guerra, A. J.; Dann, C. E.; Giedroc, D. P. Crystal Structure of the Zinc-Dependent MarR Family Transcriptional Regulator AdcR in the Zn(II)-Bound State. *J. Am. Chem. Soc.* **2011**, *133*, 19614−19617.
(219) Dintilhac, A.; Alloing, G.; Granadel, C.; Claverys, J. P. Competence and Virulence of *Streptococcus pneumoniae*: Adc and PsaA Mutants Exhibit a Requirement for Zn and Mn Resulting from Inactivation of Putative ABC Metal Permeases. *Mol. Microbiol.* **1997**, *25*, 727−739.
(220) Martin, J. E.; Edmonds, K. A.; Bruce, K. E.; Campanello, G. C.; Eijkelkamp, B. A.; Brazel, E. B.; McDevitt, C. A.; Winkler, M. E.; Giedroc, D. P. The Zinc Efflux Activator SczA Protects *Streptococcus pneumoniae* Serotype 2 D39 from Intracellular Zinc Toxicity. *Mol. Microbiol.* **2017**, *104*, 636−651.
(221) Anderson, L. A.; Palmer, T.; Price, N. C.; Bornemann, S.; Boxer, D. H.; Pau, R. N. Characterization of the Molybdenum-Responsive ModE Regulatory Protein and Its Binding to the Promoter Region of the ModABCD (Molybdenum Transport) Operon of *Escherichia coli*. *Eur. J. Biochem.* **1997**, *246*, 119−126.
(222) Massé, E.; Vanderpool, C. K.; Gottesman, S. Effect of RyhB Small RNA on Global Iron Use in *Escherichia coli*. *J. Bacteriol.* **2005**, *187*, 6962−6971.
(223) Wilderman, P. J.; Sowa, N. A.; FitzGerald, D. J.; FitzGerald, P. C.; Gottesman, S.; Ochsner, U. A.; Vasil, M. L. Identification of Tandem Duplicate Regulatory Small RNAs in *Pseudomonas aeruginosa* Involved in Iron Homeostasis. *Proc. Natl. Acad. Sci. U. S. A.* **2004**, *101*, 9792−9797.
(224) Furukawa, K.; Ramesh, A.; Zhou, Z.; Weinberg, Z.; Vallery, T.; Winkler, W. C.; Breaker, R. R. Bacterial Riboswitches Cooperatively Bind Ni^{2+} or Co^{2+} Ions and Control Expression of Heavy Metal Transporters. *Mol. Cell* **2015**, *57*, 1088−1098.
(225) Shi, Y.; Zhao, G.; Kong, W. Genetic Analysis of Riboswitch-Mediated Transcriptional Regulation Responding to Mn^{2+} in *Salmonella*. *J. Biol. Chem.* **2014**, *289*, 11353−11366.
(226) Martin, J. E.; Le, M. T.; Bhattarai, N.; Capdevila, D. A.; Shen, J.; Winkler, M. E.; Giedroc, D. P. A Mn-Sensing Riboswitch Activates Expression of a Mn^{2+}/Ca^{2+} ATPase Transporter in Streptococcus. *Nucleic Acids Res.* **2019**, *47*, 6885−6899.
(227) Johnson, J. E.; Reyes, F. E.; Polaski, J. T.; Batey, R. T. B_{12} Cofactors Directly Stabilize an MRNA Regulatory Switch. *Nature* **2012**, *492*, 133−137.
(228) Xu, J.; Cotruvo, J. A. The CzcD (NiCo) Riboswitch Responds to Iron(II). *Biochemistry* **2020**, *59*, 1508−1516.
(229) Kavita, K.; Breaker, R. R. Discovering Riboswitches: The Past and the Future. *Trends Biochem. Sci.* **2023**, *48*, 119−141.
(230) Kim, H. J.; Jeong, H.; Lee, S. J. Synthetic Biology for Microbial Heavy Metal Biosensors. *Anal Bioanal Chem.* **2018**, *410*, 1191−1203.
(231) Li, S.; Li, Z.; Tan, G.-Y.; Xin, Z.; Wang, W. *In vitro* Allosteric Transcription Factor-Based Biosensing. *Trends Biotechnol* **2023**, *41*, 1080−1095.
(232) Kim, Y.; Jeon, Y.; Na, M.; Hwang, S.-J.; Yoon, Y. Recent Trends in Chemical Sensors for Detecting Toxic Materials. *Sensors* **2024**, *24*, 431.
(233) Rawson, D. M.; Willmer, A. J.; Turner, A. P. Whole-Cell Biosensors for Environmental Monitoring. *Biosensors* **1989**, *4*, 299−311.
(234) Ralston, D. M.; O'Halloran, T. V. Ultrasensitivity and Heavy-Metal Selectivity of the Allosterically Modulated MerR Transcription Complex. *Proc. Natl. Acad. Sci. U. S. A.* **1990**, *87*, 3846−3850.
(235) Scott, D. L.; Ramanathan, S.; Shi, W.; Rosen, B. P.; Daunert, S. Genetically Engineered Bacteria: Electrochemical Sensing Systems for Antimonite and Arsenite. *Anal. Chem.* **1997**, *69*, 16−20.
(236) Ellefson, J. W.; Ledbetter, M. P.; Ellington, A. D. Directed Evolution of a Synthetic Phylogeny of Programmable Trp Repressors Article. *Nat. Chem. Biol.* **2018**, *14*, 361−367.
(237) Huang, S.; Liu, X.; Wang, D.; Chen, W.; Hu, Q.; Wei, T.; Zhou, W.; Gan, J.; Chen, H. Structural Basis for the Selective Pb(II) Recognition of Metalloregulatory Protein PbrR691. *Inorg. Chem.* **2016**, *55*, 12516−12519.
(238) Lee, C. W.; Chakravorty, D. K.; Chang, F. M. J.; Reyes-Caballero, H.; Ye, Y.; Merz, K. M.; Giedroc, D. P. Solution Structure of *Mycobacterium tuberculosis* NmtR in the Apo State: Insights into Ni(II)-Mediated Allostery. *Biochemistry* **2012**, *51*, 2619−2629.
(239) Fakhoury, J. N.; Zhang, Y.; Edmonds, K. A.; Bringas, M.; Luebke, J. L.; Gonzalez-Gutierrez, G.; Capdevila, D. A.; Giedroc, D. P. Functional Asymmetry and Chemical Reactivity of CsoR Family Persulfide Sensors. *Nucleic Acids Res.* **2021**, *49*, 12556−12576.
(240) Bahlawane, C.; Dian, C.; Muller, C.; Round, A.; Fauquant, C.; Schauer, K.; de Reuse, H.; Terradot, L.; Michaud-Soret, I. Structural and Mechanistic Insights into *Helicobacter pylori* NikR Activation. *Nucleic Acids Res.* **2010**, *38*, 3106−3118.
(241) Antelo, G. T.; Vila, A. J.; Giedroc, D. P.; Capdevila, D. A. Molecular Evolution of Transition Metal Bioavailability at the Host-Pathogen Interface. *Trends Microbiol* **2021**, *29*, 441−457.
(242) Rosinski, J. A.; Atchley, W. R. Molecular Evolution of Helix-Turn-Helix Proteins. *J. Mol. Evol* **1999**, *49*, 301−309.
(243) Zhang, T.; Akaike, T.; Sawa, T. Redox Regulation of Xenobiotics by Reactive Sulfur and Supersulfide Species. *Antioxid Redox Signal* **2024**, *40*, 679−690.
(244) Switzer, C. H. How Super Is Supersulfide? Reconsidering Persulfide Reactivity in Cellular Biology. *Redox Biol.* **2023**, *67*, 102899.
(245) Pis Diez, C. M.; Antelo, G. T.; Dalia, T. N.; Dalia, A. B.; Giedroc, D. P.; Capdevila, D. A. Increased Intracellular Persulfide Levels Attenuate HlyU-Mediated Hemolysin Transcriptional Activation in *Vibrio cholerae*. *J. Biol. Chem.* **2023**, *299*, 105147.
(246) Zhang, Y.; Martin, J. E.; Edmonds, K. A.; Winkler, M. E.; Giedroc, D. P. SifR Is an Rrf2-Family Quinone Sensor Associated with Catechol Iron Uptake in *Streptococcus pneumoniae* D39. *J. Biol. Chem.* **2022**, *298*, 102046.
(247) Roy, R.; Samanta, S.; Patra, S.; Mahato, N. K.; Saha, R. P. In Silico Identification and Characterization of Sensory Motifs in the Transcriptional Regulators of the ArsR-SmtB Family. *Metallomics* **2018**, *10*, 1476−1500.
(248) Prabaharan, C.; Kandavelu, P.; Packianathan, C.; Rosen, B. P.; Thiyagarajan, S. Structures of Two ArsR As(III)-Responsive Transcriptional Repressors: Implications for the Mechanism of Derepression. *J. Struct Biol.* **2019**, *207*, 209−217.
(249) Stoyanov, J. V.; Hobman, J. L.; Brown, N. L. CueR (Ybbl) of *Escherichia coli* Is a MerR Family Regulator Controlling Expression of the Copper Exporter CopA. *Mol. Microbiol.* **2001**, *39*, 502−512.
(250) Jordan, M. R.; Wang, J.; Capdevila, D. A.; Giedroc, D. P. Multi-Metal Nutrient Restriction and Crosstalk in Metallostasis Systems in Microbial Pathogens. *Curr. Opin Microbiol* **2020**, *55*, 17−25.
(251) Glauninger, H.; Zhang, Y.; Higgins, K. A.; Jacobs, A. D.; Martin, J. E.; Fu, Y.; Coyne, H. J., 3rd; Bruce, K. E.; Maroney, M. J.; Clemmer, D. E.; et al. Metal-Dependent Allosteric Activation and Inhibition on the Same Molecular Scaffold: The Copper Sensor CopY from *Streptococcus pneumoniae*. *Chem. Sci.* **2018**, *9*, 105−118.
(252) Ma, Z.; Faulkner, M. J.; Helmann, J. D. Origins of Specificity and Cross-Talk in Metal Ion Sensing by *Bacillus subtilis* Fur. *Mol. Microbiol.* **2012**, *86*, 1144−1155.
(253) Pis Diez, C. M.; Juncos, M. J.; Villarruel Dujovne, M.; Capdevila, D. A. Bacterial Transcriptional Regulators: A Road Map for Functional, Structural, and Biophysical Characterization. *Int. J. Mol. Sci.* **2022**, *23*, 2179.

https://doi.org/10.1021/acs.chemrev.4c00264
Chem. Rev. 2024, 124, 13574−13659

(254) Arunkumar, A. I.; Campanello, G. C.; Giedroc, D. P. Solution Structure of a Paradigm ArsR Family Zinc Sensor in the DNA-Bound State. *Proc. Natl. Acad. Sci. U. S. A.* **2009**, *106*, 18177−82.
(255) Harvie, D. R.; Andreini, C.; Cavallaro, G.; Meng, W.; Connolly, B. A.; Yoshida, K.; Fujita, Y.; Harwood, C. R.; Radford, D. S.; Tottey, S.; et al. Predicting Metals Sensed by ArsR-SmtB Repressors: Allosteric Interference by a Non-Effector Metal. *Mol. Microbiol.* **2006**, *59*, 1341−1356.
(256) Saha, R. P.; Samanta, S.; Patra, S.; Sarkar, D.; Saha, A.; Singh, M. K. Metal Homeostasis in Bacteria: The Role of ArsR-SmtB Family of Transcriptional Repressors in Combating Varying Metal Concentrations in the Environment. *BioMetals* **2017**, *30*, 459−503.
(257) Busenlehner, L. S.; Pennella, M. A.; Giedroc, D. P. The SmtB/ArsR Family of Metalloregulatory Transcriptional Repressors: Structural Insights into Prokaryotic Metal Resistance. *FEMS Microbiol. Rev.* **2003**, *27*, 131−143.
(258) Li, B.; Jo, M.; Liu, J.; Tian, J.; Canfield, R.; Bridwell-Rabb, J. Structural and Mechanistic Basis for Redox Sensing by the Cyanobacterial Transcription Regulator RexT. *Commun. Biol.* **2022**, *5*, 275.
(259) Shimizu, T.; Shen, J.; Fang, M.; Zhang, Y.; Hori, K.; Trinidad, J. C.; Bauer, C. E.; Giedroc, D. P.; Masuda, S. Sulfide-Responsive Transcriptional Repressor SqrR Functions as a Master Regulator of Sulfide-Dependent Photosynthesis. *Proc. Natl. Acad. Sci. U. S. A.* **2017**, *114*, 2355−2360.
(260) de Lira, N. P. V.; Pauletti, B. A.; Marques, A. C.; Perez, C. A.; Caserta, R.; de Souza, A. A.; Vercesi, A. E.; Paes Leme, A. F.; Benedetti, C. E. BigR Is a Sulfide Sensor That Regulates a Sulfur Transferase/Dioxygenase Required for Aerobic Respiration of Plant Bacteria under Sulfide Stress. *Sci. Rep* **2018**, *8*, 3508.
(261) Lee, S. G.; Krishnan, H. B.; Jez, J. M. Structural Basis for Regulation of Rhizobial Nodulation and Symbiosis Gene Expression by the Regulatory Protein NolR. *Proc. Natl. Acad. Sci. U. S. A.* **2014**, *111*, 6509−6514.
(262) Gao, C.; Yang, M.; He, Z.-G. Characterization of a Novel ArsR-Like Regulator Encoded by Rv2034 in *Mycobacterium tuberculosis*. *PLoS One* **2012**, *7*, No. e36255.
(263) Mazzei, L.; Musiani, F.; Zerko, S.; Koźminski, W.; Cianci, M.; Beniamino, Y.; Ciurli, S.; Zambelli, B. Structure, Dynamics, and Function of SrnR, a Transcription Factor for Nickel-Dependent Gene Expression. *Metallomics* **2021**, *13*, mfab069.
(264) Zallot, R.; Oberg, N.; Gerlt, J. A. The EFI Web Resource for Genomic Enzymology Tools: Leveraging Protein, Genome, and Metagenome Databases to Discover Novel Enzymes and Metabolic Pathways. *Biochemistry* **2019**, *58*, 4169−4182.
(265) Campanello, G. C.; Ma, Z.; Grossoehme, N. E.; Guerra, A. J.; Ward, B. P.; Dimarchi, R. D.; Ye, Y.; Dann, C. E.; Giedroc, D. P. Allosteric Inhibition of a Zinc-Sensing Transcriptional Repressor: Insights into the Arsenic Repressor (ArsR) Family. *J. Mol. Biol.* **2013**, *425*, 1143−1157.
(266) Busenlehner, L. S.; Weng, T.-C.; Penner-Hahn, J. E.; Giedroc, D. P. Elucidation of Primary (α3N) and Vestigial (α5) Heavy Metal-Binding Sites in *Staphylococcus aureus* pI258 CadC: Evolutionary Implications for Metal Ion Selectivity of ArsR/SmtB Metal Sensor Proteins. *J. Mol. Biol.* **2002**, *319*, 685−701.
(267) Capdevila, D. A.; Walsh, B. J. C. C.; Zhang, Y.; Dietrich, C.; Gonzalez-Gutierrez, G.; Giedroc, D. P. Structural Basis for Persulfide-Sensing Specificity in a Transcriptional Regulator. *Nat. Chem. Biol.* **2021**, *17*, 65−70.
(268) Thelwell, C.; Robinson, N. J.; Turner-Cavet, J. S. An SmtB-like Repressor from *Synechocystis* PCC 6803 Regulates a Zinc Exporter. *Proc. Natl. Acad. Sci. U. S. A.* **1998**, *95*, 10728−10733.
(269) Jung, J. K.; Alam, K. K.; Verosloff, M. S.; et al. Cell-Free Biosensors for Rapid Detection of Water Contaminants. *Nat. Biotechnol.* **2020**, *38*, 1451−1459.
(270) Reyes-Caballero, H.; Lee, C. W.; Giedroc, D. P. *Mycobacterium tuberculosis* NmtR Harbors a Nickel Sensing Site with Parallels to *Escherichia coli* RcnR. *Biochemistry* **2011**, *50*, 7941−7952.
(271) Lebrun, M.; Audurier, A.; Cossart, P. Plasmid-Borne Cadmium Resistance Genes in Listeria Monocytogenes Are Similar to CadA and CadC of *Staphylococcus aureus* and Are Induced by Cadmium. *J. Bacteriol.* **1994**, *176*, 3040−3048.
(272) Busenlehner, L. S.; Giedroc, D. P. Kinetics of Metal Binding by the Toxic Metal-Sensing Transcriptional Repressor *Staphylococcus aureus* pI258 CadC. *J. Inorg. Biochem* **2006**, *100*, 1024−1034.
(273) Ye, J.; Kandegedara, A.; Martin, P.; Rosen, B. P. Crystal Structure of the *Staphylococcus aureus* pI258 CadC Cd(II)/Pb(II)/Zn(II)-Responsive Repressor. *J. Bacteriol.* **2005**, *187*, 4214−4221.
(274) Pombinho, R.; Camejo, A.; Vieira, A.; Reis, O.; Carvalho, F.; Almeida, M. T.; Pinheiro, J. C.; Sousa, S.; Cabanes, D. Listeria Monocytogenes CadC Regulates Cadmium Efflux and Fine-Tunes Lipoprotein Localization to Escape the Host Immune Response and Promote Infection. *J. Infect Dis* **2017**, *215*, 1468−1479.
(275) Kandegedara, A.; Thiyagarajan, S.; Kondapalli, K. C.; Stemmler, T. L.; Rosen, B. P. Role of Bound Zn(II) in the CadC Cd(II)/Pb(II)/Zn(II)-Responsive Repressor. *J. Biol. Chem.* **2009**, *284*, 14958−14965.
(276) Liu, T.; Chen, X.; Ma, Z.; Shokes, J.; Hemmingsen, L.; Scott, R. A.; Giedroc, D. P. A Cu(I)-Sensing ArsR Family Metal Sensor Protein with a Relaxed Metal Selectivity Profile. *Biochemistry* **2008**, *47*, 10564−75.
(277) Liu, T.; Golden, J. W.; Giedroc, D. P. A Zinc(II)/Lead(II)/Cadmium(II)-Inducible Operon from the *Cyanobacterium Anabaena* Is Regulated by AztR, an α3N ArsR/SmtB Metalloregulator. *Biochemistry* **2005**, *44*, 8673−8683.
(278) Campbell, D. R.; Chapman, K. E.; Waldron, K. J.; Tottey, S.; Kendall, S.; Cavallaro, G.; Andreini, C.; Hinds, J.; Stoker, N. G.; Robinson, N. J.; et al. Mycobacterial Cells Have Dual Nickel-Cobalt Sensors. *J. Biol. Chem.* **2007**, *282*, 32298−32310.
(279) Canneva, F.; Branzoni, M.; Riccardi, G.; Provvedi, R.; Milano, A. Rv2358 and FurB: Two Transcriptional Regulators from *Mycobacterium tuberculosis* Which Respond to Zinc. *J. Bacteriol.* **2005**, *187*, 5837−5840.
(280) Goethe, E.; Laarmann, K.; Lührs, J.; Jarek, M.; Meens, J.; Lewin, A.; Goethe, R. Critical Role of Zur and SmtB in Zinc Homeostasis of *Mycobacterium Smegmatis*. *mSystems* **2020**, *5*. DOI: 10.1128/mSystems.00880-19.
(281) Wang, Y.; Kendall, J.; Cavet, J. S.; Giedroc, D. P. Elucidation of the Functional Metal Binding Profile of a Cd^{II} /Pb^{II} Sensor $CmtR^{Sc}$ from *Streptomyces coelicolor*. *Biochemistry* **2010**, *49*, 6617−6626.
(282) Banci, L.; Bertini, I.; Cantini, F.; Ciofi-Baffoni, S.; Cavet, J. S.; Dennison, C.; Graham, A. I.; Harvie, D. R.; Robinson, N. J. NMR Structural Analysis of Cadmium Sensing by Winged Helix Repressor CmtR. *J. Biol. Chem.* **2007**, *282*, 30181−30188.
(283) Beniamino, Y.; Pesce, G.; Zannoni, A.; Roncarati, D.; Zambelli, B. SrnR from *Streptomyces griseus* Is a Nickel-Binding Transcriptional Activator. *J. Biol. Inorg. Chem.* **2020**, *25*, 187−198.
(284) Kim, J.-S.; Kang, S.-O.; Lee, J. K. The Protein Complex Composed of Nickel-Binding SrnQ and DNA Binding Motif-Bearing SrnR of *Streptomyces griseus* Represses SodF Transcription in the Presence of Nickel. *J. Biol. Chem.* **2003**, *278*, 18455−18463.
(285) Brünker, P.; Rother, D.; Sedlmeier, R.; Klein, J.; Mattes, R.; Altenbuchner, J. Regulation of the Operon Responsible for Broad-Spectrum Mercury Resistance in *Streptomyces lividans* 1326. *Mol. Gen Genet* **1996**, *251*, 307−15.
(286) Boyd, E. S.; Barkay, T. The Mercury Resistance Operon: From an Origin in a Geothermal Environment to an Efficient Detoxification Machine. *Front Microbiol* **2012**, *3*, 1−13.
(287) Fernández, M.; Morel, B.; Ramos, J. L.; Krell, T. Paralogous Regulators ArsR1 and ArsR2 of *Pseudomonas putida* KT2440 as a Basis for Arsenic Biosensor Development. *Appl. Environ. Microbiol.* **2016**, *82*, 4133−4144.
(288) Qin, J.; Fu, H.-L.; Ye, J.; Bencze, K. Z.; Stemmler, T. L.; Rawlings, D. E.; Rosen, B. P. Convergent Evolution of a New Arsenic Binding Site in the ArsR/SmtB Family of Metalloregulators. *J. Biol. Chem.* **2007**, *282*, 34346−34355.
(289) Ordonez, E.; Thiyagarajan, S.; Cook, J. D.; Stemmler, T. L.; Gil, J. A.; Mateos, L. M.; Rosen, B. P. Evolution of Metal(Loid) Binding

Sites in Transcriptional Regulators. *J. Biol. Chem.* **2008**, *283*, 25706−25714.
(290) Kang, Y. S.; Brame, K.; Jetter, J.; Bothner, B. B.; Wang, G.; Thiyagarajan, S.; McDermott, T. R. Regulatory Activities of Four ArsR Proteins in *Agrobacterium tumefaciens* 5A. *Appl. Environ. Microbiol.* **2016**, *82*, 3471−3480.
(291) Rawle, R.; Saley, T. C.; Kang, Y. S.; Wang, Q.; Walk, S.; Bothner, B.; McDermott, T. R. Introducing the ArsR-Regulated Arsenic Stimulon. *Front Microbiol* **2021**, *12*, 630562.
(292) Chen, J.; Nadar, V. S.; Rosen, B. P. A Novel As(III)-Selective ArsR Transcriptional Repressor. *Mol. Microbiol.* **2017**, *106*, 469−478.
(293) Zhang, J.; Li, Y.-N.; Shen, J.; Nadar, V. S.; Chen, J. Characterization of a Novel ArsR Regulates Divergent Ars Operon in *Ensifer adhaerens* Strain ST2. *FEMS Microbiol Lett.* **2023**, *370*, 627−9.
(294) Tóth, A.; Sajdik, K.; Gyurcsik, B.; Nafaee, Z. H.; Wéber, E.; Kele, Z.; Christensen, N. J.; Schell, J.; Correia, J. G.; Sigfridsson Clauss, K. G. V.; et al. As^{III} Selectively Induces a Disorder-to-Order Transition in the Metalloid Binding Region of the *Af*ArsR Protein. *J. Am. Chem. Soc.* **2024**, *146*, 17009−17022.
(295) Shi, W.; Dong, J.; Scott, R. A.; Ksenzenko, M. Y.; Rosen, B. P. The Role of Arsenic-Thiol Interactions in Metalloregulation of the *ars* Operon. *J. Biol. Chem.* **1996**, *271*, 9291−7.
(296) Walsh, B. J. C.; Wang, J.; Edmonds, K. A.; Palmer, L. D.; Zhang, Y.; Trinidad, J. C.; Skaar, E. P.; Giedroc, D. P. The Response of *Acinetobacter baumannii* to Hydrogen Sulfide Reveals Two Independent Persulfide-Sensing Systems and a Connection to Biofilm Regulation. *mBio* **2020**, *11*, mbio01254.
(297) Giedroc, D. P.; Antelo, G. T.; Fakhoury, J. N.; Capdevila, D. A. Sensing and Regulation of Reactive Sulfur Species (RSS) in Bacteria. *Curr. Opin Chem. Biol.* **2023**, *76*, 102358.
(298) Shimizu, T.; Ida, T.; Antelo, G. T.; Ihara, Y.; Fakhoury, J. N.; Masuda, S.; Giedroc, D. P.; Akaike, T.; Capdevila, D. A.; Masuda, T. Polysulfide Metabolizing Enzymes Influence SqrR-Mediated Sulfide-Induced Transcription by Impacting Intracellular Polysulfide Dynamics. *PNAS Nexus* **2023**, *2*, 5−6.
(299) Balasubramanian, R.; Hori, K.; Shimizu, T.; Kasamatsu, S.; Okamura, K.; Tanaka, K.; Ihara, H.; Masuda, S. The Sulfide-Responsive SqrR/BigR Homologous Regulator YgaV of *Escherichia coli* Controls Expression of Anaerobic Respiratory Genes and Antibiotic Tolerance. *Antioxidants* **2022**, *11*, 2359.
(300) Li, J.; Törkel, K.; Koch, J.; Tanabe, T. S.; Hsu, H. Y.; Dahl, C. In the *Alphaproteobacterium hyphomicrobium denitrificans* SoxR Serves a Sulfane Sulfur-Responsive Repressor of Sulfur Oxidation. *Antioxidants* **2023**, *12*, 1620.
(301) Wang, Y.; Hemmingsen, L.; Giedroc, D. P. Structural and Functional Characterization of *Mycobacterium tuberculosis* CmtR, a Pb^{II} /Cd^{II} -Sensing SmtB/ArsR Metalloregulatory Repressor. *Biochemistry* **2005**, *44*, 8976−8988.
(302) Brown, N. L.; Stoyanov, J. V.; Kidd, S. P.; Hobman, J. L. The MerR Family of Transcriptional Regulators. *FEMS Microbiol Rev.* **2003**, *27*, 145−163.
(303) Tulin, G.; Figueroa, N. R.; Checa, S. K.; Soncini, F. C. The Multifarious MerR Family of Transcriptional Regulators. *Mol. Microbiol.* **2024**, *121*, 230−242.
(304) Ibáñez, M. M.; Checa, S. K.; Soncini, F. C. A Single Serine Residue Determines Selectivity to Monovalent Metal Ions in Metalloregulators of the MerR Family. *J. Bacteriol.* **2015**, *197*, 1606−1613.
(305) Watanabe, S.; Kita, A.; Kobayashi, K.; Miki, K. Crystal Structure of the [2Fe-2S] Oxidative-Stress Sensor SoxR Bound to DNA. *Proc. Natl. Acad. Sci. U. S. A.* **2008**, *105*, 4121−4126.
(306) Zheleznova Heldwein, E. E.; Brennan, R. G. Crystal Structure of the Transcription Activator BmrR Bound to DNA and a Drug. *Nature* **2001**, *409*, 378−382.
(307) Chang, C. C.; Lin, L. Y.; Zou, X. W.; Huang, C. C.; Chan, N. L. Structural Basis of the Mercury(II)-Mediated Conformational Switching of the Dual-Function Transcriptional Regulator MerR. *Nucleic Acids Res.* **2015**, *43*, 7612−7623.
(308) Wang, D.; Huang, S.; Liu, P.; Liu, X.; He, Y.; Chen, W.; Hu, Q.; Wei, T.; Gan, J.; Ma, J.; et al. Structural Analysis of the Hg(II)-Regulatory Protein Tn501 MerR from *Pseudomonas aeruginosa*. *Sci. Rep* **2016**, *6*, 33391.
(309) Liu, X.; Hu, Q.; Yang, J.; Huang, S.; Wei, T.; Chen, W.; He, Y.; Wang, D.; Liu, Z.; Wang, K.; et al. Selective Cadmium Regulation Mediated by a Cooperative Binding Mechanism in CadR. *Proc. Natl. Acad. Sci. U. S. A.* **2019**, *116*, 20398−20403.
(310) Brocklehurst, K. R.; Megit, S. J.; Morby, A. P. Characterisation of CadR from *Pseudomonas aeruginosa*: A Cd(II)-Responsive MerR Homologue. *Biochem. Biophys. Res. Commun.* **2003**, *308*, 234−239.
(311) Hobman, J. L.; Julian, D. J.; Brown, N. L. Cysteine Coordination of Pb(II) Is Involved in the PbrR-Dependent Activation of the Lead-Resistance Promoter, P^{pbrA}, from *Cupriavidus Metallidurans* CH34. *BMC Microbiol* **2012**, *12*, 109.
(312) Rutherford, J. C.; Cavet, J. S.; Robinson, N. J. Cobalt-Dependent Transcriptional Switching by a Dual-Effector MerR-like Protein Regulates a Cobalt-Exporting Variant CPx-Type ATPase. *J. Biol. Chem.* **1999**, *274*, 25827−32.
(313) Brocklehurst, K. R.; Hobman, J. L.; Lawley, B.; Blank, L.; Marshall, S. J.; Brown, N. L.; Morby, A. P. ZntR Is a Zn(II)-responsive MerR-like Transcriptional Regulator of ZntA in *Escherichia coli*. *Mol. Microbiol.* **1999**, *31*, 893−902.
(314) Pellizza, L.; Bialer, M. G.; Sieira, R.; Aran, M. MliR, a Novel MerR-like Regulator of Iron Homeostasis, Impacts Metabolism, Membrane Remodeling, and Cell Adhesion in the Marine Bacteroidetes *Bizionia argentinensis*. *Front Microbiol* **2022**, *13*, 1−20.
(315) Kidd, S. P.; Djoko, K. Y.; Ng, J.; Argente, M. P.; Jennings, M. P.; McEwan, A. G. A Novel Nickel Responsive MerR-like Regulator, NimR, from *Haemophilus influenzae*. *Metallomics* **2011**, *3*, 1009.
(316) Checa, S. K.; Espariz, M.; Audero, M. E. P.; Botta, P. E.; Spinelli, S. V.; Soncini, F. C. Bacterial Sensing of and Resistance to Gold Salts. *Mol. Microbiol.* **2007**, *63*, 1307−1318.
(317) Changela, A.; Chen, K.; Xue, Y.; Holschen, J.; Outten, C. E.; O'Halloran, T. V.; Mondragón, A. Molecular Basis of Metal-Ion Selectivity and Zeptomolar Sensitivity by CueR. *Science* **2003**, *301*, 1383−7.
(318) Lee, P. E.; Demple, B.; Barton, J. K. DNA-Mediated Redox Signaling for Transcriptional Activation of SoxR. *Proc. Natl. Acad. Sci. U. S. A.* **2009**, *106*, 13164−13168.
(319) Couñago, R. M.; Chen, N. H.; Chang, C.-W.; Djoko, K. Y.; McEwan, A. G.; Kobe, B. Structural Basis of Thiol-Based Regulation of Formaldehyde Detoxification in *H. influenzae* by a MerR Regulator with No Sensor Region. *Nucleic Acids Res.* **2016**, *44*, 6981−6993.
(320) McEwan, A. G.; Djoko, K. Y.; Chen, N. H.; Couñago, R. L. M.; Kidd, S. P.; Potter, A. J.; Jennings, M. P. Novel Bacterial MerR-Like Regulators. Their Role in the Response to Carbonyl and Nitrosative Stress. *Adv. Microb Physiol* **2011**, *58*, 1−22.
(321) Fang, C.; Li, L.; Zhao, Y.; Wu, X.; Philips, S. J.; You, L.; Zhong, M.; Shi, X.; O'Halloran, T. V.; Li, Q.; et al. The Bacterial Multidrug Resistance Regulator BmrR Distorts Promoter DNA to Activate Transcription. *Nat. Commun.* **2020**, *11*, 6284.
(322) Fang, C.; Philips, S. J.; Wu, X.; Chen, K.; Shi, J.; Shen, L.; Xu, J.; Feng, Y.; O'Halloran, T. V.; Zhang, Y. CueR Activates Transcription through a DNA Distortion Mechanism. *Nat. Chem. Biol.* **2021**, *17*, 57−64.
(323) Helmann, J. D.; Ballard, B. T.; Walsh, C. T. The MerR Metalloregulatory Protein Binds Mercuric Ion as a Tricoordinate, Metal-Bridged Dimer. *Science* **1990**, *247*, 946−8.
(324) Lee, S. W.; Glickmann, E.; Cooksey, D. A. Chromosomal Locus for Cadmium Resistance in *Pseudomonas putida* Consisting of a Cadmium-Transporting ATPase and a MerR Family Response Regulator. *Appl. Environ. Microbiol.* **2001**, *67*, 1437−1444.
(325) Busenlehner, L. S.; Cosper, N. J.; Scott, R. A.; Rosen, B. P.; Wong, M. D.; Giedroc, D. P. Spectroscopic Properties of the Metalloregulatory Cd(II) and Pb(II) Sites of *S. aureus* pI258 CadC. *Biochemistry* **2001**, *40*, 4426−4436.
(326) Apuy, J. L.; Busenlehner, L. S.; Russell, D. H.; Giedroc, D. P. Ratiometric Pulsed Alkylation Mass Spectrometry as a Probe of

Thiolate Reactivity in Different Metallodervatives of *Staphylococcus aureus* pI258 CadC. *Biochemistry* **2004**, *43*, 3824−3834.
(327) Wang, D.; Hosteen, O.; Fierke, C. A. ZntR-Mediated Transcription of ZntA Responds to Nanomolar Intracellular Free Zinc. *J. Inorg. Biochem* **2012**, *111*, 173−81.
(328) Binet, M. R. B.; Poole, R. K. Cd(II), Pb(II) and Zn(II) Ions Regulate Expression of the Metal-Transporting P-Type ATPase ZntA in *Escherichia coli*. *FEBS Lett.* **2000**, *473*, 67−70.
(329) Jeon, Y.; Lee, Y.; Jang, G.; Kim, B. G.; Yoon, Y. Design of Pb(II)-Specific *E. coli*-Based Biosensors by Engineering Regulatory Proteins and Host Cells. *Front Microbiol* **2022**, *13*, 1−12.
(330) Sheehan, L. M.; Budnick, J. A.; Roop, R. M.; Caswell, C. C. Coordinated Zinc Homeostasis Is Essential for the Wild-Type Virulence of Brucella Abortus. *J. Bacteriol.* **2015**, *197*, 1582−1591.
(331) Carlier, J. D.; dos Reis Ferreira, G. M.; Schwan, R. F.; da Silva, C. F.; Costa, M. C. Pb^{2+} Biosorption by *Serratia marcescens* CCMA 1010 and Its Relation with ZntR Gene Expression and ZntA Efflux Pump Regulation. *Environ. Adv.* **2024**, *15*, 100479.
(332) Chaoprasid, P.; Nookabkaew, S.; Sukchawalit, R.; Mongkolsuk, S. Roles of *Agrobacterium Tumefaciens* C58 ZntA and ZntB and the Transcriptional Regulator ZntR in Controlling $Cd^{2+}/Zn^{2+}/Co^{2+}$ Resistance and the Peroxide Stress Response. *Microbiology* **2015**, *161*, 1730−1740.
(333) Kim, H.; Jang, G.; Yoon, Y. Specific Heavy Metal/Metalloid Sensors: Current State and Perspectives. *Appl. Microbiol. Biotechnol.* **2020**, *104*, 907−914.
(334) Kang, Y.; Lee, W.; Jang, G.; Kim, B.; Yoon, Y. Modulating the Sensing Properties of *Escherichia coli* -Based Bioreporters for Cadmium and Mercury. *Appl. Microbiol. Biotechnol.* **2018**, *102*, 4863.
(335) Utschig, L. M.; Bryson, J. W.; O'Halloran, T. V. Mercury-199 NMR of the Metal Receptor Site in MerR and Its Protein-DNA Complex. *Science* **1995**, *268*, 380−385.
(336) Wright, J. G.; Natan, M. J.; MacDonnel, F. M.; Ralston, D. M.; O'Halloran, T. V. Mercury (II)—Thiolate Chemistry and the Mechanism of the Heavy Metal Biosensor MerR. In *Progress in Inorganic Chemistry: Bioinorganic Chemistry*; John Wiley & Sons, 1990; pp 323−412.
(337) Wright, J. G.; O'Halloran, T. V.; Tsang, H. T.; Penner-Hahn, J. E.; O'Halloran, T. V. Coordination Chemistry of the Hg-MerR Metalloregulatory Protein: Evidence for a Novel Tridentate Hg-Cysteine Receptor Site. *J. Am. Chem. Soc.* **1990**, *112*, 2434−2435.
(338) Chakraborty, S.; Yudenfreundkravitz, J.; Thulstrup, P. W.; Hemmingsen, L.; Degrado, W. F.; Pecoraro, V. L. Design of a Three-Helix Bundle Capable of Binding Heavy Metals in a Triscysteine Environment. *Angew. Chem. Int. Ed* **2011**, *50*, 2049−2053.
(339) Chen, P.; He, C. A General Strategy to Convert the MerR Family Proteins into Highly Sensitive and Selective Fluorescent Biosensors for Metal Ions. *J. Am. Chem. Soc.* **2004**, *126*, 728−729.
(340) Ralston, D. M.; O'Halloran, T. V. Ultrasensitivity and Heavy-Metal Selectivity of the Allosterically Modulated MerR Transcription Complex. *Proc. Natl. Acad. Sci. U. S. A.* **1990**, *87*, 3846−3850.
(341) Caguiat, J. J.; Watson, A. L.; Summers, A. O. Cd(II)-Responsive and Constitutive Mutants Implicate a Novel Domain in MerR. *J. Bacteriol.* **1999**, *181*, 3462−3471.
(342) Hakkila, K. M.; Nikander, P. A.; Junttila, S. M.; Lamminmäki, U. J.; Virta, M. P. Cd-Specific Mutants of Mercury-Sensing Regulatory Protein MerR, Generated by Directed Evolution. *Appl. Environ. Microbiol.* **2011**, *77*, 6215−6224.
(343) Cerminati, S.; Soncini, F. C.; Checa, S. K. A Sensitive Whole-Cell Biosensor for the Simultaneous Detection of a Broad-Spectrum of Toxic Heavy Metal Ions. *Chem. Commun.* **2015**, *51*, 5917−5920.
(344) Ibáñez, M. M.; Checa, S. K.; Soncini, F. C. A Single Serine Residue Determines Selectivity to Monovalent Metal Ions in Metalloregulators of the MerR Family. *J. Bacteriol.* **2015**, *197*, 1606−1613.
(345) Pérez Audero, M. E.; Podoroska, B. M.; Ibáñez, M. M.; Cauerhff, A.; Checa, S. K.; Soncini, F. C. Target Transcription Binding Sites Differentiate Two Groups of MerR-Monovalent Metal Ion Sensors. *Mol. Microbiol.* **2010**, *78*, 853−865.
(346) Humbert, M. V.; Rasia, R. M.; Checa, S. K.; Soncini, F. C. Protein Signatures That Promote Operator Selectivity among Paralog MerR Monovalent Metal Ion Regulators. *J. Biol. Chem.* **2013**, *288*, 20510−20519.
(347) Kobayashi, K.; Fujikawa, M.; Kozawa, T. Oxidative Stress Sensing by the Iron-Sulfur Cluster in the Transcription Factor, SoxR. *J. Inorg. Biochem* **2014**, *133*, 87−91.
(348) Hidalgo, E.; Leautaud, V.; Demple, B. The Redox-Regulated SoxR Protein Acts from a Single DNA Site as a Repressor and an Allosteric Activator. *EMBO J.* **1998**, *17*, 2629−2636.
(349) Gaudu, P.; Weiss, B. SoxR, a [2Fe-2S] Transcription Factor, Is Active Only in Its Oxidized Form. *Proc. Natl. Acad. Sci. U. S. A.* **1996**, *93*, 10094−10098.
(350) Dietrich, L. E. P.; Teal, T. K.; Price-Whelan, A.; Newman, D. K. Redox-Active Antibiotics Control Gene Expression and Community Behavior in Divergent Bacteria. *Science* **2008**, *321*, 1203−1206.
(351) Park, W.; Peña-Llopis, S.; Lee, Y.; Demple, B. Regulation of Superoxide Stress in *Pseudomonas putida* KT2440 Is Different from the SoxR Paradigm in *Escherichia coli*. *Biochem. Biophys. Res. Commun.* **2006**, *341*, 51−56.
(352) Kidd, S. P.; Potter, A. J.; Apicella, M. A.; Jennings, M. P.; McEwan, A. G. NmIR of *Neisseria gonorrhoeae*: A Novel Redox Responsive Transcription Factor from the MerR Family. *Mol. Microbiol.* **2005**, *57*, 1676−1689.
(353) Fritsch, V. N.; Linzner, N.; Busche, T.; Said, N.; Weise, C.; Kalinowski, J.; Wahl, M. C.; Antelmann, H. The MerR-Family Regulator NmlR Is Involved in the Defense against Oxidative Stress in *Streptococcus pneumoniae*. *Mol. Microbiol.* **2023**, *119*, 191−207.
(354) Huyen, N. T. T.; Eiamphungporn, W.; Mäder, U.; Liebeke, M.; Lalk, M.; Hecker, M.; Helmann, J. D.; Antelmann, H. Genome-Wide Responses to Carbonyl Electrophiles in *Bacillus subtilis*: Control of the Thiol-Dependent Formaldehyde Dehydrogenase AdhA and Cysteine Proteinase YraA by the MerR-Family Regulator YraB (AdhR). *Mol. Microbiol.* **2009**, *71*, 876−894.
(355) Chi, B. K.; Huyen, N. T. T.; Loi, V.; Van; Gruhlke, M. C. H.; Schaffer, M.; Mäder, U.; Maaß, S.; Becher, D.; Bernhardt, J.; Arbach, M.; et al. The Disulfide Stress Response and Protein *S*-Thioallylation Caused by Allicin and Diallyl Polysulfanes in *Bacillus subtilis* as Revealed by Transcriptomics and Proteomics. *Antioxidants* **2019**, *8*, 605.
(356) Higgins, K. A.; Giedroc, D. Insights into Protein Allostery in the CsoR/RcnR Family of Transcriptional Repressors. *Chem. Lett.* **2014**, *43*, 20−25.
(357) Dwarakanath, S.; Chaplin, A. K.; Hough, M. A.; Rigali, S.; Vijgenboom, E.; Worrall, J. A. R. Response to Copper Stress in *Streptomyces lividans* Extends beyond Genes under Direct Control of a Copper-Sensitive Operon Repressor Protein (CsoR). *J. Biol. Chem.* **2012**, *287*, 17833−17847.
(358) Iwig, J. S.; Rowe, J. L.; Chivers, P. T. Nickel Homeostasis in *Escherichia coli* - the RcnR-*rcnA* Efflux Pathway and Its Linkage to NikR Function. *Mol. Microbiol.* **2006**, *62*, 252−262.
(359) Festa, R. A.; Jones, M. B.; Butler-Wu, S.; Sinsimer, D.; Gerads, R.; Bishai, W. R.; Peterson, S. N.; Darwin, K. H. A Novel Copper-Responsive Regulon in *Mycobacterium tuberculosis*. *Mol. Microbiol.* **2011**, *79*, 133−148.
(360) Foster, A. W.; Patterson, C. J.; Pernil, R.; Hess, C. R.; Robinson, N. J. Cytosolic Ni(II) Sensor in Cyanobacterium: Nickel Detection Follows Nickel Affinity across Four Families of Metal Sensors. *J. Biol. Chem.* **2012**, *287*, 12142−12151.
(361) Denby, K. J.; Iwig, J.; Bisson, C.; Westwood, J.; Rolfe, M. D.; Sedelnikova, S. E.; Higgins, K.; Maroney, M. J.; Baker, P. J.; Chivers, P. T.; et al. The Mechanism of a Formaldehyde-Sensing Transcriptional Regulator. *Sci. Rep* **2016**, *6*, 38879.
(362) Osman, D.; Piergentili, C.; Chen, J.; Sayer, L. N.; Usón, I.; Huggins, T. G.; Robinson, N. J.; Pohl, E. The Effectors and Sensory Sites of Formaldehyde-Responsive Regulator FrmR and Metal-Sensing Variant. *J. Biol. Chem.* **2016**, *291*, 19502−19516.
(363) Luebke, J. L.; Shen, J.; Bruce, K. E.; Kehl-Fie, T. E.; Peng, H.; Skaar, E. P.; Giedroc, D. P. The CsoR-like Sulfurtransferase Repressor

https://doi.org/10.1021/acs.chemrev.4c00264
Chem. Rev. 2024, 124, 13574−13659

(CstR) Is a Persulfide Sensor in *Staphylococcus aureus*. *Mol. Microbiol.* **2014**, *94*, 1343−1360.
(364) Shen, J.; Walsh, B. J. C.; Flores-Mireles, A. L.; Peng, H.; Zhang, Y.; Zhang, Y.; Trinidad, J. C.; Hultgren, S. J.; Giedroc, D. P. Hydrogen Sulfide Sensing through Reactive Sulfur Species (RSS) and Nitroxyl (HNO) in *Enterococcus faecalis*. *ACS Chem. Biol.* **2018**, *13*, 1610−1620.
(365) Foster, A. W.; Pernil, R.; Patterson, C. J.; Scott, A. J. P.; Pålsson, L. O.; Pal, R.; Cummins, I.; Chivers, P. T.; Pohl, E.; Robinson, N. J. A Tight Tunable Range for Ni(II) Sensing and Buffering in Cells. *Nat. Chem. Biol.* **2017**, *13*, 409−414.
(366) Chang, F. M. J.; Coyne, H. J.; Cubillas, C.; Vinuesa, P.; Fang, X.; Ma, Z.; Ma, D.; Helmann, J. D.; García-De Los Santos, A.; Wang, Y. X.; et al. Cu(I)-Mediated Allosteric Switching in a Copper-Sensing Operon Repressor (CsoR). *J. Biol. Chem.* **2014**, *289*, 19204−19217.
(367) Sakamoto, K.; Agari, Y.; Agari, K.; Kuramitsu, S.; Shinkai, A. Structural and Functional Characterization of the Transcriptional Repressor CsoR from *Thermus thermophilus* HB8. *Microbiology* **2010**, *156*, 1993−2005.
(368) Ma, Z.; Cowart, D. M.; Ward, B. P.; Arnold, R. J.; DiMarchi, R. D.; Zhang, L.; George, G. N.; Scott, R. A.; Giedroc, D. P. Unnatural Amino Acid Substitution as a Probe of the Allosteric Coupling Pathway in a Mycobacterial Cu(I) Sensor. *J. Am. Chem. Soc.* **2009**, *131*, 18044−18045.
(369) Ma, Z.; Cowart, D. M.; Scott, R. A.; Giedroc, D. P. Molecular Insights into the Metal Selectivity of the Copper(I)-Sensing Repressor CsoR from. *Bacillus subtilis*. *Biochemistry* **2009**, *48*, 3325−3334.
(370) Grossoehme, N.; Kehl-Fie, T. E.; Ma, Z.; Adams, K. W.; Cowart, D. M.; Scott, R. A.; Skaar, E. P.; Giedroc, D. P. Control of Copper Resistance and Inorganic Sulfur Metabolism by Paralogous Regulators in *Staphylococcus aureus*. *J. Biol. Chem.* **2011**, *286*, 13522−13531.
(371) Porto, T. V.; Wilson, M. T.; Worrall, J. A. R. Copper and Nickel Bind via Two Distinct Kinetic Mechanisms to a CsoR Metalloregulator. *Dalton Trans.* **2015**, *44*, 20176−20185.
(372) Porto, T. V.; Hough, M. A.; Worrall, J. A. R. Structural Insights into Conformational Switching in the Copper Metalloregulator CsoR from *Streptomyces lividans*. *Acta Crystallogr. D Biol. Crystallogr.* **2015**, *71*, 1872−1878.
(373) Chang, F.-M. J.; Martin, J. E.; Giedroc, D. P. Electrostatic Occlusion and Quaternary Structural Ion Pairing Are Key Determinants of Cu(I)-Mediated Allostery in the Copper-Sensing Operon Repressor (CsoR). *Biochemistry* **2015**, *54*, 2463−2472.
(374) Marcus, S. A.; Sidiropoulos, S. W.; Steinberg, H.; Talaat, A. M. CsoR Is Essential for Maintaining Copper Homeostasis in *Mycobacterium tuberculosis*. *PLoS One* **2016**, *11*, e0151816.
(375) Jacobs, A. D.; Chang, F.-M. J.; Morrison, L.; Dilger, J. M.; Wysocki, V. H.; Clemmer, D. E.; Giedroc, D. P. Resolution of Stepwise Cooperativities of Copper Binding by the Homotetrameric Copper-Sensitive Operon Repressor (CsoR): Impact on Structure and Stability. *Angew. Chemie Int. Ed* **2015**, *54*, 12795−12799.
(376) Higgins, K. A.; Chivers, P. T.; Maroney, M. J. Role of the N-Terminus in Determining Metal-Specific Responses in the *E. coli* Ni- and Co-Responsive Metalloregulator, RcnR. *J. Am. Chem. Soc.* **2012**, *134*, 7081−7093.
(377) Herring, C. D.; Blattner, F. R. Global Transcriptional Effects of a Suppressor TRNA and the Inactivation of the Regulator FrmR. *J. Bacteriol.* **2004**, *186*, 6714−6720.
(378) Higgins, K. A.; Hu, H. Q.; Chivers, P. T.; Maroney, M. J. Effects of Select Histidine to Cysteine Mutations on Transcriptional Regulation by *Escherichia coli* RcnR. *Biochemistry* **2013**, *52*, 84−97.
(379) Carr, C. E.; Musiani, F.; Huang, H. T.; Chivers, P. T.; Ciurli, S.; Maroney, M. J. Glutamate Ligation in the Ni(II)- and Co(II)-Responsive *Escherichia coli* Transcriptional Regulator, RcnR. *Inorg. Chem.* **2017**, *56*, 6459−6476.
(380) Zhu, T.; Tian, J.; Zhang, S.; Wu, N.; Fan, Y. Identification of the Transcriptional Regulator NcrB in the Nickel Resistance Determinant of *Leptospirillum ferriphilum* UBK03. *PLoS One* **2011**, *6*, 2−9.
(381) Foster, A. W.; Pernil, R.; Patterson, C. J.; Robinson, N. J. Metal Specificity of Cyanobacterial Nickel-Responsive Repressor InrS: Cells Maintain Zinc and Copper below the Detection Threshold for InrS. *Mol. Microbiol.* **2014**, *92*, 797−812.
(382) Manzari, C.; Chiara, M.; Costanza, A.; Leoni, C.; Volpicella, M.; Picardi, E.; D'Erchia, A. M.; Placido, A.; Trotta, M.; Horner, D. S.; et al. Draft Genome Sequence of *Sphingobium* sp. Strain Ba1, Resistant to Kanamycin and Nickel Ions. *FEMS Microbiol Lett.* **2014**, *361*, 8−9.
(383) Tang, C.; Li, J.; Shen, Y.; Liu, M.; Liu, H.; Liu, H.; Xun, L.; Xia, Y. A Sulfide-Sensor and a Sulfane Sulfur-Sensor Collectively Regulate Sulfur-Oxidation for Feather Degradation by *Bacillus licheniformis*. *Commun. Biol.* **2023**, *6*, 1−16.
(384) Fakhoury, J. N.; Capdevila, D. A.; Giedroc, D. P. Protocol for Using Organic Persulfides to Measure the Chemical Reactivity of Persulfide Sensors. *STAR Protoc* **2022**, *3*, 101424.
(385) Lu, T.; Cao, Q.; Pang, X.; Xia, Y.; Xun, L.; Liu, H. Sulfane Sulfur-Activated Actinorhodin Production and Sporulation Is Maintained by a Natural Gene Circuit in *Streptomyces coelicolor*. *Microb Biotechnol* **2020**, *13*, 1917−1932.
(386) Portmann, R.; Poulsen, K. R.; Wimmer, R.; Solioz, M. CopY-like Copper Inducible Repressors Are Putative "winged Helix" Proteins. *BioMetals* **2006**, *19*, 61−70.
(387) Cantini, F.; Banci, L.; Solioz, M. The Copper-Responsive Repressor CopR of *Lactococcus lactis* Is a "winged helix" Protein. *Biochem. J.* **2009**, *417*, 493−499.
(388) Pazehoski, K. O.; Cobine, P. A.; Winzor, D. J.; Dameron, C. T. Evidence for Involvement of the C-Terminal Domain in the Dimerization of the CopY Repressor Protein from *Enterococcus hirae*. *Biochem. Biophys. Res. Commun.* **2011**, *406*, 183−187.
(389) Cobine, P. A.; George, G. N.; Jones, C. E.; Wickramasinghe, W. A.; Solioz, M.; Dameron, C. T. Copper Transfer from the Cu (I) Chaperone, CopZ, to the Repressor, Zn(II) CopY: Metal Coordination Environments and Protein Interactions. *Biochemistry* **2002**, *41*, 5822−5829.
(390) Shafeeq, S.; Yesilkaya, H.; Kloosterman, T. G.; Narayanan, G.; Wandel, M.; Andrew, P. W.; Kuipers, O. P.; Morrissey, J. A. The Cop Operon Is Required for Copper Homeostasis and Contributes to Virulence in *Streptococcus pneumoniae*. *Mol. Microbiol.* **2011**, *81*, 1255−1270.
(391) Magnani, D.; Barré, O.; Gerber, S. D.; Solioz, M. Characterization of the CopR Regulon of *Lactococcus lactis* IL1403. *J. Bacteriol.* **2008**, *190*, 536−545.
(392) Cobine, P. A.; George, G. N.; Jones, C. E.; Wickramasinghe, W. A.; Solioz, M.; Dameron, C. T. Copper Transfer from the Cu(I) Chaperone, CopZ, to the Repressor, Zn(II) CopY: Metal Coordination Environments and Protein Interactions. *Biochemistry* **2002**, *41*, 5822−5829.
(393) Hasman, H.; Kempf, I.; Chidaine, B.; Cariolet, R.; Ersbøll, A. K.; Houe, H.; Bruun Hansen, H. C.; Aarestrup, F. M. Copper Resistance in *Enterococcus faecium*, Mediated by the TcrB Gene, Is Selected by Supplementation of Pig Feed with Copper Sulfate. *Appl. Environ. Microbiol.* **2006**, *72*, 5784−5789.
(394) Zheng, C.; Jia, M.; Lu, T.; Gao, M.; Li, L. CopA Protects *Streptococcus suis* against Copper Toxicity. *Int. J. Mol. Sci.* **2019**, *20*, 2969.
(395) Mitrakul, K.; Loo, C. Y.; Hughes, C. V.; Ganeshkumar, N. Role of a *Streptococcus gordonii* Copper-transport Operon, *copYAZ.*, in Biofilm Detachment. *Oral Microbiol. Immunol* **2004**, *19*, 395−402.
(396) Hirsch, M.; Hofmann, L.; Shenberger, Y.; Gevorkyan-Airapetov, L.; Ruthstein, S. Conformations and Local Dynamics of the CopY Metal Sensor Revealed by EPR Spectroscopy. *Biochemistry* **2023**, *62*, 797−807.
(397) García-Castellanos, R.; Marrero, A.; Mallorquí-Fernández, G.; Potempa, J.; Coll, M.; Gomis-Rüth, F. X. Three-Dimensional Structure of MecI. Molecular Basis for Transcriptional Regulation of Staphylococcal Methicillin Resistance. *J. Biol. Chem.* **2003**, *278*, 39897−39905.
(398) Lee, J. W.; Helmann, J. D. Functional Specialization within the Fur Family of Metalloregulators. *Biometals* **2007**, *20*, 485−499.

(399) Sevilla, E.; Bes, M. T.; Peleato, M. L.; Fillat, M. F. Fur-like Proteins: Beyond the Ferric Uptake Regulator (Fur) Paralog. *Arch. Biochem. Biophys.* **2021**, *701*, 108770.
(400) Fontenot, C. R.; Tasnim, H.; Valdes, K. A.; Popescu, C. V.; Ding, H. Ferric Uptake Regulator (Fur) Reversibly Binds a [2Fe-2S] Cluster to Sense Intracellular Iron Homeostasis in *Escherichia coli*. *J. Biol. Chem.* **2020**, *295*, 15454−15463.
(401) Fillat, M. F. The FUR (Ferric Uptake Regulator) Superfamily: Diversity and Versatility of Key Transcriptional Regulators. *Arch. Biochem. Biophys.* **2014**, *546*, 41−52.
(402) Nader, S.; Pérard, J.; Carpentier, P.; Arnaud, L.; Crouzy, S.; Michaud-Soret, I. New Insights into the Tetrameric Family of the Fur Metalloregulators. *BioMetals* **2019**, *32*, 501−519.
(403) Liu, F.; Su, Z.; Chen, P.; Tian, X.; Wu, L.; Tang, D. J.; Li, P.; Deng, H.; Ding, P.; Fu, Q.; Tang, J. L.; Ming, Z. Structural Basis for Zinc-Induced Activation of a Zinc Uptake Transcriptional Regulator. *Nucleic Acids Res.* **2021**, *49*, 6511−6528.
(404) Sarvan, S.; Charih, F.; Askoura, M.; Butcher, J.; Brunzelle, J. S.; Stintzi, A.; Couture, J.-F. Functional Insights into the Interplay between DNA Interaction and Metal Coordination in Ferric Uptake Regulators. *Sci. Rep* **2018**, *8*, 7140.
(405) Grim, K. P.; San Francisco, B.; Radin, J. N.; Brazel, E. B.; Kelliher, J. L.; Párraga Solórzano, P. K.; Kim, P. C.; McDevitt, C. A.; Kehl-Fie, T. E. The Metallophore Staphylopine Enables *Staphylococcus aureus* To Compete with the Host for Zinc and Overcome Nutritional Immunity. *mBio* **2017**, *8*, 1−16.
(406) Fojcik, C.; Arnoux, P.; Ouerdane, L.; Aigle, M.; Alfonsi, L.; Borezée-Durant, E. Independent and Cooperative Regulation of Staphylopine Biosynthesis and Trafficking by Fur and Zur. *Mol. Microbiol.* **2018**, *108*, 159−177.
(407) Mazzon, R. R.; Braz, V. S.; da Silva Neto, J. F.; do Valle Marques, M. Analysis of the *Caulobacter crescentus* Zur Regulon Reveals Novel Insights in Zinc Acquisition by TonB-Dependent Outer Membrane Proteins. *BMC Genomics* **2014**, *15*, 734.
(408) Pinochet-Barros, A.; Helmann, J. D. Redox Sensing by Fe^{2+} in Bacterial Fur Family Metalloregulators. *Antioxid Redox Signal* **2018**, *29*, 1858−1871.
(409) Askoura, M.; Sarvan, S.; Couture, J. F.; Stintzi, A. The *Campylobacter jejuni* Ferric Uptake Regulator Promotes Acid Survival and Cross-Protection against Oxidative Stress. *Infect. Immun.* **2016**, *84*, 1287−1300.
(410) Husain, M.; Jones-Carson, J.; Liu, L.; Song, M.; Royden Saah, J.; Troxell, B.; Mendoza, M.; Hassan, H.; Vázquez-Torres, A. Ferric Uptake Regulator-Dependent Antinitrosative Defenses in *Salmonella enterica* Serovar Typhimurium Pathogenesis. *Infect. Immun.* **2014**, *82*, 333−340.
(411) Steingard, C. H.; Helmann, J. D. Meddling with Metal Sensors: Fur-Family Proteins as Signaling Hubs. *J. Bacteriol.* **2023**, *205*, No. e0002223.
(412) Ernst, F. D.; Homuth, G.; Stoof, J.; Mäder, U.; Waidner, B.; Kuipers, E. J.; Kist, M.; Kusters, J. G.; Bereswill, S.; Van Vliet, A. H. M. Iron-Responsive Regulation of the *Helicobacter pylori* Iron-Cofactored Superoxide Dismutase SodB Is Mediated by Fur. *J. Bacteriol.* **2005**, *187*, 3687−3692.
(413) Shin, J. H.; Helmann, J. D. Molecular Logic of the Zur-Regulated Zinc Deprivation Response in *Bacillus subtilis*. *Nat. Commun.* **2016**, *7*, 12612.
(414) Shin, J.-H.; Jung, H. J.; An, Y. J.; Cho, Y.-B.; Cha, S.-S.; Roe, J.-H. Graded Expression of Zinc-Responsive Genes through Two Regulatory Zinc-Binding Sites in Zur. *Proc. Natl. Acad. Sci. U. S. A.* **2011**, *108*, 5045−5050.
(415) Pi, H.; Helmann, J. D. Sequential Induction of Fur-Regulated Genes in Response to Iron Limitation in *Bacillus subtilis*. *Proc. Natl. Acad. Sci. U. S. A.* **2017**, *114*, 12785−12790.
(416) Sheikh, M. A.; Taylor, G. L. Crystal Structure of the *Vibrio cholerae* Ferric Uptake Regulator (Fur) Reveals Insights into Metal Co-Ordination. *Mol. Microbiol.* **2009**, *72*, 1208−1220.
(417) Traoré, D. A. K.; El Ghazouani, A.; Ilango, S.; Dupuy, J.; Jacquamet, L.; Ferrer, J. L.; Caux-Thang, C.; Duarte, V.; Latour, J. M. Crystal Structure of the Apo-PerR-Zn Protein from *Bacillus subtilis*. *Mol. Microbiol.* **2006**, *61*, 1211−1219.
(418) Ollinger, J.; Song, K. B.; Antelmann, H.; Hecker, M.; Helmann, J. D. Role of the Fur Regulon in Iron Transport in *Bacillus subtilis*. *J. Bacteriol.* **2006**, *188*, 3664−3673.
(419) Daniel, C.; Haentjens, S.; Bissinger, M. C.; Courcol, R. J. Characterization of the *Acinetobacter baumannii* Fur Regulator: Cloning and Sequencing of the Fur Homolog Gene. *FEMS Microbiol Lett.* **1999**, *170*, 199−209.
(420) Ernst, F. D.; Homuth, G.; Stoof, J.; Mäder, U.; Waidner, B.; Kuipers, E. J.; Kist, M.; Kusters, J. G.; Bereswill, S.; Van Vliet, A. H. M. Iron-Responsive Regulation of the *Helicobacter pylori* Iron-Cofactored Superoxide Dismutase SodB Is Mediated by Fur. *J. Bacteriol.* **2005**, *187*, 3687−3692.
(421) Sheikh, M. A.; Taylor, G. L. Crystal Structure of the *Vibrio cholerae* Ferric Uptake Regulator (Fur) Reveals Insights into Metal Co-Ordination. *Mol. Microbiol.* **2009**, *72*, 1208−1220.
(422) Pellicer, S.; González, A.; Peleato, M. L.; Martinez, J. I.; Fillat, M. F.; Bes, M. T. Site-Directed Mutagenesis and Spectral Studies Suggest a Putative Role of FurA from Anabaena Sp. PCC 7120 as a Heme Sensor Protein. *FEBS J.* **2012**, *279*, 2231−2246.
(423) Salinas, P. C.; Tolmasky, M. E.; Crosa, J. H. Regulation of the Iron Uptake System in *Vibrio anguillarum*: Evidence for a Cooperative Effect between Two Transcriptional Activators. *Proc. Natl. Acad. Sci. U. S. A.* **1989**, *86*, 3529−3533.
(424) Barton, H. A.; Johnson, Z.; Cox, C. D.; Vasil, A. I.; Vasil, M. L. Ferric Uptake Regulator Mutants of *Pseudomonas aeruginosa* with Distinct Alterations in the Iron-Dependent Repression of Exotoxin A and Siderophores in Aerobic and Microaerobic Environments. *Mol. Microbiol.* **1996**, *21*, 1001−1017.
(425) Deng, Z.; Wang, Q.; Liu, Z.; Zhang, M.; Machado, A. C. D.; Chiu, T.-P.; Feng, C.; Zhang, Q.; Yu, L.; Qi, L.; et al. Mechanistic Insights into Metal Ion Activation and Operator Recognition by the Ferric Uptake Regulator. *Nat. Commun.* **2015**, *6*, 7642.
(426) Pohl, E.; Haller, J. C.; Mijovilovich, A.; Meyer-Klaucke, W.; Garman, E.; Vasil, M. L. Architecture of a Protein Central to Iron Homeostasis: Crystal Structure and Spectroscopic Analysis of the Ferric Uptake Regulator. *Mol. Microbiol.* **2003**, *47*, 903−915.
(427) Muranishi, K.; Ishimori, K.; Uchida, T. Regulation of the Expression of the Nickel Uptake System in *Vibrio cholerae* by Iron and Heme via Ferric Uptake Regulator (Fur). *J. Inorg. Biochem* **2022**, *228*, 111713.
(428) Patzer, S. I.; Hantke, K. The ZnuABC High-Affinity Zinc Uptake System and Its Regulator Zur in *Escherichia coli*. *Mol. Microbiol.* **1998**, *28*, 1199−1210.
(429) Kandari, D.; Joshi, H.; Bhatnagar, R. Zur: Zinc-sensing Transcriptional Regulator in a Diverse Set of Bacterial Species. *Pathogens* **2021**, *10*, 344.
(430) Mikhaylina, A.; Ksibe, A. Z.; Scanlan, D. J.; Blindauer, C. A. Bacterial Zinc Uptake Regulator Proteins and Their Regulons. *Biochem. Soc. Trans.* **2018**, *46*, 983−1001.
(431) Gilston, B. A.; Wang, S.; Marcus, M. D.; Canalizo-Hernández, M. A.; Swindell, E. P.; Xue, Y.; Mondragón, A.; O'Halloran, T. V. Structural and Mechanistic Basis of Zinc Regulation Across the *E. coli* Zur Regulon. *PLoS Biol.* **2014**, *12*, No. e1001987.
(432) Kim, M.; Le, M. T.; Fan, L.; Campbell, C.; Sen, S.; Capdevila, D. A.; Stemmler, T. L.; Giedroc, D. P. Characterization of the Zinc Uptake Repressor (Zur) from *Acinetobacter baumannii*. *Biochemistry* **2024**, *63*, 660−670.
(433) Lucarelli, D.; Russo, S.; Garman, E.; Milano, A.; Meyer-Klaucke, W.; Pohl, E. Crystal Structure and Function of the Zinc Uptake Regulator FurB from *Mycobacterium tuberculosis*. *J. Biol. Chem.* **2007**, *282*, 9914−9922.
(434) Neupane, D. P.; Jacquez, B.; Sundararajan, A.; Ramaraj, T.; Schilkey, F. D.; Yukl, E. T. Zinc-Dependent Transcriptional Regulation in *Paracoccus denitrificans*. *Front Microbiol* **2017**, *8*, 1−15.
(435) Pawlik, M. C.; Hubert, K.; Joseph, B.; Claus, H.; Schoen, C.; Vogel, U. The Zinc-Responsive Regulon of *Neisseria meningitidis*

Comprises 17 Genes under Control of a Zur Element. *J. Bacteriol.* **2012**, *194*, 6594−6603.
(436) Maciąg, A.; Dainese, E.; Rodriguez, G. M.; Milano, A.; Provvedi, R.; Pasca, M. R.; Smith, I.; Palù, G.; Riccardi, G.; Manganelli, R. Global Analysis of the *Mycobacterium tuberculosis* Zur (FurB) Regulon. *J. Bacteriol.* **2007**, *189*, 730−740.
(437) Mikhaylina, A.; Ksibe, A. Z.; Wilkinson, R. C.; Smith, D.; Marks, E.; Coverdale, J. P. C.; Fülöp, V.; Scanlan, D. J.; Blindauer, C. A. A Single Sensor Controls Large Variations in Zinc Quotas in a Marine Cyanobacterium. *Nat. Chem. Biol.* **2022**, *18*, 869−877.
(438) Choi, Y.; Koh, J.; Cha, S.; Roe, J.-H. Activation of Zinc Uptake Regulator by Zinc Binding to Three Regulatory Sites. *Nucleic Acids Res.* **2024**, *52*, 4185−4197.
(439) Choi, S.-H.; Lee, K.-L.; Shin, J.-H.; Cho, Y.-B.; Cha, S.-S.; Roe, J.-H. Zinc-Dependent Regulation of Zinc Import and Export Genes by Zur. *Nat. Commun.* **2017**, *8*, 15812.
(440) Yang, X.; Wang, Y.; Liu, G.; Deng, Z.; Lin, S.; Zheng, J. Structural Basis of Streptomyces Transcription Activation by Zinc Uptake Regulator. *Nucleic Acids Res.* **2022**, *50*, 8363−8376.
(441) Van Vliet, A. H. M.; Baillon, M. L. A.; Penn, C. W.; Ketley, J. M. *Campylobacter jejuni* Contains Two Fur Homologs: Characterization of Iron-Responsive Regulation of Peroxide Stress Defense Genes by the PerR Repressor. *J. Bacteriol.* **1999**, *181*, 6371−6376.
(442) Wu, H. J.; Seib, K. L.; Srikhanta, Y. N.; Kidd, S. P.; Edwards, J. L.; Maguire, T. L.; Grimmond, S. M.; Apicella, M. A.; McEwan, A. G.; Jennings, M. P. PerR Controls Mn-Dependent Resistance to Oxidative Stress in *Neisseria gonorrhoeae*. *Mol. Microbiol.* **2006**, *60*, 401−416.
(443) Ji, C.-J.; Kim, J.-H.; Won, Y.-B.; Lee, Y.-E.; Choi, T.-W.; Ju, S.-Y.; Youn, H.; Helmann, J. D.; Lee, J.-W. *Staphylococcus aureus* PerR Is a Hypersensitive Hydrogen Peroxide Sensor Using Iron-Mediated Histidine Oxidation. *J. Biol. Chem.* **2015**, *290*, 20374−20386.
(444) Ahn, B. E.; Baker, T. A. Oxidization without Substrate Unfolding Triggers Proteolysis of the Peroxide-Sensor, PerR. *Proc. Natl. Acad. Sci. U. S. A.* **2016**, *113*, No. e23-e31.
(445) Traoré, D. A. K.; Ghazouani, A.; El; Jacquamet, L.; Borel, F.; Ferrer, J. L.; Lascoux, D.; Ravanat, J. L.; Jaquinod, M.; Blondin, G.; Caux-Thang, C.; et al. Structural and Functional Characterization of 2-Oxo-Histidine in Oxidized PerR Protein. *Nat. Chem. Biol.* **2009**, *5*, 53−59.
(446) Jacquamet, L.; Traoré, D. A. K.; Ferrer, J. L.; Proux, O.; Testemale, D.; Hazemann, J. L.; Nazarenko, E.; El Ghazouani, A.; Caux-Thang, C.; Duarte, V.; et al. Structural Characterization of the Active Form of PerR: Insights into the Metal-Induced Activation of PerR and Fur Proteins for DNA Binding. *Mol. Microbiol.* **2009**, *73*, 20−31.
(447) Lee, J.-W.; Helmann, J. D. The PerR Transcription Factor Senses H_2O_2 by Metal-Catalysed Histidine Oxidation. *Nature* **2006**, *440*, 363−367.
(448) Parent, A.; Caux-Thang, C.; Signor, L.; Clémancey, M.; Sethu, R.; Blondin, G.; Maldivi, P.; Duarte, V.; Latour, J. M. Single Glutamate to Aspartate Mutation Makes Ferric Uptake Regulator (Fur) as Sensitive to H_2O_2 as Peroxide Resistance Regulator (PerR). *Angew. Chemie Int. Ed* **2013**, *52*, 10339−10343.
(449) Menscher, E. A.; Caswell, C. C.; Anderson, E. S.; Roop, R. M. Mur Regulates the Gene Encoding the Manganese Transporter MntH in *Brucella abortus* 2308. *J. Bacteriol.* **2012**, *194*, 561−566.
(450) Díaz-Mireles, E.; Wexler, M.; Sawers, G.; Bellini, D.; Todd, J. D.; Johnston, A. W. B. The Fur-like Protein Mur of *Rhizobium leguminosarum* Is a Mn^{2+}-Responsive Transcriptional Regulator. *Microbiology* **2004**, *150*, 1447−1456.
(451) Hohle, T. H.; O'Brian, M. R. Metal-Specific Control of Gene Expression Mediated by *Bradyrhizobium japonicum* Mur and *Escherichia coli* Fur Is Determined by the Cellular Context. *Mol. Microbiol.* **2016**, *101*, 152.
(452) Ahn, B.; Cha, J.; Lee, E.; Han, A.; Thompson, C. J.; Roe, J. Nur, a Nickel-responsive Regulator of the Fur Family, Regulates Superoxide Dismutases and Nickel Transport in *Streptomyces coelicolor*. *Mol. Microbiol.* **2006**, *59*, 1848−1858.
(453) An, Y. J.; Ahn, B. E.; Han, A. R.; Kim, H. M.; Chung, K. M.; Shin, J. H.; Cho, Y. B.; Roe, J. H.; Cha, S. S. Structural Basis for the Specialization of Nur, a Nickel-Specific Fur Homolog, in Metal Sensing and DNA Recognition. *Nucleic Acids Res.* **2009**, *37*, 3442−3451.
(454) Hohle, T. H.; O'Brian, M. R. Transcriptional Control of the *Bradyrhizobium Japonicum* Irr Gene Requires Repression by Fur and Antirepression by Irr. *J. Biol. Chem.* **2010**, *285*, 26074−26080.
(455) Hamza, I.; Chauhan, S.; Hassett, R.; O'Brian, M. R. The Bacterial Irr Protein Is Required for Coordination of Heme Biosynthesis with Iron Availability. *J. Biol. Chem.* **1998**, *273*, 21669−21674.
(456) Merchant, A. T.; Spatafora, G. A. A Role for the DtxR Family of Metalloregulators in Gram-positive Pathogenesis. *Mol. Oral Microbiol* **2014**, *29*, 1−10.
(457) Pastor, M. M.; Sakrikar, S.; Hwang, S.; Hackley, R. K.; Soborowski, A. L.; Maupin-Furlow, J. A.; Schmid, A. K. TroR Is the Primary Regulator of the Iron Homeostasis Transcription Network in the Halophilic Archaeon *Haloferax volcanii*. *Nucleic Acids Res.* **2024**, *52*, 125−140.
(458) Marcos-Torres, F. J.; Juniar, L.; Griese, J. J. The Molecular Mechanisms of the Bacterial Iron Sensor IdeR. *Biochem. Soc. Trans.* **2023**, *51*, 1319−1329.
(459) Marcos-Torres, F. J.; Maurer, D.; Juniar, L.; Griese, J. J. The Bacterial Iron Sensor IdeR Recognizes Its DNA Targets by Indirect Readout. *Nucleic Acids Res.* **2021**, *49*, 10120−10135.
(460) Kurochkina, N.; Guha, U. SH3 Domains: Modules of Protein-Protein Interactions. *Biophys Rev.* **2013**, *5*, 29−39.
(461) Qiu, X.; Pohl, E.; Holmes, R. K.; Hol, W. G. J. High-Resolution Structure of the Diphtheria Toxin Repressor Complexed with Cobalt and Manganese Reveals an SH3-like Third Domain and Suggests a Possible Role of Phosphate as Co-Corepressor. *Biochemistry* **1996**, *35*, 12292−12302.
(462) Glasfeld, A.; Guedon, E.; Helmann, J. D.; Brennan, R. G. Structure of the Manganese-Bound Manganese Transport Regulator of *Bacillus subtilis*. *Nat. Struct. Biol.* **2003**, *10*, 652−657.
(463) Pandey, R.; Rodriguez, G. M. IdeR Is Required for Iron Homeostasis and Virulence in *Mycobacterium tuberculosis*. *Mol. Microbiol.* **2014**, *91*, 98−109.
(464) Deng, Y.; Zhang, X. DtxR, an Iron-Dependent Transcriptional Repressor That Regulates the Expression of Siderophore Gene Clusters in *Thermobifida fusca*. *FEMS Microbiol Lett.* **2015**, *362*, 1−23.
(465) Cheng, Y.; Yang, R.; Lyu, M.; Wang, S.; Liu, X.; Wen, Y.; Song, Y.; Li, J.; Chen, Z. IdeR, a DtxR Family Iron Response Regulator, Controls Iron Homeostasis, Morphological Differentiation, Secondary Metabolism, and the Oxidative Stress Response in *Streptomyces avermitilis*. *Appl. Environ. Microbiol.* **2018**, *84*, 1−19.
(466) Zondervan, N. A.; Van Dam, J. C. J.; Schaap, P. J.; Dos Santos, V. A. P. M.; Suarez-Diez, M. Regulation of Three Virulence Strategies of *Mycobacterium tuberculosis*: A Success Story. *Int. J. Mol. Sci.* **2018**, *19*, 347.
(467) Parveen, S.; Bishai, W. R.; Murphy, J. R. *Corynebacterium diphtheriae*: Diphtheria Toxin, the Tox Operon, and Its Regulation by Fe^{2+} Activation of Apo-DtxR. *Microbiol Spectr* **2019**, 1154−1164.
(468) Guedon, E.; Helmann, J. D. Origins of Metal Ion Selectivity in the DtxR/MntR Family of Metalloregulators. *Mol. Microbiol.* **2003**, *48*, 495−506.
(469) Spiering, M. M.; Ringe, D.; Murphy, J. R.; Marletta, M. A. Metal Stoichiometry and Functional Studies of the Diphtheria Toxin Repressor. *Proc. Natl. Acad. Sci. U. S. A.* **2003**, *100*, 3808−3813.
(470) Qiu, X.; Verlinde, C. L.; Zhang, S.; Schmitt, M. P.; Holmes, R. K.; Hol, W. G. Three-Dimensional Structure of the Diphtheria Toxin Repressor in Complex with Divalent Cation Co-Repressors. *Structure* **1995**, *3*, 87−100.
(471) Ding, X.; Zeng, H.; Schiering, N.; Ringe, D.; Murphy, J. R. Identification of the Primary Metal Ion-Activation Sites of the Diphtheria Tox Represser by X-Ray Crystallography and Site-Directed Mutational Analysis. *Nat. Struct Mol. Biol.* **1996**, *3*, 382−387.
(472) D'Aquino, J. A.; Tetenbaum-Novatt, J.; White, A.; Berkovitch, F.; Ringe, D. Mechanism of Metal Ion Activation of the Diphtheria Toxin Repressor DtxR. *Proc. Natl. Acad. Sci. U. S. A.* **2005**, *102*, 18408−18413.

https://doi.org/10.1021/acs.chemrev.4c00264
Chem. Rev. 2024, 124, 13574−13659

(473) Love, J. F.; vanderSpek, J. C.; Marin, V.; Guerrero, L.; Logan, T. M.; Murphy, J. R. Genetic and Biophysical Studies of Diphtheria Toxin Repressor (DtxR) and the Hyperactive Mutant DtxR(E175K) Support a Multistep Model of Activation. *Proc. Natl. Acad. Sci. U. S. A.* **2004**, *101*, 2506−2511.
(474) Pohl, E.; Holmes, R. K.; Hol, W. G. Crystal Structure of a Cobalt-Activated Diphtheria Toxin Repressor-DNA Complex Reveals a Metal-Binding SH3-like Domain. *J. Mol. Biol.* **1999**, *292*, 653−667.
(475) Stapleton, B.; Walker, L. R.; Logan, T. M. Zn(II) Stimulation of Fe(II)-Activated Repression in the Iron-Dependent Repressor from *Mycobacterium tuberculosis*. *Biochemistry* **2013**, *52*, 1927−1938.
(476) McGuire, A. M.; Cuthbert, B. J.; Ma, Z.; Grauer-Gray, K. D.; Brunjes Brophy, M.; Spear, K. A.; Soonsanga, S.; Kliegman, J. I.; Griner, S. L.; Helmann, J. D.; Glasfeld, A. Roles of the A and C Sites in the Manganese-Specific Activation of MntR. *Biochemistry* **2013**, *52*, 701−713.
(477) Lisher, J. P.; Higgins, K. A.; Maroney, M. J.; Giedroc, D. P. Physical Characterization of the Manganese-Sensing Pneumococcal Surface Antigen Repressor from *Streptococcus pneumoniae*. *Biochemistry* **2013**, *52*, 7689−7701.
(478) Mota, C.; Webster, M.; Saidi, M.; Kapp, U.; Zubieta, C.; Giachin, G.; Manso, J. A.; de Sanctis, D. Metal Ion Activation and DNA Recognition by the *Deinococcus radiodurans* Manganese Sensor DR2539. *FEBS J.* **2024**, *291*, 3384−3402.
(479) Rolerson, E.; Swick, A.; Newlon, L.; Palmer, C.; Pan, Y.; Keeshan, B.; Spatafora, G. The SloR/Dlg Metalloregulator Modulates *Streptococcus mutans* Virulence Gene Expression. *J. Bacteriol.* **2006**, *188*, 5033−44.
(480) O'Rourke, K. P.; Shaw, J. D.; Pesesky, M. W.; Cook, B. T.; Roberts, S. M.; Bond, J. P.; Spatafora, G. Genome-Wide Characterization of the SloR Metalloregulome in *Streptococcus mutans*. *J. Bacteriol.* **2010**, *192*, 1433−43.
(481) Do, H.; Makthal, N.; Chandrangsu, P.; Olsen, R. J.; Helmann, J. D.; Musser, J. M.; Kumaraswami, M. Metal Sensing and Regulation of Adaptive Responses to Manganese Limitation by MtsR Is Critical for Group A Streptococcus Virulence. *Nucleic Acids Res.* **2019**, *47*, 7476−7493.
(482) Stoll, K. E.; Draper, W. E.; Kliegman, J. I.; Golynskiy, M. V.; Brew-Appiah, R. A. T.; Phillips, R. K.; Brown, H. K.; Breyer, W. A.; Jakubovics, N. S.; Jenkinson, H. F.; et al. Characterization and Structure of the Manganese-Responsive Transcriptional Regulator ScaR. *Biochemistry* **2009**, *48*, 10308−10320.
(483) Schreiter, E. R.; Drennan, C. L. Ribbon-Helix-Helix Transcription Factors: Variations on a Theme. *Nat. Rev. Microbiol* **2007**, *5*, 710−720.
(484) Muller, C.; Bahlawane, C.; Aubert, S.; Delay, C. M.; Schauer, K.; Michaud-Soret, I.; De Reuse, H. Hierarchical Regulation of the NikR-Mediated Nickel Response in *Helicobacter pylori*. *Nucleic Acids Res.* **2011**, *39*, 7564−7575.
(485) Chivers, P. T.; Tahirov, T. H. Structure of *Pyrococcus horikoshii* NikR: Nickel Sensing and Implications for the Regulation of DNA Recognition. *J. Mol. Biol.* **2005**, *348*, 597−607.
(486) Dian, C.; Schauer, K.; Kapp, U.; McSweeney, S. M.; Labigne, A.; Terradot, L. Structural Basis of the Nickel Response in *Helicobacter pylori*: Crystal Structures of *Hp*NikR in Apo and Nickel-Bound States. *J. Mol. Biol.* **2006**, *361*, 715−730.
(487) Phillips, C. M.; Schreiter, E. R.; Guo, Y.; Wang, S. C.; Zamble, D. B.; Drennan, C. L. Structural Basis of the Metal Specificity for Nickel Regulatory Protein NikR. *Biochemistry* **2008**, *47*, 1938−1946.
(488) West, A. L.; Evans, S. E.; Gonzalez, J. M.; Carter, L. G.; Tsuruta, H.; Pozharski, E.; Michel, S. L. J. Ni(II) Coordination to Mixed Sites Modulates DNA Binding of *Hp*NikR via a Long-Range Effect. *Proc. Natl. Acad. Sci. U. S. A.* **2012**, *109*, 5633−5638.
(489) Phillips, C. M.; Schreiter, E. R.; Stultz, C. M.; Drennan, C. L. Structural Basis of Low-Affinity Nickel Binding to the Nickel-Responsive Transcription Factor NikR from *Escherichia coli*. *Biochemistry* **2010**, *49*, 7830−7838.
(490) Baksh, K. A.; Augustine, J.; Sljoka, A.; Prosser, R. S.; Zamble, D. B. Mechanistic Insights into the Nickel-Dependent Allosteric Response of the *Helicobacter pylori* NikR Transcription Factor. *J. Biol. Chem.* **2023**, *299*, 102785.
(491) Wang, S. C.; Dias, A. V.; Bloom, S. L.; Zamble, D. B. Selectivity of Metal Binding and Metal-Induced Stability of *Escherichia coli* NikR. *Biochemistry* **2004**, *43*, 10018−10028.
(492) Chivers, P. T.; Sauer, R. T. NikR Repressor: High-Affinity Nickel Binding to the C-Terminal Domain Regulates Binding to Operator DNA. *Chem. Biol.* **2002**, *9*, 1141−1148.
(493) Zambelli, B.; Danielli, A.; Romagnoli, S.; Neyroz, P.; Ciurli, S.; Scarlato, V. High-Affinity Ni^{2+} Binding Selectively Promotes Binding of *Helicobacter pylori* NikR to Its Target Urease Promoter. *J. Mol. Biol.* **2008**, *383*, 1129−1143.
(494) Danielli, A.; Scarlato, V. Regulatory Circuits in *Helicobacter pylori*: Network Motifs and Regulators Involved in Metal-Dependent Responses. *FEMS Microbiol Rev.* **2010**, *34*, 738−752.
(495) Li, Y.; Zamble, D. B. pH-Responsive DNA-Binding Activity of *Helicobacter pylori* NikR. *Biochemistry* **2009**, *48*, 2486−2496.
(496) Shepard, W.; Soutourina, O.; Courtois, E.; England, P.; Haouz, A.; Martin-Verstraete, I.al. Insights into the Rrf2 Repressor Family - The Structure of CymR, the Global Cysteine Regulator of *Bacillus subtilis*. *FEBS J.* **2011**, *278*, 2689−2701.
(497) Volbeda, A.; Martinez, M. T. P.; Crack, J. C.; Amara, P.; Gigarel, O.; Munnoch, J. T.; Hutchings, M. I.; Darnault, C.; Le Brun, N. E.; Fontecilla-Camps, J. C. Crystal Structure of the Transcription Regulator RsrR Reveals a [2Fe-2S] Cluster Coordinated by Cys, Glu, and His Residues. *J. Am. Chem. Soc.* **2019**, *141*, 2367−2375.
(498) Volbeda, A.; Dodd, E. L.; Darnault, C.; Crack, J. C.; Renoux, O.; Hutchings, M. I.; Le Brun, N. E.; Fontecilla-Camps, J. C Crystal Structures of the NO Sensor NsrR Reveal How Its Iron-Sulfur Cluster Modulates DNA Binding. *Nat. Commun.* **2017**, *8*, 15052.
(499) Keon, R. G.; Fu, R.; Voordouw, G. Deletion of Two Downstream Genes Alters Expression of the Hmc Operon of *Desulfovibrio Vulgaris* Subsp. Vulgaris Hildenborough. *Arch. Microbiol.* **1997**, *167*, 376−383.
(500) Fleischhacker, A. S.; Stubna, A.; Hsueh, K. L.; Guo, Y.; Teter, S. J.; Rose, J. C.; Brunold, T. C.; Markley, J. L.; Münck, E.; Kiley, P. J. Characterization of the [2Fe-2S] Cluster of *Escherichia coli* Transcription Factor IscR. *Biochemistry* **2012**, *51*, 4453−4462.
(501) Tanous, C.; Soutourina, O.; Raynal, B.; Hullo, M. F.; Mervelet, P.; Gilles, A. M.; Noirot, P.; Danchin, A.; England, P.; Martin-Verstraete, I. The CymR Regulator in Complex with the Enzyme CysK Controls Cysteine Metabolism in *Bacillus Subtilis*. *J. Biol. Chem.* **2008**, *283*, 35551−35560.
(502) Even, S.; Burguiere, P.; Auger, S.; Soutourina, O.; Danchin, A.; Martin-Verstraete, I. Global Control of Cysteine Metabolism by CymR in *Bacillus subtilis* Global Control of Cysteine Metabolism by CymR in *Bacillus subtilis*. *J. Bacteriol.* **2006**, *188*, 2184−2197.
(503) Pellicer Martinez, M. T.; Martinez, A. B.; Crack, J. C.; Holmes, J. D.; Svistunenko, D. A.; Johnston, A. W. B.; Cheesman, M. R.; Todd, J. D.; Le Brun, N. E. Sensing Iron Availability *via* the Fragile [4Fe-4S] Cluster of the Bacterial Transcriptional Repressor RirA. *Chem. Sci.* **2017**, *8*, 8451−8463.
(504) Pellicer Martinez, M. T.; Crack, J. C.; Stewart, M. Y.; Bradley, J. M.; Svistunenko, D. A.; Johnston, A. W.; Cheesman, M. R.; Todd, J. D.; Le Brun, N. E. Mechanisms of Iron- and O_2-Sensing by the [4Fe-4S] Cluster of the Global Iron Regulator RirA. *Elife* **2019**, *8*, No. e47804.
(505) Crack, J. C.; Amara, P.; Volbeda, A.; Mouesca, J.-M.; Rohac, R.; Pellicer Martinez, M. T.; Huang, C.-Y.; Gigarel, O.; Rinaldi, C.; Le Brun, N. E.; Fontecilla-Camps, J. C. Electron and Proton Transfers Modulate DNA Binding by the Transcription Regulator RsrR. *J. Am. Chem. Soc.* **2020**, *142*, 5104−5116.
(506) Loi, V. V.; Busche, T.; Tedin, K.; Bernhardt, J.; Wollenhaupt, J.; Huyen, N. T. T.; Weise, C.; Kalinowski, J.; Wahl, M. C.; Fulde, M.; Antelmann, H. Redox-Sensing Under Hypochlorite Stress and Infection Conditions by the Rrf2-Family Repressor HypR in *Staphylococcus aureus*. *Antioxid Redox Signal* **2018**, *29*, 615−636.
(507) Nakano, M. M.; Kominos-Marvell, W.; Sane, B.; Nader, Y. M.; Barendt, S. M.; Jones, M. B.; Zuber, P. SpxA2, Encoding a Regulator of

Stress Resistance in *Bacillus anthracis*, Is Controlled by SaiR, a New Member of the Rrf2 Protein Family. *Mol. Microbiol.* **2014**, *94*, 815−827.
(508) Nakano, M. M.; Geng, H.; Nakano, S.; Kobayashi, K. The Nitric Oxide-Responsive Regulator NsrR Controls ResDE-Dependent Gene Expression. *J. Bacteriol.* **2006**, *188*, 5878−5887.
(509) Munnoch, J. T.; Martinez, M. T. P.; Svistunenko, D. A.; Crack, J. C.; Le Brun, N. E.; Hutchings, M. I. Characterization of a Putative NsrR Homologue in *Streptomyces venezuelae* Reveals a New Member of the Rrf2 Superfamily. *Sci. Rep* **2016**, *6*, 31597.
(510) Crack, J. C.; Gray, E.; Le Brun, N. E. Sensing Mechanisms of Iron-Sulfur Cluster Regulatory Proteins Elucidated Using Native Mass Spectrometry. *Dalton Trans* **2021**, *50*, 7887−7897.
(511) Giel, J. L.; Nesbit, A. D.; Mettert, E. L.; Fleischhacker, A. S.; Wanta, B. T.; Kiley, P. J. Regulation of Iron-Sulphur Cluster Homeostasis through Transcriptional Control of the Isc Pathway by [2Fe-2S]-IscR in *Escherichia coli*. *Mol. Microbiol.* **2013**, *87*, 478−492.
(512) Hibbing, M. E.; Fuqua, C. Antiparallel and Interlinked Control of Cellular Iron Levels by the Irr and RirA Regulators of *Agrobacterium tumefaciens*. *J. Bacteriol.* **2011**, *193*, 3461−3472.
(513) Crack, J. C.; Munnoch, J.; Dodd, E. L.; Knowles, F.; Al Bassam, M. M.; Kamali, S.; Holland, A. A.; Cramer, S. P.; Hamilton, C. J.; Johnson, M. K.; et al. NsrR from *Streptomyces coelicolor* Is a Nitric Oxide-Sensing [4Fe-4S] Cluster Protein with a Specialized Regulatory Function. *J. Biol. Chem.* **2015**, *290*, 12689−12704.
(514) Yeo, W. S.; Lee, J. H.; Lee, K. C.; Roe, J. H. IscR Acts as an Activator in Response to Oxidative Stress for the *suf* Operon Encoding Fe-S Assembly Proteins. *Mol. Microbiol.* **2006**, *61*, 206−218.
(515) Ji, Q.; Zhang, L.; Sun, F.; Deng, X.; Liang, H.; Bae, T.; He, C. *Staphylococcus aureus* CymR Is a New Thiol-Based Oxidation-Sensing Regulator of Stress Resistance and Oxidative Response. *J. Biol. Chem.* **2012**, *287*, 21102−21109.
(516) Zhang, Y.; Edmonds, K. A.; Raines, D. J.; Murphy, B. A.; Wu, H.; Guo, C.; Nolan, E. M.; VanNieuwenhze, M. S.; Duhme-Klair, A. K.; Giedroc, D. P. The Pneumococcal Iron Uptake Protein A (PiuA) Specifically Recognizes Tetradentate Fe^{III} *bis*- and Mono-Catechol Complexes. *J. Mol. Biol.* **2020**, *432*, 5390−5410.
(517) Singh, B.; Arya, G.; Kundu, N.; Sangwan, A.; Nongthombam, S.; Chaba, R. Molecular and Functional Insights into the Regulation of D-Galactonate Metabolism by the Transcriptional Regulator DgoR in *Escherichia coli*. *J. Bacteriol.* **2019**, *201*, jb00281.
(518) Jain, D. Allosteric Control of Transcription in GntR Family of Transcription Regulators: A Structural Overview. *IUBMB Life* **2015**, *67*, 556−563.
(519) Suvorova, I. A.; Korostelev, Y. D.; Gelfand, M. S. GntR Family of Bacterial Transcription Factors and Their DNA Binding Motifs: Structure, Positioning and Co-Evolution. *PLoS One* **2015**, *10*, No. e0132618.
(520) Vindal, V.; Suma, K.; Ranjan, A. GntR Family of Regulators in *Mycobacterium smegmatis*: A Sequence and Structure Based Characterization. *BMC Genomics* **2007**, *8*, 1−12.
(521) Tsypik, O.; Yushchuk, O.; Zaburannyi, N.; Flärdh, K.; Walker, S.; Fedorenko, V.; Ostash, B. Transcriptional Regulators of GntR Family in *Streptomyces coelicolor* A3(2): Analysis in Silico and in Vivo of YtrA Subfamily. *Folia Microbiol* **2016**, *61*, 209−220.
(522) Rigali, S.; Derouaux, A.; Giannotta, F.; Dusart, J. Subdivision of the Helix-Turn-Helix GntR Family of Bacterial Regulators in the FadR, HutC, MocR, and YtrA Subfamilies. *J. Biol. Chem.* **2002**, *277*, 12507−12515.
(523) Rao, M.; Liu, H.; Yang, M.; Zhao, C.; He, Z.-G. A Copper-Responsive Global Repressor Regulates Expression of Diverse Membrane-Associated Transporters and Bacterial Drug Resistance in Mycobacteria. *J. Biol. Chem.* **2012**, *287*, 39721−39731.
(524) Blancato, V. S.; Pagliai, F. A.; Magni, C.; Gonzalez, C. F.; Lorca, G. L. Functional Analysis of the Citrate Activator CitO from *Enterococcus faecalis* Implicates a Divalent Metal in Ligand Binding. *Front Microbiol* **2016**, *7*, 1−12.
(525) Gao, Y. G.; Suzuki, H.; Itou, H.; Zhou, Y.; Tanaka, Y.; Wachi, M.; Watanabe, N.; Tanaka, I.; Yao, M. Structural and Functional Characterization of the LldR from *Corynebacterium glutamicum*: A Transcriptional Repressor Involved in L-Lactate and Sugar Utilization. *Nucleic Acids Res.* **2008**, *36*, 7110−7123.
(526) Lin, Z.; Sun, Y.; Liu, Y.; Tong, S.; Shang, Z.; Cai, Y.; Lin, W. Structural and Functional Analyses of the Transcription Repressor DgoR From *Escherichia coli* Reveal a Divalent Metal-Containing D-Galactonate Binding Pocket. *Front. Microbiol.* **2020**, *11*, 1−13.
(527) Bouvier, J. T.; Sernova, N. V.; Ghasempur, S.; Rodionova, I. A.; Vetting, M. W.; Al-Obaidi, N. F.; Almo, S. C.; Gerlt, J. A.; Rodionov, D. A. Novel Metabolic Pathways and Regulons for Hexuronate Utilization in Proteobacteria. *J. Bacteriol.* **2019**, *201*, jb00431.
(528) Arya, G.; Pal, M.; Sharma, M.; Singh, B.; Singh, S.; Agrawal, V.; Chaba, R. Molecular Insights into Effector Binding by DgoR, a GntR/FadR Family Transcriptional Repressor of D-Galactonate Metabolism in *Escherichia coli*. *Mol. Microbiol.* **2021**, *115*, 591−609.
(529) Tutukina, M. N.; Potapova, A. V.; Vlasov, P. K.; Purtov, Y. A.; Ozoline, O. N. Structural Modeling of the ExuR and UxuR Transcription Factors of *E. coli*: Search for the Ligands Affecting Their Regulatory Properties. *J. Biomol Struct Dyn* **2016**, *34*, 2296−2304.
(530) Perera, I. C.; Grove, A. Molecular Mechanisms of Ligand-Mediated Attenuation of DNA Binding by MarR Family Transcriptional Regulators. *J. Mol. Cell Biol.* **2010**, *2*, 243−254.
(531) Grove, A. MarR Family Transcription Factors. *Curr. Biol.* **2013**, *23*, R142−R143.
(532) Deochand, D. K.; Grove, A. MarR Family Transcription Factors: Dynamic Variations on a Common Scaffold. *Crit Rev. Biochem Mol. Biol.* **2017**, *52*, 595−613.
(533) Perera, I. C.; Grove, A. Molecular Mechanisms of Ligand-Mediated Attenuation of DNA Binding by MarR Family Transcriptional Regulators. *J. Mol. Cell Biol.* **2010**, *2*, 243−254.
(534) Hao, Z.; Lou, H.; Zhu, R.; Zhu, J.; Zhang, D.; Zhao, B. S.; Zeng, S.; Chen, X.; Chan, J.; He, C.; Chen, P. R. The Multiple Antibiotic Resistance Regulator MarR Is a Copper Sensor in *Escherichia coli*. *Nat. Chem. Biol.* **2014**, *10*, 21−28.
(535) Gao, Y.-R.; Li, D.-F.; Fleming, J.; Zhou, Y.-F.; Liu, Y.; Deng, J.-Y.; Zhou, L.; Zhou, J.; Zhu, G.-F.; Zhang, X.-E.; et al. Structural Analysis of the Regulatory Mechanism of MarR Protein Rv2887 in *M. tuberculosis*. *Sci. Rep* **2017**, *7*, 6471.
(536) Kim, Y.; Joachimiak, G.; Bigelow, L.; Babnigg, G.; Joachimiak, A. How Aromatic Compounds Block DNA Binding of HcaR Catabolite Regulator. *J. Biol. Chem.* **2016**, *291*, 13243−13256.
(537) Kim, M. Il; Cho, M. U.; Hong, M. Structure Analysis of *Bacillus cereus* MepR-like Transcription Regulator, BC0657, in Complex with Pseudo-Ligand Molecules. *Biochem. Biophys. Res. Commun.* **2015**, *458*, 644−649.
(538) Wilke, M. S.; Heller, M.; Creagh, A. L.; Haynes, C. A.; McIntosh, L. P.; Poole, K.; Strynadka, N. C. J. The Crystal Structure of MexR from *Pseudomonas aeruginosa* in Complex with Its Antirepressor ArmR. *Proc. Natl. Acad. Sci. U. S. A.* **2008**, *105*, 14832−14837.
(539) Liguori, A.; Malito, E.; Lo Surdo, P.; Fagnocchi, L.; Cantini, F.; Haag, A. F.; Brier, S.; Pizza, M.; Delany, I.; Bottomley, M. J. Molecular Basis of Ligand-Dependent Regulation of NadR, the Transcriptional Repressor of Meningococcal Virulence Factor NadA. *PLoS Pathog* **2016**, *12*, e1005557.
(540) Perera, I. C.; Grove, A. Urate Is a Ligand for the Transcriptional Regulator PecS. *J. Mol. Biol.* **2010**, *402*, 539−551.
(541) Yu, L.; Fang, J.; Wei, Y. Characterization of the Ligand and DNA Binding Properties of a Putative Archaeal Regulator ST1710. *Biochemistry* **2009**, *48*, 2099−2108.
(542) Chang, Y. M.; Chen, C. K. M.; Ko, T. P.; et al. Structural Analysis of the Antibiotic-Recognition Mechanism of MarR Proteins. *Acta Crystallogr. D Biol. Crystallogr.* **2013**, *69*, 1138−1149.
(543) Gupta, A.; Grove, A. Ligand-Binding Pocket Bridges DNA-Binding and Dimerization Domains of the Urate-Responsive Marr Homologue MftR from *Burkholderia thailandensis*. *Biochemistry* **2014**, *53*, 4368−4380.
(544) Lim, D.; Poole, K.; Strynadka, N. C. J. Crystal Structure of the MexR Repressor of the MexRAB-OprM Multidrug Efflux Operon of *Pseudomonas aeruginosa*. *J. Biol. Chem.* **2002**, *277*, 29253−29259.

https://doi.org/10.1021/acs.chemrev.4c00264
Chem. Rev. 2024, 124, 13574−13659

(545) Otani, H.; Stogios, P. J.; Xu, X.; Nocek, B.; Li, S.-N.; Savchenko, A.; Eltis, L. D. The Activity of CouR, a MarR Family Transcriptional Regulator, Is Modulated through a Novel Molecular Mechanism. *Nucleic Acids Res.* **2016**, *44*, 595−607.
(546) Zuo, G.; Chen, Z. P.; Jiang, Y. L.; Zhu, Z.; Ding, C.; Zhang, Z.; Chen, Y.; Zhou, C. Z.; Li, Q. Structural Insights into Repression of the Pneumococcal Fatty Acid Synthesis Pathway by Repressor FabT and Co-Repressor Acyl-ACP. *FEBS Lett.* **2019**, *593*, 2730−2741.
(547) Liu, G.; Liu, X.; Xu, H.; Liu, X.; Zhou, H.; Huang, Z.; Gan, J.; Chen, H.; Lan, L.; Yang, C.-G. Structural Insights into the Redox-Sensing Mechanism of MarR-Type Regulator AbfR. *J. Am. Chem. Soc.* **2017**, *139*, 1598−1608.
(548) Dolan, K. T.; Duguid, E. M.; He, C. Crystal Structures of SlyA Protein, a Master Virulence Regulator of Salmonella, in Free and DNA-Bound States. *J. Biol. Chem.* **2011**, *286*, 22178−22185.
(549) Chen, P. R.; Bae, T.; Williams, W. A.; et al. An Oxidation-Sensing Mechanism Is Used by the Global Regulator MgrA in *Staphylococcus aureus*. *Nat. Chem. Biol.* **2006**, *2*, 591−595.
(550) Lee, J.-W.; Soonsanga, S.; Helmann, J. D. A Complex Thiolate Switch Regulates the *Bacillus Subtilis* Organic Peroxide Sensor OhrR. *Proc. Natl. Acad. Sci. U. S. A.* **2007**, *104*, 8743−8748.
(551) Fuangthong, M.; Helmann, J. D. The OhrR Repressor Senses Organic Hydroperoxides by Reversible Formation of a Cysteine-Sulfenic Acid Derivative. *Proc. Natl. Acad. Sci. U. S. A.* **2002**, *99*, 6690−6695.
(552) Xu, H.; Xuan, G.; Liu, H.; Liu, H.; Xia, Y.; Xun, L. Sulfane Sulfur Is an Intrinsic Signal for the Organic Peroxide Sensor OhrR of *Pseudomonas aeruginosa*. *Antioxidants* **2022**, *11*, 1667.
(553) Newberry, K. J.; Fuangthong, M.; Panmanee, W.; Mongkolsuk, S.; Brennan, R. G. Structural Mechanism of Organic Hydroperoxide Induction of the Transcription Regulator OhrR. *Mol. Cell* **2007**, *28*, 652−64.
(554) Hong, M.; Fuangthong, M.; Helmann, J. D.; Brennan, R. G. Structure of an OhrR-OhrA Operator Complex Reveals the DNA Binding Mechanism of the MarR Family. *Mol. Cell* **2005**, *20*, 131−141.
(555) Chen, H.; Yi, C.; Zhang, J.; Zhang, W.; Ge, Z.; Yang, C.-G.; He, C. Structural Insight into the Oxidation-Sensing Mechanism of the Antibiotic Resistance of Regulator MexR. *EMBO Rep* **2010**, *11*, 685−90.
(556) Poor, C. B.; Chen, P. R.; Duguid, E.; Rice, P. A.; He, C. Crystal Structures of the Reduced, Sulfenic Acid, and Mixed Disulfide Forms of SarZ, a Redox Active Global Regulator in *Staphylococcus aureus*. *J. Biol. Chem.* **2009**, *284*, 23517−23524.
(557) Martin, R. G.; Rosner, J. L. Binding of Purified Multiple Antibiotic-Resistance Repressor Protein (MarR) to Mar Operator Sequences. *Proc. Natl. Acad. Sci. U. S. A.* **1995**, *92*, 5456−5460.
(558) Xiong, A.; Gottman, A.; Park, C.; Baetens, M.; Pandza, S.; Matin, A. The EmrR Protein Represses the *Escherichia coli* EmrRAB Multidrug Resistance Operon by Directly Binding to Its Promoter Region. *Antimicrob. Agents Chemother.* **2000**, *44*, 2905−2907.
(559) Roy, A.; Ranjan, A. HosA, a MarR Family Transcriptional Regulator, Represses Nonoxidative Hydroxyarylic Acid Decarboxylase Operon and Is Modulated by 4-Hydroxybenzoic Acid. *Biochemistry* **2016**, *55*, 1120−1134.
(560) Will, W. R.; Fang, F. C. The Evolution of MarR Family Transcription Factors as Counter-Silencers in Regulatory Networks. *Curr. Opin Microbiol* **2020**, *55*, 1−8.
(561) Sanson, M.; Makthal, N.; Flores, A. R.; Olsen, R. J.; Musser, J. M.; Kumaraswami, M. Adhesin Competence Repressor (AdcR) from *Streptococcus pyogenes* Controls Adaptive Responses to Zinc Limitation and Contributes to Virulence. *Nucleic Acids Res.* **2015**, *43*, 418−432.
(562) Llull, D.; Son, O.; Blanié, S.; Briffotaux, J.; Morello, E.; Rogniaux, H.; Danot, O.; Poquet, I. *Lactococcus lactis* ZitR Is a Zinc-Responsive Repressor Active in the Presence of Low, Nontoxic Zinc Concentrations *in Vivo*. *J. Bacteriol.* **2011**, *193*, 1919−29.
(563) Guerra, A. J.; Dann, C. E.; Giedroc, D. P. Crystal Structure of the Zinc-Dependent MarR Family Transcriptional Regulator AdcR in the Zn(II)-Bound State. *J. Am. Chem. Soc.* **2011**, *133*, 19614−19617.
(564) Shafeeq, S.; Kloosterman, T. G.; Kuipers, O. P. Transcriptional Response of *Streptococcus pneumoniae* to Zn^{2+} Limitation and the Repressor/Activator Function of AdcR. *Metallomics* **2011**, *3*, 609−618.
(565) Reyes-Caballero, H.; Guerra, A. J.; Jacobsen, F. E.; Kazmierczak, K. M.; Cowart, D.; Koppolu, U. M. K.; Scott, R. A.; Winkler, M. E.; Giedroc, D. P. The Metalloregulatory Zinc Site in *Streptococcus pneumoniae* AdcR, a Zinc-Activated MarR Family Repressor. *J. Mol. Biol.* **2010**, *403*, 197−216.
(566) Varela, P. F.; Velours, C.; Aumont-Niçaise, M.; Pineau, B.; Legrand, P.; Poquet, I. Biophysical and Structural Characterization of a Zinc-Responsive Repressor of the MarR Superfamily. *PLoS One* **2019**, *14*, No. e0210123.
(567) Cao, K.; Li, N.; Wang, H.; Cao, X.; He, J.; Zhang, B.; He, Q. Y.; Zhang, G.; Sun, X. Two Zinc-Binding Domains in the Transporter AdcA from *Streptococcus pyogenes* Facilitate High-Affinity Binding and Fast Transport of Zinc. *J. Biol. Chem.* **2018**, *293*, 6075−6089.
(568) Zhu, R.; Song, Y.; Liu, H.; Yang, Y.; Wang, S.; Yi, C.; Chen, P. R. Allosteric Histidine Switch for Regulation of Intracellular Zinc(II) Fluctuation. *Proc. Natl. Acad. Sci. U. S. A.* **2017**, *114*, 13661−13666.
(569) Makthal, N.; Nguyen, K.; Do, H.; Gavagan, M.; Chandrangsu, P.; Helmann, J. D.; Olsen, R. J.; Kumaraswami, M. A Critical Role of Zinc Importer AdcABC in Group A Streptococcus -Host Interactions During Infection and Its Implications for Vaccine Development. *EBioMedicine* **2017**, *21*, 131−141.
(570) Randazzo, P.; Aubert-Frambourg, A.; Guillot, A.; Auger, S. The MarR-like Protein PchR (YvmB) Regulates Expression of Genes Involved in Pulcherriminic Acid Biosynthesis and in the Initiation of Sporulation in *Bacillus subtilis*. *BMC Microbiol* **2016**, *16*, 1−16.
(571) Chen, H.; Hu, J.; Chen, P. R.; Lan, L.; Li, Z.; Hicks, L. M.; Dinner, A. R.; He, C. The *Pseudomonas aeruginosa* Multidrug Efflux Regulator MexR Uses an Oxidation-Sensing Mechanism. *Proc. Natl. Acad. Sci. U. S. A.* **2008**, *105*, 13586−91.
(572) Xuan, G.; Chuanjuan, L.; Xu, H.; Chen, Z.; Li, K.; Liu, H.; Liu, H.; Xia, Y.; Xun, L. Sulfane Sulfur Is an Intrinsic Signal Activating MexR-Regulated Antibiotic Resistance in *Pseudomonas aeruginosa*. *Mol. Microbiol.* **2020**, *114*, 1038−1048.
(573) Zhu, R.; Hao, Z.; Lou, H.; Song, Y.; Zhao, J.; Chen, Y.; Zhu, J.; Chen, P. R. Structural Characterization of the DNA-Binding Mechanism Underlying the Copper(II)-Sensing MarR Transcriptional Regulator. *J. Biol. Inorg. Chem.* **2017**, *22*, 685−693.
(574) Cuthbertson, L.; Nodwell, J. R. The TetR Family of Regulators. *Microbiol Mol. Biol. Rev.* **2013**, *77*, 440−475.
(575) Capdevila, D. A.; Edmonds, K. A.; Giedroc, D. P. Metallochaperones and Metalloregulation in Bacteria. *Essays Biochem* **2017**, *61*, 177−200.
(576) Zotta, T.; Ricciardi, A.; Ianniello, R. G.; Parente, E.; Reale, A.; Rossi, F.; Iacumin, L.; Comi, G.; Coppola, R. Assessment of Aerobic and Respiratory Growth in the *Lactobacillus casei* Group. *PLoS One* **2014**, *9*, No. e99189.
(577) Sawai, H.; Yamanaka, M.; Sugimoto, H.; Shiro, Y.; Aono, S. Structural Basis for the Transcriptional Regulation of Heme Homeostasis in *Lactococcus lactis*. *J. Biol. Chem.* **2012**, *287*, 30755−30768.
(578) Gray, M. J.; Li, Y.; Leichert, L. I.-O.; Xu, Z.; Jakob, U. Does the Transcription Factor NemR Use a Regulatory Sulfenamide Bond to Sense Bleach? *Antioxid Redox Signal* **2015**, *23*, 747−754.
(579) Shi, K.; Radhakrishnan, M.; Dai, X.; Rosen, B. P.; Wang, G. NemA Catalyzes Trivalent Organoarsenical Oxidation and Is Regulated by the Trivalent Organoarsenical-Selective Transcriptional Repressor NemR. *Environ. Sci. Technol.* **2021**, *55*, 6485−6494.
(580) Ray, A.; Edmonds, K. A.; Palmer, L. D.; Skaar, E. P.; Giedroc, D. P. *Staphylococcus aureus* Glucose-Induced Biofilm Accessory Protein A (GbaA) Is a Monothiol-Dependent Electrophile Sensor. *Biochemistry* **2020**, *59*, 2882−2895.
(581) Van Loi, V.; Busche, T.; Fritsch, V. N.; Weise, C.; Gruhlke, M. C. H.; Slusarenko, A. J.; Kalinowski, J.; Antelmann, H. The Two-Cys-Type TetR Repressor GbaA Confers Resistance under Disulfide and Electrophile Stress in *Staphylococcus aureus*. *Free Radic Biol. Med.* **2021**, *177*, 120−131.

https://doi.org/10.1021/acs.chemrev.4c00264
Chem. Rev. 2024, 124, 13574−13659

(582) Murarka, P.; Bagga, T.; Singh, P.; Rangra, S.; Srivastava, P. Isolation and Identification of a TetR Family Protein That Regulates the Biodesulfurization Operon. *AMB Express* **2019**, *9*, 1−16.
(583) Kloosterman, T. G.; Van Der Kooi-Pol, M. M.; Bijlsma, J. J. E.; Kuipers, O. P. The Novel Transcriptional Regulator SczA Mediates Protection against Zn^{2+} Stress by Activation of the Zn^{2+}-Resistance Gene CzcD in *Streptococcus pneumoniae*. *Mol. Microbiol.* **2007**, *65*, 1049−1063.
(584) Young, T. R.; Xiao, Z. Principles and Practice of Determining Metal-Protein Affinities. *Biochem. J.* **2021**, *478*, 1085−1116.
(585) Xu, X.; Zhang, L.; Cui, Y.; Kong, J.; Guo, T. Development of Zn^{2+}-Controlled Expression System for Lactic Acid Bacteria and Its Application in Engineered Probiotics. *Synth Syst. Biotechnol* **2024**, *9*, 152−158.
(586) Große, C.; Schleuder, G.; Schmole, C.; Nies, D. H. Survival of *Escherichia coli* Cells on Solid Copper Surfaces Is Increased by Glutathione. *Appl. Environ. Microbiol.* **2014**, *80*, 7071−7078.
(587) Mermod, M.; Magnani, D.; Solioz, M.; Stoyanov, J. V. The Copper-Inducible ComR (YcfQ) Repressor Regulates Expression of ComC (YcfR), Which Affects Copper Permeability of the Outer Membrane of *Escherichia coli*. *BioMetals* **2012**, *25*, 33−43.
(588) Mayo-Pérez, S.; Gama-Martínez, Y.; Dávila, S.; Rivera, N.; Hernández-Lucas, I. LysR-Type Transcriptional Regulators: State of the Art. *Crit Rev. Microbiol* **2023**, *50*, 598−630.
(589) Choi, H.-J.; Kim, S.-J.; Mukhopadhyay, P.; Cho, S.; Woo, J.-R.; Storz, G.; Ryu, S.-E. Structural Basis of the Redox Switch in the OxyR Transcription Factor. *Cell* **2001**, *105*, 103−113.
(590) Hillion, M.; Antelmann, H. Thiol-Based Redox Switches in Prokaryotes. *Biol. Chem.* **2015**, *396*, 415−444.
(591) Hoffmann, M.-C.; Ali, K.; Sonnenschein, M.; Robrahn, L.; Strauss, D.; Narberhaus, F.; Masepohl, B. Molybdate Uptake by *Agrobacterium tumefaciens* Correlates with the Cellular Molybdenum Cofactor Status. *Mol. Microbiol.* **2016**, *101*, 809−822.
(592) Xuan, G.; Lv, C.; Xu, H.; Li, K.; Liu, H.; Xia, Y.; Xun, L. Sulfane Sulfur Regulates LasR-Mediated Quorum Sensing and Virulence in *Pseudomonas aeruginosa* PAO1. *Antioxidants* **2021**, *10*, 1498.
(593) Bang, Y. J.; Lee, Z. W.; Kim, D.; Jo, I.; Ha, N. C.; Choi, S. H. OxyR2 Functions as a Three-State Redox Switch to Tightly Regulate Production of Prx2, a Peroxiredoxin of *Vibrio vulnificus*. *J. Biol. Chem.* **2016**, *291*, 16038−16047.
(594) Antelmann, H. *Chapter 13 - Oxidative Stress Responses and Redox Signalling Mechanisms in Bacillus Subtilis and Staphylococcus aureus*; Elsevier Ltd, 2015.
(595) Åslund, F.; Zheng, M.; Beckwith, J.; Storz, G. Regulation of the OxyR Transcription Factor by Hydrogen Peroxide and the Cellular Thiol - Disulfide Status. *Proc. Natl. Acad. Sci. U. S. A.* **1999**, *96*, 6161−6165.
(596) Pedre, B.; Young, D.; Charlier, D.; Mourenza, Á.; Rosado, L. A.; Marcos-Pascual, L.; Wahni, K.; Martens, E.; de la Rubia, A. G.; Belousov, V. V.; et al. Structural Snapshots of OxyR Reveal the Peroxidatic Mechanism of H_2O_2 Sensing. *Proc. Natl. Acad. Sci. U. S. A.* **2018**, *115*, No. e11623-e11632.
(597) Schüttelkopf, A. W.; Boxer, D. H.; Hunter, W. N. Crystal Structure of Activated ModE Reveals Conformational Changes Involving Both Oxyanion and DNA-Binding Domains. *J. Mol. Biol.* **2003**, *326*, 761−767.
(598) Wedekind, J. E.; Dutta, D.; Belashov, I. A.; Jenkins, J. L. Metalloriboswitches: RNA-Based Inorganic Ion Sensors That Regulate Genes. *J. Biol. Chem.* **2017**, *292*, 9441−9450.
(599) Breaker, R. R. The Biochemical Landscape of Riboswitch Ligands. *Biochemistry* **2022**, *61*, 137−149.
(600) Regulski, E. E.; Moy, R. H.; Weinberg, Z.; Barrick, J. E.; Yao, Z.; Ruzzo, W. L.; Breaker, R. R. A Widespread Riboswitch Candidate That Controls Bacterial Genes Involved in Molybdenum Cofactor and Tungsten Cofactor Metabolism. *Mol. Microbiol.* **2008**, *68*, 918−932.
(601) Lofgren, M.; Padovani, D.; Koutmos, M.; Banerjee, R. A Switch III Motif Relays Signaling between a B12 Enzyme and Its G-Protein Chaperone. *Nat. Chem. Biol.* **2013**, *9*, 535−541.
(602) Xu, J.; Cotruvo, J. A. Iron-Responsive Riboswitches. *Curr. Opin Chem. Biol.* **2022**, *68*, 102135.
(603) Baker, J. L.; Sudarsan, N.; Weinberg, Z.; Roth, A.; Stockbridge, R. B.; Breaker, R. R. *Widespread Genetic Switches and Toxicity Resistance Proteins for Fluoride*. **2012**, *335*, 233−235.
(604) White, N.; Sadeeshkumar, H.; Sun, A.; Sudarsan, N.; Breaker, R. R. Na+ Riboswitches Regulate Genes for Diverse Physiological Processes in Bacteria. *Nat. Chem. Biol.* **2022**, *18*, 878−885.
(605) Sherlock, M. E.; Sudarsan, N.; Stav, S.; Breaker, R. R. Tandem Riboswitches Form a Natural Boolean Logic Gate to Control Purine Metabolism in Bacteria. *Elife* **2018**, *7*, No. e33908.
(606) Price, I. R.; Gaballa, A.; Ding, F.; Helmann, J. D.; Ke, A. Mn^{2+}-Sensing Mechanisms of YybP-YkoY Orphan Riboswitches. *Mol. Cell* **2015**, *57*, 1110−1123.
(607) Xu, J.; Cotruvo, J. A. Reconsidering the CzcD (NiCo) Riboswitch as an Iron Riboswitch. *ACS Bio Med. Chem. Au* **2022**, *2*, 376−385.
(608) Kennedy, K. J.; Widner, F. J.; Sokolovskaya, O. M.; Innocent, L. V.; Procknow, R. R.; Mok, K. C.; Taga, M. E. Cobalamin Riboswitches Are Broadly Sensitive to Corrinoid Cofactors to Enable an Efficient Gene Regulatory Strategy. *mBio* **2022**, *13*, mbio01121.
(609) Updegrove, T. B.; Storz, G.; Sandoval, M.; Dambach, M.; Aravind, L.; Anantharaman, V.; Waters, L. S. The Ubiquitous YybP-YkoY Riboswitch Is a Manganese-Responsive Regulatory Element. *Mol. Cell* **2015**, *57*, 1099−1109.
(610) Sung, H.-L.; Nesbitt, D. J. Single-Molecule FRET Kinetics of the Mn^{2+} Riboswitch: Evidence for Allosteric Mg^{2+} Control of "Induced-Fit" vs "Conformational Selection" Folding Pathways. *J. Phys. Chem. B* **2019**, *123*, 2005−2015.
(611) Suddala, K. C.; Price, I. R.; Dandpat, S. S.; Janeček, M.; Kührová, P.; Šponer, J.; Banáš, P.; Ke, A.; Walter, N. G. Local-to-Global Signal Transduction at the Core of a Mn^{2+} Sensing Riboswitch. *Nat. Commun.* **2019**, *10*, 4304.
(612) Bachas, S. T.; Ferré-D'Amaré, A. R. Convergent Use of Heptacoordination for Cation Selectivity by RNA and Protein Metalloregulators. *Cell Chem. Biol.* **2018**, *25*, 962.
(613) Anton, A.; Große, C.; Reißmann, J.; Pribyl, T.; Nies, D. H. CzcD Is a Heavy Metal Ion Transporter Involved in Regulation of Heavy Metal Resistance in *Ralstonia sp*. Strain CH34. *J. Bacteriol.* **1999**, *181*, 6876−6881.
(614) Nies, D. H.; Nies, A.; Chu, L.; Silver, S. Expression and Nucleotide Sequence of a Plasmid-Determined Divalent Cation Efflux System from *Alcaligenes eutrophus*. *Proc. Natl. Acad. Sci. U. S. A.* **1989**, *86*, 7351−7355.
(615) Bradley, M. J.; Chivers, P. T.; Baker, N. A. Molecular Dynamics Simulation of the *Escherichia coli* NikR Protein: Equilibrium Conformational Fluctuations Reveal Interdomain Allosteric Communication Pathways. *J. Mol. Biol.* **2008**, *378*, 1155−1173.
(616) Zambelli, B.; Bellucci, M.; Danielli, A.; Scarlato, V.; Ciurli, S. The Ni^{2+} Binding Properties of *Helicobacter pylori* NikR. *Chem. Commun. (Camb)* **2007**, 3649−3651.
(617) Ren, A.; Rajashankar, K. R.; Patel, D. J. Fluoride Ion Encapsulation by Mg^{2+} Ions and Phosphates in a Fluoride Riboswitch. *Nature* **2012**, *486*, 85−89.
(618) Thavarajah, W.; Silverman, A. D.; Verosloff, M. S.; Kelley-Loughnane, N.; Jewett, M. C.; Lucks, J. B. Point-of-Use Detection of Environmental Fluoride via a Cell-Free Riboswitch-Based Biosensor. *ACS Synth. Biol.* **2020**, *9*, 10−18.
(619) Vörösmarty, C. J.; McIntyre, P. B.; Gessner, M. O.; Dudgeon, D.; Prusevich, A.; Green, P.; Glidden, S.; Bunn, S. E.; Sullivan, C. A.; Liermann, C. R.; Davies, P. M. Global Threats to Human Water Security and River Biodiversity. *Nature* **2010**, *467*, 555−561.
(620) Jung, J. K.; Archuleta, C. M.; Alam, K. K.; Lucks, J. B. Programming Cell-Free Biosensors with DNA Strand Displacement Circuits. *Nat. Chem. Biol.* **2022**, *18*, 385−393.
(621) Berset, Y.; Merulla, D.; Joublin, A.; Hatzimanikatis, V.; Van Der Meer, J. R. Mechanistic Modeling of Genetic Circuits for ArsR Arsenic Regulation. *ACS Synth. Biol.* **2017**, *6*, 862−874.

https://doi.org/10.1021/acs.chemrev.4c00264
Chem. Rev. 2024, 124, 13574−13659

(622) Beabout, K.; Bernhards, C. B.; Thakur, M.; Turner, K. B.; Cole, S. D.; Walper, S. A.; Chávez, J. L.; Lux, M. W. Optimization of Heavy Metal Sensors Based on Transcription Factors and Cell-Free Expression Systems. *ACS Synth. Biol.* **2021**, *10*, 3040−3054.
(623) Novichkov, P. S.; Kazakov, A. E.; Ravcheev, D. A.; Leyn, S. A.; Kovaleva, G. Y.; Sutormin, R. A.; Kazanov, M. D.; Riehl, W.; Arkin, A. P.; Dubchak, I.; Rodionov, D. A. RegPrecise 3.0 - A Resource for Genome-Scale Exploration of Transcriptional Regulation in Bacteria. *BMC Genomics* **2013**, *14*, 745.
(624) d' Oelsnitz, S.; Stofel, S. K.; Love, J. D.; Ellington, A. D. Snowprint: A Predictive Tool for Genetic Biosensor Discovery. *Commun. Biol.* **2024**, *7*, 163.
(625) Santos-Zavaleta, A.; Salgado, H.; Gama-Castro, S.; Sánchez-Pérez, M.; Gómez-Romero, L.; Ledezma-Tejeida, D.; García-Sotelo, J. S.; Alquicira-Hernández, K.; Muñiz-Rascado, L. J.; Peña-Loredo, P.; et al. RegulonDB v 10.5: Tackling Challenges to Unify Classic and High Throughput Knowledge of Gene Regulation in *E. coli* K-12. *Nucleic Acids Res.* **2019**, *47*, D212−D220.
(626) Omidi, S.; Zavolan, M.; Pachkov, M.; Breda, J.; Berger, S.; van Nimwegen, E. Automated Incorporation of Pairwise Dependency in Transcription Factor Binding Site Prediction Using Dinucleotide Weight Tensors. *PLoS Comput. Biol.* **2017**, *13*, e1005176.
(627) d' Oelsnitz, S.; Love, J. D.; Diaz, D. J.; Ellington, A. D. GroovDB: A Database of Ligand-Inducible Transcription Factors. *ACS Synth. Biol.* **2022**, *11*, 3534−3537.
(628) Thavarajah, W.; Verosloff, M. S.; Jung, J. K.; Alam, K. K.; Miller, J. D.; Jewett, M. C.; Young, S. L.; Lucks, J. B. A Primer on Emerging Field-Deployable Synthetic Biology Tools for Global Water Quality Monitoring. *NPJ. Clean Water* **2020**, *3*, 18.
(629) d'Oelsnitz, S.; Nguyen, V.; Alper, H. S.; Ellington, A. D. Evolving a Generalist Biosensor for Bicyclic Monoterpenes. *ACS Synth. Biol.* **2022**, *11*, 265−272.
(630) Hou, Q.; Ma, A.; Wang, T.; Lin, J.; Wang, H.; du, B.; Zhuang, X.; Zhuang, G. Detection of Bioavailable Cadmium, Lead, and Arsenic in Polluted Soil by Tailored Multiple *Escherichia coli* Whole-Cell Sensor Set. *Anal Bioanal Chem.* **2015**, *407*, 6865−6871.
(631) Chen, S.; Chen, X.; Su, H.; Guo, M.; Liu, H. Advances in Synthetic-Biology-Based Whole-Cell Biosensors: Principles, Genetic Modules, and Applications in Food Safety. *Int. J. Mol. Sci.* **2023**, *24*, 7989.
(632) Kaur, P.; Rosen, B. P. Plasmid-Encoded Resistance to Arsenic and Antimony. *Plasmid* **1992**, *27*, 29−40.
(633) Ji, G.; Silver, S. Regulation and Expression of the Arsenic Resistance Operon from *Staphylococcus aureus* Plasmid pI258. *J. Bacteriol.* **1992**, *174*, 3684−3694.
(634) Stocker, J.; Balluch, D.; Gsell, M.; Harms, H.; Feliciano, J.; Daunert, S.; Malik, K. A.; Van der Meer, J. R. Development of a Set of Simple Bacterial Biosensors for Quantitative and Rapid Measurements of Arsenite and Arsenate in Potable Water. *Environ. Sci. Technol.* **2003**, *37*, 4743−4750.
(635) Hui, C. Y.; Liu, M. Q.; Guo, Y. Synthetic Bacteria Designed Using Ars Operons: A Promising Solution for Arsenic Biosensing and Bioremediation. *World J. Microbiol. Biotechnol.* **2024**, *40*, 1−17.
(636) Tauriainen, S.; Karp, M.; Chang, W.; Virta, M. Recombinant Luminescent Bacteria for Measuring Bioavailable Arsenite and Antimonite. *Appl. Environ. Microbiol.* **1997**, *63*, 4456−4461.
(637) Hynninen, A.; Tõnismann, K.; Virta, M. Improving the Sensitivity of Bacterial Bioreporters for Heavy Metals. *Bioeng Bugs* **2010**, *1*, 132−138.
(638) Kaur, H.; Kumar, R.; Babu, J. N.; Mittal, S. Advances in Arsenic Biosensor Development - A Comprehensive Review. *Biosens Bioelectron* **2015**, *63*, 533−545.
(639) Barone, F.; Dorr, F.; Marasco, L. E.; Mildiner, S.; Patop, I. L.; Sosa, S.; Vattino, L. G.; Vignale, F. A.; Altszyler, E.; Basanta, B.; et al. Design and Evaluation of an Incoherent Feed-Forward Loop for an Arsenic Biosensor Based on Standard IGEM Parts. *Synth Biol.* **2017**, *2*, 1−10.
(640) Chen, J.; Zhu, Y. G.; Rosen, B. P. A Novel Biosensor Selective for Organoarsenicals. *Appl. Environ. Microbiol.* **2012**, *78*, 7145−7147.
(641) Chen, J.; Galván, A. E.; Nadar, V. S.; Yoshinaga, M.; Rosen, B. P. An ArsRC Fusion Protein Enhances Arsenate Sensing and Detoxification. *Environ. Microbiol* **2022**, *24*, 1977−1987.
(642) Kim, H. J.; Lim, J. W.; Jeong, H.; Lee, S. J.; Lee, D. W.; Kim, T.; Lee, S. J. Development of a Highly Specific and Sensitive Cadmium and Lead Microbial Biosensor Using Synthetic CadC-T7 Genetic Circuitry. *Biosens Bioelectron* **2016**, *79*, 701−708.
(643) Wei, W.; Liu, X.; Sun, P.; Wang, X.; Zhu, H.; Hong, M.; Mao, Z. W.; Zhao, J. Simple Whole-Cell Biodetection and Bioremediation of Heavy Metals Based on an Engineered Lead-Specific Operon. *Environ. Sci. Technol.* **2014**, *48*, 3363−3371.
(644) Li, P. S.; Peng, Z. W.; Su, J.; Tao, H. C. Construction and Optimization of a *Pseudomonas putida* Whole-Cell Bioreporter for Detection of Bioavailable Copper. *Biotechnol. Lett.* **2014**, *36*, 761−766.
(645) Cerminati, S.; Soncini, F. C.; Checa, S. K. Selective Detection of Gold Using Genetically Engineered Bacterial Reporters. *Biotechnol. Bioeng.* **2011**, *108*, 2553−2560.
(646) Michelini, E.; Cevenini, L.; Calabretta, M. M.; Spinozzi, S.; Camborata, C.; Roda, A. Field-Deployable Whole-Cell Bioluminescent Biosensors: So near and yet so far. *Anal Bioanal Chem.* **2013**, *405*, 6155−6163.
(647) Cao, J.; Yao, Y.; Fan, K.; Tan, G.; Xiang, W.; Xia, X.; Li, S.; Wang, W.; Zhang, L. Harnessing a Previously Unidentified Capability of Bacterial Allosteric Transcription Factors for Sensing Diverse Small Molecules *In vitro*. *Sci. Adv.* **2018**, *4*, No. eaau4602.
(648) Yao, Y.; Li, S.; Cao, J.; Liu, W.; Fan, K.; Xiang, W.; Yang, K.; Kong, D.; Wang, W. Development of Small Molecule Biosensors by Coupling the Recognition of the Bacterial Allosteric Transcription Factor with Isothermal Strand Displacement Amplification. *Chem. Commun.* **2018**, *54*, 4774−4777.
(649) Li, S.; Zhou, L.; Yao, Y.; Fan, K.; Li, Z.; Zhang, L.; Wang, W.; Yang, K. A Platform for the Development of Novel Biosensors by Configuring Allosteric Transcription Factor Recognition with Amplified Luminescent Proximity Homogeneous Assays. *Chem. Commun.* **2017**, *53*, 99−102.
(650) Khan, S. S.; Shen, Y.; Fatmi, M. Q.; Campbell, R. E.; Bokhari, H. Design and Prototyping of Genetically Encoded Arsenic Biosensors Based on Transcriptional Regulator *Af*ArsR. *Biomolecules* **2021**, *11*, 1276.
(651) Zhang, Y.; Zhao, C.; Bi, H.; Zhang, X.; Xue, B.; Li, C.; Wang, S.; Yang, X.; Qiu, Z.; Wang, J.; Shen, Z. A Cell-Free Paper-Based Biosensor Dependent on Allosteric Transcription Factors (ATFs) for on-Site Detection of Harmful Metals Hg^{2+} and Pb^{2+} in Water. *J. Hazard Mater.* **2022**, *438*, 129499.
(652) Wang, X.; Zhu, K.; Chen, D.; Wang, J.; Wang, X.; Xu, A.; Wu, L.; Li, L.; Chen, S. Monitoring Arsenic Using Genetically Encoded Biosensors *in vitro*: The Role of Evolved Regulatory Genes. *Ecotoxicol Environ. Saf* **2021**, *207*, 111273.
(653) Thavarajah, W.; Silverman, A. D.; Verosloff, M. S.; Kelley-Loughnane, N.; Jewett, M. C.; Lucks, J. B. Point-of-Use Detection of Environmental Fluoride via a Cell-Free Riboswitch-Based Biosensor. *ACS Synth. Biol.* **2020**, *9*, 10−18.
(654) Saunders, A. M.; DeRose, V. J. Beyond Mg^{2+}: Functional Interactions between RNA and Transition Metals. *Curr. Opin Chem. Biol.* **2016**, *31*, 153−159.
(655) Li, Y.; Arce, A.; Lucci, T.; Rasmussen, R. A.; Lucks, J. B. Dynamic RNA Synthetic Biology: New Principles, Practices and Potential. *RNA Biol.* **2023**, *20*, 817−829.
(656) Silverman, A. D.; Akova, U.; Alam, K. K.; Jewett, M. C.; Lucks, J. B. Design and Optimization of a Cell-Free Atrazine Biosensor. *ACS Synth. Biol.* **2020**, *9*, 671−677.
(657) Soudier, P.; Zúñiga, A.; Duigou, T.; Voyvodic, P. L.; Bazi-Kabbaj, K.; Kushwaha, M.; Vendrell, J. A.; Solassol, J.; Bonnet, J.; Faulon, J. L. PeroxiHUB: A Modular Cell-Free Biosensing Platform Using H2O2 as Signal Integrator. *ACS Synth. Biol.* **2022**, *11*, 2578−2588.
(658) Silverman, A. D.; Kelley-Loughnane, N.; Lucks, J. B.; Jewett, M. C. Deconstructing Cell-Free Extract Preparation for *in vitro* Activation

https://doi.org/10.1021/acs.chemrev.4c00264
Chem. Rev. 2024, 124, 13574−13659

of Transcriptional Genetic Circuitry. *ACS Synth. Biol.* **2019**, *8*, 403−414.
(659) Arce, A.; Guzman Chavez, F.; Gandini, C.; Puig, J.; Matute, T.; Haseloff, J.; Dalchau, N.; Molloy, J.; Pardee, K.; Federici, F. Decentralizing Cell-Free RNA Sensing With the Use of Low-Cost Cell Extracts. *Front Bioeng Biotechnol* **2021**, *9*, 727584.
(660) Brookwell, A. W.; Gonzalez, J. L.; Martinez, A. W.; Oza, J. P. Development of Solid-State Storage for Cell-Free Expression Systems. *ACS Synth. Biol.* **2023**, *12*, 2561−2577.
(661) He, M. Y.; Lin, Y. J.; Kao, Y. L.; Kuo, P.; Grauffel, C.; Lim, C.; Cheng, Y. S.; Chou, H. H. D. Sensitive and Specific Cadmium Biosensor Developed by Reconfiguring Metal Transport and Leveraging Natural Gene Repositories. *ACS Sens* **2021**, *6*, 995−1002.
(662) Libis, V.; Delépine, B.; Faulon, J.-L. Sensing New Chemicals with Bacterial Transcription Factors. *Curr. Opin Microbiol* **2016**, *33*, 105−112.
(663) Kim, H.; Jang, G.; Kim, B.-G.; Yoon, Y. Modulation of the Metal(Loid) Specificity of Whole-Cell Bioreporters by Genetic Engineering of ZntR Metal-Binding Loops. *J. Microbiol Biotechnol* **2020**, *30*, 681−688.
(664) Kang, Y.; Lee, W.; Jang, G.; Kim, B. G.; Yoon, Y. Modulating the Sensing Properties of *Escherichia coli*-Based Bioreporters for Cadmium and Mercury. *Appl. Microbiol. Biotechnol.* **2018**, *102*, 4863−4872.
(665) Mendoza, J. I.; Soncini, F. C.; Checa, S. K. Engineering of a Au-Sensor to Develop a Hg-Specific, Sensitive and Robust Whole-Cell Biosensor for on-Site Water Monitoring. *Chem. Commun.* **2020**, *56*, 6590−6593.
(666) Jia, X.; Ma, Y.; Bu, R.; Zhao, T.; Wu, K. Directed Evolution of a Transcription Factor PbrR to Improve Lead Selectivity and Reduce Zinc Interference through Dual Selection. *AMB Express* **2020**, *10*. DOI: 10.1186/s13568-020-01004-8.
(667) Li, L.; Liang, J.; Hong, W.; Zhao, Y.; Sun, S.; Yang, X.; Xu, A.; Hang, H.; Wu, L.; Chen, S. Evolved Bacterial Biosensor for Arsenite Detection in Environmental Water. *Environ. Sci. Technol.* **2015**, *49*, 6149−6155.
(668) d' Oelsnitz, S.; Kim, W.; Burkholder, N. T.; Javanmardi, K.; Thyer, R.; Zhang, Y.; Alper, H. S.; Ellington, A. D. Using Fungible Biosensors to Evolve Improved Alkaloid Biosyntheses. *Nat. Chem. Biol.* **2022**, *18*, 981−989.
(669) d'Oelsnitz, S.; Diaz, D. J.; Kim, W.; Acosta, D. J.; Dangerfield, T. L.; Schechter, M. W.; Minus, M. B.; Howard, J. R.; Do, H.; Loy, J. M.; et al. Biosensor and Machine Learning-Aided Engineering of an Amaryllidaceae Enzyme. *Nat. Commun.* **2024**, *15*, 2084.
(670) Dauparas, J.; Lee, G. R.; Pecoraro, R.; An, L.; Anishchenko, I.; Glasscock, C.; Baker, D. Atomic Context-Conditioned Protein Sequence Design Using LigandMPNN. *bioRxiv* **2023**. DOI: 10.1101/2023.12.22.573103
(671) Krishna, R.; Wang, J.; Ahern, W.; Sturmfels, P.; Venkatesh, P.; Kalvet, I.; Lee, G. R.; Morey-Burrows, F. S.; Anishchenko, I.; Humphreys, I. R.; et al. Generalized Biomolecular Modeling and Design with RoseTTAFold All-Atom. *Science* **2024**, *384*, No. eadl2528.
(672) Jha, R. K.; Chakraborti, S.; Kern, T. L.; Fox, D. T.; Strauss, C. E. M. Rosetta Comparative Modeling for Library Design: Engineering Alternative Inducer Specificity in a Transcription Factor. *Proteins* **2015**, *83*, 1327−1340.
(673) Pi, H.; Sun, R.; McBride, J. R.; Kruse, A. R. S.; Gibson-Corley, K. N.; Krystofiak, E. S.; Nicholson, M. R.; Spraggins, J. M.; Zhou, Q.; Skaar, E. P. *Clostridioides difficile* Ferrosome Organelles Combat Nutritional Immunity. *Nature* **2023**, *623*, 1009−1016.
(674) Grant, C. R.; Amor, M.; Trujillo, H. A.; Krishnapura, S.; Iavarone, A. T.; Komeili, A. Distinct Gene Clusters Drive Formation of Ferrosome Organelles in Bacteria. *Nature* **2022**, *606*, 160−164.
(675) Osterman, A.; Overbeek, R. Missing Genes in Metabolic Pathways: A Comparative Genomics Approach. *Curr. Opin Chem. Biol.* **2003**, *7*, 238−251.
(676) de Crécy-Lagard, V.; El Yacoubi, B.; de la Garza, R. D.; Noiriel, A.; Hanson, A. D. Comparative Genomics of Bacterial and Plant Folate Synthesis and Salvage: Predictions and Validations. *BMC Genomics* **2007**, *8*, 245.
(677) El Yacoubi, B.; Bonnett, S.; Anderson, J. N.; Swairjo, M. A.; Iwata-Reuyl, D.; De Crécy-Lagard, V. Discovery of a New Prokaryotic Type I GTP Cyclohydrolase Family. *J. Biol. Chem.* **2006**, *281*, 37586−37593.
(678) Sankaran, B.; Bonnett, S. A.; Shah, K.; Gabriel, S.; Reddy, R.; Schimmel, P.; Rodionov, D. A.; De Crécy-Lagard, V.; Helmann, J. D.; Iwata-Reuyl, D.; Swairjo, M. A. Zinc-Independent Folate Biosynthesis: Genetic, Biochemical, and Structural Investigations Reveal New Metal Dependence for GTP Cyclohydrolase IB. *J. Bacteriol.* **2009**, *191*, 6936−6949.
(679) Pribat, A.; Jeanguenin, L.; Lara-Núñez, A.; Ziemak, M. J.; Hyde, J. E.; De Crécy-Lagard, V.; Hanson, A. D. 6-Pyruvoyltetrahydropterin Synthase Paralogs Replace the Folate Synthesis Enzyme Dihydroneopterin Aldolase in Diverse Bacteria. *J. Bacteriol.* **2009**, *191*, 4158−4165.
(680) Sendra, K. M.; Barwinska-Sendra, A.; Mackenzie, E. S.; Baslé, A.; Kehl-Fie, T. E.; Waldron, K. J. An Ancient Metalloenzyme Evolves through Metal Preference Modulation. *Nat. Ecol Evol* **2023**, *7*, 732−744.
(681) Frye, K. A.; Sendra, K. M.; Waldron, K. J.; Kehl-Fie, T. E. Old Dogs, New Tricks: New Insights into the Iron/Manganese Superoxide Dismutase Family. *J. Inorg. Biochem* **2022**, *230*, 111748.
(682) Martin, J. E.; Imlay, J. A. The Alternative Aerobic Ribonucleotide Reductase of *Escherichia coli*, NrdEF, Is a Manganese-Dependent Enzyme That Enables Cell Replication during Periods of Iron Starvation. *Mol. Microbiol.* **2011**, *80*, 319−334.
(683) Rohaun, S. K.; Sethu, R.; Imlay, J. A. Microbes Vary Strategically in Their Metalation of Mononuclear Enzymes. *Proc. Natl. Acad. Sci. U. S. A.* **2024**, *121*, 2017.
(684) Natheer, S. E.; Muthukkaruppan, S. Assessing the *In vitro* Zinc Solubilization Potential and Improving Sugarcane Growth by Inoculating *Gluconacetobacter diazotrophicus*. *Ann. Microbiol* **2012**, *62*, 435−441.
(685) Saravanan, V. S.; Subramoniam, S. R.; Raj, S. A. Assessing *in vitro* Solubilization Potential of Different Zinc Solubilizing Bacterial (Zsb) Isolates. *Brazil J. Microbiol* **2004**, *34*, 121−125.
(686) Cunden, L. S.; Nolan, E. M. Bioinorganic Explorations of Zn(II) Sequestration by Human S100 Host-Defense Proteins. *Biochemistry* **2018**, *57*, 1673−1680.
(687) Gabriel, S. E.; Helmann, J. D. Contributions of Zur-Controlled Ribosomal Proteins to Growth under Zinc Starvation Conditions. *J. Bacteriol.* **2009**, *191*, 6116−6122.
(688) Haas, C. E.; Rodionov, D. A.; Kropat, J.; Malasarn, D.; Merchant, S. S.; de Crecy-Lagard, V. A Subset of the Diverse COG0523 Family of Putative Metal Chaperones Is Linked to Zinc Homeostasis in All Kingdoms of Life. *BMC Genomics* **2009**, *10*, 470.
(689) Jordan, M. R.; Villarruel Dujovne, M.; Capdevila, D. A.; Giedroc, D. P. Metal Ion Homeostasis: Metalloenzyme Paralogs in the Bacterial Adaptative Response to Zinc Restriction. In *Comprehensive Inorganic Chemistry III*; Reedijk, J., Poeppelmeier, K. R., Eds.; Elsevier, 2023; pp 30−52.
(690) Pederick, V. G.; Eijkelkamp, B. A.; Begg, S. L.; Ween, M. P.; McAllister, L. J.; Paton, J. C.; McDevitt, C. A. ZnuA and Zinc Homeostasis in *Pseudomonas aeruginosa*. *Sci. Rep* **2015**, *5*, 13139.
(691) Edmonds, K. A.; Jordan, M. R.; Giedroc, D. P. COG0523 Proteins: A Functionally Diverse Family of Transition Metal-Regulated G3E P-Loop GTP Hydrolases from Bacteria to Man. *Metallomics* **2021**, *13*, mfab046.
(692) Makarova, K. S.; Ponomarev, V. A.; Koonin, E. V. Two C or Not Two C: Recurrent Disruption of Zn-Ribbons, Gene Duplication, Lineage-Specific Gene Loss, and Horizontal Gene Transfer in Evolution of Bacterial Ribosomal Proteins. *Genome Biol.* **2001**, *2*, 0033.
(693) Panina, E. M.; Mironov, A. A.; Gelfand, M. S. Comparative Genomics of Bacterial Zinc Regulons: Enhanced Ion Transport, Pathogenesis, and Rearrangement of Ribosomal Proteins. *Proc. Natl. Acad. Sci. U. S. A.* **2003**, *100*, 9912−9917.
(694) Hemm, M. R.; Paul, B. J.; Miranda-Ríos, J.; Zhang, A.; Soltanzad, N.; Storz, G. Small Stress Response Proteins in *Escherichia*

coli: Proteins Missed by Classical Proteomic Studies. *J. Bacteriol.* **2010**, *192*, 46−58.
(695) Rasmussen, R. A.; Wang, S.; Camarillo, J. M.; Sosnowski, V.; Cho, B. K.; Goo, Y. A.; Lucks, J. B.; O'Halloran, T. V. Zur and Zinc Increase Expression of *E. coli* Ribosomal Protein L31 through RNA-Mediated Repression of the Repressor L31p. *Nucleic Acids Res.* **2022**, *50*, 12739−12753.
(696) Sheng, K.; Li, N.; Rabuck-Gibbons, J. N.; Dong, X.; Lyumkis, D.; Williamson, J. R. Assembly Landscape for the Bacterial Large Ribosomal Subunit. *Nat. Commun.* **2023**, *14*, 5220.
(697) Li, Y.; Sharma, M. R.; Koripella, R. K.; Yang, Y.; Kaushal, P. S.; Lin, Q.; Wade, J. T.; Gray, T. A.; Derbyshire, K. M.; Agrawal, R. K.; Ojha, A. K. Zinc Depletion Induces Ribosome Hibernation in Mycobacteria. *Proc. Natl. Acad. Sci. U. S. A.* **2018**, *115*, 8191−8196.
(698) Hentschel, J.; Burnside, C.; Mignot, I.; Leibundgut, M.; Boehringer, D.; Ban, N. The Complete Structure of the *Mycobacterium smegmatis* 70S Ribosome. *Cell Rep* **2017**, *20*, 149−160.
(699) Li, Y.; Koripella, R. K.; Sharma, M. R.; Lee, R. E.; Agrawal, R. K.; Ojha, A. K. Replacement of S14 Protein in Ribosomes of Zinc-Starved Mycobacteria Reduces Spectinamide Sensitivity. *Antimicrob. Agents Chemother.* **2021**, *65*, No. e01833-20.
(700) Chen, Y.-X.; Xu, Z.-y.; Ge, X.; Hong, J.-Y.; Sanyal, S.; Lu, Z. J.; Javid, B. Selective Translation by Alternative Bacterial Ribosomes. *Proc. Natl. Acad. Sci. U. S. A.* **2020**, *117*, 19487−19496.
(701) Dow, A.; Burger, A.; Marcantonio, E.; Prisic, S. Multi-Omics Profiling Specifies Involvement of Alternative Ribosomal Proteins in Response to Zinc Limitation in *Mycobacterium smegmatis*. *Front Microbiol* **2022**, *13*, 1−16.
(702) Dworkin, J. Understanding the Stringent Response: Experimental Context Matters. *mBio* **2023**, *14*, mbio03404.
(703) Wang, B.; Dai, P.; Ding, D.; Del Rosario, A.; Grant, R. A.; Pentelute, B. L.; Laub, M. T. Affinity-Based Capture and Identification of Protein Effectors of the Growth Regulator ppGpp. *Nat. Chem. Biol.* **2019**, *15*, 141−150.
(704) Irving, S. E.; Choudhury, N. R.; Corrigan, R. M. The Stringent Response and Physiological Roles of (Pp)PGpp in Bacteria. *Nat. Rev. Microbiol* **2021**, *19*, 256−271.
(705) Kang, P. J.; Craig, E. A. Identification and Characterization of a New *Escherichia coli* Gene That Is a Dosage-Dependent Suppressor of a DnaK Deletion Mutation. *J. Bacteriol.* **1990**, *172*, 2055−2064.
(706) Gourse, R. L.; Chen, A. Y.; Gopalkrishnan, S.; Sanchez-Vazquez, P.; Myers, A.; Ross, W. Transcriptional Responses to ppGpp and DksA. *Annu. Rev. Microbiol.* **2018**, *72*, 163−184.
(707) Cohen, H.; Adani, B.; Cohen, E.; Piscon, B.; Azriel, S.; Desai, P.; Bähre, H.; McClelland, M.; Rahav, G.; Gal-Mor, O. The Ancestral Stringent Response Potentiator, DksA Has Been Adapted throughout Salmonella Evolution to Orchestrate the Expression of Metabolic, Motility, and Virulence Pathways. *Gut Microbes* **2022**, *14*, No. e1997294.
(708) Crawford, M. A.; Tapscott, T.; Fitzsimmons, L. F.; Liu, L.; Reyes, A. M.; Libby, S. J.; Trujillo, M.; Fang, F. C.; Radi, R.; Vázquez-Torres, A. Redox-Active Sensing by Bacterial DksA Transcription Factors Is Determined by Cysteine and Zinc Content. *mBio* **2016**, *7*, No. e02161-e0215.
(709) Molodtsov, V.; Sineva, E.; Zhang, L.; Huang, X.; Cashel, M.; Ades, S. E.; Murakami, K. S. Allosteric Effector PpGpp Potentiates the Inhibition of Transcript Initiation by DksA. *Mol. Cell* **2018**, *69*, 828−839.
(710) Perederina, A.; Svetlov, V.; Vassylyeva, M. N.; Tahirov, T. H.; Yokoyama, S.; Artsimovitch, I.; Vassylyev, D. G. Regulation through the Secondary Channel—Structural Framework for ppGpp-DksA Synergism during Transcription. *Cell* **2004**, *118*, 297−309.
(711) Paul, B. J.; Barker, M. M.; Ross, W.; Schneider, D. A.; Webb, C.; Foster, J. W.; Gourse, R. L. DksA: A Critical Component of the Transcription Initiation Machinery That Potentiates the Regulation of RRNA Promoters by ppGpp and the Initiating NTP. *Cell* **2004**, *118*, 311−322.
(712) Crawford, M. A.; Henard, C. A.; Tapscott, T.; Porwollik, S.; McClelland, M.; Vázquez-Torres, A. DksA-Dependent Transcriptional Regulation in Salmonella Experiencing Nitrosative Stress. *Front Microbiol* **2016**, *7*, 1−8.
(713) Symersky, J.; Perederina, A.; Vassylyeva, M. N.; Svetlov, V.; Artsimovitch, I.; Vassylyev, D. G. Regulation through the RNA Polymerase Secondary Channel Structural and Functional Variability Of The Coiled-Coil. *J. Biol. Chem.* **2006**, *281*, 1309−1312.
(714) Stebbins, C. E.; Borukhov, S.; Orlova, M.; Polyakov, A.; Goldfarb, A.; Darst, S. A. Crystal Structure of the GreA Transcript Cleavage Factor from *Escherichia coli*. *Nature* **1995**, *373*, 636−640.
(715) Furman, R.; Biswas, T.; Danhart, E. M.; Foster, M. P.; Tsodikov, O. V.; Artsimovitch, I. DksA2, a Zinc-Independent Structural Analog of the Transcription Factor DksA. *FEBS Lett.* **2013**, *587*, 614−619.
(716) Blaby-Haas, C. E.; Furman, R.; Rodionov, D. A.; Artsimovitch, I.; De Crécy-Lagard, V. Role of a Zn-Independent DksA in Zn Homeostasis and Stringent Response. *Mol. Microbiol.* **2011**, *79*, 700−715.
(717) de Crecy-Lagard, V.; Jaroch, M. Functions of Bacterial TRNA Modifications: From Ubiquity to Diversity. *Trends Microbiol* **2021**, *29*, 41−53.
(718) Edwards, A. M.; Addo, M. A.; Dos Santos, P. C. Extracurricular Functions of tRNA Modifications in Microorganisms. *Genes* **2020**, *11*, 907.
(719) Zaborske, J. M.; Bauer DuMont, V. L.; Wallace, E. W. J.; Pan, T.; Aquadro, C. F.; Drummond, D. A. A Nutrient-Driven tRNA Modification Alters Translational Fidelity and Genome-Wide Protein Coding across an Animal Genus. *PLoS Biol.* **2014**, *12*, No. e1002015.
(720) Muller, M.; Legrand, C.; Tuorto, F.; Kelly, V. P.; Atlasi, Y.; Lyko, F.; Ehrenhofer-Murray, A. E. Queuine Links Translational Control in Eukaryotes to a Micronutrient from Bacteria. *Nucleic Acids Res.* **2019**, *47*, 3711−3727.
(721) Harada, F.; Nishimura, S. Possible Anticodon Sequences of $tRNA^{His}$, $tRNA^{Asn}$, and $tRNA^{Asp}$ from *Escherichia coli*. Universal Presence of Nucleoside O in the First Position of the Anticodons of These Transfer Ribonucleic Acid. *Biochemistry* **1972**, *11*, 301−308.
(722) Tuorto, F.; Legrand, C.; Cirzi, C.; Federico, G.; Liebers, R.; Müller, M.; Ehrenhofer-Murray, A. E.; Dittmar, G.; Gröne, H.; Lyko, F. Queuosine-modified TRNAs Confer Nutritional Control of Protein Translation. *EMBO J.* **2018**, *37*, 1−14.
(723) Meier, F.; Suter, B.; Grosjean, H.; Keith, G.; Kubli, E. Queuosine Modification of the Wobble Base in $tRNA^{His}$ Influences '*in Vivo*' Decoding Properties. *EMBO J.* **1985**, *4*, 823−827.
(724) Dixit, S.; Kessler, A. C.; Henderson, J.; Pan, X.; Zhao, R.; D'Almeida, G. S.; Kulkarni, S.; Rubio, M. A. T.; Hegedüsová, E.; Ross, R. L.; Limbach, P. A.; Green, B. D.; Paris, Z.; Alfonzo, J. D. Dynamic Queuosine Changes in tRNA Couple Nutrient Levels to Codon Choice in *Trypanosoma brucei*. *Nucleic Acids Res.* **2021**, *49*, 12986−12999.
(725) Kulkarni, S.; Rubio, M. A. T.; Hegedüsová, E.; Ross, R. L.; Limbach, P. A.; Alfonzo, J. D.; Paris, Z. Preferential Import of Queuosine-Modified tRNAs into *Trypanosoma brucei* Mitochondrion Is Critical for Organellar Protein Synthesis. *Nucleic Acids Res.* **2021**, *49*, 8247−8260.
(726) Manickam, N.; Joshi, K.; Bhatt, M. J.; Farabaugh, P. J. Effects of yRNA Modification on Translational Accuracy Depend on Intrinsic Codon-Anticodon Strength. *Nucleic Acids Res.* **2016**, *44*, 1871−1881.
(727) Diaz-Rullo, J.; Gonzalez-Pastor, J. E. tRNA Queuosine Modification Is Involved in Biofilm Formation and Virulence in Bacteria. *Nucleic Acids Res.* **2023**, *51*, 9821−9837.
(728) Babosan, A.; Fruchard, L.; Krin, E.; Carvalho, A.; Mazel, D.; Baharoglu, Z. Nonessential tRNA and rRNA Modifications Impact the Bacterial Response to sub-MIC Antibiotic Stress. *Microlife* **2022**, *3*, uqac019.
(729) McCarty, R. M.; Somogyi, A.; Bandarian, V. *Escherichia coli* QueD Is a 6-Carboxy-5,6,7,8-Tetrahydropterin Synthase. *Biochemistry* **2009**, *48*, 2301−2303.
(730) Auerbach, G.; Herrmann, A.; Bracher, A.; Bader, G.; Gütlich, M.; Fischer, M.; Neukamm, M.; Garrido-Franco, M.; Richardson, J.; Nar, H.; Huber, R.; Bacher, A. Zinc Plays a Key Role in Human and Bacterial GTP Cyclohydrolase I. *Proc. Natl. Acad. Sci. U. S. A.* **2000**, *97*, 13567−13572.

(731) Nelp, M. T.; Bandarian, V. A Single Enzyme Transforms a Carboxylic Acid into a Nitrile through an Amide Intermediate. *Angew. Chemie Int. Ed* **2015**, *127*, 10773−10775.
(732) Chong, S.; Curnow, A. W.; Huston, T. J.; Garcia, G. A. Site-Directed Mutagenesis of *Escherichia coli* tRNA-Guanine Transglycosylase Zinc Metalloprotein to Identify Zinc Ligands. *Biochemistry* **1995**, *34*, 3694−3701.
(733) McCarty, R. M.; Krebs, C.; Bandarian, V. Spectroscopic, Steady-State Kinetic, and Mechanistic Characterization of the Radical SAM Enzyme QueE, Which Catalyzes a Complex Cyclization Reaction in the Biosynthesis of 7-Deazapurines. *Biochemistry* **2013**, *52*, 188−198.
(734) Miles, Z. D.; Myers, W. K.; Kincannon, W. M.; Britt, R. D.; Bandarian, V. Biochemical and Spectroscopic Studies of Epoxyqueuosine Reductase: A Novel Iron-Sulfur Cluster- and Cobalamin-Containing Protein Involved in the Biosynthesis of Queuosine. *Biochemistry* **2015**, *54*, 4927−4935.
(735) Li, Q.; Zallot, R.; MacTavish, B. S.; Montoya, A.; Payan, D. J.; Hu, Y.; Gerlt, J. A.; Angerhofer, A.; de Crécy-Lagard, V.; Bruner, S. D. Epoxyqueuosine Reductase QueH in the Biosynthetic Pathway to tRNA Queuosine Is a Unique Metalloenzyme. *Biochemistry* **2021**, *60*, 3152−3161.
(736) Pollo-Oliveira, L.; Davis, N. K.; Hossain, I.; Ho, P.; Yuan, Y.; Salguero Garcia, P.; Pereira, C.; Byrne, S. R.; Leng, J.; Sze, M.; Blaby-Haas, C. E.; et al. The Absence of the Queuosine TRNA Modification Leads to Pleiotropic Phenotypes Revealing Perturbations of Metal and Oxidative Stress Homeostasis in *Escherichia coli* K12. *Metallomics* **2022**, *14*, mfac065.
(737) McCarty, R. M.; Somogyi, Á.; Lin, G.; Jacobsen, N. E.; Bandarian, V. The Deazapurine Biosynthetic Pathway Revealed: *In vitro* Enzymatic Synthesis of PreQ0 from Guanosine 5′-Triphosphate in Four Steps. *Biochemistry* **2009**, *48*, 3847−3852.
(738) Wang, J.; Lonergan, Z. R.; Gonzalez-Gutierrez, G.; Nairn, B. L.; Maxwell, C. N.; Zhang, Y.; Andreini, C.; Karty, J. A.; Chazin, W. J.; Trinidad, J. C.; et al. Multi-Metal Restriction by Calprotectin Impacts *De Novo* Flavin Biosynthesis in *Acinetobacter baumannii*. *Cell Chem. Biol.* **2019**, *26*, 745−755.
(739) Phillips, G.; Grochowski, L. L.; Bonnett, S.; Xu, H.; Bailly, M.; Blaby-Haas, C.; El Yacoubi, B.; Iwata-Reuyl, D.; White, R. H.; De Crécy-Lagard, V. Functional Promiscuity of the COG0720 Family. *ACS Chem. Biol.* **2012**, *7*, 197−209.
(740) Miles, Z. D.; Roberts, S. A.; McCarty, R. M.; Bandarian, V. Biochemical and Structural Studies of 6-Carboxy-5,6,7,8-Tetrahydropterin Synthase Reveal the Molecular Basis of Catalytic Promiscuity within the Tunnel-Fold Superfamily. *J. Biol. Chem.* **2014**, *289*, 23641−23652.
(741) Kim, G.-J.; Kim, H.-S. Identification of the Structural Similarity in the Functionally Related Amidohydrolases Acting on the Cyclic Amide Ring. *Biochem. J.* **1998**, *330*, 295−302.
(742) Davidson, J. N.; Chen, K. C.; Jamison, R. S.; Musmanno, L. A.; Kern, C. B. The Evolutionary History of the First Three Enzymes in Pyrimidine Biosynthesis. *BioEssays* **1993**, *15*, 157−164.
(743) Samant, S.; Lee, H.; Ghassemi, M.; Chen, J.; Cook, J. L.; Mankin, A. S.; Neyfakh, A. A. Nucleotide Biosynthesis Is Critical for Growth of Bacteria in Human Blood. *PLoS Pathog* **2008**, *4*, No. e37.
(744) Forsyth, R. A.; Haselbeck, R. J.; Ohlsen, K. L.; Yamamoto, R. T.; Xu, H.; Trawick, J. D.; Wall, D.; Wang, L.; Brown-Driver, V.; Froelich, J. M.; et al. A Genome-Wide Strategy for the Identification of Essential Genes in *Staphylococcus aureus*. *Mol. Microbiol.* **2002**, *43*, 1387−1400.
(745) Sassetti, C. M.; Boyd, D. H.; Rubin, E. J. Genes Required for Mycobacterial Growth Defined by High Density Mutagenesis. *Mol. Microbiol.* **2003**, *48*, 77−84.
(746) Mehboob, S.; Mulhearn, D. C.; Truong, K.; Johnson, M. E.; Santarsiero, B. D. Structure of Dihydroorotase from Bacillus Anthracis at 2.6 Å Resolution. *Acta Crystallogr. Sect F Struct Biol. Cryst. Commun.* **2010**, *66*, 1432−1435.
(747) Rice, A. J.; Lei, H.; Santarsiero, B. D.; Lee, H.; Johnson, M. E. Ca-Asp Bound X-Ray Structure and Inhibition of Bacillus Anthracis Dihydroorotase (DHOase). *Bioorg. Med. Chem.* **2016**, *24*, 4536−4543.
(748) Thoden, J. B.; Phillips, J.; Neal, T. M.; Raushel, F. M.; Holden, H. M. Molecular Structure of Dihydroorotase: A Paradigm for Catalysis through the Use of a Binuclear Metal Center. *Biochemistry* **2001**, *40*, 6989−6997.
(749) Porter, T. N.; Li, Y.; Raushel, F. M. Mechanism of the Dihydroorotase Reaction. *Biochemistry* **2004**, *43*, 16285−16292.
(750) Huang, D. T. C.; Thomas, M. A. W.; Christopherson, R. I. Divalent Metal Derivatives of the Hamster Dihydroorotase Domain. *Biochemistry* **1999**, *38*, 9964−9970.
(751) Pettigrew, D. W.; Mehta, B. J.; Bidigare, R. R.; Choudhury, R. R.; Scheffler, J. E.; Sander, E. G. Enzyme Elements Involved in the Interconversion of L-Carbamylaspartate and L-Dihydroorotate by Dihydroorotase from *Clostridium oroticum*. *Arch. Biochem. Biophys.* **1985**, *243*, 447−453.
(752) Brown, D. C.; Collins, K. D. Dihydroorotase from *Escherichia coli*. *J. Biol. Chem.* **1991**, *266*, 1597−1604.
(753) Ehrnstorfer, I. A.; Geertsma, E. R.; Pardon, E.; Steyaert, J.; Dutzler, R. Crystal Structure of a SLC11 (NRAMP) Transporter Reveals the Basis for Transition-Metal Ion Transport. *Nat. Struct Mol. Biol.* **2014**, *21*, 990−996.
(754) Lee, M.; Chan, C. W.; Guss, J. M.; Christopherson, R. I.; Maher, M. J. Dihydroorotase from *Escherichia coli*: Loop Movement and Cooperativity between Subunits. *J. Mol. Biol.* **2005**, *348*, 523−533.
(755) Reader, J. S.; Metzgar, D.; Schimmel, P.; De Crécy-Lagard, V. Identification of Four Genes Necessary for Biosynthesis of the Modified Nucleoside Queuosine. *J. Biol. Chem.* **2004**, *279*, 6280−6285.
(756) Rebelo, J.; Auerbach, G.; Bader, G.; Bracher, A.; Nar, H.; Hösl, C.; Schramek, N.; Kaiser, J.; Bacher, A.; Huber, R.; et al. Biosynthesis of Pteridines. Reaction Mechanism of GTP Cyclohydrolase I. *J. Mol. Biol.* **2003**, *326*, 503−516.
(757) Auerbach, G.; Herrmann, A.; Bracher, A.; Bader, G.; Gütlich, M.; Fischer, M.; Neukamm, M.; Garrido-Franco, M.; Richardson, J.; et al. Zinc Plays a Key Role in Human and Bacterial GTP Cyclohydrolase I. *Proc. Natl. Acad. Sci. U. S. A.* **2000**, *97*, 13567−13572.
(758) Schulz, V.; Galea, D.; Herzberg, M.; Nies, D. H. Protecting the Achilles Heel: Three FolE_I-Type GTP-Cyclohydrolases Needed for Full Growth of Metal-Resistant *Cupriavidus metallidurans* under a Variety of Conditions. *J. Bacteriol.* **2024**, *206*, No. e0039523.
(759) Paranagama, N.; Bonnett, S. A.; Alvarez, J.; Luthra, A.; Stec, B.; Gustafson, A.; Iwata-Reuyl, D.; Swairjo, M. A. Mechanism and Catalytic Strategy of the Prokaryotic-Specific GTP Cyclohydrolase-IB. *Biochem. J.* **2017**, *474*, 1017−1039.
(760) Shin, J.-H.; Helmann, J. D. Molecular Logic of the Zur-Regulated Zinc Deprivation Response in *Bacillus subtilis*. *Nat. Commun.* **2016**, *7*, 12612.
(761) Chandrangsu, P.; Huang, X.; Gaballa, A.; Helmann, J. D. *Bacillus Subtilis* FolE Is Sustained by the ZagA Zinc Metallochaperone and the Alarmone ZTP under Conditions of Zinc Deficiency. *Mol. Microbiol.* **2019**, *112*, 751−765.
(762) Shin, J.-H.; Helmann, J. D. Molecular Logic of the Zur-Regulated Zinc Deprivation Response in *Bacillus subtilis*. *Nat. Commun.* **2016**, *7*, 12612.
(763) Nies, D. H. The Ancient Alarmone ZTP and Zinc Homeostasis in *Bacillus subtilis*. *Mol. Microbiol.* **2019**, *112*, 741−746.
(764) Rebelo, J.; Auerbach, G.; Bader, G.; Bracher, A.; Nar, H.; Hösl, C.; Schramek, N.; Kaiser, J.; Bacher, A.; Huber, R.; Fischer, M. Biosynthesis of Pteridines. Reaction Mechanism of GTP Cyclohydrolase I. *J. Mol. Biol.* **2003**, *326*, 503−516.
(765) Beckett, D. Specificity and Selectivity in Post-Translational Biotin Addition. *Biochem. Soc. Trans.* **2018**, *46*, 1577−1591.
(766) Supuran, C. T.; Capasso, C. Biomedical Applications of Prokaryotic Carbonic Anhydrases. *Expert Opin Ther Pat* **2018**, *28*, 745−754.
(767) Supuran, C.; Capasso, C. An Overview of the Bacterial Carbonic Anhydrases. *Metabolites* **2017**, *7*, 56.
(768) Nocentini, A.; Donald, W. A.; Supuran, C. T. Human Carbonic Anhydrases. In *Carbonic Anhydrases*; Supuran, C. T., Nocentini, A. B. T.-C. A., Eds.; Elsevier, 2019; pp 151−185.

https://doi.org/10.1021/acs.chemrev.4c00264
Chem. Rev. 2024, 124, 13574−13659

(769) Campestre, C.; De Luca, V.; Carradori, S.; Grande, R.; Carginale, V.; Scaloni, A.; Supuran, C. T.; Capasso, C. Carbonic Anhydrases: New Perspectives on Protein Functional Role and Inhibition in *Helicobacter pylori*. *Front Microbiol* **2021**, *12*, 629163.
(770) Jensen, E. L.; Clement, R.; Kosta, A.; Maberly, S. C.; Gontero, B. A New Widespread Subclass of Carbonic Anhydrase in Marine Phytoplankton. *ISME J.* **2019**, *13*, 2094−2106.
(771) MacAuley, S. R.; Zimmerman, S. A.; Apolinario, E. E.; Evilia, C.; Hou, Y.-M.; Ferry, J. G.; Sowers, K. R. The Archetype γ-Class Carbonic Anhydrase (Cam) Contains Iron When Synthesized in Vivo. *Biochemistry* **2009**, *48*, 817−819.
(772) Tripp, B. C.; Bell, C. B.; Cruz, F.; Krebs, C.; Ferry, J. G. A Role for Iron in an Ancient Carbonic Anhydrase. *J. Biol. Chem.* **2004**, *279*, 6683−6687.
(773) De Simone, G.; Monti, S. M.; Alterio, V.; Buonanno, M.; De Luca, V.; Rossi, M.; Carginale, V.; Supuran, C. T.; Capasso, C.; Di Fiore, A. Crystal Structure of the Most Catalytically Effective Carbonic Anhydrase Enzyme Known, SazCA from the Thermophilic Bacterium *Sulfurihydrogenibium azorense*. *Bioorg. Med. Chem. Lett.* **2015**, *25*, 2002−2006.
(774) Covarrubias, A. S.; Bergfors, T.; Jones, T. A.; Högbom, M. Structural Mechanics of the PH-Dependent Activity of β-Carbonic Anhydrase from *Mycobacterium tuberculosis*. *J. Biol. Chem.* **2006**, *281*, 4993−4999.
(775) Peña, K. L.; Castel, S. E.; De Araujo, C.; Espie, G. S.; Kimber, M. S. Structural Basis of the Oxidative Activation of the Carboxysomal γ-Carbonic Anhydrase, CcmM. *Proc. Natl. Acad. Sci. U. S. A.* **2010**, *107*, 2455−2460.
(776) Buvelot, H.; Posfay-Barbe, K. M.; Linder, P.; Schrenzel, J.; Krause, K. H. *Staphylococcus aureus*, Phagocyte NADPH Oxidase and Chronic Granulomatous Disease. *FEMS Microbiol Rev.* **2016**, *41*, 139−157.
(777) Broxton, C. N.; Culotta, V. C. SOD Enzymes and Microbial Pathogens: Surviving the Oxidative Storm of Infection. *PLoS Pathog* **2016**, *12*, No. e1005295.
(778) Sheng, Y.; Abreu, I. A.; Cabelli, D. E.; Maroney, M. J.; Miller, A. F.; Teixeira, M.; Valentine, J. S. Superoxide Dismutases and Superoxide Reductases. *Chem. Rev.* **2014**, *114*, 3854−3918.
(779) Abreu, I. A.; Cabelli, D. E. Superoxide Dismutases-a Review of the Metal-Associated Mechanistic Variations. *Biochim. Biophys. Acta* **2010**, *1804*, 263−274.
(780) Massé, E.; Gottesman, S. A Small RNA Regulates the Expression of Genes Involved in Iron Metabolism in *Escherichia coli*. *Proc. Natl. Acad. Sci. U. S. A.* **2002**, *99*, 4620−4625.
(781) Jung, Y. S.; Kwon, Y. M. Small RNA ArrF Regulates the Expression of SodB and FeSII Genes in *Azotobacter vinelandii*. *Curr. Microbiol.* **2008**, *57*, 593−597.
(782) Khakh, S. K.; Antelmann, H.; Helmann, J. D.; Song, K.-B.; Aguilar, C.; Smaldone, G. T.; Gaballa, A. The *Bacillus subtilis* Iron-Sparing Response Is Mediated by a Fur-Regulated Small RNA and Three Small, Basic Proteins. *Proc. Natl. Acad. Sci. U. S. A.* **2008**, *105*, 11927−11932.
(783) Ernst, F. D.; Homuth, G.; Stoof, J.; Mäder, U.; Waidner, B.; Kuipers, E. J.; Kist, M.; Kusters, J. G.; Bereswill, S.; Van Vliet, A. H. M. Iron-Responsive Regulation of the *Helicobacter pylori* Iron-Cofactored Superoxide Dismutase SodB Is Mediated by Fur. *J. Bacteriol.* **2005**, *187*, 3687−3692.
(784) Kim, H. M.; Shin, J. H.; Cho, Y. B.; Roe, J. H. Inverse Regulation of Fe-And Ni-Containing SOD Genes by a Fur Family Regulator Nur through Small RNA Processed from 3′UTR of the *sodF* mRNA. *Nucleic Acids Res.* **2014**, *42*, 2003−2014.
(785) Smethurst, D. G. J.; Shcherbik, N. Interchangeable Utilization of Metals: New Perspectives on the Impacts of Metal Ions Employed in Ancient and Extant Biomolecules. *J. Biol. Chem.* **2021**, *297*, 101374.
(786) Karavolos, M. H.; Horsburgh, M.; Ingham, E.; Foster, S. J. Role and Regulation of the Superoxide Dismutases of *Staphylococcus aureus*. *Microbiology* **2003**, *149*, 2749−2758.
(787) Barwinska-Sendra, A.; Garcia, Y. M.; Sendra, K. M.; Baslé, A.; Mackenzie, E. S.; Tarrant, E.; Card, P.; Tabares, L. C.; Bicep, C.; Un, S.; et al. An Evolutionary Path to Altered Cofactor Specificity in a Metalloenzyme. *Nat. Commun.* **2020**, *11*, 2738.
(788) Spagnolo, L.; Töro, I.; D'Orazio, M.; O'Neill, P.; Pedersen, J. Z.; Carugo, O.; Rotilio, G.; Battistoni, A.; Djinović-Carugo, K. Unique Features of the SodC-Encoded Superoxide Dismutase from *Mycobacterium tuberculosis*, a Fully Functional Copper-Containing Enzyme Lacking Zinc in the Active Site. *J. Biol. Chem.* **2004**, *279*, 33447−33455.
(789) Robinett, N. G.; Peterson, R. L.; Culotta, V. C. Eukaryotic Copper-Only Superoxide Dismutases (SODs): A New Class of SOD Enzymes and SOD-like Protein Domains. *J. Biol. Chem.* **2018**, *293*, 4636−4643.
(790) Schatzman, S. S.; Peterson, R. L.; Teka, M.; He, B.; Cabelli, D. E.; Cormack, B. P.; Culotta, V. C. Copper-Only Superoxide Dismutase Enzymes and Iron Starvation Stress in Candida Fungal Pathogens. *J. Biol. Chem.* **2020**, *295*, 570−583.
(791) Miller, A. F. Redox Tuning over Almost 1 V in a Structurally Conserved Active Site: Lessons from Fe-Containing Superoxide Dismutase. *Acc. Chem. Res.* **2008**, *41*, 501−510.
(792) Barwinska-Sendra, A.; Baslé, A.; Waldron, K. J.; Un, S. A Charge Polarization Model for the Metal-Specific Activity of Superoxide Dismutases. *Phys. Chem. Chem. Phys.* **2018**, *20*, 2363−2372.
(793) Levitz, T. S.; Drennan, C. L. Starting a New Chapter on Class Ia Ribonucleotide Reductases. *Curr. Opin Struct Biol.* **2022**, *77*, 102489.
(794) Blaesi, E. J.; Palowitch, G. M.; Hu, K.; Kim, A. J.; Rose, H. R.; Alapati, R.; Lougee, M. G.; Kim, H. J.; Taguchi, A. T.; Tan, K. O.; et al. Metal-Free Class Ie Ribonucleotide Reductase from Pathogens Initiates Catalysis with a Tyrosine-derived Dihydroxyphenylalanine Radical. *Proc. Natl. Acad. Sci. U. S. A.* **2018**, *115*, 10022−10027.
(795) Boal, A. K.; Cotruvo, J. A.; Stubbe, J.; Rosenzweig, A. C. Structural Basis for Activation of Class Ib Ribonucleotide Reductase. *Science* **2010**, *329*, 1526−1530.
(796) Čapek, J.; Večerek, B. Why Is Manganese so Valuable to Bacterial Pathogens? *Front Cell Infect Microbiol* **2023**, *13*, 1−29.
(797) Hammerstad, M.; Hersleth, H. P.; Tomter, A. B.; Røhr, Å. K.; Andersson, K. K. Crystal Structure of *Bacillus cereus* Class Ib Ribonucleotide Reductase di-Iron NrdF in Complex with NrdI. *ACS Chem. Biol.* **2014**, *9*, 526−537.
(798) Grave, K.; Griese, J. J.; Berggren, G.; Bennett, M. D.; Högbom, M. The *Bacillus anthracis* Class Ib Ribonucleotide Reductase Subunit NrdF Intrinsically Selects Manganese over Iron. *J. Biol. Inorg. Chem.* **2020**, *25*, 571−582.
(799) Robinson, N. J.; Winge, D. R. Copper Metallochaperones. *Annu. Rev. Biochem.* **2010**, *79*, 537−562.
(800) Boal, A. K.; Rosenzweig, A. C. Structural Biology of Copper Trafficking. *Chem. Rev.* **2009**, *109*, 4760−4779.
(801) Vaccaro, F. A.; Drennan, C. L. The Role of Nucleoside Triphosphate Hydrolase Metallochaperones in Making Metalloenzymes. *Metallomics* **2022**, *14*, mfac030.
(802) Bublitz, M.; Poulsen, H.; Morth, J. P.; Nissen, P. In and out of the Cation Pumps: P-Type ATPase Structure Revisited. *Curr. Opin Struct Biol.* **2010**, *20*, 431−439.
(803) Mattle, D.; Sitsel, O.; Autzen, H. E.; Meloni, G.; Gourdon, P.; Nissen, P. On Allosteric Modulation of P-Type Cu+-ATPases. *J. Mol. Biol.* **2013**, *425*, 2299−2308.
(804) Banci, L.; Bertini, I.; Ciofi-Baffoni, S.; Kandias, N. G.; Robinson, N. J.; Spyroulias, G. A.; Su, X. C.; Tottey, S.; Vanarotti, M. The Delivery of Copper for Thylakoid Import Observed by NMR. *Proc. Natl. Acad. Sci. U. S. A.* **2006**, *103*, 8320−8325.
(805) Banci, L.; Bertini, I.; Ciofi-Baffoni, S.; Kozyreva, T.; Zovo, K.; Palumaa, P. Affinity Gradients Drive Copper to Cellular Destinations. *Nature* **2010**, *465*, 645−648.
(806) Rosenzweig, A. C. Metallochaperones: Bind and Deliver. *Chem. Biol.* **2002**, *9*, 673−677.
(807) Banci, L.; Bertini, I.; Cantini, F.; Felli, I. C.; Gonnelli, L.; Hadjiliadis, N.; Pierattelli, R.; Rosato, A.; Voulgaris, P. The Atx1-Ccc2 Complex Is a Metal-Mediated Protein-Protein Interaction. *Nat. Chem. Biol.* **2006**, *2*, 367−8.
(808) Berg, J. M.; Lippard, S. J. *Principles of Bioinorganic Chemistry*; University Science Books, 1994.

https://doi.org/10.1021/acs.chemrev.4c00264
Chem. Rev. 2024, 124, 13574−13659

(809) Pufahl, R. A.; Singer, C. P.; Peariso, K. L.; Lin, S. J.; Schmidt, P. J.; Fahrni, C. J.; Culotta, V. C.; Penner-Hahn, J. E.; O'Halloran, T. V. Metal Ion Chaperone Function of the Soluble Cu(I) Receptor Atx1. *Science* **1997**, *278*, 853−856.
(810) Zangger, K.; Oz, G.; Otvos, J. D.; Armitage, I. M. Three-Dimensional Solution Structure of Mouse [Cd7]-Metallothionein-1 by Homonuclear and Heteronuclear NMR Spectroscopy. *Protein Sci.* **1999**, *8*, 2630−2638.
(811) Banci, L.; Bertini, I.; McGreevy, K. S.; Rosato, A. Molecular Recognition in Copper Trafficking. *Nat. Prod Rep* **2010**, *27*, 695−710.
(812) Lacasse, M. J.; Zamble, D. B. [NiFe]-Hydrogenase Maturation. *Biochemistry* **2016**, *55*, 1689−1701.
(813) Farrugia, M. A.; Macomber, L.; Hausinger, R. P. Biosynthesis of the Urease Metallocenter. *J. Biol. Chem.* **2013**, *288*, 13178−13185.
(814) Pasquini, M.; Grosjean, N.; Hixson, K. K.; Nicora, C. D.; Yee, E. F.; Lipton, M.; Blaby, I. K.; Haley, J. D.; Blaby-Haas, C. E. Zng1 Is a GTP-Dependent Zinc Transferase Needed for Activation of Methionine Aminopeptidase. *Cell Rep* **2022**, *39*, 110834.
(815) Campanello, G. C.; Lofgren, M.; Yokom, A. L.; Southworth, D. R.; Banerjee, R. Switch I-Dependent Allosteric Signaling in a G-Protein Chaperone-B_{12} enzyme Complex. *J. Biol. Chem.* **2017**, *292*, 17617−17625.
(816) Lofgren, M.; Padovani, D.; Koutmos, M.; Banerjee, R. A Switch III Motif Relays Signaling between a B_{12} Enzyme and Its G-Protein Chaperone. *Nat. Chem. Biol.* **2013**, *9*, 535−539.
(817) Wittinghofer, A.; Vetter, I. R. Structure-Function Relationships of the G Domain, a Canonical Switch Motif. *Annu. Rev. Biochem.* **2011**, *80*, 943−971.
(818) Sydor, A. M.; Jost, M.; Ryan, K. S.; Turo, K. E.; Douglas, C. D.; Drennan, C. L.; Zamble, D. B. Metal Binding Properties of *Escherichia coli* YjiA, a Member of the Metal Homeostasis-Associated COG0523 Family of GTPases. *Biochemistry* **2013**, *52*, 1788−1801.
(819) Gasper, R.; Scrima, A.; Wittinghofer, A. Structural Insights into HypB, a GTP-Binding Protein That Regulates Metal Binding. *J. Biol. Chem.* **2006**, *281*, 27492−27502.
(820) Osterberg, M. K.; Smith, A. K.; Campbell, C.; Deredge, D. J.; Stemmler, T. L.; Giedroc, D. P. Coupling of Zinc and GTP Binding Drives G-Domain Folding in *Acinetobacter baumannii* ZigA. *Biophys. J.* **2024**, *123*, 979−991.
(821) Yuen, M. H.; Fong, Y. H.; Nim, Y. S.; Lau, P. H.; Wong, K. Structural Insights into How GTP-Dependent Conformational Changes in a Metallochaperone UreG Facilitate Urease Maturation. *Proc. Natl. Acad. Sci. U. S. A.* **2017**, *114*, No. e10890-e10898.
(822) Xia, W.; Li, H.; Yang, X.; Wong, K.-B.; Sun, H. Metallo-GTPase HypB from *Helicobacter pylori* and Its Interaction with Nickel Chaperone Protein HypA. *J. Biol. Chem.* **2012**, *287*, 6753−6763.
(823) Benoit, S. L.; McMurry, J. L.; Hill, S. A.; Maier, R. J. *Helicobacter pylori* Hydrogenase Accessory Protein HypA and Urease Accessory Protein UreG Compete with Each Other for UreE Recognition. *Biochim. Biophys. Acta* **2012**, *1820*, 1519−1525.
(824) Tsang, K. L.; Wong, K. B. Moving Nickel along the Hydrogenase-Urease Maturation Pathway. *Metallomics* **2022**, *14*, mfac003.
(825) Leipe, D. D.; Wolf, Y. I.; Koonin, E. V.; Aravind, L. Classification and Evolution of P-Loop GTPases and Related ATPases. *J. Mol. Biol.* **2002**, *317*, 41−72.
(826) Gasper, R.; Meyer, S.; Gotthardt, K.; Sirajuddin, M.; Wittinghofer, A. It Takes Two to Tango: Regulation of G Proteins by Dimerization. *Nat. Rev. Mol. Cell Biol.* **2009**, *10*, 423−429.
(827) Boer, J. L.; Quiroz-Valenzuela, S.; Anderson, K. L.; Hausinger, R. P. Mutagenesis of *Klebsiella Aerogenes* UreG to Probe Nickel Binding and Interactions with Other Urease-Related Proteins. *Biochemistry* **2010**, *49*, 5859−5869.
(828) Sydor, A. M.; Lebrette, H.; Ariyakumaran, R.; Cavazza, C.; Zamble, D. B. Relationship between Ni(II) and Zn(II) Coordination and Nucleotide Binding by the *Helicobacter pylori* [NiFe]-Hydrogenase and Urease Maturation Factor HypB. *J. Biol. Chem.* **2014**, *289*, 3828−3841.
(829) Douglas, C. D.; Ngu, T. T.; Kaluarachchi, H.; Zamble, D. B. Metal Transfer within the *Escherichia coli* HypB-HypA Complex of Hydrogenase Accessory Proteins. *Biochemistry* **2013**, *52*, 6030−9.
(830) Fong, Y. H.; Wong, H. C.; Yuen, M. H.; Lau, P. H.; Chen, Y. W.; Wong, K.-B. Structure of UreG/UreF/UreH Complex Reveals How Urease Accessory Proteins Facilitate Maturation of *Helicobacter pylori* Urease. *PLoS Biol.* **2013**, *11*, No. e1001678.
(831) Jabri, E.; Carr, M. B.; Hausinger, R. P.; Karplus, P. A. The Crystal Structure of Urease from *Klebsiella aerogenes*. *Science* **1995**, *268*, 998−1004.
(832) Zhang, S.; Shen, Y.; Liu, H.; Zhu, D.; Fang, J.; Pan, H.; Liu, W. Inflammatory Microenvironment in Gastric Premalignant Lesions: Implication and Application. *Front Immunol* **2023**, *14*, 1297101.
(833) Nim, Y. S.; Fong, I. Y. H.; Deme, J.; Tsang, K. L.; Caesar, J.; Johnson, S.; Pang, L. T. H.; Yuen, N. M. H.; Ng, T. L. C.; Choi, T.; et al. Delivering a Toxic Metal to the Active Site of Urease. *Sci. Adv.* **2023**, *9*, No. eadf7790.
(834) Chovancova, E.; Pavelka, A.; Benes, P.; Strnad, O.; Brezovsky, J.; Kozlikova, B.; Gora, A.; Sustr, V.; Klvana, M.; Medek, P.; et al. CAVER 3.0: A Tool for the Analysis of Transport Pathways in Dynamic Protein Structures. *PLoS Comput. Biol.* **2012**, *8*, e1002708.
(835) Mascarenhas, R.; Ruetz, M.; Gouda, H.; Heitman, N.; Yaw, M.; Banerjee, R. Architecture of the Human G-Protein-Methylmalonyl-CoA Mutase Nanoassembly for B_{12} Delivery and Repair. *Nat. Commun.* **2023**, *14*, 4332.
(836) Li, Z.; Gouda, H.; Pillay, S.; Yaw, M.; Ruetz, M.; Banerjee, R. The Human B(12) Trafficking Chaperones: CblA, ATR, CblC and CblD. *Methods Enzymol* **2022**, *668*, 137−156.
(837) Vaccaro, F. A.; Born, D. A.; Drennan, C. L. Structure of Metallochaperone in Complex with the Cobalamin-Binding Domain of Its Target Mutase Provides Insight into Cofactor Delivery. *Proc. Natl. Acad. Sci. U. S. A.* **2023**, *120*, No. e2214085120.
(838) Padovani, D.; Banerjee, R. A G-Protein Editor Gates Coenzyme B_{12} Loading and Is Corrupted in Methylmalonic Aciduria. *Proc. Natl. Acad. Sci. U. S. A.* **2009**, *106*, 21567−21572.
(839) Padovani, D.; Labunska, T.; Banerjee, R. Energetics of Interaction between the G-Protein Chaperone, MeaB, and B_{12}-Dependent Methylmalonyl-CoA Mutase. *J. Biol. Chem.* **2006**, *281*, 17838−17844.
(840) Jost, M.; Cracan, V.; Hubbard, P. A.; Banerjee, R.; Drennan, C. L. Visualization of a Radical B_{12} Enzyme with Its G-Protein Chaperone. *Proc. Natl. Acad. Sci. U. S. A.* **2015**, *112*, 2419−2424.
(841) Vaccaro, F. A.; Faber, D. A.; Andree, G. A.; Born, D. A.; Kang, G.; Fonseca, D. R.; Jost, M.; Drennan, C. L. Structural Insight into G-Protein Chaperone-Mediated Maturation of a Bacterial Adenosylcobalamin-Dependent Mutase. *J. Biol. Chem.* **2023**, *299*, 105109.
(842) Hubbard, P. A.; Padovani, D.; Labunska, T.; Mahlstedt, S. A.; Banerjee, R.; Drennan, C. L. Crystal Structure and Mutagenesis of the Metallochaperone MeaB: Insight into the Causes of Methylmalonic Aciduria. *J. Biol. Chem.* **2007**, *282*, 31308−31316.
(843) Gumataotao, N.; Lankathilaka, K. P. W.; Bennett, B.; Holz, R. C. The Iron-Type Nitrile Hydratase Activator Protein Is a GTPase. *Biochem. J.* **2017**, *474*, 247−258.
(844) Lankathilaka, K. P. W.; Bennett, B.; Holz, R. C. The Fe-Type Nitrile Hydratase from *Rhodococcus equi* TG328−2 Forms an Alpha-Activator Protein Complex. *J. Biol. Inorg. Chem.* **2020**, *25*, 903−911.
(845) Crouzet, J.; Levy-Schil, S.; Cameron, B.; Cauchois, L.; Rigault, S.; Rouyez, M. C.; Blanche, F.; Debussche, L.; Thibaut, D. Nucleotide Sequence and Genetic Analysis of a 13.1-Kilobase-Pair *Pseudomonas denitrificans* DNA Fragment Containing Five Cob Genes and Identification of Structural Genes Encoding Cob(I)Alamin Adenosyltransferase, Cobyric Acid Synthase, and Bifunctional Cob. *J. Bacteriol.* **1991**, *173*, 6074−6087.
(846) Zhang, L.; Braynen, J.; Fahey, A.; Chopra, K.; Cifani, P.; Tadesse, D.; Regulski, M.; Hu, F.; van Dam, H. J. J.; Xie, M.; et al. Two Related Families of Metal Transferases, ZNG1 and ZNG2, Are Involved in Acclimation to Poor Zn Nutrition in *Arabidopsis*. *Front Plant Sci.* **2023**, *14*, 1237722.

(847) Khil, P. P.; Obmolova, G.; Teplyakov, A.; Howard, A. J.; Gilliland, G. L.; Camerini-Otero, R. D. Crystal Structure of the *Escherichia coli* YjiA Protein Suggests a GTP-Dependent Regulatory Function. *Proteins* **2004**, *54*, 371−4.
(848) Blaby-Haas, C. E.; Flood, J. A.; Crecy-Lagard, V.; Zamble, D. B. YeiR: A Metal-Binding GTPase from *Escherichia coli* Involved in Metal Homeostasis. *Metallomics* **2012**, *4*, 488−497.
(849) Jordan, M. R.; Wang, J.; Weiss, A.; Skaar, E. P.; Capdevila, D. A.; Giedroc, D. P. Mechanistic Insights into the Metal-Dependent Activation of Zn^{II} -Dependent Metallochaperones. *Inorg. Chem.* **2019**, *58*, 13661−13672.
(850) Bennison, D. J.; Nakamoto, J. A.; Craggs, T. D.; Milon, P.; Rafferty, J. B.; Corrigan, R. M. The Stringent Response Inhibits 70S Ribosome Formation in *Staphylococcus aureus* by Impeding GTPase-Ribosome Interactions. *mBio* **2021**, *12*, No. e0267921.
(851) Young, T. R.; Deery, E.; Foster, A. W.; Martini, M. A.; Osman, D.; Warren, M. J.; Robinson, N. J. Two Distinct Thermodynamic Gradients for Cellular Metalation of Vitamin B_{12}. *JACS Au* **2023**, *3*, 1472−1483.
(852) Saudino, G.; Ciofi-Baffoni, S.; Banci, L. Protein-Interaction Affinity Gradient Drives [4Fe-4S] Cluster Insertion in Human Lipoyl Synthase. *J. Am. Chem. Soc.* **2022**, *144*, 5713−5717.
(853) Schedlbauer, A.; Iturrioz, I.; Ochoa-Lizarralde, B.; Diercks, T.; Lopez-Alonso, J. P.; Lavin, J. L.; Kaminishi, T.; Capuni, R.; Dhimole, N.; de Astigarraga, E.; et al. A Conserved rRNA Switch Is Central to Decoding Site Maturation on the Small Ribosomal Subunit. *Sci. Adv.* **2021**, *7*, No. eabf7547.
(854) Zhou, Z.; Hashimoto, Y.; Kobayashi, M. Self-Subunit Swapping Chaperone Needed for the Maturation of Multimeric Metalloenzyme Nitrile Hydratase by a Subunit Exchange Mechanism Also Carries out the Oxidation of the Metal Ligand Cysteine Residues and Insertion of Cobalt. *J. Biol. Chem.* **2009**, *284*, 14930−14938.
(855) Zhou, Z.; Hashimoto, Y.; Shiraki, K.; Kobayashi, M. Discovery of Posttranslational Maturation by Self-Subunit Swapping. *Proc. Natl. Acad. Sci. U. S. A.* **2008**, *105*, 14849−14854.
(856) Xia, Y.; Cheng, Z.; Hou, C.; Peplowski, L.; Zhou, Z.; Chen, X. Discovery of the ATPase Activity of a Cobalt-Type Nitrile Hydratase Activator and Its Promoting Effect on Enzyme Maturation. *Biochemistry* **2022**, *61*, 2940−2947.
(857) Hashimoto, Y.; Ube, Y.; Doi, S.; Kumano, T.; Kobayashi, M. Metal Chaperone, Nhpc, Involved in the Metallocenter Biosynthesis of Nitrile Hydratase. *J. Gen Appl. Microbiol* **2021**, *67*, 24−32.
(858) Miyanaga, A.; Fushinobu, S.; Ito, K.; Wakagi, T. Crystal Structure of Cobalt-Containing Nitrile Hydratase. *Biochem. Biophys. Res. Commun.* **2001**, *288*, 1169−1174.
(859) Endo, I.; Nojiri, M.; Tsujimura, M.; Nakasako, M.; Nagashima, S.; Yohda, M.; Odaka, M. Fe-Type Nitrile Hydratase. *J. Inorg. Biochem* **2001**, *83*, 247−253.
(860) Nelp, M. T.; Astashkin, A. V.; Breci, L. A.; McCarty, R. M.; Bandarian, V. The Alpha Subunit of Nitrile Hydratase Is Sufficient for Catalytic Activity and Post-Translational Modification. *Biochemistry* **2014**, *53*, 3990−3994.
(861) Song, L.; Wang, M.; Shi, J.; Xue, Z.; Wang, M. X.; Qian, S. High Resolution X-Ray Molecular Structure of the Nitrile Hydratase from *Rhodococcus erythropolis* AJ270 Reveals Posttranslational Oxidation of Two Cysteines into Sulfinic Acids and a Novel Biocatalytic Nitrile Hydration Mechanism. *Biochem. Biophys. Res. Commun.* **2007**, *362*, 319−324.
(862) Tanaka, Y.; Nakagawa, N.; Kuramitsu, S.; Yokoyama, S.; Masui, R. Novel Reaction Mechanism of GTP Cyclohydrolase I. High-Resolution X-Ray Crystallography of *Thermus thermophilus* HB8 Enzyme Complexed with a Transition State Analogue, the 8-Oxoguanine Derivative. *J. Biochem* **2005**, *138*, 263−275.
(863) Schussler, S.; Haase, I.; Perbandt, M.; Illarionov, B.; Siemens, A.; Richter, K.; Bacher, A.; Fischer, M.; Grawert, T. Structure of GTP Cyclohydrolase I from *Listeria monocytogenes*, a Potential Anti-Infective Drug Target. *Acta Crystallogr. F Struct Biol. Commun.* **2019**, *75*, 586−592.
(864) Saio, T.; Guan, X.; Rossi, P.; Economou, A.; Kalodimos, C. G. Structural Basis for Protein Antiaggregation Activity of the Trigger Factor Chaperone. *Science* **2014**, *344*, 1250494.
(865) Deuerling, E.; Gamerdinger, M.; Kreft, S. G. Chaperone Interactions at the Ribosome. *Cold Spring Harb Perspect Biol.* **2019**, *11*, a033977.
(866) Kohl, M. P.; Chane-Woon-Ming, B.; Bahena-Ceron, R.; Jaramillo-Ponce, J.; Antoine, L.; Herrgott, L.; Romby, P.; Marzi, S. Ribosome Profiling Methods Adapted to the Study of RNA-Dependent Translation Regulation in *Staphylococcus aureus*. *Methods Mol. Biol.* **2024**, *2741*, 73−100.
(867) Gamerdinger, M.; Jia, M.; Schloemer, R.; Rabl, L.; Jaskolowski, M.; Khakzar, K. M.; Ulusoy, Z.; Wallisch, A.; Jomaa, A.; Hunaeus, G.; et al. NAC Controls Cotranslational N-Terminal Methionine Excision in Eukaryotes. *Science* **2023**, *380*, 1238−1243.
(868) Addlagatta, A.; Hu, X.; Liu, J. O.; Matthews, B. W. Structural Basis for the Functional Differences between Type I and Type II Human Methionine Aminopeptidases. *Biochemistry* **2005**, *44*, 14741−14749.
(869) Wang, Y.; Weisenhorn, E.; Macdiarmid, C. W.; Andreini, C.; Bucci, M.; Taggart, J.; Banci, L.; Russell, J.; Coon, J. J.; Eide, D. J. The Cellular Economy of the *Saccharomyces cerevisiae* Zinc Proteome. *Metallomics* **2018**, *10*, 1755−1776.
(870) Braymer, J. J.; Giedroc, D. P. Recent Developments in Copper and Zinc Homeostasis in Bacterial Pathogens. *Curr. Opin Chem. Biol.* **2014**, *19*, 59−66.
(871) Osman, D.; Cavet, J. S. Copper Homeostasis in Bacteria. *Adv. Appl. Microbiol* **2008**, *65*, 217−247.
(872) Andrei, A.; Öztürk, Y.; Khalfaoui-Hassani, B.; Rauch, J.; Marckmann, D.; Trasnea, P.-I.; Daldal, F.; Koch, H.-G. Cu Homeostasis in Bacteria: The Ins and Outs. *Membranes* **2020**, *10*, 242.
(873) Huokko, T.; Ni, T.; Dykes, G. F.; Simpson, D. M.; Brownridge, P.; Conradi, F. D.; Beynon, R. J.; Nixon, P. J.; Mullineaux, C. W.; Zhang, P.; et al. Probing the Biogenesis Pathway and Dynamics of Thylakoid Membranes. *Nat. Commun.* **2021**, *12*, 3475.
(874) Rosenzweig, A. C.; O'Halloran, T. V. Structure and Chemistry of the Copper Chaperone Proteins. *Curr. Opin Chem. Biol.* **2000**, *4*, 140−147.
(875) Fu, Y.; Tsui, H.-C. T. H.; Bruce, K. E.; Sham, L.-T. L.; Higgins, K. A.; Lisher, J. P.; Kazmierczak, K. M.; Maroney, M. J.; Dann, C. E.; Winkler, M. E.; Giedroc, D. P. A New Structural Paradigm in Copper Resistance in *Streptococcus pneumoniae*. *Nat. Chem. Biol.* **2013**, *9*, 177−83.
(876) Chaplin, A. K.; Tan, B. G.; Vijgenboom, E.; Worrall, J. A. R. Copper Trafficking in the CsoR Regulon of *Streptomyces lividans*. *Metallomics* **2015**, *7*, 145−155.
(877) Novoa-Aponte, L.; Ramirez, D.; Arguello, J. M. The Interplay of the Metallosensor CueR with Two Distinct CopZ Chaperones Defines Copper Homeostasis in *Pseudomonas aeruginosa*. *J. Biol. Chem.* **2019**, *294*, 4934−4945.
(878) Cobine, P.; Wickramasinghe, W. A.; Harrison, M. D.; Weber, T.; Solioz, M.; Dameron, C. T. The *Enterococcus Hirae* Copper Chaperone CopZ Delivers Copper(I) to the CopY Repressor. *FEBS Lett.* **1999**, *445*, 27−30.
(879) Kosman, D. J. Multicopper Oxidases: A Workshop on Copper Coordination Chemistry, Electron Transfer, and Metallophysiology. *J. Biol. Inorg. Chem.* **2010**, *15*, 15−28.
(880) Zapotoczna, M.; Riboldi, G. P.; Moustafa, A. M.; Dickson, E.; Narechania, A.; Morrissey, J. A.; Planet, P. J.; Holden, M. T. G.; Waldron, K. J.; Geoghegan, J. A. Mobile-Genetic-Element-Encoded Hypertolerance to Copper Protects *Staphylococcus aureus* from Killing by Host Phagocytes. *mBio* **2018**, *9*, mbio00550.
(881) Rowland, J. L.; Niederweis, M. A Multicopper Oxidase Is Required for Copper Resistance in *Mycobacterium tuberculosis*. *J. Bacteriol.* **2013**, *195*, 3724−3733.
(882) Achard, M. E.; Tree, J. J.; Holden, J. A.; Simpfendorfer, K. R.; Wijburg, O. L.; Strugnell, R. A.; Schembri, M. A.; Sweet, M. J.; Jennings, M. P.; McEwan, A. G. The Multi-Copper-Ion Oxidase CueO of

Salmonella enterica Serovar Typhimurium Is Required for Systemic Virulence. *Infect. Immun.* **2010**, *78*, 2312−2319.
(883) Arnesano, F.; Banci, L.; Bertini, I.; Mangani, S.; Thompsett, A. R. A Redox Switch in CopC: An Intriguing Copper Trafficking Protein That Binds Copper(I) and Copper(II) at Different Sites. *Proc. Natl. Acad. Sci. U. S. A.* **2003**, *100*, 3814−3819.
(884) Wernimont, A. K.; Huffman, D. L.; Finney, L. A.; Demeler, B.; O'Halloran, T. V.; Rosenzweig, A. C. Crystal Structure and Dimerization Equilibria of PcoC, a Methionine- Rich Copper Resistance Protein from *Escherichia coli*. *J. Biol. Inorg. Chem.* **2003**, *8*, 185−194.
(885) Zhang, L.; Koay, M.; Maher, M. J.; Xiao, Z.; Wedd, A. G. Intermolecular Transfer of Copper Ions from the CopC Protein of *Pseudomonas syringae*. Crystal Structures of Fully Loaded Cu(I)Cu(II) Forms. *J. Am. Chem. Soc.* **2006**, *128*, 5834−5850.
(886) Chacon, K. N.; Perkins, J.; Mathe, Z.; Alwan, K.; Ho, E. N.; Ucisik, M. N.; Merz, K. M.; Blackburn, N. J. Trapping Intermediates in Metal Transfer Reactions of the CusCBAF Export Pump of *Escherichia coli*. *Commun. Biol.* **2018**, *1*, 192.
(887) Franke, S.; Grass, G.; Rensing, C.; Nies, D. H. Molecular Analysis of the Copper-Transporting Efflux System CusCFBA of *Escherichia coli*. *J. Bacteriol.* **2003**, *185*, 3804−3812.
(888) Purves, J.; Thomas, J.; Riboldi, G. P.; Zapotoczna, M.; Tarrant, E.; Andrew, P. W.; Londoño, A.; Planet, P. J.; Geoghegan, J. A.; Waldron, K. J.; et al. A Horizontally Gene Transferred Copper Resistance Locus Confers Hyper-Resistance to Antibacterial Copper Toxicity and Enables Survival of Community Acquired Methicillin Resistant *Staphylococcus aureus* USA300 in Macrophages. *Environ. Microbiol* **2018**, *20*, 1576−1589.
(889) Rosario-Cruz, Z.; Eletsky, A.; Daigham, N. S.; Al-Tameemi, H.; Swapna, G. V. T.; Kahn, P. C.; Szyperski, T.; Montelione, G. T.; Boyd, J. M. The CopBL Operon Protects *Staphylococcus aureus* from Copper Toxicity: CopL Is an Extracellular Membrane-Associated Copper-Binding Protein. *J. Biol. Chem.* **2019**, *294*, 4027−4044.
(890) Gold, B.; Deng, H.; Bryk, R.; Vargas, D.; Eliezer, D.; Roberts, J.; Jiang, X.; Nathan, C. Identification of a Copper-Binding Metallothionein in Pathogenic Mycobacteria. *Nat. Chem. Biol.* **2008**, *4*, 609−616.
(891) Latorre, M.; Olivares, F.; Reyes-Jara, A.; Lopez, G.; Gonzalez, M. CutC Is Induced Late during Copper Exposure and Can. Modify Intracellular Copper Content in *Enterococcus faecalis*. *Biochem. Biophys. Res. Commun.* **2011**, *406*, 633−637.
(892) Dennison, C.; David, S.; Lee, J. Bacterial Copper Storage Proteins. *J. Biol. Chem.* **2018**, *293*, 4616−4627.
(893) Vita, N.; Platsaki, S.; Basle, A.; Allen, S. J.; Paterson, N. G.; Crombie, A. T.; Murrell, J. C.; Waldron, K. J.; Dennison, C. A Four-Helix Bundle Stores Copper for Methane Oxidation. *Nature* **2015**, *525*, 140−143.
(894) Straw, M. L.; Hough, M. A.; Wilson, M. T.; Worrall, J. A. R. A Histidine Residue and a Tetranuclear Cuprous-Thiolate Cluster Dominate the Copper Loading Landscape of a Copper Storage Protein from *Streptomyces lividans*. *Chemistry* **2019**, *25*, 10678−10688.
(895) Lee, J.; Dalton, R. A.; Baslé, A.; Vita, N.; Dennison, C. Important Structural Features of Thiolate-Rich Four-Helix Bundles for Cu(I) Uptake and Removal. *Inorg. Chem.* **2023**, *62*, 6617−6628.
(896) Straw, M. L.; Chaplin, A. K.; Hough, M. A.; Paps, J.; Bavro, V. N.; Wilson, M. T.; Vijgenboom, E.; Worrall, J. A. R. A Cytosolic Copper Storage Protein Provides a Second Level of Copper Tolerance in *Streptomyces lividans*. *Metallomics* **2018**, *10*, 180−193.
(897) Vita, N.; Landolfi, G.; Basle, A.; Platsaki, S.; Lee, J.; Waldron, K. J.; Dennison, C. Bacterial Cytosolic Proteins with a High Capacity for Cu(I) That Protect against Copper Toxicity. *Sci. Rep* **2016**, *6*, 39065.
(898) Lee, J.; Dennison, C. Cytosolic Copper Binding by a Bacterial Storage Protein and Interplay with Copper Efflux. *Int. J. Mol. Sci.* **2019**, *20*, 4144.
(899) Lee, J.; Dalton, R. A.; Dennison, C. Copper Delivery to an Endospore Coat. Protein of *Bacillus subtilis*. *Front Cell Dev Biol.* **2022**, *10*, 916114.
(900) Nicolas, P.; Mader, U.; Dervyn, E.; Rochat, T.; Leduc, A.; Pigeonneau, N.; Bidnenko, E.; Marchadier, E.; Hoebeke, M.; Aymerich, S.; et al. Condition-Dependent Transcriptome Reveals High-Level Regulatory Architecture in *Bacillus subtilis*. *Science* **2012**, *335*, 1103−1106.
(901) Palmgren, M. G.; Nissen, P. P-Type ATPases. *Annu. Rev. Biophys* **2011**, *40*, 243−266.
(902) Albers, R. W. Biochemical Aspects of Active Transport. *Annu. Rev. Biochem.* **1967**, *36*, 727−756.
(903) Palmgren, M. P-Type ATPases: Many More Enigmas Left to Solve. *J. Biol. Chem.* **2023**, *299*, 105352.
(904) Dyla, M.; Basse Hansen, S.; Nissen, P.; Kjaergaard, M. Structural Dynamics of P-Type ATPase Ion Pumps. *Biochem. Soc. Trans.* **2019**, *47*, 1247−1257.
(905) Purohit, R.; Ross, M. O.; Batelu, S.; Kusowski, A.; Stemmler, T. L.; Hoffman, B. M.; Rosenzweig, A. C. Cu(+)-Specific CopB Transporter: Revising P_{1B}-Type ATPase Classification. *Proc. Natl. Acad. Sci. U. S. A.* **2018**, *115*, 2108−2113.
(906) Vanoevelen, J.; Dode, L.; Van Baelen, K.; Fairclough, R. J.; Missiaen, L.; Raeymaekers, L.; Wuytack, F. The Secretory Pathway Ca^{2+}/Mn^{2+}-ATPase 2 Is a Golgi-Localized Pump with High Affinity for Ca^{2+} Ions. *J. Biol. Chem.* **2005**, *280*, 22800−22808.
(907) Wu, M.; Wu, C.; Song, T.; Pan, K.; Wang, Y.; Liu, Z. Structure and Transport Mechanism of the Human Calcium Pump SPCA1. *Cell Res.* **2023**, *33*, 533−545.
(908) Chen, Z.; Watanabe, S.; Hashida, H.; Inoue, M.; Daigaku, Y.; Kikkawa, M.; Inaba, K. Cryo-EM Structures of Human SPCA1a Reveal the Mechanism of Ca^{2+}/Mn^{2+}Transport into the Golgi Apparatus. *Sci. Adv.* **2023**, *9*, No. eadd9742.
(909) Gronberg, C.; Hu, Q.; Mahato, D. R.; Longhin, E.; Salustros, N.; Duelli, A.; Lyu, P.; Bagenholm, V.; Eriksson, J.; Rao, K. U.; et al. Structure and Ion-Release Mechanism of P_{IB-4}-Type ATPases. *Elife* **2021**, *10*, No. e73124.
(910) Smith, A. T.; Smith, K. P.; Rosenzweig, A. C. Diversity of the Metal-Transporting P1B-Type ATPases. *J. Biol. Inorg. Chem.* **2014**, *19*, 947−960.
(911) Gonzalez-Guerrero, M.; Arguello, J. M. Mechanism of Cu^+-Transporting ATPases: Soluble Cu^+ Chaperones Directly Transfer Cu^+ to Transmembrane Transport Sites. *Proc. Natl. Acad. Sci. U. S. A.* **2008**, *105*, 5992−5997.
(912) Fu, Y.; Bruce, K. E.; Wu, H.; Giedroc, D. P. The S2 Cu(I) Site in CupA from *Streptococcus pneumoniae* Is Required for Cellular Copper Resistance. *Metallomics* **2016**, *8*, 61−70.
(913) Salustros, N.; Gronberg, C.; Abeyrathna, N. S.; Lyu, P.; Oradd, F.; Wang, K.; Andersson, M.; Meloni, G.; Gourdon, P. Structural Basis of Ion Uptake in Copper-Transporting P_{1B}-Type ATPases. *Nat. Commun.* **2022**, *13*, 5121.
(914) Mattle, D.; Zhang, L.; Sitsel, O.; Pedersen, L. T.; Moncelli, M. R.; Tadini-Buoninsegni, F.; Gourdon, P.; Rees, D. C.; Nissen, P.; Meloni, G. A Sulfur-Based Transport Pathway in Cu^+-ATPases. *EMBO Rep* **2015**, *16*, 728−740.
(915) Gallenito, M. J.; Irvine, G. W.; Zhang, L.; Meloni, G. Coordination Promiscuity Guarantees Metal Substrate Selection in Transmembrane Primary-Active Zn^{2+} Pumps. *Chem. Commun.* **2019**, *55*, 10844−10847.
(916) Raimunda, D.; Subramanian, P.; Stemmler, T.; Arguello, J. M. A Tetrahedral Coordination of Zinc during Transmembrane Transport by P-Type Zn^{2+}-ATPases. *Biochim Biophys Acta Biomembr* **2012**, *1818*, 1374−1377.
(917) Gourdon, P.; Liu, X. Y.; Skjorringe, T.; Morth, J. P.; Moller, L. B.; Pedersen, B. P.; Nissen, P. Crystal Structure of a Copper-Transporting P_{IB}-Type ATPase. *Nature* **2011**, *475*, 59−64.
(918) Wang, K.; Sitsel, O.; Meloni, G.; Autzen, H. E.; Andersson, M.; Klymchuk, T.; Nielsen, A. M.; Rees, D. C.; Nissen, P.; Gourdon, P. Structure and Mechanism of Zn^{2+}-Transporting P-Type ATPases. *Nature* **2014**, *514*, 518−522.
(919) Raimunda, D.; Long, J. E.; Sassetti, C. M.; Arguello, J. M. Role in Metal Homeostasis of CtpD, a Co(2)(+) Transporting P_{1B4}-ATPase of *MycobacteriumsSmegmatis*. *Mol. Microbiol.* **2012**, *84*, 1139−1149.

https://doi.org/10.1021/acs.chemrev.4c00264
Chem. Rev. 2024, 124, 13574−13659

(920) Pi, H.; Patel, S. J.; Arguello, J. M.; Helmann, J. D. The *Listeria monocytogenes* Fur-Regulated Virulence Protein FrvA Is an Fe(II) Efflux P_{1B4} -Type ATPase. *Mol. Microbiol.* **2016**, *100*, 1066−1079.
(921) Patel, S. J.; Lewis, B. E.; Long, J. E.; Nambi, S.; Sassetti, C. M.; Stemmler, T. L.; Arguello, J. M. Fine-Tuning of Substrate Affinity Leads to Alternative Roles of *Mycobacterium tuberculosis* Fe^{2+}-ATPases. *J. Biol. Chem.* **2016**, *291*, 11529−11539.
(922) Guan, G.; Pinochet-Barros, A.; Gaballa, A.; Patel, S. J.; Argüello, J. M.; Helmann, J. D. PfeT, a P1B4-Type ATPase, Effluxes Ferrous Iron and Protects *Bacillus subtilis* against Iron Intoxication. *Mol. Microbiol.* **2015**, *98*, 787−803.
(923) Turner, A. G.; Djoko, K. Y.; Ong, C. Y.; Barnett, T. C.; Walker, M. J.; McEwan, A. G. Group A Streptococcus Co-Ordinates Manganese Import and Iron Efflux in Response to Hydrogen Peroxide Stress. *Biochem. J.* **2019**, *476*, 595−611.
(924) VanderWal, A. R.; Makthal, N.; Pinochet-Barros, A.; Helmann, J. D.; Olsen, R. J.; Kumaraswami, M. Iron Efflux by PmtA Is Critical for Oxidative Stress Resistance and Contributes Significantly to Group A Streptococcus Virulence. *Infect. Immun.* **2017**, *85*, No. e00091.
(925) Brenot, A.; Weston, B. F.; Caparon, M. G. A PerR-Regulated Metal Transporter (PmtA) Is an Interface between Oxidative Stress and Metal Homeostasis in *Streptococcus pyogenes*. *Mol. Microbiol.* **2007**, *63*, 1185−1196.
(926) Gonciarz, R. L.; Renslo, A. R. Emerging Role of Ferrous Iron in Bacterial Growth and Host-Pathogen Interaction: New Tools for Chemical (Micro)Biology and Antibacterial Therapy. *Curr. Opin Chem. Biol.* **2021**, *61*, 170−178.
(927) Blank, B. R.; Talukder, P.; Muir, R. K.; Green, E. R.; Skaar, E. P.; Renslo, A. R. Targeting Mobilization of Ferrous Iron in *Pseudomonas aeruginosa* Infection with an Iron(II)-Caged LpxC Inhibitor. *ACS Infect Dis* **2019**, *5*, 1366−1375.
(928) Aron, A. T.; Heffern, M. C.; Lonergan, Z. R.; Vander Wal, M. N.; Blank, B. R.; Spangler, B.; Zhang, Y.; Park, H. M.; Stahl, A.; Renslo, A. R.; Skaar, E. P.; Chang, C. J. *In Vivo* Bioluminescence Imaging of Labile Iron Accumulation in a Murine Model of *Acinetobacter baumannii* Infection. *Proc. Natl. Acad. Sci. U. S. A.* **2017**, *114*, 12669.
(929) Brown, J. B.; Lee, M. A.; Smith, A. T. Ins and Outs: Recent Advancements in Membrane Protein-Mediated Prokaryotic Ferrous Iron Transport. *Biochemistry* **2021**, *60*, 3277−3291.
(930) Pi, H.; Helmann, J. D. Ferrous Iron Efflux Systems in Bacteria. *Metallomics* **2017**, *9*, 840−851.
(931) Sestok, A. E.; Linkous, R. O.; Smith, A. T. Toward a Mechanistic Understanding of Feo-Mediated Ferrous Iron Uptake. *Metallomics* **2018**, *10*, 887−898.
(932) Komeili, A. Molecular Mechanisms of Magnetosome Formation. *Annu. Rev. Biochem.* **2007**, *76*, 351−366.
(933) Byrne, M. E.; Ball, D. A.; Guerquin-Kern, J. L.; Rouiller, I.; Wu, T. D.; Downing, K. H.; Vali, H.; Komeili, A. *Desulfovibrio magneticus* RS-1 Contains an Iron- and Phosphorus-Rich Organelle Distinct from Its Bullet-Shaped Magnetosomes. *Proc. Natl. Acad. Sci. U. S. A.* **2010**, *107*, 12263−12268.
(934) Mridha, S.; Abt, M. C. Starvation Helps Transition to Abundance - a Ferrosome Story. *Trends Microbiol* **2024**, *32*, 219−220.
(935) Boudehen, Y. M.; Faucher, M.; Marechal, X.; Miras, R.; Rech, J.; Rombouts, Y.; Seneque, O.; Wallat, M.; Demange, P.; Bouet, J. Y.; et al. Mycobacterial Resistance to Zinc Poisoning Requires Assembly of P-ATPase-Containing Membrane Metal Efflux Platforms. *Nat. Commun.* **2022**, *13*, 4731.
(936) Martin, J. E.; Waters, L. S.; Storz, G.; Imlay, J. A. The *Escherichia coli* Small Protein MntS and Exporter MntP Optimize the Intracellular Concentration of Manganese. *PLoS Genet* **2015**, *11*, No. e1004977.
(937) Wright, Z.; Seymour, M.; Paszczak, K.; Truttmann, T.; Senn, K.; Stilp, S.; Jansen, N.; Gosz, M.; Goeden, L.; Anantharaman, V.; et al. The Small Protein MntS Evolved from a Signal Peptide and Acquired a Novel Function Regulating Manganese Homeostasis in *Escherichia coli*. *Mol. Microbiol.* **2024**, *121*, 152−166.
(938) Rosenzweig, A. C. Copper Delivery by Metallochaperone Proteins. *Acc. Chem. Res.* **2001**, *34*, 119−128.
(939) Fu, Y.; Tsui, H. C.; Bruce, K. E.; Sham, L. T.; Higgins, K. A.; Lisher, J. P.; Kazmierczak, K. M.; Maroney, M. J.; Dann, C. E., 3rd; Winkler, M. E.; et al. A New Structural Paradigm in Copper Resistance in *Streptococcus pneumoniae*. *Nat. Chem. Biol.* **2013**, *9*, 177−183.
(940) Fu, Y.; Chang, F. M.; Giedroc, D. P. Copper Transport and Trafficking at the Host-Bacterial Pathogen Interface. *Acc. Chem. Res.* **2014**, *47*, 3605−3613.
(941) Botella, H.; Stadthagen, G.; Lugo-Villarino, G.; de Chastellier, C.; Neyrolles, O. Metallobiology of Host-Pathogen Interactions: An Intoxicating New Insight. *Trends Microbiol* **2012**, *20*, 106−112.
(942) Ward, S. K.; Abomoelak, B.; Hoye, E. A.; Steinberg, H.; Talaat, A. M. CtpV: A Putative Copper Exporter Required for Full Virulence of *Mycobacterium tuberculosis*. *Mol. Microbiol.* **2010**, *77*, 1096−1110.
(943) Botella, H.; Peyron, P.; Levillain, F.; Poincloux, R.; Poquet, Y.; Brandli, I.; Wang, C.; Tailleux, L.; Tilleul, S.; Charrière, G. M.; et al. Mycobacterial P1-Type ATPases Mediate Resistance to Zinc Poisoning in Human Macrophages. *Cell Host Microbe* **2011**, *10*, 248−259.
(944) Dupuy, P.; Gutierrez, C.; Neyrolles, O. Modulation of Bacterial Membrane Proteins Activity by Clustering into Plasma Membrane Nanodomains. *Mol. Microbiol.* **2023**, *120*, 502−507.
(945) Patel, S. J.; Padilla-Benavides, T.; Collins, J. M.; Arguello, J. M. Functional Diversity of Five Homologous Cu^{+}-ATPases Present in *Sinorhizobium meliloti*. *Microbiology* **2014**, *160*, 1237−1251.
(946) Padilla-Benavides, T.; George Thompson, A. M.; McEvoy, M. M.; Arguello, J. M. Mechanism of ATPase-Mediated Cu^{+} Export and Delivery to Periplasmic Chaperones: The Interaction of *Escherichia coli* CopA and CusF. *J. Biol. Chem.* **2014**, *289*, 20492−20501.
(947) Maltman, C.; Yurkov, V. Extreme Environments and High-Level Bacterial Tellurite Resistance. *Microorganisms* **2019**, *7*, 601.
(948) Mason, S.; Vornhagen, J.; Smith, S. N.; Mike, L. A.; Mobley, H. L. T.; Bachman, M. A. The *Klebsiella pneumoniae* Ter Operon Enhances Stress Tolerance. *Infect. Immun.* **2023**, *91*, No. e0055922.
(949) Paruthiyil, S.; Pinochet-Barros, A.; Huang, X.; Helmann, J. D. *Bacillus subtilis* TerC Family Proteins Help Prevent Manganese Intoxication. *J. Bacteriol.* **2020**, *202*, No. e00624-19.
(950) Sharma, R.; Mishanina, T. V. A Riboswitch-Controlled Manganese Exporter (Alx) Tunes Intracellular Mn^{2+} Concentration in *E. coli* at Alkaline PH. *bioRxiv* **2023**. DOI: 10.1101/2023.05.07.539761
(951) Zeinert, R.; Martinez, E.; Schmitz, J.; Senn, K.; Usman, B.; Anantharaman, V.; Aravind, L.; Waters, L. S. Structure-Function Analysis of Manganese Exporter Proteins across Bacteria. *J. Biol. Chem.* **2018**, *293*, 5715−5730.
(952) He, B.; Sachla, A. J.; Helmann, J. D. TerC Proteins Function during Protein Secretion to Metalate Exoenzymes. *Nat. Commun.* **2023**, *14*, 6186.
(953) Andreini, C.; Rosato, A. Structural Bioinformatics and Deep Learning of Metalloproteins: Recent Advances and Applications. *Int. J. Mol. Sci.* **2022**, *23*, 7684.
(954) Yan, Z.; Wang, J. Evolution Shapes Interaction Patterns for Epistasis and Specific Protein Binding in a Two-Component Signaling System. *Commun. Chem.* **2024**, *7*, 1−11.
(955) Freiberger, M. I.; Ruiz-Serra, V.; Pontes, C.; Romero-Durana, M.; Galaz-Davison, P.; Ramírez-Sarmiento, C. A.; Schuster, C. D.; Marti, M. A.; Wolynes, P. G.; Ferreiro, D. U.; et al. Local Energetic Frustration Conservation in Protein Families and Superfamilies. *Nat. Commun.* **2023**, *14*, 8379.
(956) Monteiro da Silva, G.; Cui, J. Y.; Dalgarno, D. C.; Lisi, G. P.; Rubenstein, B. M. High-Throughput Prediction of Protein Conformational Distributions with Subsampled AlphaFold2. *Nat. Commun.* **2024**, *15*, 2464.
(957) Gelman, S.; Johnson, B.; Freschlin, C.; D'costa, S.; Gitter, A.; Romero, P. A. Biophysics-Based Protein Language Models for Protein Engineering. *bioRxiv* **2024**, DOI: 10.1101/2024.03.15.585128.
(958) Peinetti, A. S.; Lake, R.; Lu, Y. Functional DNA Sensors for Heavy Metal Ions and Microbial Contaminants in Water. In *World Scientific Series in Nanoscience and Nanotechnology*; World Scientific, 2023; pp 137−170.

(959) Grant, C. R.; Amor, M.; Trujillo, H. A.; Krishnapura, S.; Iavarone, A. T.; Komeili, A. Distinct Gene Clusters Drive Formation of Ferrosome Organelles in Bacteria. *Nature* **2022**, *606*, 160−164.
(960) Nordlund, P.; Reichard, P. Ribonucleotide Reductases. *Annu. Rev. Biochem.* **2006**, *75*, 681−706.
(961) Cotruvo, J. A.; Stubbe, J. Class I Ribonucleotide Reductases: Metallocofactor Assembly and Repair *In vitro* and *In vivo*. *Annu. Rev. Biochem.* **2011**, *80*, 733−767.
(962) Srinivas, V.; Lebrette, H.; Lundin, D.; Kutin, Y.; Sahlin, M.; Lerche, M.; Eirich, J.; Branca, R. M. M.; Cox, N.; Sjöberg, B. M.; Högbom, M. Metal-Free Ribonucleotide Reduction Powered by a DOPA Radical in Mycoplasma Pathogens. *Nature* **2018**, *563*, 416−420.
(963) Hood, M. I.; Skaar, E. P. Nutritional Immunity: Transition Metals at the Pathogen-Host Interface. *Nat. Rev. Microbiol* **2012**, *10*, 525−537.
(964) Chen, Y. Y.; O'Halloran, T. V. A Zinc Chaperone Mediates the Flow of an Inorganic Commodity to an Important Cellular Client. *Cell* **2022**, *185*, 2013−2015.
(965) Maret, W. Escort Proteins for Cellular Zinc Ions. *Nature* **2022**, *608*, 38−39.
(966) Foster, A. W.; Young, T. R.; Chivers, P. T.; Robinson, N. J. Protein Metalation in Biology. *Curr. Opin Chem. Biol.* **2022**, *66*, 102095.
(967) Zeng, X.; Wei, T.; Wang, X.; Liu, Y.; Tan, Z.; Zhang, Y.; Feng, T.; Cheng, Y.; Wang, F.; Ma, B.; et al. Discovery of Metal-Binding Proteins by Thermal Proteome Profiling. *Nat. Chem. Biol.* **2024**, *20*, 770−778.
(968) Zeng, X.; Cheng, Y.; Wang, C. Global Mapping of Metalloproteomes. *Biochemistry* **2021**, *60*, 3507−3514.
(969) Maret, W. Metalloproteomics, Metalloproteomes, and the Annotation of Metalloproteins. *Metallomics* **2010**, *2*, 117−125.

https://doi.org/10.1021/acs.chemrev.4c00264
Chem. Rev. 2024, 124, 13574−13659